LATE HOLOCENE MUD SEDIMENTATION AND DIAGENESIS IN THE FIRTH OF THAMES:

BENTONITES IN THE MAKING

A thesis submitted in partial

fulfilment of the requirements for the

Degree of

Master of Science in Earth Sciences

at the

University of Waikato

by

Timothy R. Naish

UNIVERSITY OF WAIKATO

1990

ABSTRACT

Late Holocene mud sedimentation in the southern Firth of Thames has been described from analysis of a number of shallow marine sediment cores. Three distinct lithofacies are distinguished on the basis of sediment texture and mineralogy. A laterally extensive greenish grey mud, typically bioturbated and massive, with sporadic uncorrelatable interbedded shell layers is termed the Firth of Thames mud facies. Nearer shore sediments are usually coarser and are subdivided into two facies: a siliciclastic sand facies (river mouth sand facies) comprising more prominent interbeds of sand in mud and associated with sedimentation at the mouth of the Waihou River; and a mixed terrigenous-carbonate gravel facies (delta fan gravel facies) associated with deposition on small delta fans adjacent to streams draining the Coromandel Range. The areal distribution of all three facies over the late Holocene has been controlled largely by northward progradation of the coastal Hauraki Lowland associated with the rapid sediment infilling of the Firth of Thames since sea level reached its present height 6500 y B.P. From seismic evidence the Holocene muds are up to 10 m thick. The cores in this study penetrated only to 5.5m sub-bottom depth and yielded an oldest radiocarbon age of 5000 y B.P. The age data indicate an average rate of offshore vertical sediment accumulation of 1.5 mm/y.

Up to 15 km of progradation of the southern shoreline of the coastal Hauraki Lowland has occurred over the late Holocene at an average rate of up to 2.5 m/y, notably from 3500 y B.P to 1200 y B.P. Progradation is evidenced by the occurrence of coarsening-upward sequences in nearer shore cores of the Firth of Thames, as well as their changing faunal composition, particularly the upward increase in abundance of the foraminifer *Ammonia beccarri*, a good indicator of brackish water conditions, which suggests a gradual seaward encroachment of the freshwater influence of the Waihou River over the late Holocene. Basal muds which are similar in composition to marine sediments of the Firth of Thames are overlain by peat dated at 6025 y B.P in a peat core from Kopouatai Peat Bog, and suggest that marine conditions existed in this inland region of the Hauraki Depression prior to 6025 y B.P.

Muds range from silty clays to clayey silts and consist principally of volcanic glass, smectite and halloysite, with smaller amounts of other volcanic-derived siliciclasts and allophane and illite, as well as skeletal carbonate (mainly aragonite) and organic matter. A contemporaneous decrease in the abundance of volcanic glass (55-15 wt% down-core) and an increase in smectite concentration (8-45 wt % down-core) occurs with sub-bottom depth. Specific mineralogical analyses (XRD and IR) and evidence from scanning electron microscopy suggest the smectite is montmorillonitic in composition and authigenic in nature. Moreover, the absence of smectite in the bottom sediments of rivers draining the Hauraki Lowland precludes a detrital origin.

The diagenetic transformation of volcanic glass to smectite in sediments of the Firth of Thames is described by a sequential kinetic model which involves a parabolic dissolution coupled with a first order precipitation of smectite via the formation of an intermediate hydrated glass phase. The rate constant calculated from the sequential kinetic model is $3.35 \times 10^{-4} y^{-1}$. The half-life of the glass is 1475 y, implying rapid early diagenetic alteration of volcanic glass to smectite to form late Holocene bentonitic deposits. Thermodynamic stability considerations imply that the first order precipitaion of smectite may be favoured by conditions of pH and Na^+ activity typical of interstitial fluids having sea water salinity under mildly anoxic conditions.

ACKNOWLEDGEMENTS

First and foremost I thank my supervisors Cam Nelson and Terry Healy for their continued interest and enthusiasm in the topic, in particular Terry for setting up the project and for entrusting me with his P.C., and Cam for the patient and skillful editing of an often tortuous manuscript. Peter Hodder is also thanked for his guidance with "kinetic-related text" and editing of Chapter 7.

Advice, help and interest from other staff members has been greatly appreciated. In particular, Chris Hendy, Mike Dravitzki, Steve Bergin, Dudley Bell and Steve Stokes are thanked for assistance with field and laboratory work. Sydney Wright and Elaine Norton (Earth Sciences secretaries) are warmly thanked for help with preparation of the final manuscript.

Peter de Lange is thanked for his comments and for "lending me" one of his peat cores.

Dr Alan Hogg of the University of Waikato Radiocarbon Dating Laboratory is thanked for dating and advice on samples.

Alf Harris and David Wild (MIRINZ, Ruakura - Hamilton) are thanked for assistance with SEM work and David Stringer (School of Engineering, University of Auckland) is also thanked for allowing me access to the School of Engineering SEM.

Terry Hume (DSIR Water Quality Centre - Hamilton) is thanked for his interest and comments on the project and Hamish Spencer (University of Waikato) is thanked for help with identification of molluscs. Drs G. Gibson (University of Auckland) and N. Hornibrook (retired) are thanked for assistance with the identification of ostracods and forams and Dr L. Carter (DSIR, New Zealand Oceanographic Institute - Wellington) is thanked for making available seismic charts of the Firth of Thames. Ken Palmer (Analytical Facility - Victoria University) is acknowledged for X-ray fluorescence spectroscopy.

Thanks to Tim Bamford (University of Waikato photographer) for superb production of photographic plates.

To my fellow "third years" - Glen B., Rob, Wayne, Glenn W., Grant, Hobbs, Frances, Gary, Kay, Vance and Barry thanks for the comradeship during those long months and late nights of thesis writing. Helen, thanks for everything and Abby just think, no more Firth of Thames mud stinking your room out!.

And last but certainly not least I'd like to thank my family for their support and encouragement, and in particular Karen for her love, support and endless encouragement during my Masters resarch.

TABLE OF CONTENTS

	Page
Abstract	i
Acknowledgements	iii
Table of contents	iv
CHAPTER ONE - INTRODUCTION	
1.1 Introduction	1
1.2 Objectives of study	3
1.3 Approach to study	3
CHAPTER TWO - REGIONAL SETTING	
2.1 Introduction	5
2.2 Coastal geomorphology	5
2.3 Drainage	6
2.4 Regional geology	7
2.5 Tectonic setting	8
2.6 Holocene sea level fluctuations	9
2.7 Bathymetry	9
2.8 Hydrodynamic setting	10
Tidal currents	10
Wave-generated currents	10
CHAPTER THREE - CORE STRATIGRAPHY	
3.1 Introduction	12
3.2 Site selection	12
3.3 Core recovery	14
3.4 Core stratigraphy	16
Firth of Thames mud facies	18
River mouth sand facies	18
Delta fan gravel facies	19
3.5 Storm bed shell layers	19
3.6 ^{14}C Chronology	22
3.7 Discussion	24

CHAPTER FOUR - SEDIMENT TEXTURE

4.1 Introduction 25
4.2 Ternary texture plots 25
4.3 Lateral variations in sediment texture 27
4.4 Vertical variations in sediment texture 29

CHAPTER FIVE - SEDIMENT MINERALOGY

5.1 Introduction 32
5.2 Clay mineralogy 32
X-ray diffraction analysis 32
Differential thermal analysis 34
Infrared absorption analysis 35
5.3 Silt fraction mineralogy 38
X-ray diffraction analysis 38
Differential thermal analysis 40
Infrared absorption analysis 40
5.4 Sand mineralogy 40
5.5 Quantitative estimation of sediment composition 41
Smectite, halloysite and illite 42
Allophane 43
Calcium carbonate 44
Volcanic glass 45
Organic matter 46
5.6 Discussion 47
Lateral variations in sediment mineralogy 47
Vertical variations in sediment mineralogy 50
Sediment geochemistry 51

CHAPTER SIX - SEDIMENT FAUNA

6.1 Introduction 52
6.2 Microfossil components 52
Foraminifera 52
Ostracods 56
Diatoms 59

6.3 Macrofossil components 60
Bivalves 60
Gastropods 62

CHAPTER SEVEN - SEDIMENT DIAGENESIS

7.1 Introduction 63
7.2 Part A - Evidence supporting a diagenetic origin for smectite 64
X-ray diffraction analysis 64
Infrared absorption analysis 67
Scanning electron microscopy 68
7.3 Discussion 68
7.4 Part B - A proposed kinetic weathering model for the transformation of glass to smectite 72
Stability and thermodynamic considerations 72
Summary of previous glass studies 75
Assumptions 76
Kinetics of volcanic glass dissolution and smectite precipitation 77
7.5 Discussion: Implications of the sequential kinetic model 83

CHAPTER EIGHT - THE LATE HOLOCENE SEDIMENTATION HISTORY OF THE SOUTHERN FIRTH OF THAMES

8.1 Introduction 86
8.2 Evidence supporting rapid late Holocene sediment infilling and progradation 86
8.3 Thickness and distribution of the Holocene sediments 87
Rates of sediment accumulation 88
Seismic stratigraphy 89
8.4 Late Holocene eustatic movement in sea level 90
8.5 Vertical fault movement: An estimated rate of regional subsidence for the late Holocene 90
8.6 Estimated rates of sediment infilling and shoreline progradation 91
8.7 A late Holocene developmental history for the Firth of Thames 92
6500-3500 y B.P 92
3500-1500 y B.P 93
1500 y B.P-Recent 94

CHAPTETR NINE - SUMMARY AND CONCLUSIONS

Stratigraphy of the late Holocene sequence 95
Late Holocene sediment infilling and shoreline progradation 96
Sediment mineralogy 98
Nature of smectite 98
Origin of smectite 99
Late Holocene diagenetic transformation of volcanic glass to smectite 100

APPENDIX ONE - CORE DESCRIPTIONS 102

APPENDIX TWO - SEDIMENT TEXTURE DATA 113

APPENDIX THREE - SEDIMENT MINERALOGY DATA 118

APPENDIX FOUR - BULK SEDIMENT GEOCHEMISTRY 120

APPENDIX FIVE - METHODOLOGY 129

APPENDIX SIX - SAMPLE ARCHIVE NUMBERS 137

REFERENCES 142

-CHAPTER ONE-

INTRODUCTION

CHAPTER ONE: INTRODUCTION

1.1 INTRODUCTION

The Firth of Thames is a low-wave energy, mud-filled, shallow-marine embayment structurally confined within the central portion of the Hauraki Rift. Located in the sourthern Hauraki Gulf (Figure 1.1), it's situation is unique compared to the generally high energy nature of the coastal waters about the majority of the New Zealand coastline. For example:

1. Mud sedimentation on the open or semi-open New Zealand coastline is generally uncommon, where mixed sand-gravel sediments are the norm due to dominantly high-wave energy conditions (Healy and Kirk 1982).

2. Consequently, preservation of "relatively thick" sequences of shallow-marine Holocene mud deposits are not widely recognised in New Zealand. This is in part due to the general lack of constructional coastline features of late Holocene age.

3. The large quantities of volcanogenically-derived fine sediments in the Firth of Thames contrasts with the predominance of micaceous greywacke-derived sediments about much of the New Zealand coastline (Carter 1975; Hume and Nelson 1985; Churchman et al 1988).

The Firth of Thames is enclosed to the east and west by the uplifted blocks of the Coromandel Range and Hunua Range respectively, and to the south by the low laying Hauraki Lowland, which limits the role of wave- and wind-generated currents in transporting sediment in the Firth. A high rate of sediment supply, from the rivers draining the southern Hauraki Depression, into a low energy, protected embayment has been the major factor controlling active sedimentation during the Holocene. Moreover, the narrow width of the coastal Hauraki Lowland, a consequence of the confining effect of the Hauraki Rift, has restricted the area available for lateral dispersal of sediment alongshore and

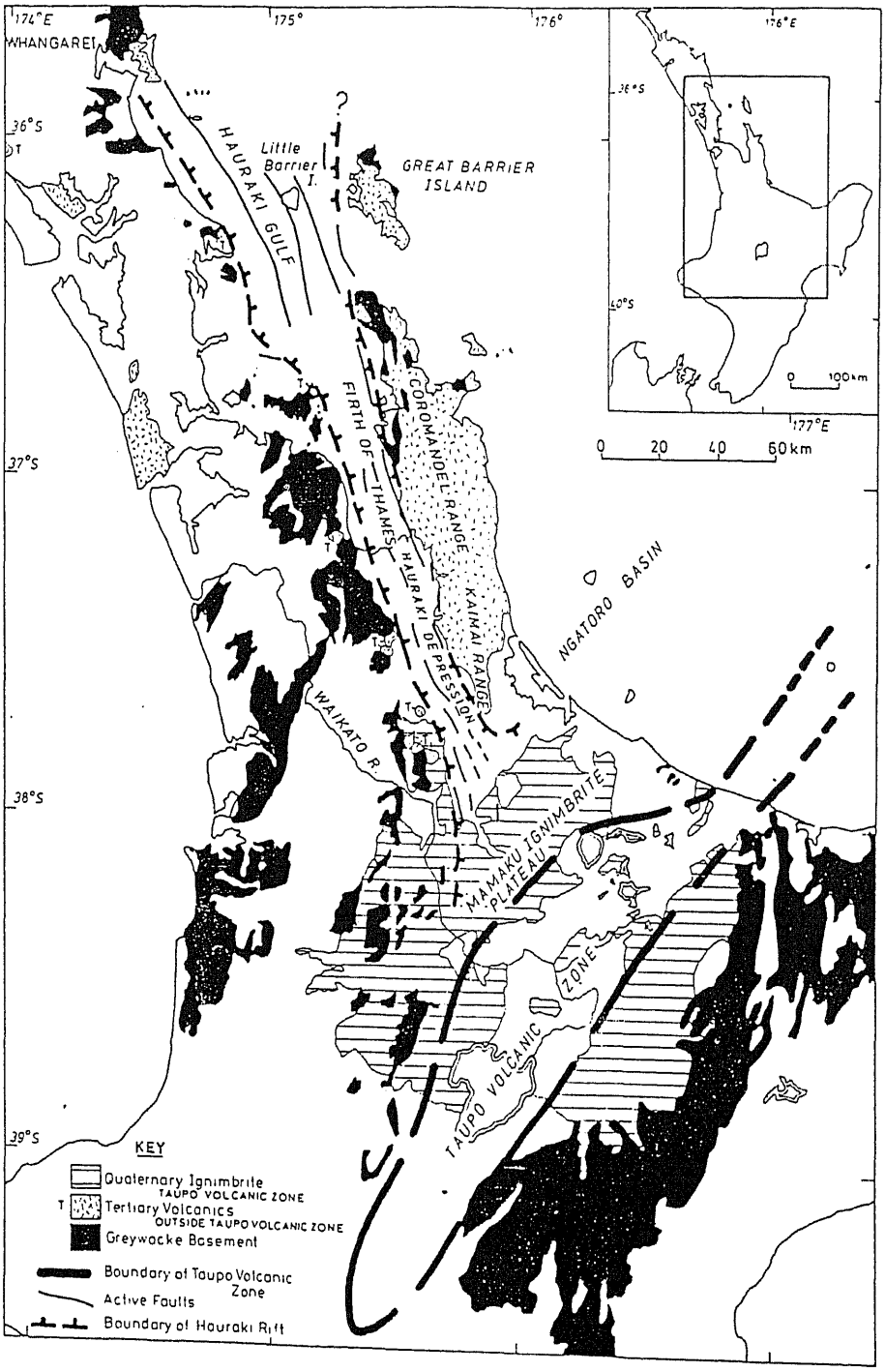

Figure 1.1
Location map of the Firth of Thames and the greater area (from Hochstein and Nixon 1986).

favoured vertical accretion. Consequently a well preserved sequence of mud sediments of Holocene age have accumulated in the Firth of Thames. It is these sediments that are the subject of this study, principally based on the analysis of a number of shallow marine cores collected from the southern Firth.

Prior to Holocene sedimentation, during the last glaciation, this region of the Hauraki Graben was subaerially exposed. Subsidence controlled deposition of pumiceous sands and gravels on a prograding braided alluvial fan resulted in the accumulation of a thick sequence of Pleistocene sediments (Kear and Tolley 1953; Cuthbertson 1981; Houghton and Cuthbertson 1989). These sediments are volcaniclastic in nature dominated by pumice and glass shards from erosion of the mid-Pleistocene ignimbrites of the Taupo Volcanic Zone (TVZ) to the south and the erosion of Neogene andesite-dacite volcanics of the Coromandel-Kaimai Range (Fig. 1.1). During the Holocene, rising sea level caused the rivers of the Hauraki Plains to aggrade and meander, reworking the cap of earlier braided alluvial sediments and delivering large amounts of volcanic glass-dominated suspended sediments to the Firth of Thames.

The stability of volcanic glass in the marine environment is a topic that has received much discussion in recent years (Peterson and Griffen 1964; Biscaye 1965; Melson and Thompson 1973; Chamley 1990). The intimate association of authigenic smectite-rich deposits (bentonites) with mid-ocean ridge basalts is well documented (Mathews 1962). Analysis of Deep Sea Drilling Project (DSDP) core sediments has revealed the same association of authigenic smectite clay minerals with volcaniclastic sediments and discretely preserved ash layers (Hein and Scholl 1978; Hein et al. 1978; Gardener et al. 1985). Early stage diagenetic reactions involving the transformation of glass to smectite in marine volcanogenic sediments are still poorly understood and given the general consensus that these reactions may be very slow, bentonites are not generally regarded as forming in sediments of young age. The possibility of marine diagenetic alteration of glass is investigated in this study.

Due to a low-angle sea floor gradient in the Firth of 1:2000, small fluctuations in relative sea level during the Holocene may have had a profound effect on the position of shoreline. Holocene coastal

plain progradation of barrier-dune systems has been described for various areas around the New Zealand coastline (Pullar and Selby 1971; Schofield 1975, Marks and Nelson 1979; Gibb and Aburn 1986b; Wigley 1990). However the recognition of progradational features associated with mud-dominated systems is more problematic, in particular the interpretation of older shorelines.

1.2 OBJECTIVES OF STUDY

With regard to the above discussion, an analysis of the shallow marine sediments of the southern Firth of Thames has been undertaken with the following two major objectives in mind:

1) To use compositional, textural, faunal and stratigraphic information from core sediments to reconstruct the late Holocene sedimentation history of the Firth of Thames. Of particular interest is the interplay between the rates of sediment accumulation, regional subsidence and eustatic fluctuations in sea level, and how these factors have influenced the late Holocene position of shoreline of the very low-lying (low gradient) Hauraki Plain.

2) To evaluate the nature and extent of early diagenetic processes occurring in sediment cores from detailed consideration of their mineralogy, and paticularly to ascertain whether "bentonite formation" is occurring from the alteration of volcanic glass.

1.3 APPROACH TO STUDY

This study involves the analysis of sediments from a number of cores collected from southern Firth of Thames. From an early stage it was decided to select from theses five representative cores for high resolution sampling (every 20 cm down-core) and subsequent comprehensive analysis. Other cores were logged and used primarily for analysis of surficial samples. The thesis presentation begins with a general discussion of the regional setting of the Firth of Thames and outlines some controlls that may have influenced the nature of sedimentation during the late Holocene (Chap. 2). Following this is four

largely descriptive chapters in which data are presented for a number of specific core properties including stratigraphy (Chap. 3), sediment texture (Chap.4), sediment mineralogy (Chap.5) and sediment faunal composition (Chap. 6). The laboratory procedures and analyses carried out in this thesis are outlined in Appendix 5. Subsequently these data are synthesised into a detailed discussion of i) diagenetic processes (Chap. 7) and ii) a history of late Holocene sedimentation for the Firth of Thames (Chap. 8).

-CHAPTER TWO-

REGIONAL SETTING

CHAPTER TWO: REGIONAL SETTING

2.1 INTRODUCTION

The aim of this chapter is to provide the regional setting in which the late Holocene mud sediments of the Firth of Thames have accumulated. In particular some controls on sedimentation and post-depostional processes are outlined and include such influences as onland sediment source, late Holocene vertical tectonic movements, eustatic sea level fluctuations and hydrodynamic processes. Much of the information presented here will be referred to in later chapters.

The Firth of Thames is situated in the central section of the Hauraki Rift, a young continental rift which extends south for over 300 km from Whangarei through the Hauraki Gulf and the Hauraki Depression into the Taupo Volcanic Zone (Hochstein and Nixon 1979; Figs.1.1 and 2.1). It is bounded by uplifted blocks, the Hunua-Hapuakohe Range in the west comprising Jurassic metagreywackes and the Coromandel-Kaimai Range in the east comprising Neogene volcanics capping Jurassic metagreywackes (Skinner 1986). To the south is the low-lying Hauraki Lowland considered by Cuthbertson (1981) to have formed during the Pleistocene from the northwards coalescence of a number of discrete alluvial fans into a single braided river outwash plain. The modern Hauraki Lowland consists of peat deposits in the northwest and two meandering river systems which drain the Hauraki Depression and enter the southern Firth of Thames.

2.2 COASTAL GEOMORPHOLOGY

The intertidal zone of the southern Firth of Thames coastline is characterised by a broad expanse of mudflats, up to 1.5 km wide. The mudflats are traversed by the channels of the Waihou, Kauraeranga, Piako and Waitakaruru Rivers in the south and numerous streams and tidal creeks elsewhere. Reclaimation and tailing deposits, associated with gold mining, have altered the position of much of the shoreline in the vicinity of Thames during historic times. North of Tararu, along the escarpment of the

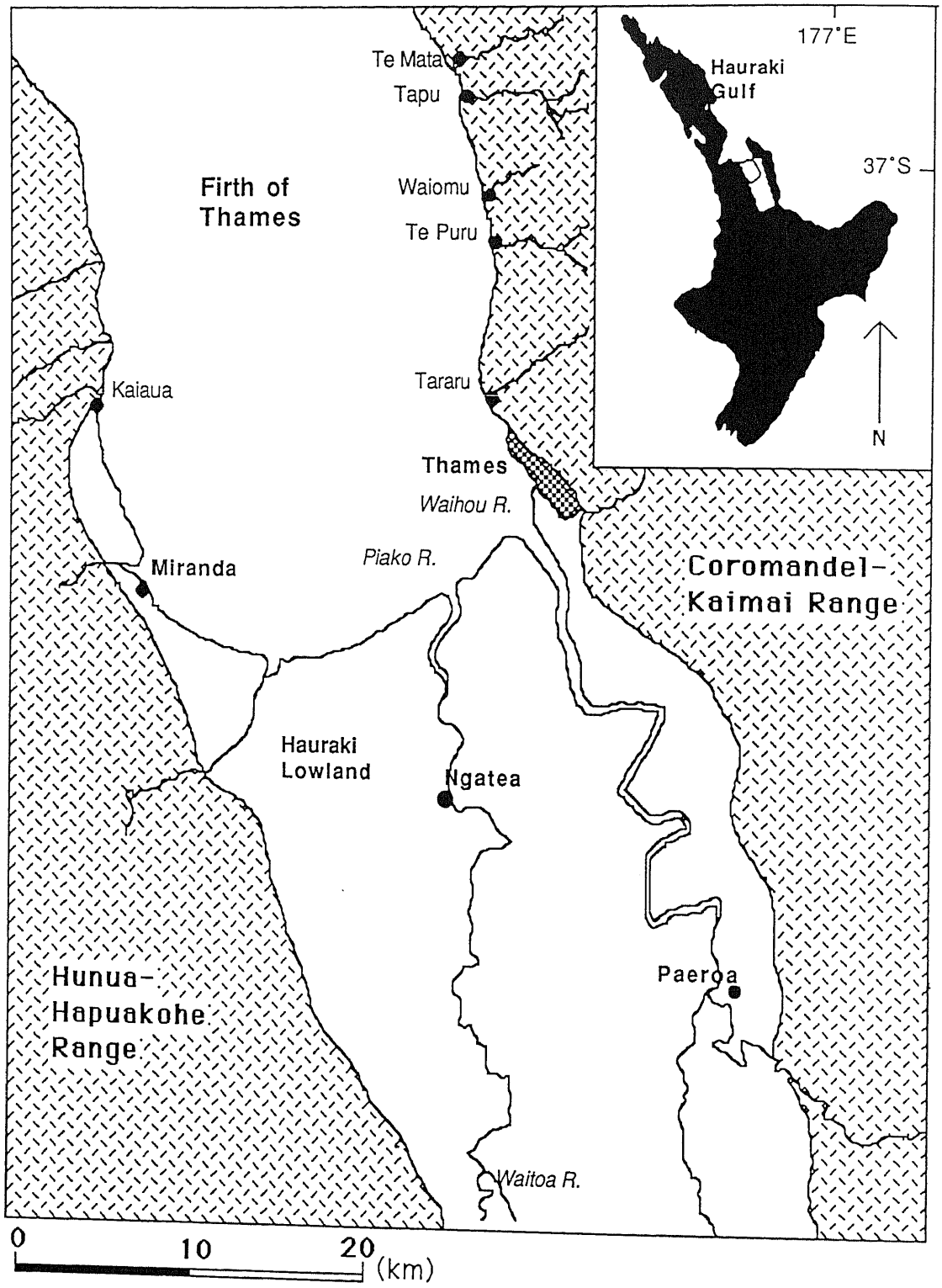

Figure 2.1
Location map of the study area.

Hauraki Fault, there is a dramatic change in coastline morphology (Figs. 1.1 and 2.3). Small rocky bays and narrow mixed sand and gravel beaches predominate. Gravel delta fans form at the mouths of the steep gradient streams that drain the Coromandel Range. Morphologically the gravel delta fans consist of a shore terrace, an active beach face, and a back-shore region (Dravitzki 1988). North of Tapu, Manaia Hill basement greywacke is exposed on the coast. Steep coastal cliffs and subaerially exposed wave cut platforms are characteristic of the northern coastline. Coastal exposures of basement rock tend to form predominantly rocky shores with conspicuous headlands, wave cut platforms and pebbly to bouldery beaches. On the southwestern coast of the Firth of Thames a well preserved system of raised beach ridges near Miranda has been described by Schofield (1960) and Woodroffe et al. (1983) as a chenier plain and is believed to recorded eustaic sea level fluctuations over the late Holocene (discussed in Section 2.6).

2.3 DRAINAGE

The major river draining the Hauraki Depression is the Waihou River which, together with it's tributaries, drains from the Whakamarama and Mamaku Plateaus in the south along the eastern side of the lowland into the Firth of Thames near Thames. The Waitoa River drains the western side of the depression from the Hinuera Valley northwards into the Piako River, which then meanders across the Kopouatai Dpression (described in Section 2.5) towards the Firth of Thames. Both river systems are illustrated in Figure 2.1. Radiocarbon dating of ancestral Waikato River sediments (Cuthbertson 1981) indicate that the Waikato River entered the Hauraki Depression about 23,000 y B.P, only to abort from it's channel around 19,000 y B.P possibly because it aggraded to a level which enabled drainage to be directed back into the Hamilton Basin (Fig. 1.1). The Waihou and Waitoa River systems have become entrenched within the confines of the Waikato paleochannels where they meander across the Hauraki Lowland.

Sediment discharge from the Waihou River is estimated to be 0.343×10^6 tonnes y^{-1} and from the Piako River 0.082×10^6 tonnes y^{-1} (Griffiths and Glasby 1985). They are considered the principal

GEOLOGICAL LEGEND

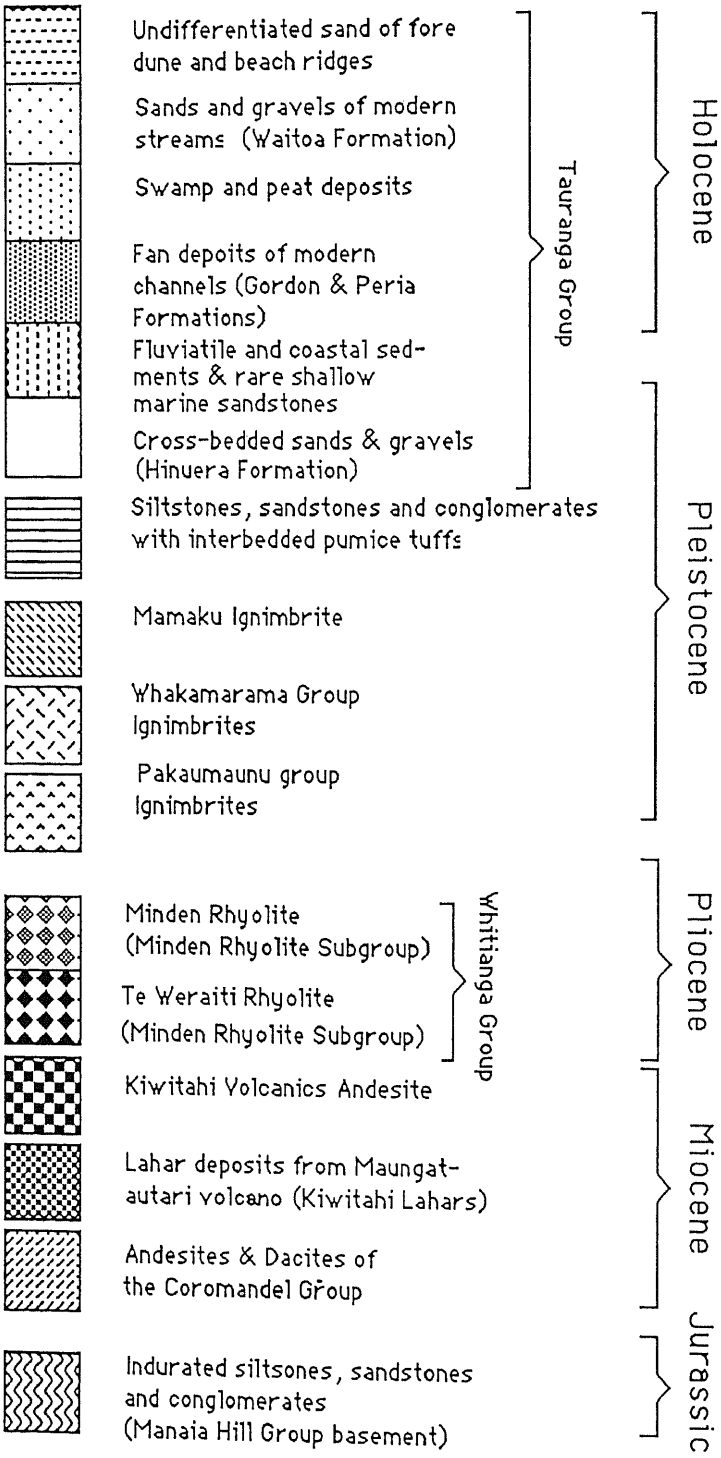

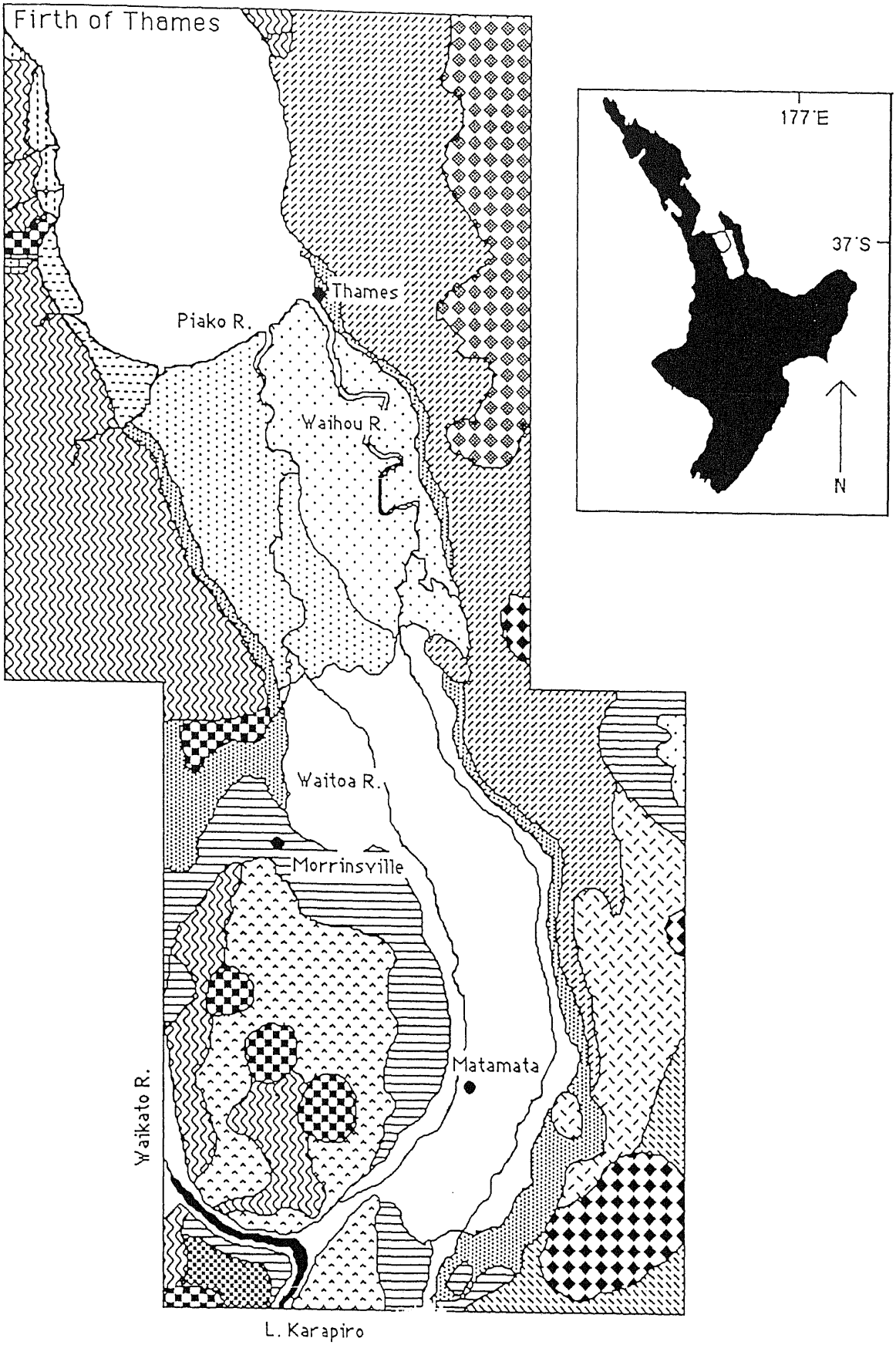

Figure 2.2

Regional geology of the Hauraki Depression.

suppliers of clastic detritus to the Firth of Thames. In contrast the streams draining the adjacent Coromandel Range are characterised by very steep gradients, commonly in excess of 1:100, formed as a consequence of rapid movement along the Hauraki Fault. These streams are considered to be important local suppliers of sediment which accumulates in small delta fans that prograde offshore (Dravitzki 1988).

Average annual rainfall (for the period 1950-1981, Dravitzki 1988) is highly variable over the region from 1278 mm at Thames, to 1843 mm at Coromandel. Flash floods are common in the region. In 1981, 383 mm fell in a 72 h period at Coromandel. Such storm events result in large inputs to the Firth of Thames of fine-grained sediment from rivers draining the Hauraki Depression and large pulses of poorly sorted coarse material to the delta fans bordering the Coromandel and Hunua Ranges.

2.4 REGIONAL GEOLOGY

Possible source areas of the late Holocene sediments include the Hauraki Depression, the adjacent ranges and the TVZ to the south (Figs. 1.1 and 2.2).

The Quaternary sediments of the Hauraki Lowlands belong to the Tauranga Group (Schofield 1959) and are dominated by the upper Pleistocene Hinuera Formation (Healy 1964) which consists of cross-bedded fluivatile pumiceous, rhyolitic and ignimbritic sands and gravels (Hume et al. 1975). Post-Hinuera sedimentation in the lowlands is confined to alluvial reworking in the modern Waitoa and Waihou river systems (Waitoa Formation), and continued fan growth along the margin of the Kaimai Range (Gordon Formation) and the Hunua-Hapuakohe Range (Peria Formation; Houghton and Cuthbertson 1989).

Mid-Pleistocene ignimbrites of Whakamarama Plateau form the southern Kaimai Range and abut onto the Mamaku Plateau in the south. These ignimbrites include the pumice-rich Aongatete Ignimbrite and the underlying crystal-rich Waitekariki Ignimbrite (Healy 1969). Together they form the Whakamarama

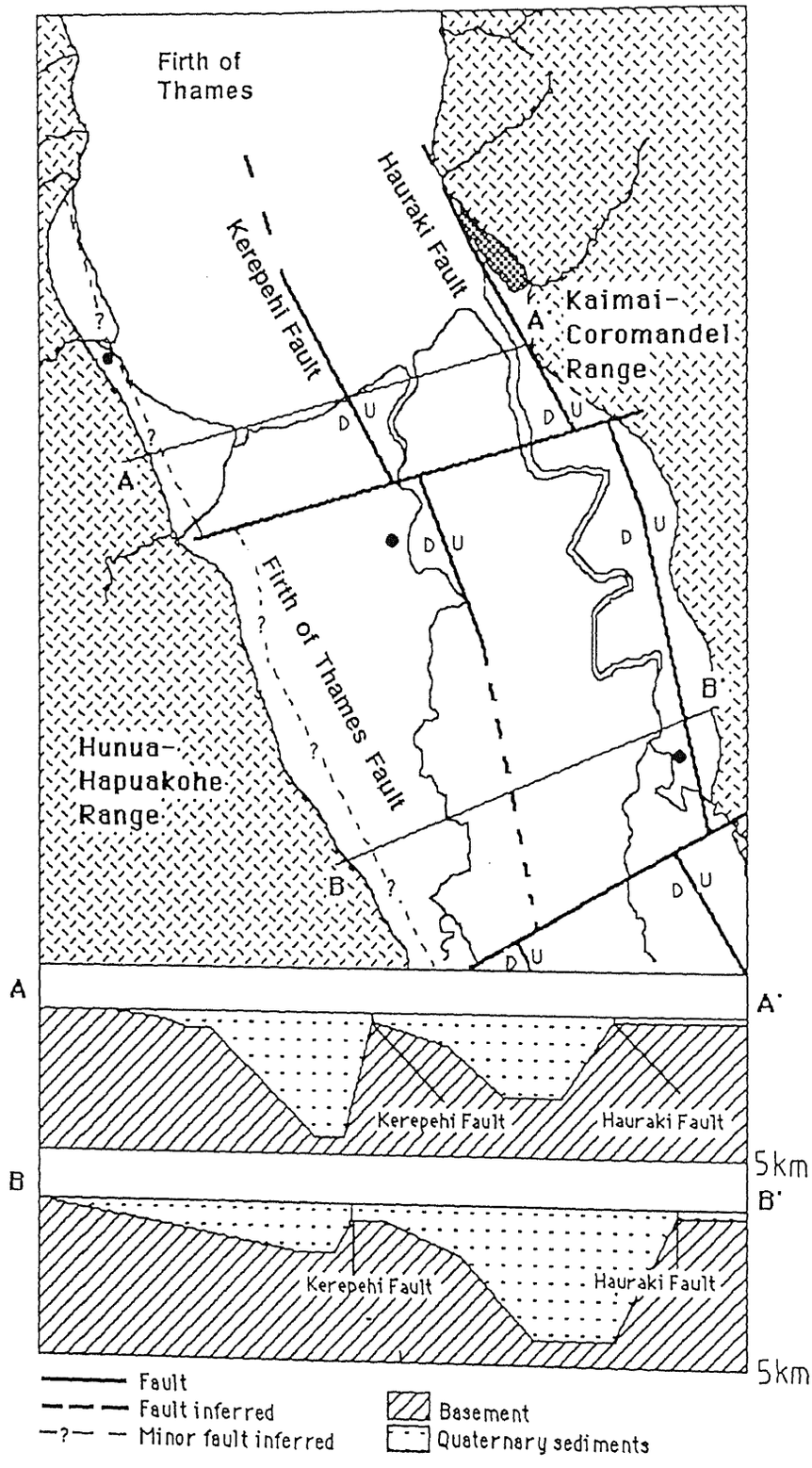

Figure 2.3

Structure map of the Hauraki Depression. Shown are the major normal faults and accomodation zones. Cross-sections are constructed from gravity and magnetic anomaly profiles (after Hochstein and Nixon 1979).

Group (Houghton and Cuthbertson 1989; Fig. 2.2). Both ignimbrites are dacitic and include predominantly rhyolitic lithics. These ignimbrites crop out extensively along the western margin of the Hauraki Depression. Pakamaunu Group Ignimbrites are exposed in the south-western region of the graben and consist of three pumice-rich ignimbrite formations: the Rocky Hill Ignimbrite, the Ahuroa Ignimbrite and the Ongatiti Ignimbrite (Healy et al. 1964). The Mamaku Pataeu comprises eroded Mamaku Ignimbrite atop the former ignimbrites, and is the ultimate provenance of much of the sediment in the Hauraki Lowlands (i.e., the Tauranga Formation) and the Firth of Thames.

Whitianga Group Rhyolite (Healy et al. 1964) and Coromandel Group andesites, intrusions, tuffs and breccias make up the northern Kaimai-Coromandel range (Skinner 1976). Mesozoic basement greywacke (Manaia Hill Group) is exposed north of Tapu in the Coromandel Range and forms the Hunua Ranges on the western boundary of the Firth of Thames.

2.5 TECTONIC SETTING

As mentioned earlier, the Firth of Thames is structurally confined within the central portion of the Hauraki Rift. Interpretation of gravity and magnetic data by Hochstein and Nixon (1979, 1986) has alluded to the structure of the rift. From west to east it consists of a fault-angle deprssion, a medial horst and a half graben (Figure 2.3). Bounding faults strike north northwest regionally and are dislocated into blocks by northeasterly to east northeasterly cross faults (Hochstein and Nixon 1979; Skinner 1986).

The age of rifitng is problematic. Hochstein and Nixon (1986) inferred that the rift is young and has experienced rapid subsidence during the Quaternary as indicated by the thick fill (0.7 to 1.0 km) of unconsolidated Pleistocene sediments. Allowing for the elevation of the rift shoulders, they deduced 2.5 to 4 km of of rift floor subsidence since the Pliocene. A regional subsidence rate for the Quaternary of 1.5 mm/y is estimated by Pillans (1986) from the above geophysical data. Quaternary uplift of the Hunua block is poorly understood. The western boundary fault of the rift, the Firth of Thames Fault, is inferred by Hochstein and Nixon (1979) to be a minor hinge fault and consequently that there has been

comparatively less subsidence in the fault-angle depression forming the western half of the rift. Moreover, no evidence exists for Holocene uplift adjacent to the Hunua Range. However, in the half graben east of the Kerepehi Fault, subsidence has been substantial.

Recent rifting is recognised beneath the Firth of Thames from seismic evidence. Pleistocene and Holocene strata are bisected by faults and tilted to the east, east of the Kerepehi Fault (Greig 1982). Cross-cutting transverse faults offset the major normal faults, in some places by up to 3 km.

2.6 HOLOCENE SEA LEVEL FLUCTUATIONS

Gibb (1986a) has summarised sea level data for a variety of sites around New Zealand and suggested that sea level reached its maximum about 6500 y B.P and has not fluctuated by more than ± 1 m since that time. However, local relative sea level movements have long been recognised for the Firth of Thames region (Schofield 1960; Woodroffe et al. 1983) and for the Northland and Auckland region (Schofield 1973). Marks and Nelson (1976) cite dune progradation at Omoro barrier spit on northern Coromandel Peninsula as evidence for a 2m lowering of sea level in the last 5000 years. Schofield (1960) described the extensive beach ridge system near Miranda as evidence for a 2 m lowering of sea level in the last 4000 years. More recently Woodroffe et al. (1983) have interpreted new data from the same area and suggested that sea level showed a eustatic lowering of 0.7-0.9 in the last 3900 years and reached it's present level about 1200 y B.P. Both Schofield (1960) and Woodroffe et al. (1983) found no evidence to suggest vertical uplift has occurred during the late Holocene along the Firth of Thames Fault.

2.7 BATHYMETRY

The Firth of Thames is a shallow semi-enclosed embayment with a maximum water depth of 30 m where it is open to the Hauraki Gulf. A generalised bathymetry of the region is illustrated in Figure 2.4 The southern Firth gradually shoals southwards from 10 m water depth to broad mudflats. There is a

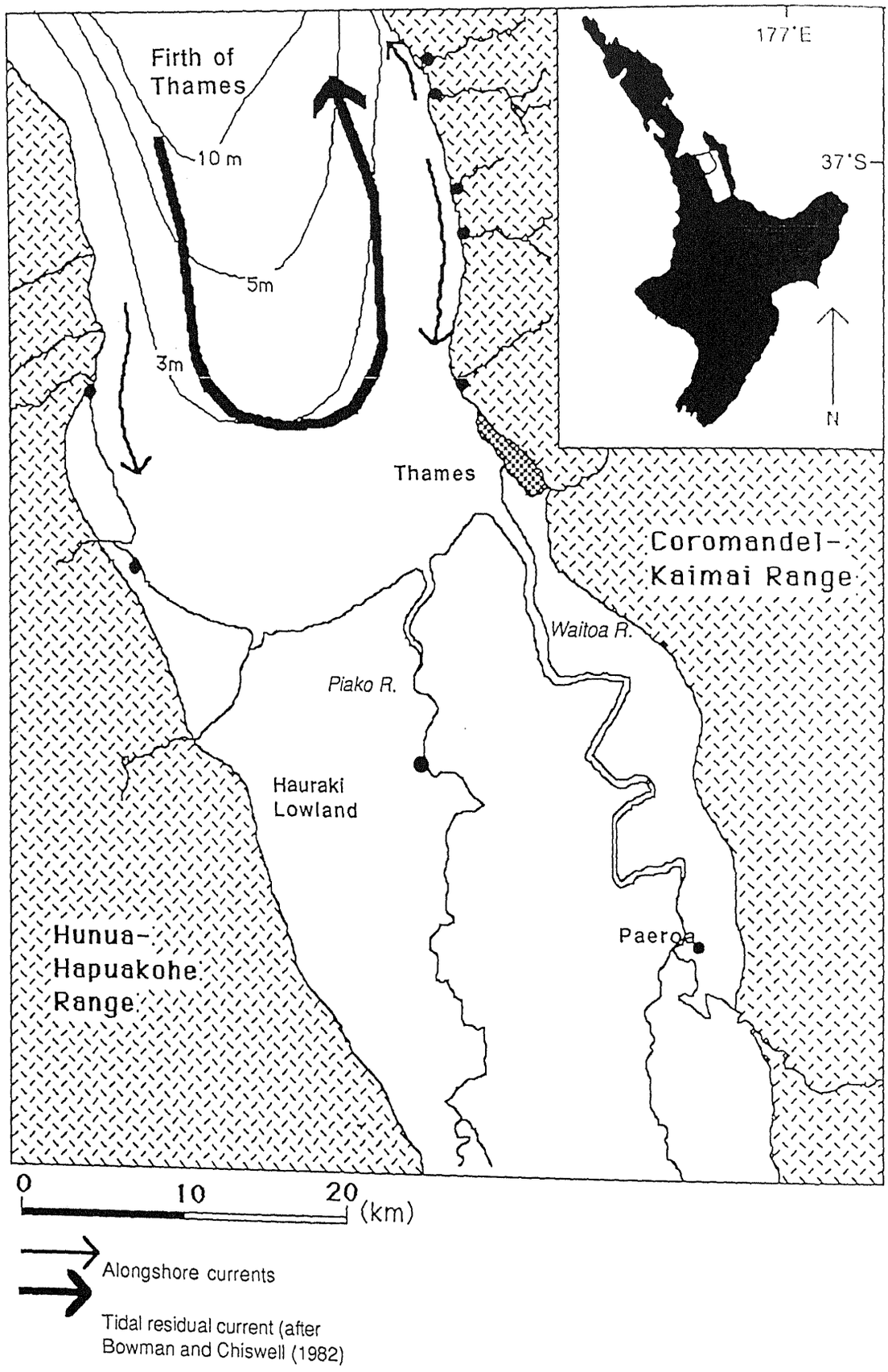

Figure 2.4

A generalised bathymetric map of the Firth of Thames. Also shown are the possible directions of sediment movement due to tidal and longshore cuurents (bathymetry from, N.Z. hydrographic chart - NZ 533, 1:100000).

general lack of subsurface relief. Side-scan sonorgraphs exhibit relatively coarse-grained lobate fan structures prograding up to 300 m offshore from the small deltas associated with Tapu, Te Mata and Tararu Streams (side-scan sonar is discussed in detail by D. Allen, in prep).

2.8 HYDRODYNAMIC SETTING

Tidal currents

The semi-diurnal tide over the New Zealand shelf forms a resonant trapped standing wave which rotates anticlockwise with a 12.42 h period (Heath 1977). The tidal wave sweeps up the east coast of the North Island and into the Hauraki Gulf. Its amplitude increases significantly on entering the Hauraki Gulf, from 85 cm at Port Jackson to 135 cm near Thames (Bowman and Chiswell 1982; Greig and Proctor 1988). The tidal range in the Firth is 2.0 m neap and 2.8 m spring. Tidal currents for the Hauraki Gulf have been numerically modelled by Bowman and Chiswell (1982) and by Greig and Proctor (1988). Results show that the residual current of the principal M_2 tide move anticlockwise around the Firth of Thames (Fig. 2.4). The flood tide is suggested to be strongest along the eastern margin. Maximum computed velocities of approximately 40 cm s^{-1} are expected at mid-tide. However the model does not allow for the considerable tidal discharge from the Waihou River and therefore underestimates current velocities along the Thames coast which can reach 103 cm s^{-1} up to 5 km off Thames (M. Dravitzki pers. commun.). In the centre of the Firth speeds of 50-70 cm s^{-1} have been measured.

Wave-generated currents

Dravitzki (1988) constructed a wind rose for the Firth of Thames. These winds were dominantly northwesterly (35.8%), westerly (24.7%) and northerly (18.5%). The wave climate within the Firth of Thames is generally low energy and is characterised by low amplitude, short period waves generated locally by the prevailing northerly and northwesterly winds. Deeper water long period swell waves can

enter the Firth via the Hauraki Gulf from the north where it is open to the ocean. However, most waves entering the Hauraki Gulf are greatly reduced in amplitude before reaching the Firth of Thames by boundary retardation effects due to a progressive shallowing southwards. Southwesterly waves are less significant in the southern region of the Firth as fetch is restricted (Dravitzki 1988).

Very little wave height data are avaliable for the Firth of Thames. Consequently the direction and magnitude of longshore currents are poorly understood. A tracer experiment conducted by Dravitzki (1988) offshore of the delta fans of Tapu, Te Puru and Te Mata indicated the net direction of littoral drift to be marginally southwards. It is possible that longshore sediment movement may be bi-directional, particularly in the northern Firth where wave approach from the south becomes more significant producing possible reversals in the direction of littoral drift (Fig. 2.3).

-CHAPTER THREE-

CORE STRATIGRAPHY

CHAPTER THREE: CORE STRATIGRAPHY

3.1 INTRODUCTION

Sediment cores were collected over the southern Firth of Thames . From these twelve cores, spaced evenly over the study area and representing different depositional settings and water depths, were selected for stratigraphic interpretation. Detailed core logs are presented in Appendix 1 and of these, logs of five "Master Cores" are discussed in detail. This information is used to categorise the core sediments into broad facies and to draw conclusions about conditions of depositional paleoenvironments. Also in this chapter the core recovery techniques and factors controlling the selection of sample sites are discussed. The main objective here is to provide a descriptive account of stratigraphy and facies relationships. A more detailed reconstruction of late Holocene mud sedimentation in the Firth of Thames, based on the stratigraphy presented in this chapter and the results of subsequent chapters, is outlined in Chapter 8.

3.2 SITE SELECTION

The core recovery program was undertaken on a contract basis for Applied Geology Associates Ltd. as part of an exploration program for placer mineral deposits in the southern Firth of Thames. Consequently, the selection of sites to be cored was determined in consultation with Applied Geology Associates Ltd. It was agreed that: (i) a number of cores should be taken offshore directly adjacent to the major stream valleys draining the Coromandel Range, in particular those whose catchments included historic or modern mining sites. Such sites may consist of sediments eroded out of the valleys and subsequently reworked and concentrated by wave action during the Holocene rise in sea level; (ii) a number of cores to be taken close to Thames where there is known historical dumping of mine tailings in the nearshore region; and (iii) a few cores be taken over the wider licence area.

The location of core sites is shown in Figure 3.1. The sites are not distributed evenly across the

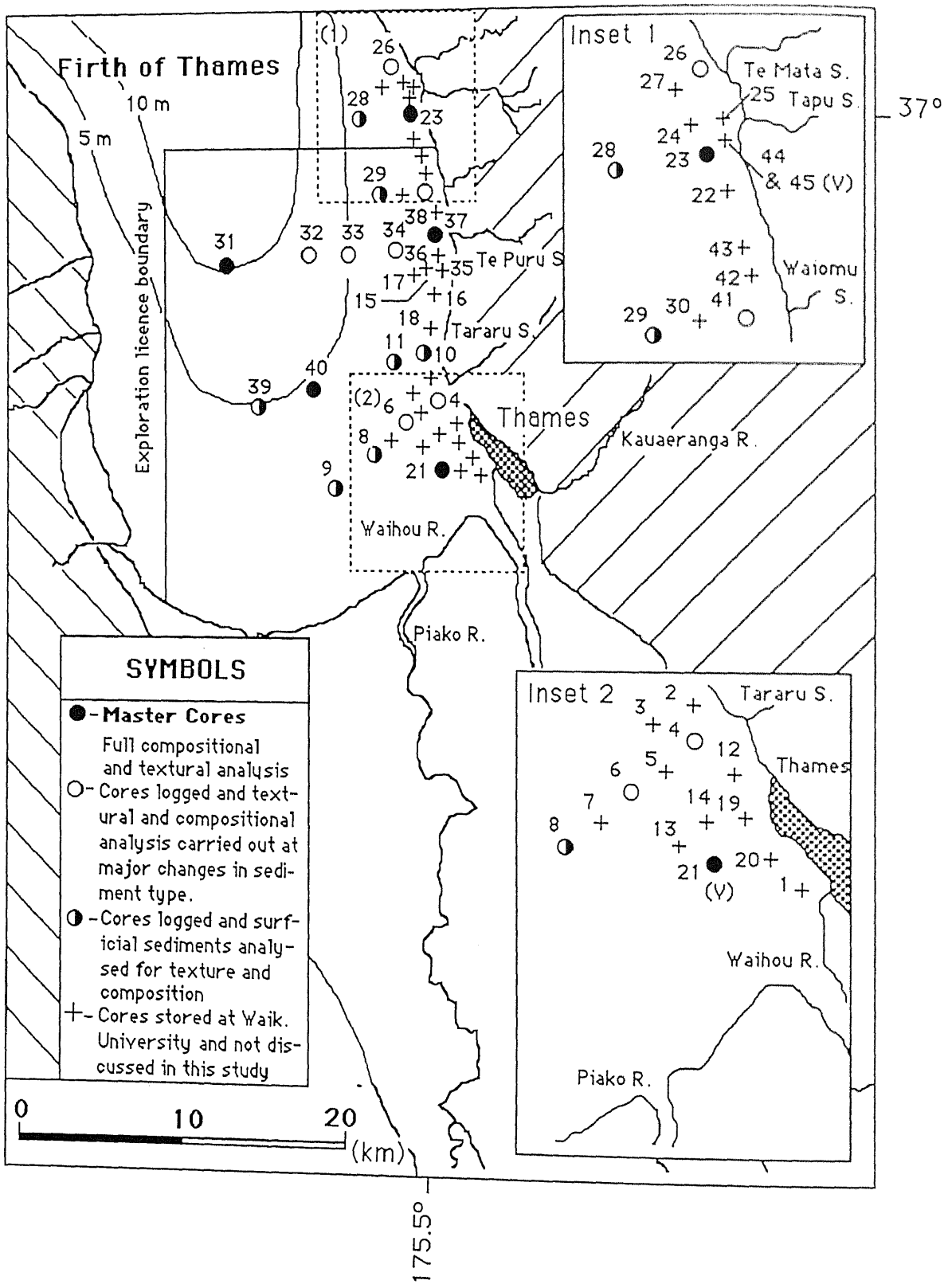

Figure 3.1
Location of core sample sites.

study area and there is a high concentration of sites in the nearshore Thames region and north along the Thames coast to Tapu. This was due to the above considerations, and the limits of the licence area

(Fig. 3.1). Within the constraints of this study it was not possible, or necessary , to analyse every core as many were taken within only a few hundred metres of each other and exhibited similar characteristics.

Five "master cores" (Cores 21, 23, 31, 37 and 40), considered to be representative of the different environments within the Firth of Thames, were selected for logging of stratigraphy, ^{14}C chronology, and detailed textural and compositional analyses . Although the master cores often contained similar lithofacies to adjacent cores they were selected on the following basis:

(i) Completeness of the sediment sequence.
(ii) Length of core recovered.
(iii) Core 21 was selected as it is a vibracore and therefore provides a larger core section for analysis.
(iv) To provide a reasonably even spread of sites across the study area.

Seven other cores (4, 6, 32, 33, 34, and 41), were also selected following the above criteria, for stratigraphic logging and less detailed compositional and textural analysis (Fig. 3.1). All master cores were sampled at 20 cm intervals. For the latter set of cores surficial sediments were sampled and further samples were taken down-core at obvious changes in sediment type. Master Core 31 was selected for detailed quantitative compositional analysis of mineralogy and is discussed in relation to diagenetic processes occurring within the sediments in Chapter 7.

Position fixing of sample sites was carried out by sextant fixes for Cores 1-20. For the remaining cores position fixing was by *FURUNO Position Fixing Radar* to an accuracy of 0.01 of a nautical mile (i.e. within 20 m). Grid references and water depths for all core sites appear in Appendix 1.

3.3 CORE RECOVERY PROGRAM

The coring program commenced in late December 1987. It was planned that cores would be recovered in two phases.

(i) A series of nearshore shallow-water (0-5 m) cores (Cores 1-20, Fig. 3.1) were obtained from predominantly muddy sediments using a "Livingstone" Piston Coring System developed by Drs David Lowe and John Green of the University of Waikato to sample lake sediments. This system, illustrated in Figure 3.2 B and Plate 3.1 A, involved manually driving 50 mm diameter PVC pipe into the sea floor. The core barrel was then extracted manually, or by electrical winch when required. Using this technique cores up to 6 m long in predominantly muddy sediments were obtained. Prior to coring some of the core barrels were pre-cut down their length and taped together. This enabled the recovered cores to be separated into two halves relatively simply, without disturbing the sediment, by working a piano wire down the length of the core between the two segments. The separated halves were then bagged, ready for logging. Unfortunately, where shell hash layers were encountered, abrasion of the tape resulted in the core barrel falling apart. Consequently un-cut cores were used in these conditions. Back in the laboratory the core sediment was extruded and measured. Up to 5% reduction in core length was noted due to compaction. During this phase of the core recovery program 20 (1-20) cores were taken in shallow-water (0-5 m) from the neashore region between Thames and Te Puru.

(ii) It was anticipated that the second phase of the core recovery program would involve the use of a shallow marine vibracoring system developed by Dr R. Davis at the University of Florida, and used successfully with Dr T.R Healy of Waikato University on the shallow shelf off the Florida Gulf coast in 1988. This system is illustrated in Figure 3.2 and Plate 3.1 B and was initially considered ideal for deeper water coring (5-10 m) in the Firth of Thames, particularly where it was anticipated coarser sediments may be encountered. However the generally muddy water-logged nature of most sediments encountered

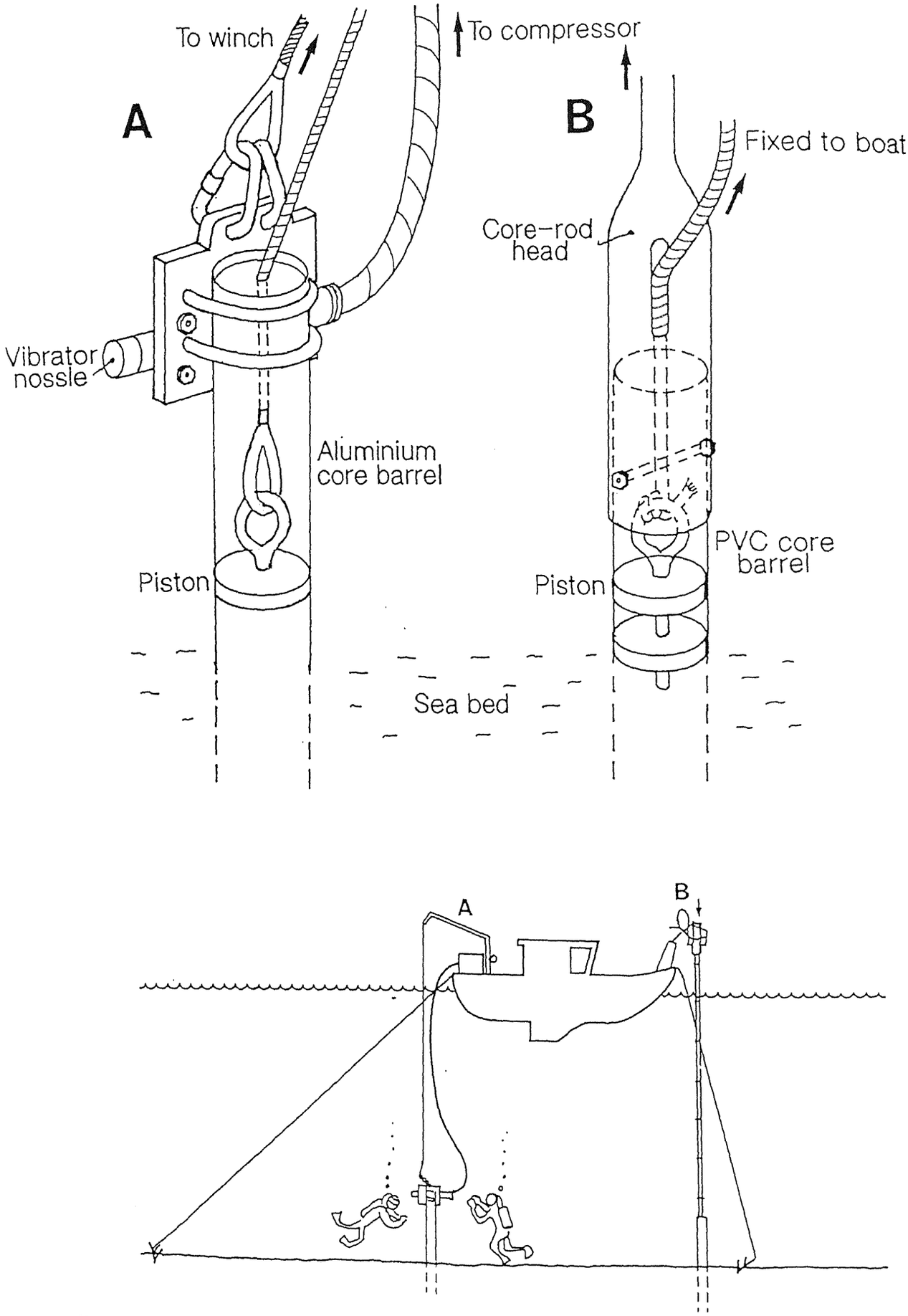

Figure 3.2
A diagrammatic view of the coring techniques used in the Firth of Thames. A) The vibracorer and B) The Livingstone corer.

A

B

Plate 3.1

Photo A shows a Livingstone core being mechanically winched out of the sea floor. In Photo B the end of a 6 m long aluminium vibracore barrel disappears as it is vibrated into the seafloor. Divers assist the entry of the barrel into the bottom sediments. Note the concrete vibrator nozzel attachment. The black cable is attached to a compressor aboard the ship.

meant they were easily penetrated by the Livingstone Corer which had the added advantages of being less time consuming, less expensive to operate and didn't require the logistical support of divers necessary for vibracoring. Two vibracores were recovered from sand-dominated regions. Core 21 adjacent to the Waihou River mouth and Core 44 adjacent to the Tapu River Mouth. Cores 21-45 were recovered during the second phase in a series of shore normal transects from Tararu, Te Puru, Tapu and Te Mata. Cores were sampled along the Te Puru and Tararu transects as far as the western boundary of the licence area (Figure 3.1).

3.4 CORE STRATIGRAPHY

In the laboratory the cores were split in half and one half was bagged and delivered to Applied Geology Associates Ltd. The other half was described, photographed and sampled for analysis of sediment texture (Chapter 4), mineral composition (Chapter 5), faunal composition (Chapter 6) and determinations of bulk sediment chemistry (Appendix 4). Core logs were constructed (Appendix 1) based upon visual observation and qualitative assessment of composition and texture. Colours were recorded using a Munsell Standard Soil Colour Book. Detailed core logs summarising lithologic units, texture, bulk density, colour and age are presented in Appendix 1.

The sediment sequence recovered in the Firth of Thames cores is dominated by a greenish grey strongly bioturbated massive plastic mud unit of late Holocene age. The oldest dated sediments occur at the base of Core 37 at 5.5m sub-bottom depth (^{14}C age = 4960 yrs, Wk 1285) . The mud unit (offshore) is broken by sporadic, uncorrelatable fine sand to gravel sized-skeletal carbonate layers consisting mainly of bivalves and subordinate amounts of benthic foraminifera and ostracods. These carbonate layers are in situ exhibiting no signs of damage from transportation processes. Nearshore, coarser layers also occur with a higher frequency within mud-dominated sediments and are composed of fragmented fine sand to gravel-sized mixed terrigenous-skeletal carbonate material. Diatoms are abundant in both sand and mud dominated sediments.

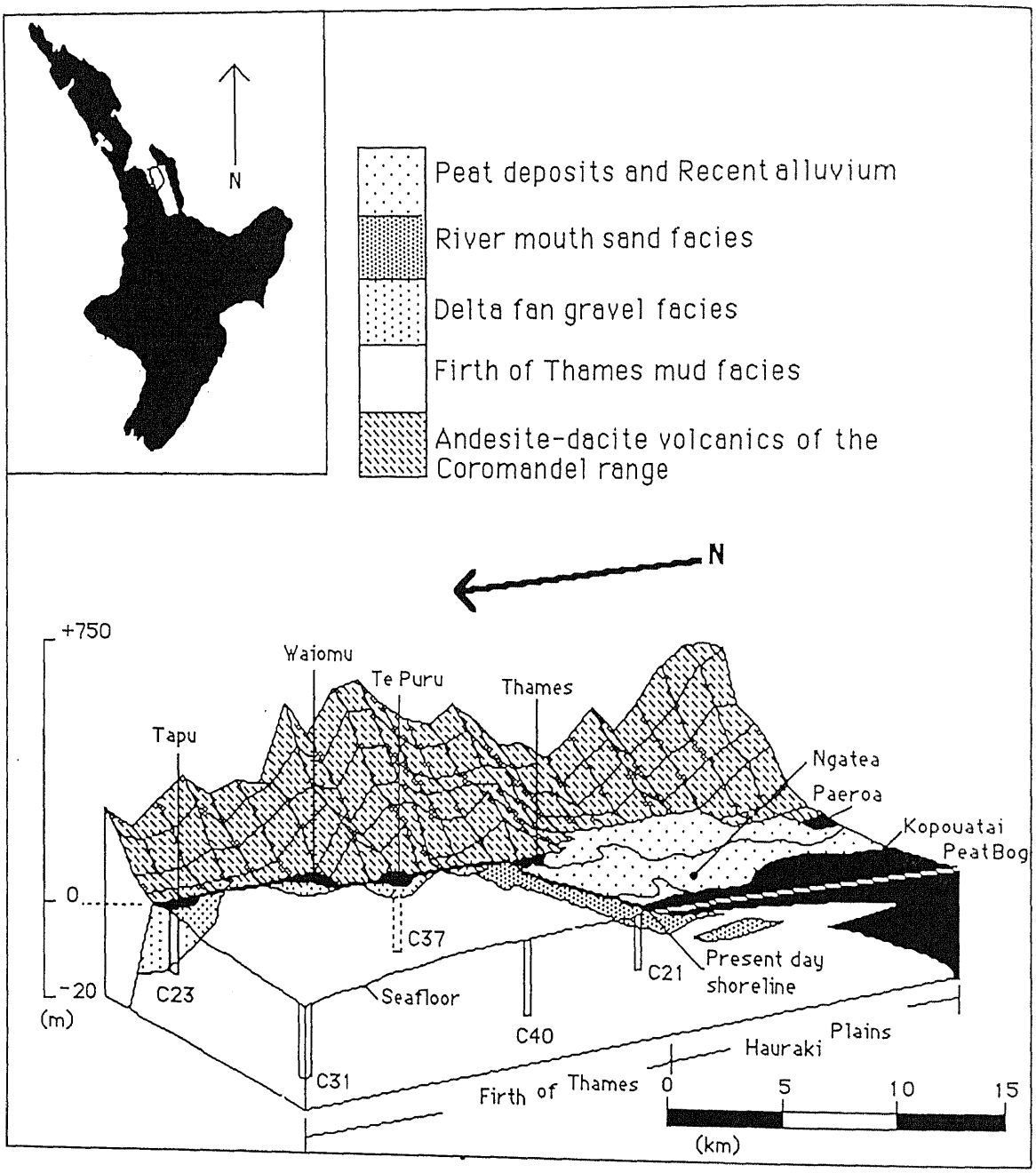

Figure 3.3
Three dimensional schematic block diagram illustrates the distribution of lithofacies represented in Master Cores from the Firth of Thames.

The core sediments were assigned to three lithofacies primarily on the basis of texture. The above greenish grey mud-dominated facies isthe major unit recognised in all offshore cores and is considered to be the same unit that Greig (1982) refers to in the northern Firth of Thames as the "Firth of Thames facies". For consistency the same name is adopted here, however this unit is further qualified with a textural term and well be referred to as the Firth of Thames mud facies. Two other facies are recognised in cores from the nearshore region, a River mouth sand facies and a Delta fan gravel facies.

Given the likelihood that the late Holocene depositional environment was not substantially different from that of the present, genetic names pertaining to modern depositional environments are assigned to all facies. Spatial and temporal relationships of the different facies are illustrated in Figure 3.3.

Firth of Thames mud facies

The Firth of Thames mud facies consists of a massive greenish grey (10GY 5/1) plastic mud interspersed with intact individual shells of *Austrovenus stutchburyi* and shell layers of predominantly *Mactra (Cyclomactra) ovata ovata*, *Mactra ordinaria* and *Nucula hartivigiana*. Microfauna characterisic of shallow marine muds occur throughout the unit and include the following dominant foraminifera and ostracod taxa: *Ammonia beccarri, Elphidium sp., Cytherella sp.* and *Kotoracythere formosa*. The facies is widespread and appears to be represented in all offshore cores recovered from the Firth of Thames. Master Cores 31, 40 and the lower portion of 21 all contain the Firth of Thames mud facies (Figure 3.4). Due to a general lack of sedimentary structures, a lack of colour changes and the presence of burrowing bivalve species (see Chap. 6) it is suggested that bioturbation of the mud unit has been intense and extensive.

River mouth sand facies

This unit is characterised by mixed terrigenous-skeletal carbonate layers ranging in texture from predominantly muddy sands to rarer sandy gravel layers and composed of glass shards, shell hash,

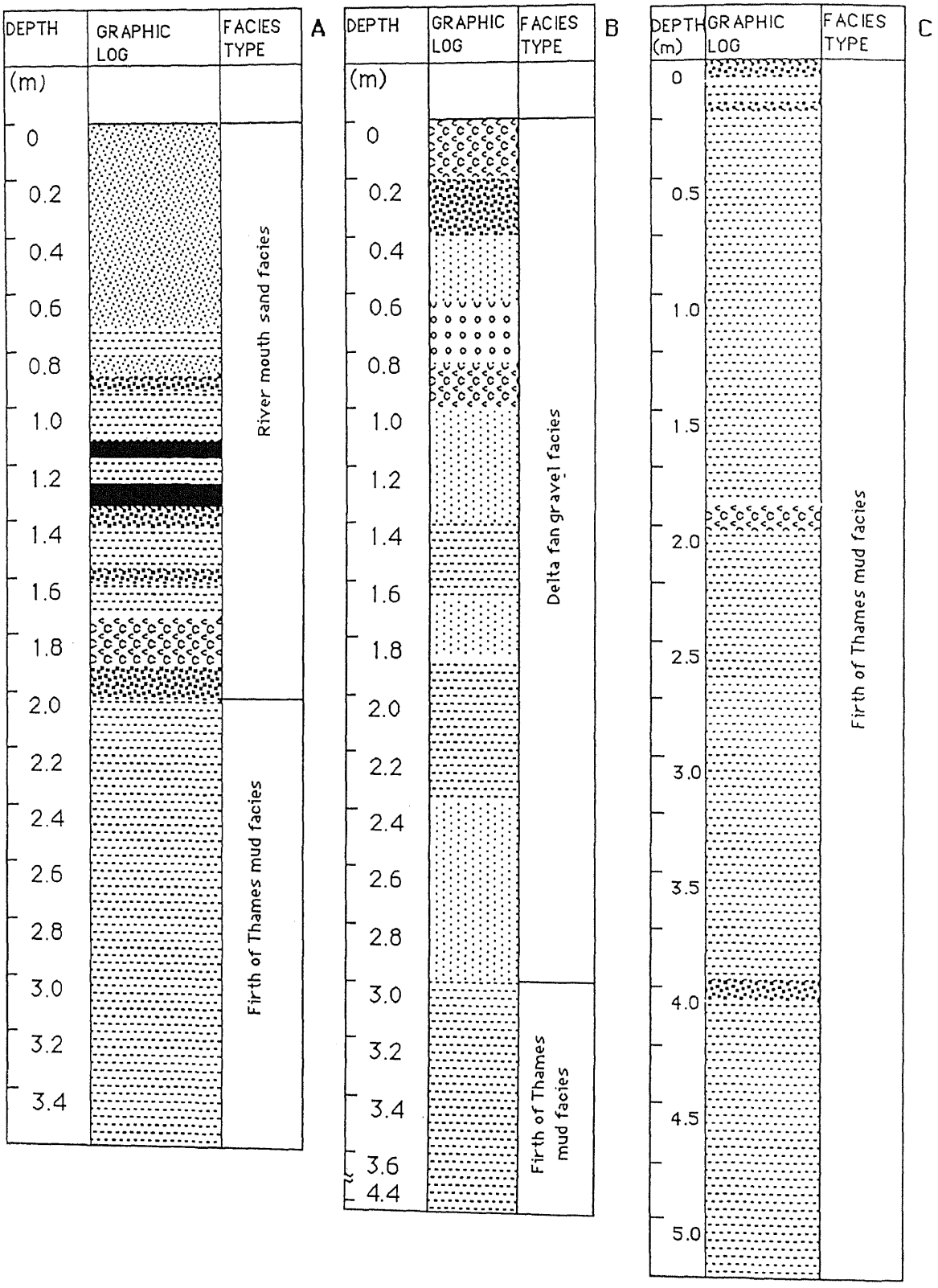
DEPTH
GRAPHIC LOG
FACIES TYPE
A
(m)
0
0.2
0.4
0.6
0.8
1.0
1.2
1.4
1.6
1.8
2.0
2.2
2.4
2.6
2.8
3.0
3.2
3.4
River mouth sand facies
Firth of Thames mud facies
DEPTH
GRAPHIC LOG
FACIES TYPE
B
(m)
0
0.2
0.4
0.6
0.8
1.0
1.2
1.4
1.6
1.8
2.0
2.2
2.4
2.6
2.8
3.0
3.2
3.4
3.6
4.4
Delta fan gravel facies
Firth of Thames mud facies
DEPTH (m)
GRAPHIC LOG
FACIES TYPE
C
0
0.5
1.0
1.5
2.0
2.5
3.0
3.5
4.0
4.5
5.0
Firth of Thames mud facies

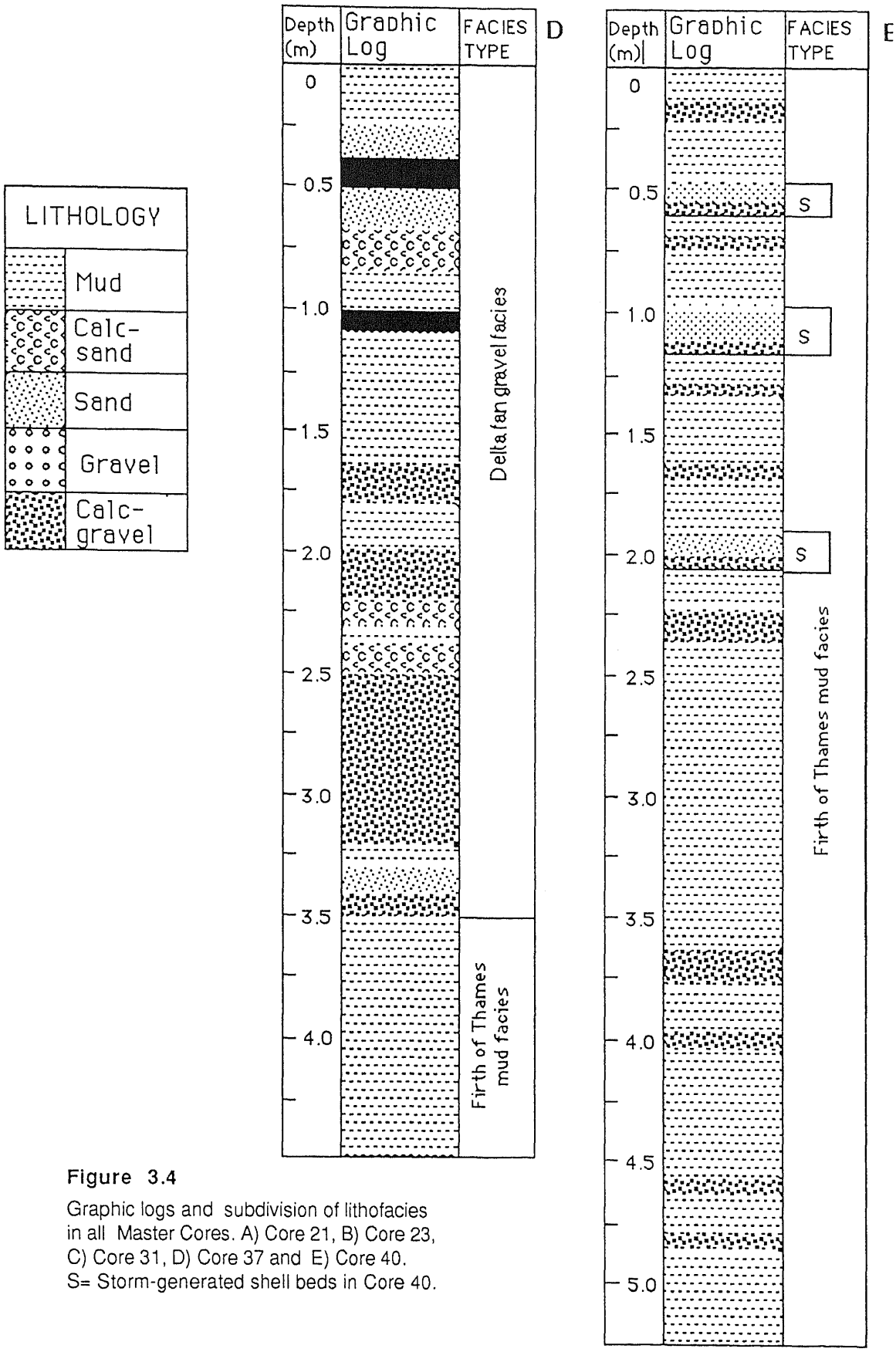

Figure 3.4

Graphic logs and subdivision of lithofacies in all Master Cores. A) Core 21, B) Core 23, C) Core 31, D) Core 37 and E) Core 40. S= Storm-generated shell beds in Core 40.

quartz and ignimbritic and rhyolitic rock fragments, with subordinate altered andesite fragments and feldspar. Interspersed between these layers are beds of calcareous poorly sorted, muddy sand and gravel shell layers dominated by *Paphies australis, Gari hodgei, Tawera spissa* and *Perna canaliculus*. This facies is represented in the upper portion of Core 21 (Fig. 3.4 A) and in Cores 4 and 6 (Appendix 1) and is considered to reflect the proximity of the Waihou, Piako and Kauaeranga River mouths and the coastline. In most cases this unit becomes considerably finer near it's base with coarser layers grading into mud-dominated sediments.

Delta fan gravel facies

This lithofacies is a correlative of the above river mouth facies. It is characterised by poorly sorted subangular terrigenous layers and mixed terrigenous-carbonate muddy gravelly sand layers of predominantly shell fragments, weathered andesite and greywacke clasts. Unlike the river mouth facies the coarse nature of this unit is less continuous and in a vertical sequence occurs as sporadic lenses of sandy gravel bands which interlayer between muds typical of the Firth of Thames mud facies. The lithofacies occurs locally in cores proximal to the delta fans of Te Puru, Waiomu, Tapu and Te Mata along the eastern boundary of the Firth of Thames (Fig. 3.1) and is well represented in Core 23 near Tapu and Core 26 adjacent to Te Mata (Appendix 1). Core 37, taken from the distal region of the Te Puru delta fan (Fig. 3.4 D), exhibits a greater occurrence of mud layers interbedded between the coarser layers.

3.5 STORM BED SHELL LAYERS

Shell layers have been described in all three of the above facies interspersed in both sand and mud units. The frequency of shell layers in cores decreases progressively with distance from shore. Two types of shell layers were observed: 1) a layer composed entirely of *Mactra* sp., predominantly *Mactra ordinaria* in growth position and generally surrounded by muds; 2) a shell hash layer associated with a normally graded mixed terrigenous-carbonate sequence. The characteristics of the two layers are summarised in Table 3.1.

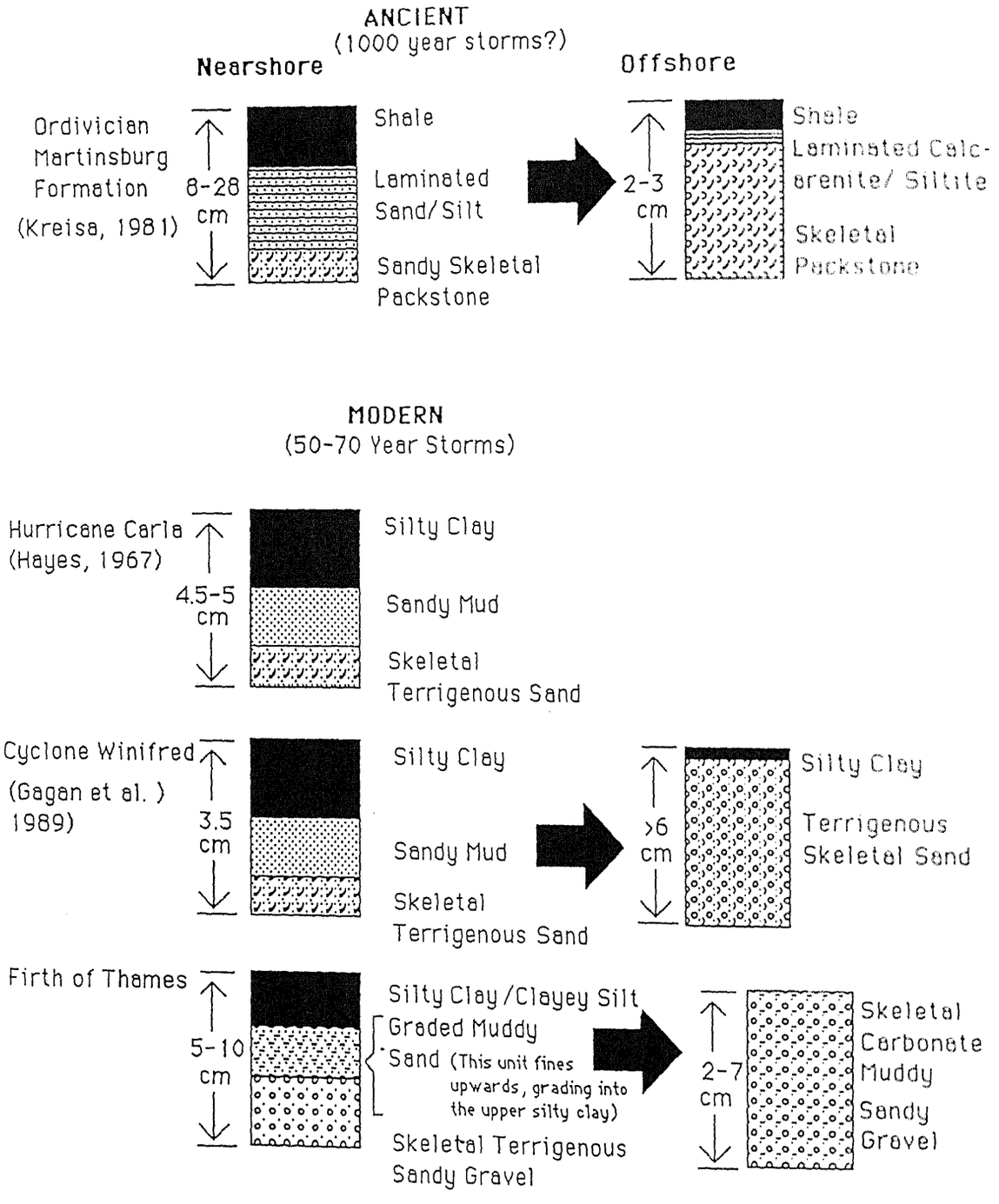

Figure 3.5
The idealised sequence of mixed-terrigenous skeletal carbonate, graded storm beds from the Firth of Thames. Also illustrated are similar storm bed sequences from other studies (after Gagen et al. 1989).

Table 3.1

Characteristics of in situ shell layers vs shell hash layers.

Properties		In situ shell layers	Shell hash layers
Textural type	-	Muddy gravel	Muddy sand-muddy sandy gravel
Sorting	-	Moderate	Poorly sorted
Thickness	-	1-5 cm	2-20 cm
Sed. structures	-	None - shells supported in growth position by muds	Basal skeletal carbonate grades into a mixed terrigenous-carbonate sand and is capped by a veneer of mud
Siliciclasts	-	None	Glass shards quartz feldspar and rock fragments
Macrofauna	-	*Mactra ordinaria Mactra ovata ovata*	*Tawera spissa, Paphies australis, Perna canaliculus, Venerupis largillierti and Austrovenus stutch buryi* (shell fragments)
Microfauna	-	*Elphidium sp. Ammonia beccarri*	*Notorotalia zealandica Ammonia beccarri* and ostracods Forams and ostracods exhibit abraded damaged tests
Contacts	-	Gradational - surrounding mud occurs throughout the shell layer.	Gradational upper contact-sharp lower boundary

The idealised shell hash sequence is illustrated in Figure 3.5 and includes a basal skeletal carbonate gravel which sharply overlies a mud unit. The basal gravel unit grades upwards into a mixed terrigenous -carbonate muddy sand and is capped by a veneer of mud. The sequence incorporates a large amount of rootlets and other organic material.

The sequence in Figure 3.5 exhibits striking similarities to storm bed layers described by Gagan et al. (1988) on the Great Barrier Reef Shelf after Cyclone Winifred (Feb, 1987) and storm-generated beds described by Hayes (1967) after Hurricane Carla in the Gulf of Mexico. The recognition of shelf storm

beds in the ancient stratigraphic record has been a topic of active debate. Graded bedding (Hayes 1967; Kreisa 1981) and more recently hummocky cross-stratification have been proposed as features of storm-induced sedimentation. However, modern analogues of these deposits appear to be limited. Gagan et al. (1988) were able to collect sediments before and immediately after Cyclone Winifred crossed the central Great Barrier Reef Shelf. Elsewhere, graded beds in Holocene shelf sediments interpreted as storm layers have been reported from the North Sea (Reineck and Singh 1972) and the Bering Sea (Nelson 1982). It is proposed that the normally graded mixed terrigenous-carbonate sequences occurring in cores from the Firth of Thames represent storm-generated beds.

These sequences are well preserved in Core 40 (Fig. 3.4) and are recognised in the river mouth sand facies of Core 21. However, it is likely that reworking of the sediment during fair-weather conditions has partially destroyed the storm beds in the latter core. Given the more distant setting of Core 40 in relation to the shoreline it is suggested that the storm beds are less susceptible to reworking, and given the high sedimentation rates (described in Chapter 8) are better preserved.

3.6 ^{14}C CHRONOLOGY

Various shell and wood samples were submitted for radiocarbon dating at the University of Waikato to enhance the understanding of the late Holocene sedimentation history (discussed in Chapter 8). Table 3.1 is a list of radiocarbon ages for samples from the master cores and Core 33 and shows that sediments represented in the dated cores are all younger 5000 y B.P. The use of wood material for dating proved problematic and consequently shell material was preferred wherever possible. Wood from some species may remain intact in the surface of bogs or stream catchments for many years before becoming entrained by fluvial processes during flood events (Butler and Stein 1988). This may be of particular significance in New Zealand with it's generally long-living indigenous trees. The problem is further compounded if fluvial activity entrains previously buried or long-dead wood. Appendix 1 (Core 37) and Table 3.1 show an age inversion for dates on wood. Wk 1284 (stratigraphically lower in the core) appears to be yonger than Wk 1283. A second date on shell (Wk 1666) taken from just below Wk 1284

yielded a more reliable date. The bivalve *Austrovenus stutchburyi* was preferred for dating as it is not a burrower. In it's absence *Mactra* sp. were used. Of these, the smaller *M. ordinaria* was preferred as *M. ovata ovata* is known to burrow down to 20 cm depth (Morton and Miller 1972), thus producing a younger apparent age. The more weakly developed palial sinus of *M. ordinaria* suggests it does not burrow as extensively as M. *ovata ovata*.

Table 5.1
Radiocarbon dating results. Wk No. refers to the University of Waikato radiocarbon dating laboratory number. Dates have been "reservoir corrected" (330 years subtracted for New Zealand carbonates).

Wk No.	Type of material	Sample site	Conv. age (y B.P)
1280	*A. stutchburyi*	Core 31, 4.6 m	2370 ± 80
1281	*M. ordinaria*	Core 33, 2.4 m	3370 ± 110
1282	*Mactra sp.*	Core 37, 0m	> Modern
1283	Wood	Core 37, 0.23m	1750 ± 90
1284	Wood	Core 37, 1.0 m	540 ± 115
1285	*A. stutchburyi*	Core 37, 3.2 m	4960 ± 54
1447	*M. ordinaria*	Core 40, 1.3 m	2590 ± 100
1448	*A. stutchburyi*	Core 40, 5.0 m	4260± 28
1663	*M. ordinaria*	Core 21, 2.0 m	3580 ± 170
1664	*A. stutchburyi*	Core 21, 1.0 m	1170 ± 90
1665	*A. stutchburyi*	Core 21, 0.2 m	730 ± 70
1666	*M. ordinaria*	Core 37, 1.1 m	2740 ± 90

The major applications of radiocarbon dating to this study are: 1) the calculation of sediment accumulation rates (Chapter 8);-2) to provide age data for Core 31 so that the kinetics of smectite formation and consequently glass dissolution can be quantified (Chapter 7); and 3) to establish a chronolgy for the core sediments.

Plate 3.2

Damage on the Te Puru delta fan following Cyclone Bola (May 1988). Note the large clast sizes of material capable of being delivered to shoreline under such conditions.

3.7 DISCUSSION

In summary, the core stratigraphy described in this chapter exhibits a complex sequence of skeletal carbonate shell layers interbedded in a broad expansive terrigenous mud unit of late Holocene age, termed the Firth of Thames mud facies. Greig (1982) makes reference to this facies in a study of the Hauraki Gulf sediments. He suggests that the facies is a Holocene feature that has been rapidly accumulating since sea level stabilised at 6500 y B.P at the culmination of the Holocene post-glacial transgression (Gibb 1986). Radiocarbon dates support this contention (see Chap. 8)

From the nearshore cores local facies adjacent to the the present Waihou River mouth and delta fans along the fault bounded eastern boundary of the Firth of Thames are also recognised. The distribution of the facies has been controlled largely by lateral migration of the mouths of rivers draining the Hauraki Lowland during the late Holocene, and it's modern day extent covers southeastern Firth of Thames adjacent to the Waihou and Piako Rivers. A radiocarbon date of 1500 y B.P near the base of the river mouth sand facies in Core 21, but above mud sediments typical of the of the Firth of Thames mud facies, suggests that the influence of the Waihou River on sedimentation was less significant prior to 1500 y B.P and may suggest that the shoreline has been prograding northwards over the late Holocene.

The delta fan gravel facies is localised to the Coromandel Range coastline and occurs as a series of discrete low-angle submarine fans. The interlayering of coarse and fine sediments of the delta fan facies is considered to be due to large pulses of sediment delivered periodically during storms to the fans. Plate 3.2 illustrates the rapid increase in discharge and erosive power that these otherwise low-flow streams that form the fans are capable of producing during storm events, thus forming characteristic, poorly sorted gravelly sand and gravel deposits in the offshore sediments.

-CHAPTER FOUR-

SEDIMENT TEXTURE

CHAPTER FOUR: SEDIMENT TEXTURE

4.1 INTRODUCTION

A qualitative assessment of sediment texture undertaken during the initial logging of cores indicated that the majority of sediments are fine-grained with sporadically interbedded with coarser skeletal carbonate layers. In the previous chapter, three lithofacies were described from the core sediments which are considered to have been deposited in environments similar to that of the modern setting.

The method of sediment grainsize analysis used in this study is outlined in Appendix 5. In effect the grainsize analysis involved seperation of the sediment into gravel (> 2mm), sand (2mm-63μm), silt (63μm-4μm) and clay (<4 μm) fractions for the five master cores and for all surficial core samples and a selected number of other cores spaced evenly over the study area. Results have been tabulated and are presented in Appendix 2. Sediment grainsize parameters were not attempted in this study largely because of the lack of sand and consequntly the dominance of mud. A detailed sediment grainsize analysis was not within the scope of this study, however van Leewue (in prep) presents a more comprehensive grainsize analysis as part of an investigation into transportation of mud sediments of the Firth of Thames.

The aim of this chapter is to present results of a sediment grain size analysis and to relate down-core and lateral variations in texture to the lithofacies already described. Some inferrences are also made about late Holocene sedimentation of the southern Firth of Thames.

4.2 TERNARY TEXTURE PLOTS

Textural results are plotted on a ternary diagram in Figure 4.1A (after Folk et al. 1970). Three lithofacies are clearly delineated on the basis of their grainsize distribution and are classified by the

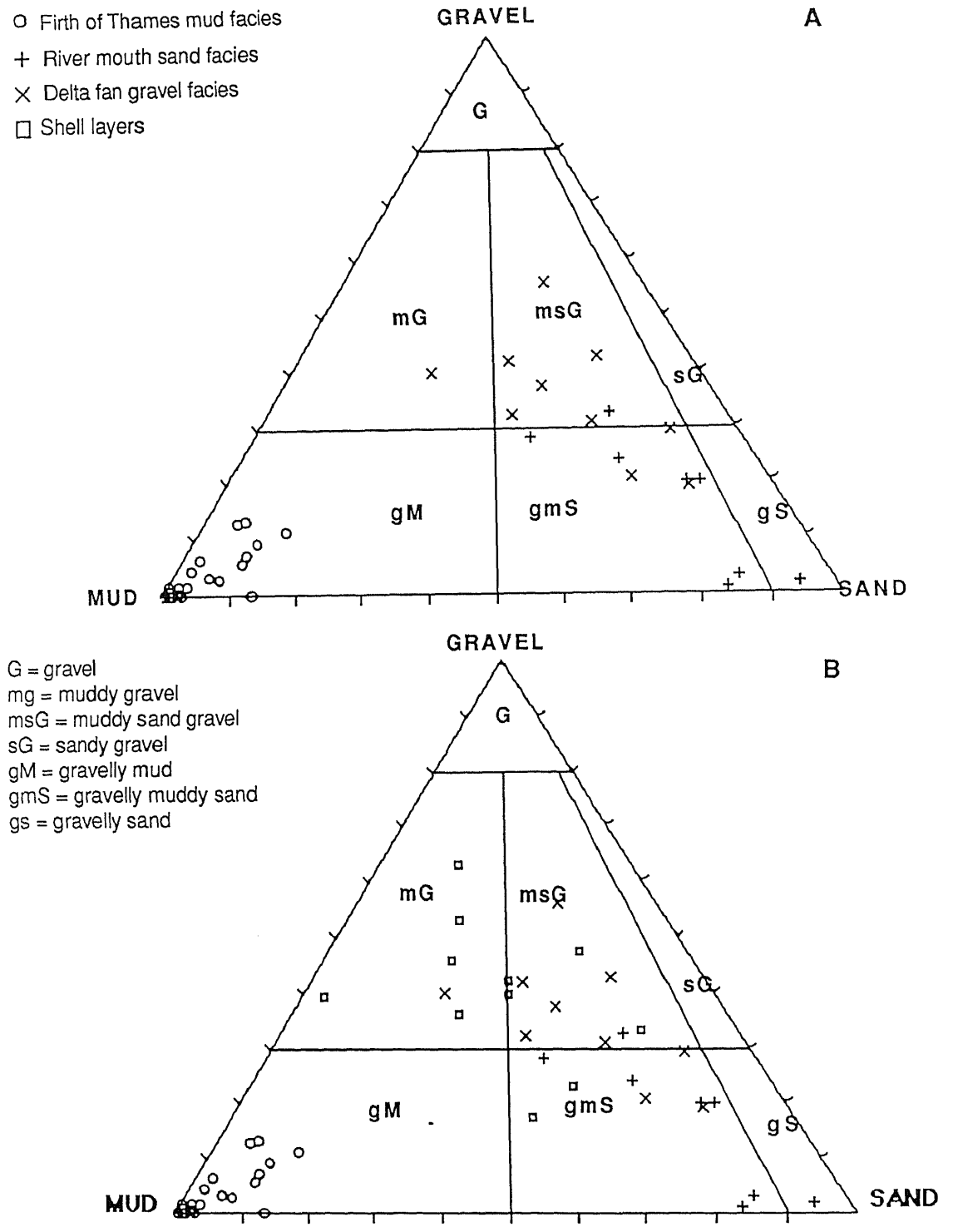

Figure 4.1

Classification of texture for core sediments of the Firth of Thames (after Folk et al. 1970). In A) the discrimination of lithofacies on the basis of sediment texture is shown. In B) shell layers from within the Firth of Thames mud facies are added .

following textural classes: (i) *mud, gravelly mud and sandy mud (Firth of Thames mud facies); (2) sand, muddy sand, gravelly muddy sand (river mouth sand facies); (iii) muddy sandy gravel and sandy gravel (delta fan gravel facies). In Table 3.1 the textural properties of the three lithofacies are summarised.

The coarseness of shell fragments in the mixed terrigenous-skeletal carbonate sediments of the Firth of Thames may not necessarliy relate to the hydrodynamic conditions of the depositional environment. Nelson (1977) notes that this is due to the wide variations in size of hydraulically equivalent skeletal carbonate grains and suggests that grainsize parametres derived from the acid-insoluble residue following acid digestion of carbonate sediments are more valid for making hydrodynamic interpretations. In the previous chapter, shell hash layers were shown to imply significant sediment reworking and hence a relatively high energy wave climate, and were probably deposited during episodic storm events. However, hydraulically equivalent intact shell beds also occur within mud sediments and these are suggested to be in situ, implying little or no post-mortem mixing or transportation. In Figure 4.1B shell layers that occur within the Firth of Thames mud facies plot in the same muddy sand to muddy gravel fields as the river mouth and delta fan facies.

Table 3.1
Textural characteristics of the sediments.

Lithofacies type	Sediment texture	Carbonate (%)
Firth of Thames facies	mud to gravelly mud	0-10
River mouth facies	sand to gravelly muddy sand	0-60
Delta fan facies	muddy gravel to muddy sandy gravel	0-60
In situ shell layers	muddy gravel	50-90
Storm shell hash layers	gravelly muddy sand to muddy sandy gravel	50-75

* the dominant textural class of each lithofacies is underlined.

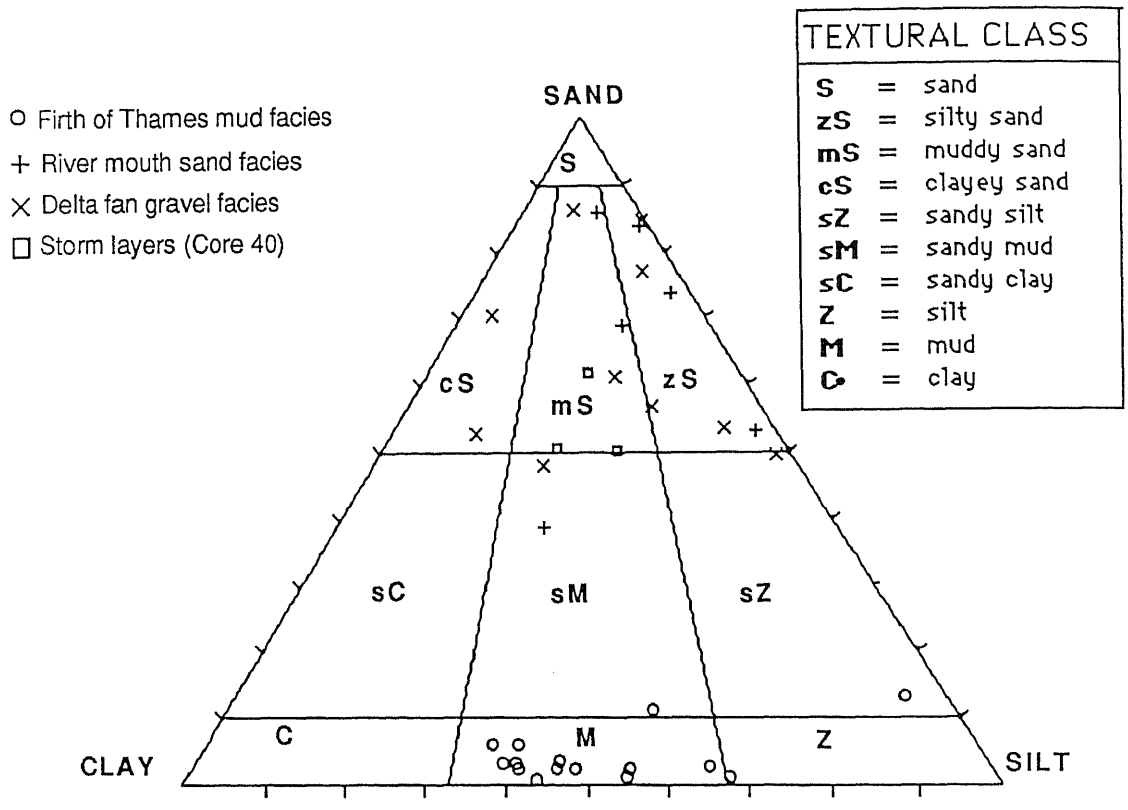

Figure 4.2

Carbonate-free textural classification of core sediments from the Firth of Thames (after Folk et al. 1970). Samples are plotted on a sand-silt-clay ternary diagram as there was no gravel component in the acid-insoluble residue.

Given the above considerations a carbonate-free textural analysis was performed on alternate samples (i.e. every second sample down-core, at 40 cm intervals) for all master cores. Calcium carbonate was dissolved from the > 63 µm fraction with 4.4 M acetic acid and the weight percente abundance of sand, silt and clay determined and tabulated in Appendix 2. Grainsizes of the acid-insoluble residues were less than 2 mm with the exception of two samples from Core 23 adjacent to Tapu. Thus the gravel component of the bulk sediment is entirely composed of calcium carbonate. In Figure 4.2 carbonate-free textural data are plotted on a sand-silt-clay ternary diagram. The ratio of silt:clay for mud facies samples is approximately 1. Sediments from delta fan and river mouth facies plot in a similar field to one another, although the river mouth sediments tend to be characterised by a higher silt component. Shell layer samples from the Firth of Thames mud facies that classified as muddy gravels in Figure 4.1B generally plotted in the mud field of Figure 4.2 after acid digestion. The exceptions are three shell layers from Core 40 (Figure 3.4), which have a muddy sand texture and are interpreted as storm beds with a mixed terrigenous-skeletal carbonate composition. This is possibly an important method for recognising mixed terrigenous-skeletal carbonate layers as storm layers.

4.3 LATERAL VARIATIONS IN SEDIMENT TEXTURE

The areal variations of texture in the surficial sediments of the southern Firth of Thames are related to a number of factors. In particular, the influence of the Waihou River and streams draining the Coromandel and Hunua Ranges, the occurence of modern accumulations of bivalves, and the influence tidal and wave/wind-generated currents. In Figure 4.3 a texture map of the surficial sediments is presented. This map enhances the accuracy of a sediment map produced for the Hauraki Gulf by Carter and Eade (1980) in the eastern Firth of Thames and relies on some of it's information for the far western region where samples were lacking. Surficial sediments range from muds to gravels. Muddy sands to sands occur adjacent to the Waihou River mouth and are recognised as the modern expression of the river mouth facies. Muddy sands to muddy sandy gravels of the delta fan facies occur adjacent to the delta fans of the Coromandel and Hunua Ranges. Variations in texture of this facies occur northwards.

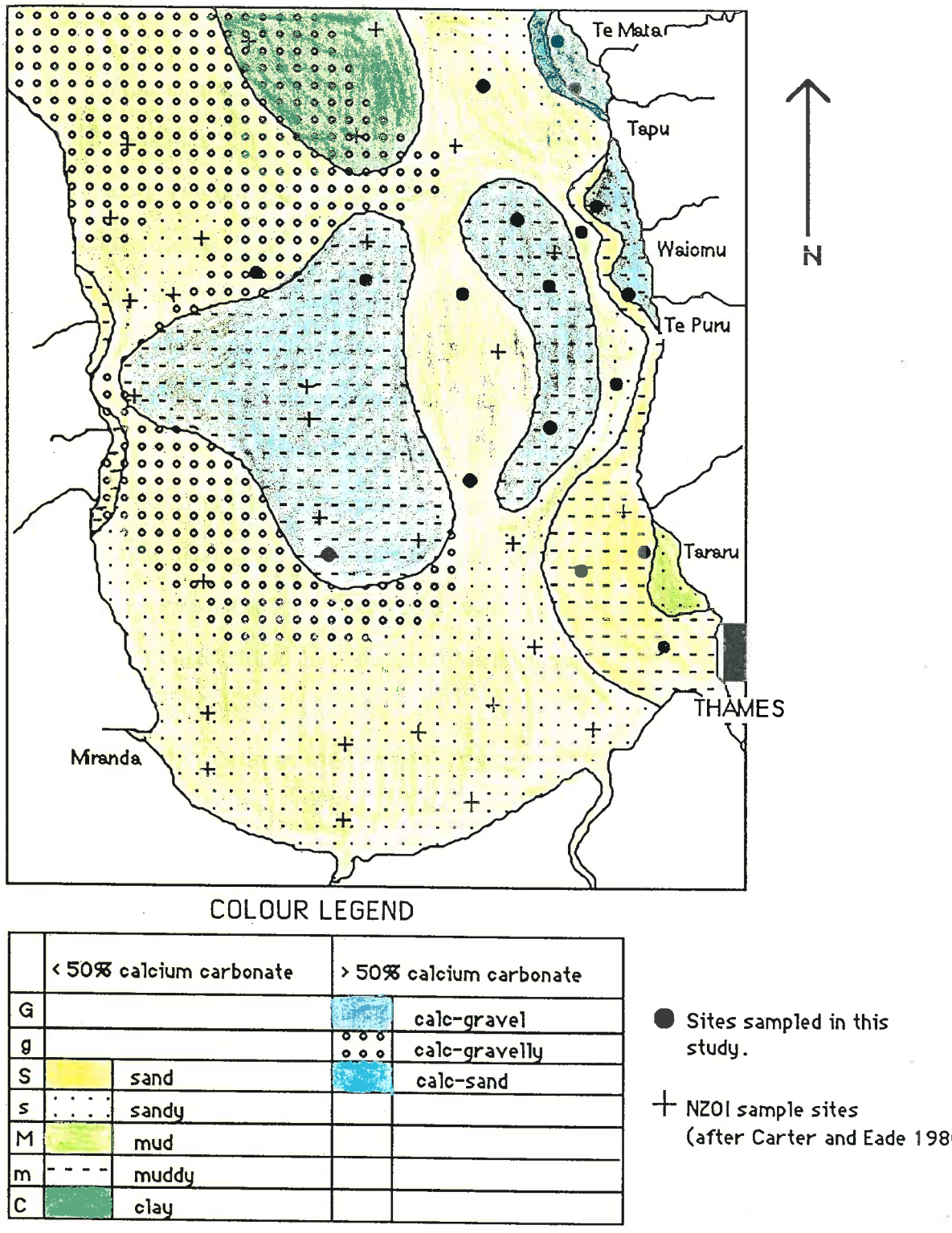

Figure 4.3

Surficial sediment texture map of the southern Firth of Thames. Samples from this study received a full textural analysis. NZOI data were used to supplement data from this study. It should be noted that most NZOI sediment texture data for the Firth of Thames are from visual determination of small samples or British Admiralty sediment notations. Textural classes were determined from ternary diagrams after Folk et al. (1970) as in Figures 4.1 and 4.2.

The delta fan gravel facies at Te Puru and Waiomu is dominated by muddy sands and some carbonate gravels, whereas at Te Mata and Tapu it consists predominantly of sandy gravels. The northwards coarsening in texture (Fig. 3.5) reflects an increased exposure to a relatively higher energy wave climate and an increased supply of coarse sediments from the Tapu River which has a higher discharge than other streams draining the Coromandel Range (Dravitzki 1988). However, coarser sediments are generally localised to the nearshore region adjacent to the mouths of streams and rivers. The majority of the Firth of Thames sediments are mud-dominated forming the far more laterally expansive Firth of Thames mud facies. Calc-gravels occur either as modern in situ shell beds or as carbonate lag deposits. The latter correspond to regions where high tidal velocites are inferred (Bowman and Chsiwell 1982) along the western boundary of the Firth during the flood tide and along the eastern boundary during the ebb tide. A carbonate bank in the central southern Firth of Thames has a predominantly muddy gravel texture and results from the presence of in situ living shell fish beds.

4.4 VERTICAL VARIATIONS IN SEDIMENT TEXTURE

Down-core profiles illustrating variations in sediment texture with depth were constructed for the master cores and are presented in Appendices 1 and 2. In general a coarsening upwards in grainsize of the acid-insoluble residue occurs in all cores. This trend is most pronounced in nearshore cores (Cores 21 and 37) and can be recognised by a significant increase in sand content up core (Figure 4.4) and may be more subtly recognised offshore in Core 31 by an up-core increase in the silt:clay ratio. However, in the latter case it is possible that variations in sediment texture result from diagenetic processes discussed in Chapter 7.

The progressive upward increase in grainsize of the acid-insoluble residue illustated in Figure 4.4 for Core 21 is considered to reflect (i) the hydrodynamic conditions of the depositional environment and/or (ii) the proximity of source. A useful textural classification for mud-dominated sediments is outlined by Pejrup (1988) and is an alternative scheme to that proposed by Folk et al (1970; Fig. 4.2). It relates the hydrodynamic conditions of the depositional environment to the percent of sand,silt and clay

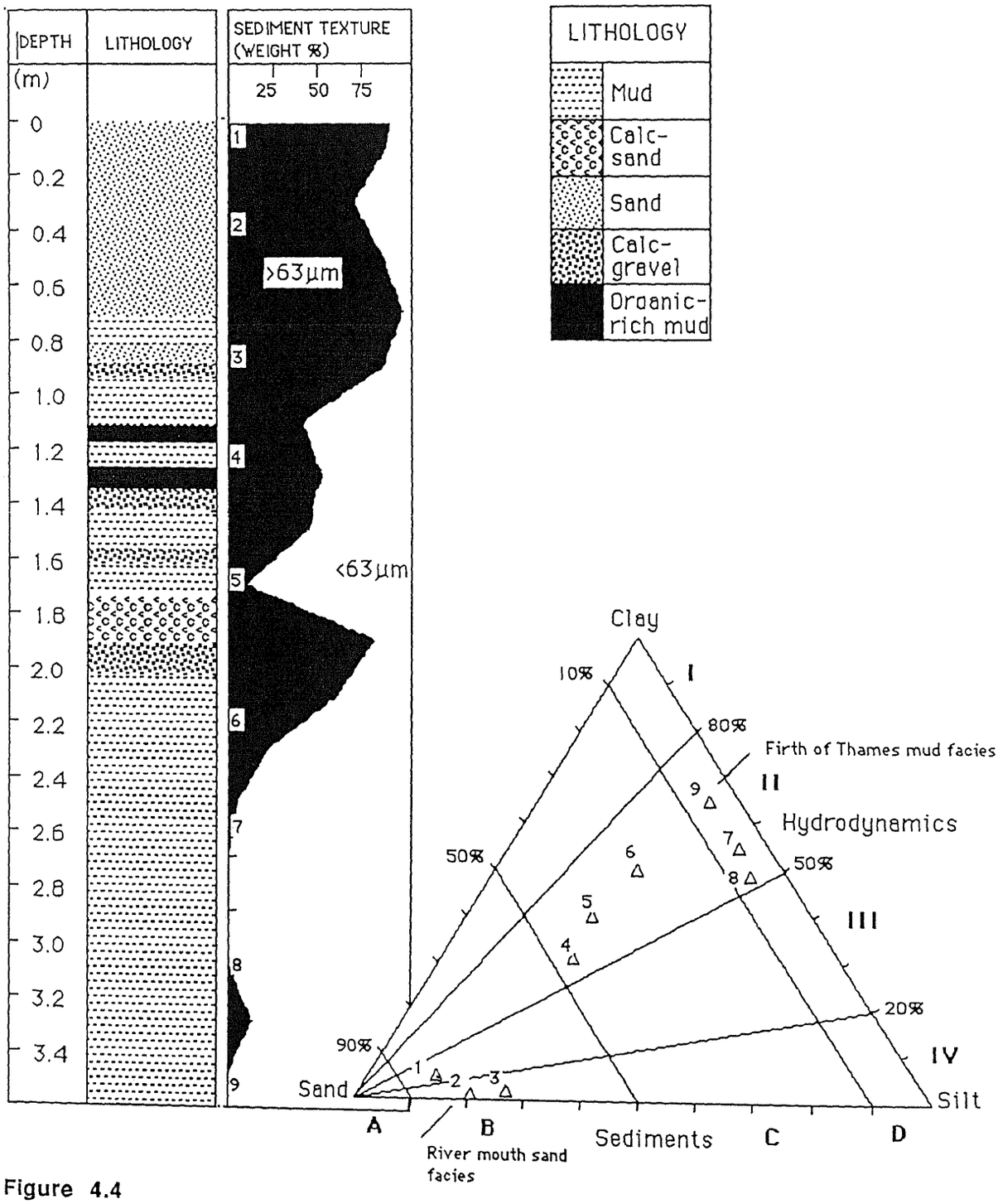

Figure 4.4

Core 21 exhibits a coarsening up-core in sediment texture. Basal core sediments belong to the Firth of Thames mud facies and grade upwards into the coarser River mouth sand facies deposited in shallower, higher energy conditions and in close proximity to the shoreline and Waihou River mouth. The ternary plot is a variation on that of Folk et al. (1970), and is after Pejrup (1988). For muddy sediments the degree of clay is considered to be related to the hydrodynamic setting of the depositional environment. Hence fields I-IV represent an increase in energy of the depositional environment. The sand content is related to the factor of supply and may be an indication of the proximity of source (i.e. Waihou River mouth; A=near source, D=distal from source). For Core 31 the acid-insoluble residue are plotted on the "Pejrup diagram" and reveals a coarsening up-core trend from muds deposited under relatively calm hydrodynamic conditions (D,II) to sands deposited under higher energy conditions closer to source (B,IV).

in the acid-insoluble residue (Figure 4.4). Samples 1,2 and 3 of the river mouth facies from Core 21, are predominantly muddy sands (Folk et al. 1970) and plot in a field on the Pejrup (1988) diagram charcterised by >70% sand content implying a relatively higher energy setting than samples 4, 5,6,7,8 and 9, which progressively decrease in grainsize from sandy mud to muds and plot in a field characterised by < 50% sand and relatively calm hydrodynamic conditions. The up-core textural trends suggest a gradual shallowing of the Firth of Thames has occurred during the late Holocene, possibly associated with northwards progradation of ther southern shoreline. Other faunal and compositional evidence supports this premise, as synthesised in a discussion of the late Holocene sedimentation for the southern history for the southern Firth of Thames, in Chapter 8.

The sediments of Core 40 are classified as mud to muddy sandy gravel. Samples exhibiting muddy gravel to muddy sandy gravel textures all correspond to shell layers and are interbedded within predominantly mud sediments of the Firth of Thames facies (Appendix 2). Muddy gravel shell layers are generally in situ, whereas muddy sandy gravel shell hash layers are associated with graded storm bed sequences. These storm layers are best preserved in Core 40 which is situated far enough offshore not to be affected by nearshore wave processes under fair-weather wave conditions. However, during large storm events gravel-sized terrigenous-skeletal carbonate material is transported offshore and, under waning storm conditions, deposited as storm beds. Also offshore carbonate sediments may be reworked. Subsequently, during fair-weather conditions, these layers remain undisturbed and are quickly preserved by continued mud deposition. The lack of storm beds and shell hash layers in the lower portion of Core 40 (below 2 m sub-bottom depth) seems to indicate a deeper setting in the past, more distal from the shoreline, perhaps similar to the present day position of Core 31 where no storm layers are evident.

Cores 37 and 23 represent muddy sandy gravels of the Delta fan facies. Down core textural variation plots in Appendix 2 exhibit a complex interlayering of muds and gravels. The coarser layers represent the offshore manifestation of large pulses of poorly sorted angular material brought down out of the Coromandel Range and delivered to the delta fans during storms, whereas the mud layers

represent deposition under fair-weather conditions.

-CHAPTER FIVE-

SEDIMENT MINERALOGY

CHAPTER FIVE: SEDIMENT MINERALOGY

5.1 INTRODUCTION

The principal aims of this chapter are to determine the mineralogical composition of the core sediments and to quantify the mineralogy of the individual clay, silt and sand fractions in Core 31. The surficial sediments from cores 4, 6, 8, 10, 21, 26, 31, 32, 33, 34, 37, 40 and 41, and samples from the Waihou, Piako, Ohinemuri, and Waitoa Rivers have been selected for detailed bulk quantitative compositional anaysis (see Fig. 3.1). Core 31 was used for high-resolution down-core compositional analysis (sampled every 20 cm) because it is the longest continuous core recovered from the late Holocene mud facies infilling the Firth of Thames (see Chapter 3).

In this chapter the application and limitations of standard techniques such as XRD, DTA and IR for analysis of mineral phases are discussed and the quantitative procedures used are outlined. Results are presented of the lateral and vertical distribution of mineral components in cores. These, along with results from Chapters 4 and 5, are interpreted with a view to identifying processes of sediment diagenesis discussed in Chapter 7, and are used to develop a model of late Holocene sedimentation in the Firth of Thames presented in Chapter 8.

5.2 CLAY MINERALOGY

X-Ray Diffraction Analysis

XRD analysis of clay minerals was carried out following the procedure outlined in Appendix 5 (Methodology). Samples of the < 2 μm fraction from Core 31 and surficial samples were run from 3° -35°O with some slow scans (0.05° 2Θ min^{-1}) over the 3°-14° 2Θ region to allow more accurate determination of the clay mineral peak positions. Samples from other cores were scanned in the 3° to

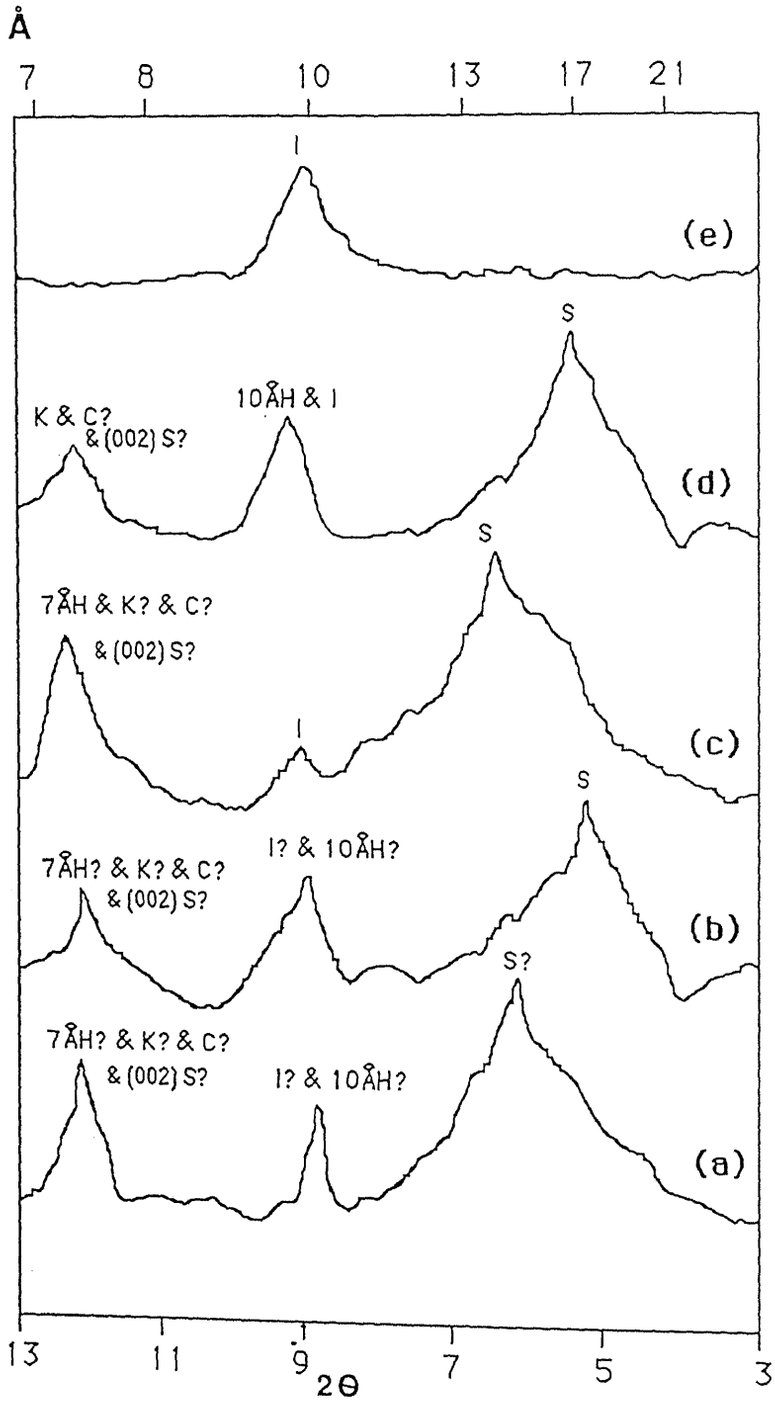

Figure 5.1

X-ray diffractogram of the < 2 μm fraction (sample 31.17) following various treatments. a) An untreated sample. b) After vapour solvation in ethylene glycol. c) Heating to 110 °C. d) Formamide treatment of an untreated specimen. e) Heating to 550 °C (Treatments discussed in text and Appendix 5). C=chlorite,I=illite, K=kaolinite, H=halloysite, S=smectite.

14° 2Θ region only for more qualitative assessment of the clay mineralogy. Clay minerals are distinguished by their characteristic basal (001) reflection after various pretreatments outlined in Appendix 5 (Fig. A5.1).

Results show little variation in the clay mineralogy between samples. Major basal (001) reflections occur at 14.6, 9.9, and 7.2Å (Fig. 5.1). A broad basal reflection from 12-15Å which expands to 17Å after the sample is vapour solvated with ethylene glycol, and collapses to 10Å after heating to 500°C, is positively identified as smectite. Higher order basal reflections are extremely weak, probably the result of small grainsize and turbostratic structure, caused by random stacking of the clay plates. This disordered structural arrangement gives rise to an 001 peak and a series of low-intensity asymmetric two-dimensional hk-diffraction bands commonly found in smectites (Brindley and Brown 1980, p171).

Basal 001 reflections at 7.2 and 9.9Å appear to be interrelated. Heating to 110°C caused a reduction in size of the 9.9Å peak and a subsequent increase in magnitude of the 7.2Å which indicates the presence of 10Å hydrated halloysite (Fig. 5.1). Conversely a decrease in the 7Å peak following formamide treatment of an untreated sample and a subsequent increase in the 10Å peak indicates the presence of 7Å halloysite. In both cases residual peaks remained at 10Å after dehydration of halloysite by heating and at 7Å following formamide intercalation. Heating of formamide treated samples at 550° C for 1 h resulted in collapse of the residual 7Å peak, suggesting minor kaolinite rather than chlorite. The residual 10Å peak increased in magnitude after heating to 550° C due to collapse of the 17Å smectite peak superimposed on naturally occurring illite (Fig. 5.1).

According to Hume and Nelson (1982) chlorite is an important component of many clay mineral suites in the South Auckland region sediments and often occurs as a mixed-layer clay. In the Firth of Thames chlorite is expected along with illite and kaolinite in clay mineral assemblages of sediments derived from greywacke source rocks in the northeast and along the western margin. However the identification of chlorite may be problematic because of the low intensity of the 14Å peak. Masking of the chlorite 002 basal reflection can occur particularly if kaolinite and chlorite are both present together.

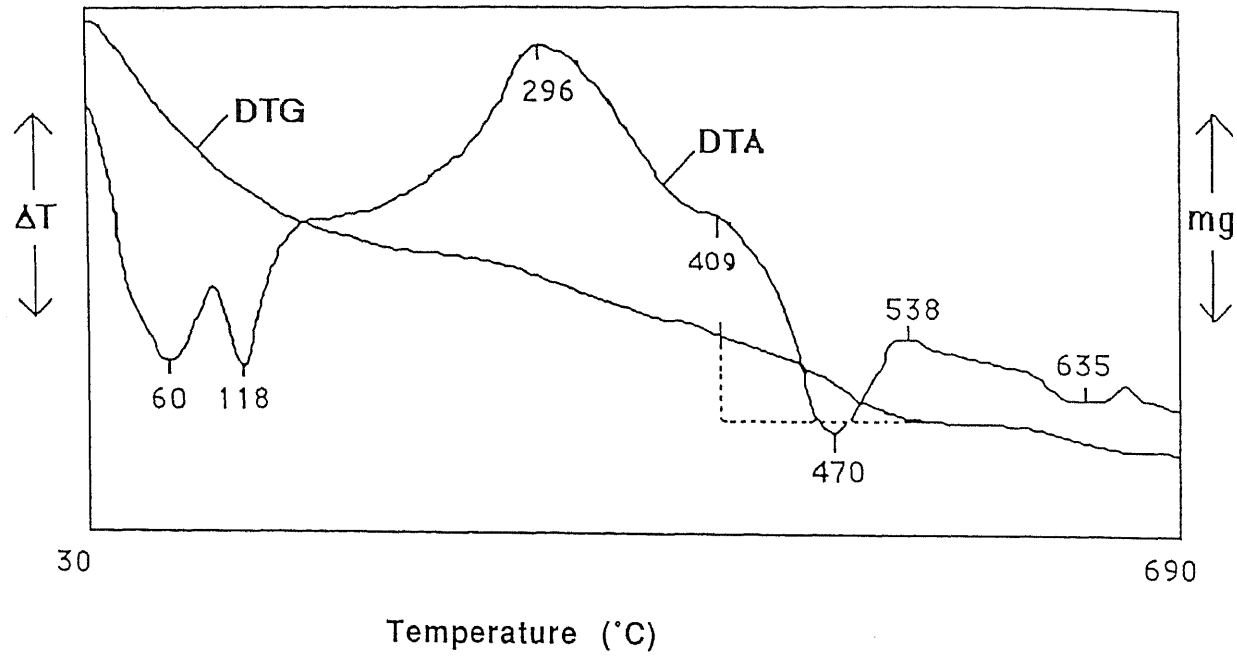

Figure 5.2

DTA and DGA traces from differential thermogravimetric analysis of the < 2 μm fraction (sample 31.9). The 470 °C endotherm = halloysite; 118 °C endotherm = halloysite (+ allophane). The slope of the DGA line corresponding to the 470 °C endotherm for halloysite is compared to the slope of a 100% standard and wt% halloysite is calculated by a computer program.

The presence of heat-laible chlorite species whose basal peaks collapse on heating as low as 350°C is a further problem encountered when heating the sample to 550°C as a test for chlorite.

From XRD analysis of the clay fraction, smectite is the dominant clay mineral. Significant amounts of both 10Å and 7Å halloysite, indicated by peak intensities, are also present, along with subordinate kaolinite and illite. Chlorite may also be present.

Differential Thermogravimetric Analysis

The primary use of differential thermogravimetric analysis (DTG) in this study was to determine quantitatively the abundance of halloysite, as discussed in Section 5.5. However DTG is also a useful technique for identifying the presence of short-range order constituents, as it is applicable irrespective of crystallinity. It is used here to identify allophane. The method of analysis used is outlined in MacKenzie (1970) and Lowe and Nelson (1982), and is summarised in Appendix 5.

DTG thermograms for most samples (Fig. 5.2) were similar, exhibiting a low-temperature endotherm at 100-120°C and a higher-temperature endotherm at approximately 500°C. In some samples an endotherm at approximately 60°C was also present and is considered to reflect the varying humidities of the samples. Although low-T endotherms due to moisture could have been avoided by equilibrating all samples to a constant humidity following the procedures outlined in Lowe and Nelson (1983), this was not considered necessary as only the 500°C endotherm is used for quantitative analysis.

In Figure 5.2 a low-T dehydration endotherm at 118°C is attributed to the presence of allophane. However some ambiguity exists as water absorbed on most clay-sized minerals (i.e. halloysite) and organic matter will contribute to the magnitude of this peak. Therefore, although the presence of allophane is implied, unequivocal recognition was not possible using this technique. In the next section allophane is identified by infrared absorption analysis and quantified by atomic absorption

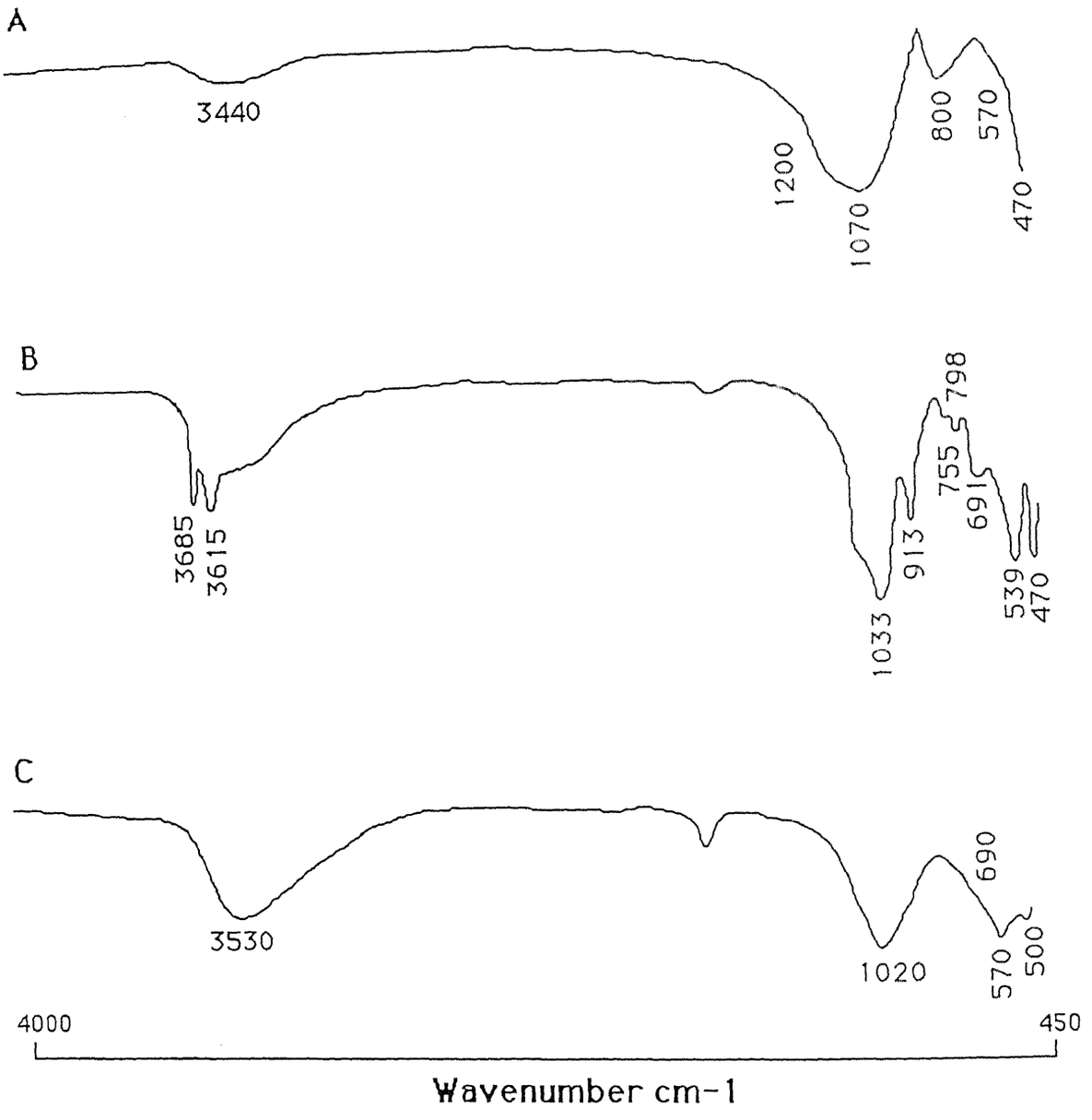

Figure 5.3
Infrared spectra of a) volcanic glass, b) halloysite (wagon wheel halloysite) and c) allophane (proto-imogolite).

spectroscopy following ammonium oxalate-extraction of Si and Al (see section 5.5).

Halloysite is identified by a weak to strong dehydroxylation endothermic peak at about 500°C (MacKenzie 1970; Fig. 5.2). Dehydroxylation of kaolinite also occurs at the same temperature so that halloysite abundances determined by this method include kaolinite, although from XRD analysis the latter appears to be subordinate to halloysite. A small endotherm or shoulder at 409°C may reflect the presence of minor imogolite (Yoshinga 1977), and an endothermic peak at 635° C could be due to crystalline silica phase changes (MacKenzie 1970).

Infrared Absorption Analysis

Infrared absorption spectroscopy (IR), like DTA, is a useful technique for the identification of X-ray amorphous minerals such as allophane, and is also used to identify volcanic glass. Quantitative estimations of the latter are discussed in Section 5.5. The theory behind IR involves passing a beam of infrared radiation (4000-200 cm^{-1}) through a sample and measuring the amount of absorption. Absorption bands are recorded as spectra corresponding to the vibrational frequencies of bonds between atoms in the clay mineral structure (Pecsok et al. 1976).

According to Parfitt and Hemni (1980) allophane is characterised by diagnostic bands at 3530, 1020, 975, 690, 570, 500, 428 and 348 cm^{-1} (Fig. 5.3A). The position of the main Si-O-Al bond can range from 975-1020 cm^{-1} depending on the Al:Si molar ratio. Al-rich allophanes are identified at 975 cm^{-1} whereas Si-rich allophanes are identified by a shift in the band to 1020 cm^{-1}. The IR spectrum of imogolite exhibits absorption bands at 990-1010 and 925-935 which distinguishes it from allophane.

Volcanic glass has a well defined spectrum (Fig. 5.3B) with main absorption bands at 3490, 1070, 800 and 470 cm^{-1} and shoulders at 1200, 512 and 540 cm^{-1}(van der Marel and Beutelspacher 1976). The length of the diagnostic 800 cm^{-1} band is used for quantifying volcanic glass (Section 5.5).

Halloysite exhibits absorption bands due to OH-stretching vibrations at 3685 and 3615 cm^{-1}. Bands also occur at 1033, 913, 798, 755, 691, 539,470, 429 and 343 cm^{-1} with shoulders at 113, 1014, 937, 780, 367 cm^{-1}; Fig 5.3C (Kirkman 1975; van der Marel and Beutelspacher 1976; Stevens and Vucetich 1986).

Pure montmorillonite (smectite) is characterised in the 3000-4000 cm^{-1} region by OH absorption bands at 3640 and 3620 cm^{-1} due to Al-OH-Mg stretching. A broad band due to Si-O-Al stretching occurs at 1035 cm^{-1} (Furket and Smidt 1972; van der Marel and Beutelspacher1976). Other bands also occur a913, 845, 790, 522, and 468 cm^{-1}(see Fig. 7.7, Chapter 7)

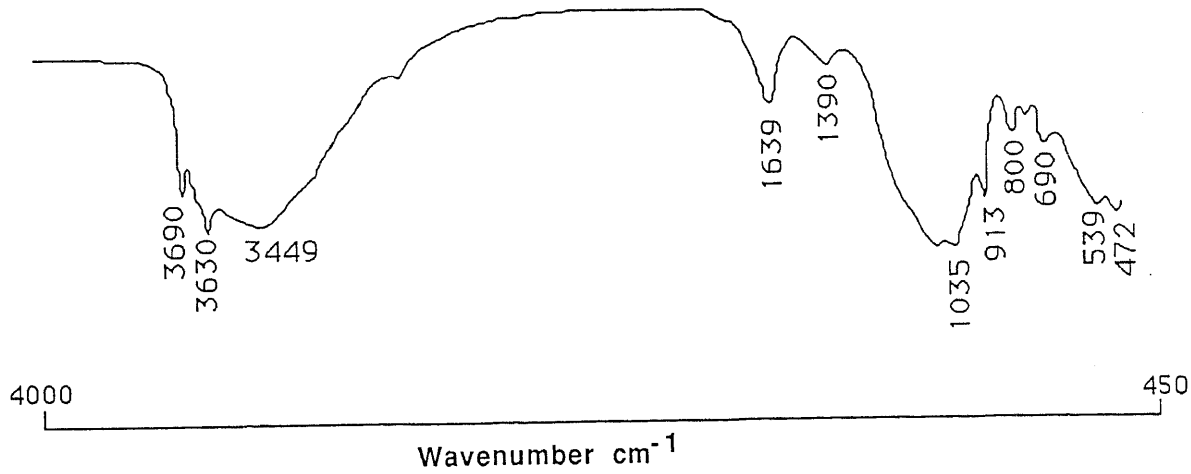

Figure 5.4

Infrared spectrum of < 2 µm fraction (Sample 31.17). Absorption bands are diagnostic of halloysite/smectite > allophane > volcanic glass. See text for details.

Figure 5.4 illustrates a typical IR spectrum for the < 2 μm fraction. Spectra were similar for all samples analysed. The only variation was due to an increased influence of smectite absorption bands in samples progressively deeper down Core 31, making the unequivocal distinction of halloysite difficult due to the overprinting of halloysite absorption bands by similar montmorillonite bands. This is particularly problematic in the 3000-4000 cm^{-1} region where OH-stretching vibrations of various clay minerals, due to structural OH groups or absorbed water (Decarreau et al.1985), may mask each other. Ideally a well defined pair of absorption bands should occur at 3685 and 3615 cm^{-1} for halloysite and at 3640 and 3620 cm^{-1} for montmorillonite. However a band at 3690 cm^{-1} accompanied by a band at 3630 cm^{-1} is observed in most spectra. The broad morphology of the 3630 cm^{-1} band is due to smectite superimposed on halloysite, producing a single broad peak. Stevens and Vucetich (1986) highlight some of the difficulties encountered when interpeting IR spectra containing several different clay species. They note that samples containing only 2% halloysite may exhibit strong halloysite absorption bands masking diagnostic bands of other aluminosilicate minerals.That the 3685 cm^{-1}band in the halloysite OH-doublet is the longer of the two is characteristic of 10Å halloysite. 7Å halloysite exhibits similar sized peaks.

A broad band at 3449 cm^{-1} in Figure 5.4 is similar to that for OH-absorption frequencies in allophanes (3550 cm^{-1}). However this band is rather broad, suggesting that a combination of species may be present, including variable composition allophanes, imogolite, and volcanic glass (3440 cm^{-1}). Absorption at 1639 cm^{-1} is caused by H_2O remaining after heating and possible COO stretching due to humic material.

Absorption at 1035, 913, 539 and 472 cm^{-1} indicates the presence of halloysite. Allophane may also be present and the position of the Si-O-(Al) band at 1035 cm^{-1} (Fig. 5.4) woud be indicative of Si-rich allophane, although the general morphology of the peak suggests that absorption in this region is due to halloysite. However absorption at 1035 cm^{-1} in combination with 690 cm^{-1} is likely to be due

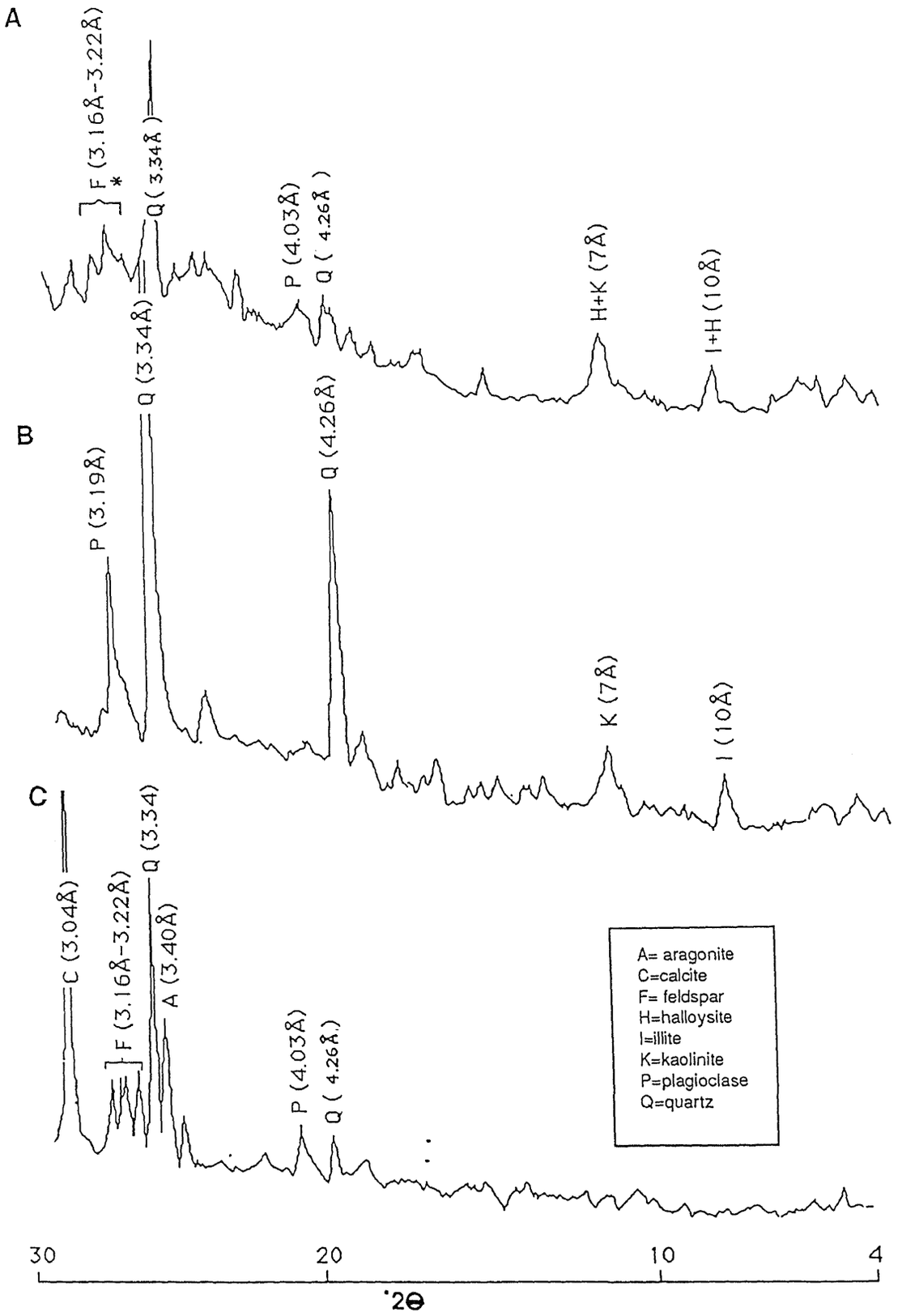

* Multiple peak feldspar (040, 220, 002 peaks between 28.2-27.7 °2Θ). The 040 peak at 27.5 °2Θ masks the 27.5 °2Θ reflection of potash feldspar.

Figure 5.5

X-ray diffractograms of 2-63 μm fraction. a) A sample (37.09) from the Firth of Thames mud facies. Multiple peak plagioclase feldspar in combination with halloysite is consistant with a volcanic source described in the text for this facies. b) Sample (26.03) is from the delta fan gravel facies adjacent to Te Mata. Single peak feldspar and the dominance of kaolinite and illite suggest greywacke derivation for this facies. c) A shell hash layer exhibiting aragonite and calcite peaks.

to Si-rich allophane.

Bands at 3449, 1035 and 470, and a diagnostic band at 800 cm^{-1}, suggest the presence of volcanic glass. From qualitative IR analysis of the clay fraction the dominant clay mineral species in Figure 5.4 (sample 31.17) are smectite/halloysite> glass> Si-rich allophane.

5.3 SILT FRACTION MINERALOGY

X-Ray Diffraction Analysis

Diagnostic peaks of minerals identified are listed in Table 5.1 and representative diffractograms are presented in Fig 5.5. The results from XRD indicate that the constituents of the silt fraction are relatively similar for all samples analysed. Variation in peak height intensity of mineral species (relative abundance) occur locally. In particular, samples from cores taken near the delta fans of Tapu and Te Mata exhibit illite and minor kaolinite as the only clays in the silt fraction (Fig. 5.5B). Elsewhere halloysite and minor illite are the dominant clay minerals in the silt fraction (Fig. 5.5A). Variations in plagioclase composition are also indicated for sediments proximal to to the northern delta fans with respect to sediments from the mud-dominated Firth of Thames facies. Samples exhibit multiple feldspar peaks at 27.8° 2Θ, 28.0° 2Θ, 28.5° 2Θ (Fig. 5.5A). However samples proximal to Te Mata and Tapu delta fans exhibit a single peak at 28.0° 2Θ (Fig. 5.5B). Symes and Wells (1973) suggest that multiple peaks are common in acidic feldspars derived from andesites or rhyolites (Fig. 5.5A), whereas diffractograms exhibiting single peaks (Fig. 5.5B) represent feldspars derived from greywackes. Correlation of X-ray peak reflections for plagioclases with optical identification of feldspar composition for South Auckland sediments by Hume and Nelson (1982) indicates that feldspar characterised by an 002 basal reflection and corresponding to 28° 2Θ is oligoclase-andesine in composition. Feldspar characterised by a 040 basal reflection and corresponding to 27.8° 2Θ is andesine-labradorite in composition. The occurrence of single peak feldspar (28.0° 2Θ) adjacent to Tapu and Te Mata reflects a change in onland geology from Coromandel Group andesite to Mania Hill Group basement greywacke. The multiple peak plagioclase feldspars and

potash feldspar (27.5° 2Θ) exhibited in the majority of diffractograms reflects an andesite-rhyolite volcanic component to the sediments (Fig. 5.2B). Potash feldspar (orthoclase) is generally poorly resolved in diffractograms as the major K-feldspar peak at 26.95° 2Θ is obscured by the strong 101 reflection from quartz at 26.6° 2Θ. However minor K-feldspar was recognised in many samples.

Table 5.1
Diagnostic mineral peaks from silt diffractograms.

	dÅ	°2Θ	hkl
Plagioclase	3.16-3.22	28.2-27.7	040, 220, 002
	4.03	22.05	201
	6.38	13.96	001,020
Quartz	4.26	20.85	100
	3.34	26.65	101
K-Feldspar	3.24	27.50	220
Calcite	3.04	29.50	104
Aragonite	3.24	26.20	311

Diffractograms of samples from shell hash layers exhibit a pronounced calcite peak at 29.4° 2Θ and an aragonite peak at 26.2° 2Θ (Fig 5.2C). The occurrence of both calcite and aragonite is due to aragonitic bivalve detritus and calcitic foram tests and ostracod carapaces in skeletal carbonate layers. The occurrence of carbonate in the mud fraction is due to physical breakdown of skeletal carbonate material in shell hash layers.

In most samples a broad elevation of background between 17° and 30° 2Θ together with diminished intensity of all diffraction peaks indicates the presence of short-range order constituents. Subsequent

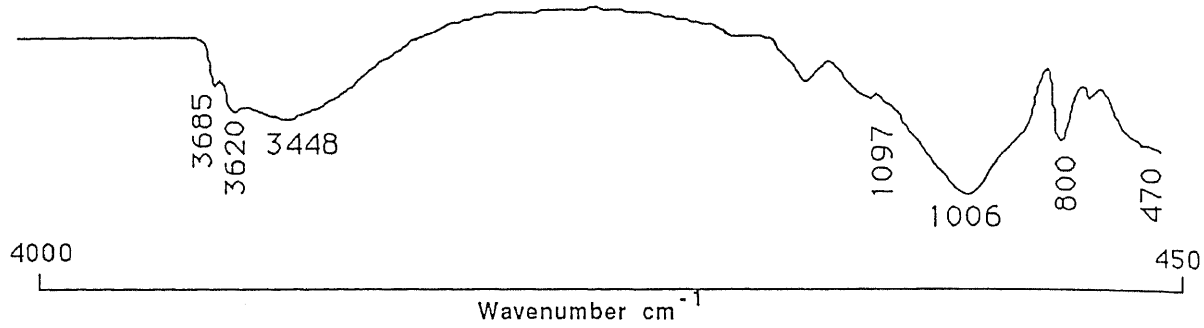

Figure 5.6

Infrared spectrum of the 2-63 µm fraction (sample 31.07). Major absorption bands characteristic of volcanic glass occur at 3448, 1006, 800 and 470 cm-1.

SEM analysis of the silt fraction reveals substantial amounts of X-ray amorphous volcanic glass.

Differential Gravimetric Analysis

Halloysite and/or kaolinite were identified in the 2-63 μm size range by a characteristic 500°C dehydroxylation endotherm. A low-T endotherm at 110°C was attributed to silt-sized allophane. DTG was used primarily to quantify halloysite and kaolinite in the silt fraction and is discussed in Section 5.5.

Infrared Absorption Analysis

Figure 5.6 illustrates the characteristic IR spectra obtained on silt samples. Major features include a broad OH-absorption band at 3448 cm^{-1}, similar to that of volcanic glass and allopohane. A weakly developed hydroxyl absorption doublet characteristic of smectite/halloysite occurs at 3685 and 3620 cm^{-1}. The main Si-O-(Al) absorption band is characterised by a broad band at 1066 cm^{-1}, similar to that of Si-rich allophane, volcanic glass and halloysite/smectite. A shoulder at 1097 cm^{-1} is also characteristic of Si-rich allophane. The most pronounced absorption bands occur at 3448, 1006, 800 and 470 cm^{-1} and are identical to that of pure volcanic glass (Fig. 5.6). In general, silt IR spectra are typified by volcanic glass with subodinate Si-rich allophane identified by bands at 3448, 1066, 694 and a shoulder at 1098 cm-1, and halloysite identified by bands at 3685, 3615, 1066 and a shoulder at 913 cm^{-1}.

5.4 SAND MINERALOGY

Three main mineral components, identified by optical microscope analysis, make up the sand fraction. They are: i) volcanic glass in the form of vesiculated pumice fragments and angular conchoidially fractured shards; ii) skeletal calcium carbonate in the form of shell and foram detritus and iii) other siliciclastic detritus - rock fragments of rhyolite, andestite and greywacke and quartz and feldspar.

Some clay/mud aggregates occur as well. Most terrigenous sand-size material is confined to regions proximal to river mouths and the delta fans. Core sediments from the Firth of Thames mud facies are genarally 90% by weight mud.

5.5 QUANTITATIVE ESTIMATION OF SEDIMENT COMPOSITION

The total composition of the bulk sediment is calculated for the surficial samples and samples from Core 31 by assuming 100% by weight = [wt%smectite + wt%halloysite + wt% illite + wt%organic matter + wt%volcanic glass + wt%$CaCO_3$ + wt% rock fragments, quartz and feldspar]

The composition of the clay, silt and sand fractions was quantified separately for Core 31 after separation of the 2 μm, 2-63 μm and the > 63 μm size ranges by centrifugation methods discussed in Appendix 5, where for the < 2μm fraction 100% = [wt%smectite + wt%halloysite + wt%illite + wt% allophane + wt%glass]; for the silt fraction 100%= [wt%halloysite + wt%allophane + wt%illite + wt%rock fragments and quartz and feldspar + wt% volcanic glass] and for the sand fraction 100% = [wt% volcanic glass + wt% $CaCO_3$ + wt%rock fragments and quartz and feldspar].

NOTE

wt% smectite = wt% smectite from XRD

wt% illite = wt% illite from XRD

wt% halloysite = wt% halloysite from DTG

wt% allophane = wt% allophane from oxalate extractable-Al and-Si

wt% glass = wt% glass from IR (< 63 μm) + from HF dissolution (> 63 μm)

wt% $CaCO_3$ = wt% $CaCO_3$ from acetic acid dissolution

wt% org. mat. = wt%organic carbon from Cr_2O_7 oxidation

wt% (rock frags. + qtz. + felds.) = 100 - (wt% tot. clays + wt% glass + wt% org. mat. + wt% CaCO3)

The results of all mineral determinations are tabulated in Appendix 2 and discussed in Section 5.6.

Smectite, Halloysite and Illite

Much discussion has centred around the various schemes for determinig quantitatively, by comparing XRD peak areas, the abundance of individual clay minerals in a clay mineral assemblage. Pierce and Siegel (1969) compared some of the weighting methods and demonstrated that gross changes in the apparent quantity of clay minerals may occur using the different methods devised. Gibbs (1967) outlined what he considered was the most reliable method, using standards of clay minerals extracted from the samples to be analysed. However, this method was precluded because of the lack of time, sample and facilities for undertaking such a procedure and because of the complexity of the clay minerals present.

Vertical changes in clay mineral abundance can be adequately estimated using the semi-quantitative techniques of Johns et al. (1954), Biscaye (1965), or Scafe and Kunze (1971). The technique described by Hume and Nelson (1982) incorporates many of the features from the above methods and is adpated in this study to include 10Å halloysite. A weighting procedure is required to compensate for the different efficiencies of clays in scattering along the 001 row line due to low angle polarisation. Details of the weighting method are described in Appendix 5. The abundance of smectite, halloysite (at 7Å , includes minor kaolinite) and illite for the individual size fractions and bulk samples was determined by this method and results are presented in Appendix 2.

Given the degree of uncertainty often associated with clay mineral abundances determined by XRD, halloysite and kaolinite were also determined quantitatively by DTG analysis (see Appendix 5) and used as a standard for calibration of values obtained by XRD. Results of halloysite abundance for the clay fraction of Core 31 are listed in Table 5.2. The difference between halloysite values of the bulk sample and values of the clay fraction expressed as on a whole sample basis was used to calculate the halloysite present in the silt fraction listed in Appendix 2. In general, good correlation was achieved with the halloysite results determined by XRD. This would suggest that chlorite, if it occurs at all, is present in very small quantities. Given the close agreement of both techniques it seems reasonable to assume that

Table 5.3

Data used in the calculation of allophane content. Si factors are extrapolated from Fig. 5.8

Sample #	wt% Al(ox)	wt% Si(ox)	Al:Si	Si Factor *	wt% allophane
Surficial samples					
4.1	0.5	0.2	2.6	10.0	2.0
6.1	0.6	0.3	1.9	13.0	2.2
21.1	0.6	0.3	1.8	13.0	2.5
23.1	0.6	0.4	1.5	13.0	3.0
26.1	0.4	0.2	2.3	11.5	1.6
23.1	0.6	0.4	1.7	15.0	2.3
33.1	0.5	0.4	1.3	17.0	2.2
34.1	0.5	0.4	1.3	17.0	2.3
37.1	0.4	0.3	1.5	16.0	2.0
39.1	0.7	0.4	1.8	14.0	2.9
40.1	0.9	0.5	1.7	15.0	3.3
41.1	0.4	0.3	1.2	17.5	1.7
Core 31 *(bulk)*					
31.1	0.8	0.6	1.4	16.5	3.5
31.2	0.7	0.5	1.4	16.5	3.0
31.3	1.2	0.5	2.3	12.0	4.3
31.4	1.1	0.5	2.1	12.5	3.3
31.5	0.4	0.4	1.1	18.0	2.2
31.6	0.5	0.4	1.2	17.5	2.6
31.7	1.0	0.5	2.1	12.5	3.1
31.8	0.7	0.5	1.4	16.5	3.0
31.9	0.7	0.6	1.1	18.0	3.4
31.10	0.7	0.5	1.4	16.5	2.8
31.11	0.7	0.5	1.4	16.5	2.7
31.12	0.7	0.5	1.4	16.5	3.0
31.13	0.7	0.6	1.2	18.0	3.3
31.14	0.7	0.7	1.1	18.0	3.7
31.15	0.5	0.3	1.4	17.0	2.1
31.16	0.5	0.3	1.4	17.0	2.0
31.17	0.7	0.5	1.4	16.5	3.0
31.18	0.7	0.4	1.8	14.0	2.8
31.19	0.4	0.3	1.5	16.0	2.0
31.20	0.5	0.4	1.3	17.0	2.2
31.21	0.5	0.4	1.2	17.5	2.4
31.22	0.7	0.5	1.4	16.5	2.8
31.23	0.8	0.5	1.5	16.0	3.2
31.24	0.5	0.4	1.3	15.5	2.5
River samples					
Ohinemuri	0.7	0.4	1.9	13.5	2.8
Waitoa	0.4	0.3	1.3	16.0	1.9
Piako	0.7	0.3	2.2	12.0	2.7
Waihou	0.6	0.4	1.6	14.0	2.8
< 2μm					
31.1	2.1	1.2	1.7	15.0	8.2
31.3	1.7	1.1	1.6	15.0	7.0
31.5	1.1	0.6	1.4	16.5	3.5
31.7	1.2	0.9	1.4	18.5	4.7
31.9	1.1	1.0	1.1	18.0	5.4
31.13	0.8	0.8	1.1	18.5	4.2
31.15	0.5	0.4	1.2	17.5	2.5
31.17	0.5	0.4	1.3	17.0	2.2
31.19	0.5	0.4	1.2	17.5	2.6
31.21	2.1	1.8	1.2	18.0	9.8
31.24	0.7	0.3	2.2	12.0	2.7

the errors involved in clay mineral estimations may be less than the standard 10% error proposed by Hume and Nelson (1982) for XRD analysis.

Table 5.2
Comparison between halloysite contents determined by XRD ($7Å_{110}$) and DTG.

Sample #	XRD (wgt%)	DTG (wgt%)
31.1	45.8	50.8
31.3	35.1	40.3
31.5	58.0	60.0
31.7	61.2	65.3
31.9	53.2	60.0
31.13	29.8	30.0
31.15	28.6	34.5
31.17	34.6	30.0
31.19	35.0	39.2
31.21	26.6	30.0
31.24	22.3	22.6

Allophane

Allophane is an hydrated aluminosilicate clay mineral characterised by a predominance of Si-O-Al bonds with a variable Al:Si molar ratio between 1.0 and 4.0 (Wada 1977 1980; Parfitt and Hemni 1980; Parfitt et al. 1980; Parfitt 1990). In New Zealand three types of allophane are recognised. They are Al-rich allophane characterised by a proto-imogolite structure and an Al:Si ratio of 2.0-4.0; Si-rich allophane known as pumice allophane or halloysite-like allophane with an Al:Si ratio of 1.0; and stream deposited allophane often found in hydrothermal or silica-rich systems and known as hydrous feldspathoid allophane and characterised by an Al:Si ratio of 0.9-1.8. 70% of New Zealand allophanes are the Al-rich types Parfitt (1990).

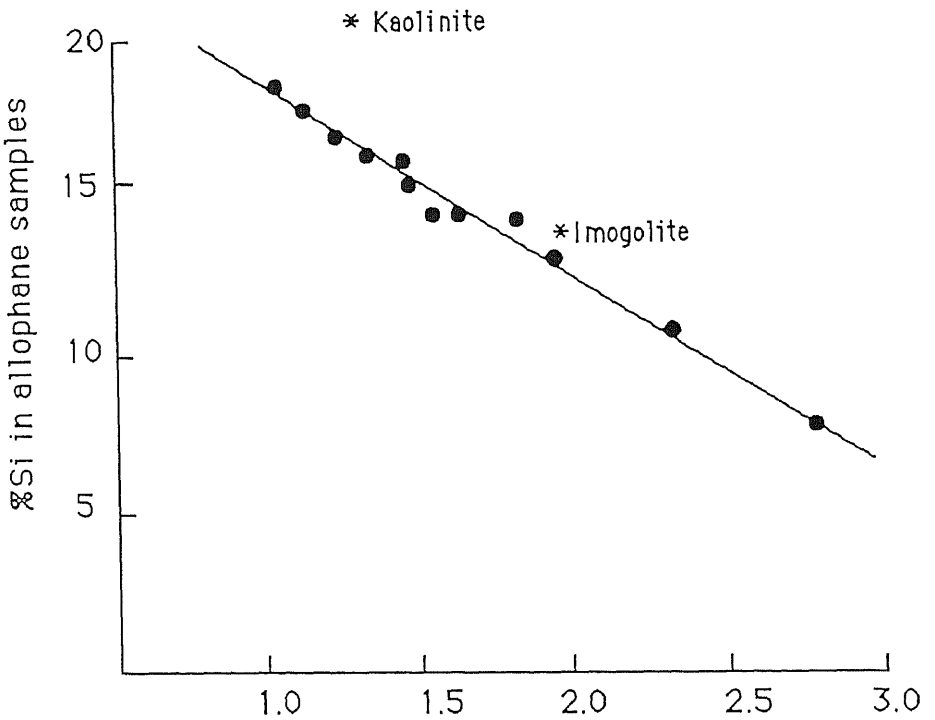

Figure 5.7

Silica content of allophanes of various Al:Si ratios (after Parfitt and Wilson 1986).

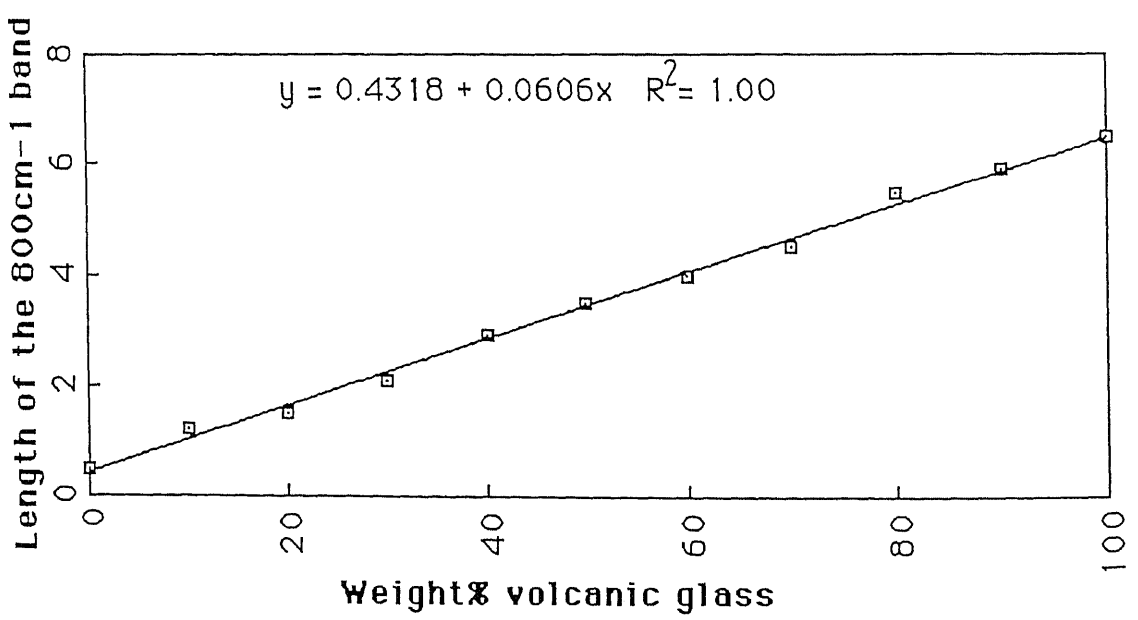

Figure 5.8

Absorption band (800 cm-1) intensity vs volcanic glass content standard curve.

Al:Si molar ratios of surficial sediments from samples listed in Table 5.3 range from 1.2-2.6 indicating variable composition allophanes which would include both Si-rich and Al-rich allophane varieties. Samples analysed down Core 31 exhibit a progressive decrease in the Al:Si ratio suggesting a predominance of Si-rich allophane with depth. Green (1987) describes both Si- and Al-rich allophanes forming from the weathering of a series of late Quaternary rhyolitic tephras in the Taupo Volcanic Zone. Given that the source material described in Section 2.4 may be very similar in composition this would be in accordance with Al-and Si-rich allophane varieties in the sediments of the Firth of Thames. The predominance of Si-rich allophane with depth may be due to post-depositional alteration of Al-rich allophane once in contact with interstitial solutions high in dissolved silica.

Ammonium oxalate extraction is a method for selectively removing Al and Si solely derived from short range order minerals. Therefore the weight% Al and Si extracted by this method, discussed in Appendix 5, was used to estimate allophane proportions. Figure 5.7 gives the silica content of allophanes of various Al:Si molar ratios according to Parfitt and Wilson (1986). Extrapolated Si contents from Figure 5.7 using the Al:Si ratios calculated from oxalate extractable Si and Al enables a calculation of weight% allophane using the following equation.

100 / %Si in allophane * wt% extract. Si = wt% allophane.

Oxalate extractable Al and Si, Al:Si ratios and weight% allophane for Core 31 bulk, and clay fractions and river samples and surficial core samples are shown in Table 5.3 (allophane calculated in the silt fraction is shown in Appendix 3).

Calcium carbonate

The wt% calcium carbonate is determined by digestion in 4.4 M acetic acid of pre-weighed samples (> 63 μm). Samples were then dried, re-weighed and the loss in weight expressed as the weight% $CaCO_3$. The same sample is then used for HF dissolution analysis for the determination of of volcanic

glass.

Volcanic glass

Volcanic glass is determined by infrared absorption analysis. Much discussion has evolved over the applicability of IR as a tool for quantittaive analysis (Furket and Schmidt 1972; Farmer et al. 1976; Parfitt and Furket1980; Parfitt and Hemni 1982). A major limitation is the particulate nature of minerals and the light scattering phenomenom known as the "Christiansen Effect" producing a non-linear relationship between the concentration of a given mineral component and the degree of absorption of infrared radiation. Other factors limiting the accuracy of quantitative determinations are the lack of standardised reference material having the same structure, particle size distribution, composition and spectral features as the component in the sample (Lowe and Nelson 1983).

In order that these variables leading to inaccuracies be minimised the following precautions were taken when preparing standards and samples (Preparation methods are described in more detail in Appendix 5). i). Silt (2-63 μm) samples were carefully ground to a size approximating 2 μm or less in order that distortion of absorption bands due to the Christiansen Effect be minimised. This distortion is overcome if the particle size is less than the wave length of infrared radiation used. ii) Standards used for constructing a calibration curve (Fig. 5.8) for quantitative estimations of volcanic glass were made from glasses extracted from the material being analysed. Glass shards were "picked" under a microscope from the sand fractien of the sample in question. The length of the diagnostic 800 cm^{-1} band is used in quantifying the wt% abunbance of glass in the silt and clay size fractions (Fig. 5.8).

Glass contents in the >63 μm fraction were estimated for the sand fraction by dissolution in concentrated hydrofluoric acid following the procedure outlined by Green (1987) and summarised in Appendix 5. Volcanic glass is known to almost instantly dissolve upon contact with hydrofluoric acid. Using this procedure glass rims around crystal phases which might be expected to contribute to secondary mineral formation, together with glass shards, are dissolved and weight loss calculated with minimal loss of crystalline minerals through acid dissolution.

Organic Matter

Organic matter in the sediments is a mixture of humic and non-humic substances. The non-humic material is predominantly peat remnants, mangrove roots, leaves and wood fragments deposited in large quantities during flood events and also entrained in ambient flow conditions. Dead shell fish and other dead marine fauna also contribute to the non-humic component. Non-humic material comprises a large proportion of the organic matter component of the sediments. The end products of the degradation of these substances are the humic components such as organic acids, lipids, waxes, polycyclic aromatic hydrocarbons and lignin fragments. The more stable compounds in sediments are humic substances partitioned into the fractions of humic acid, fulvic acid, and humin.

Organic carbon concentration provides a means of depicting the organic matter component and is discussed along with concentrations of transition metals in a breif account of sediment geochemistry in Appendix 4. Owing to the particular combination of different groups (mainly OH and SH), humic substances are able to form organically bound complexes with certain cations, in particular Fe, Cu, Ni, Cd, Cu and Mn. These substances are easily adsorbed by clay and oxide particles in the marine environment (Kababt-Pendias and Pendius 1984).

The wt% organic matter for all samples analysed is listed in Appendix 2. Organic matter decreases marginally with sub-bottom depth down Core 31 (see Fig. 5.13A) due to continued degradation of organic residues and cessation of fresh organic matter input after burial. A wide range of organic matter values in surficial sediments which show no relationship to clay content probably reflects the low values of total humic substances (THS) in the total organic carbon (TOC) and the sporadic distribution of non-humic, macro-organic components such as roots, wood fragments and shell fish remains which are estimated to be well in excess of 70% of the TOC for surficial sediments. Boldrin (1987), in a similar study of prodeltaic late Holocene mud sediments of the Po Delta, Italy, suggested that low THS's of the TOC occur due to high sedimentation rates and a correlated reduction in degradtion processes.

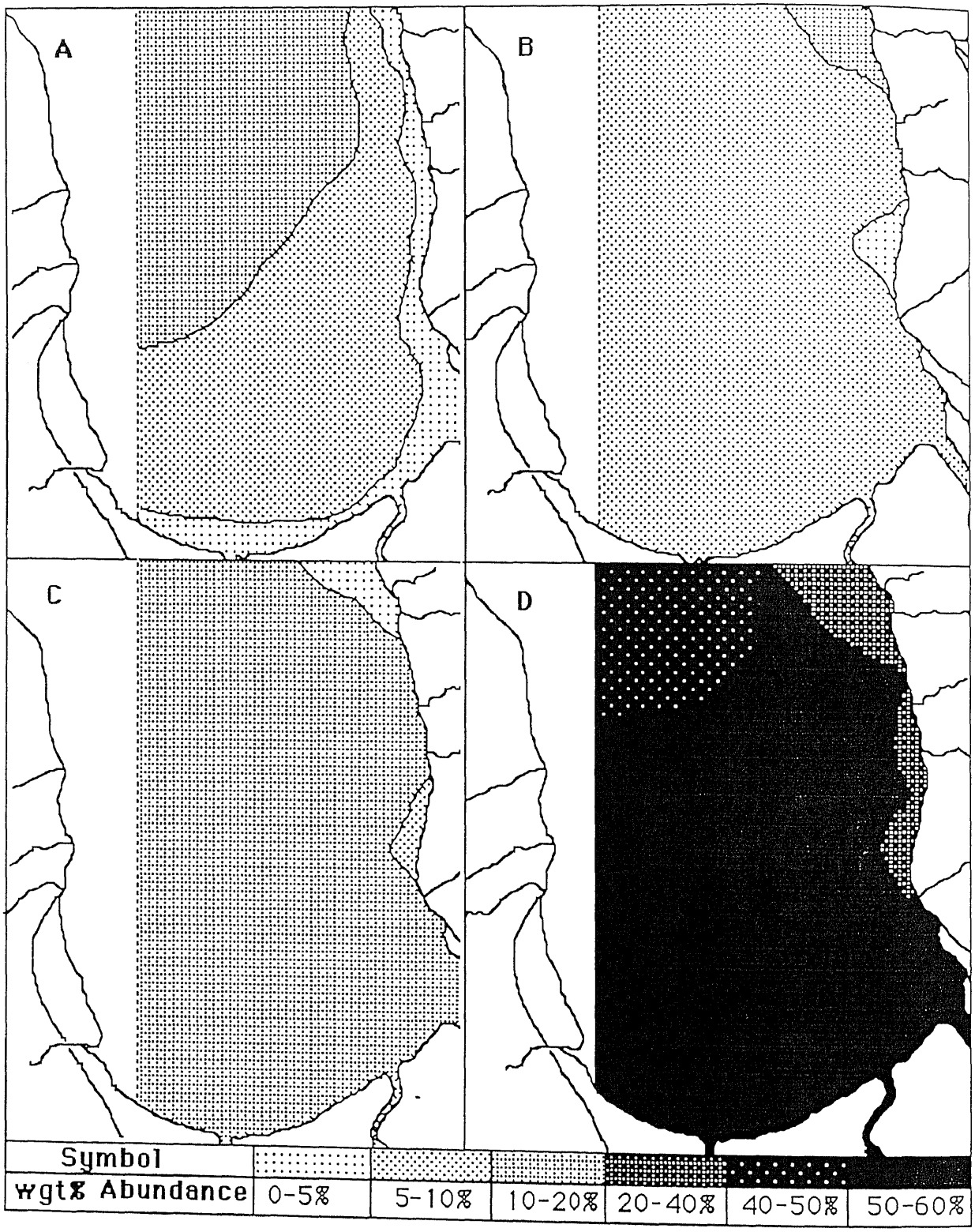

Figure 5.9

Areal distribution of A) smectite, B) illite and kaolinite, C) halloysite and allophane, and D) volcanic glass. Compositions are reported on a whole sample basis.

5.6 DISCUSSION

Lateral variations in sediment mineralogy

From the data presented in this chapter, there appears to be no significant areal variation in the mineralogy of bottom sediments throughout the Firth of Thames. The clay mineralogy in all regions is essentially the same. The only changes evident are in the abundance of various clay minerals. A pronounced increase in smectite abundance occurs northwards of the Waihou river mouth (Fig. 5.9A) and although illite and kaolinite are generally subordinate to smectite and halloysite the former dominate the clay mineral assemblage of sediments proximal to the delta fans of Tapu and Te Mata (Fig. 5.9B). Conversely, halloysite and allophane exhibit an areal distribution similar to that of smectite (Fig 5.9C).

Studies on Recent and oceanic deep sea clays (e.g. Biscaye 1965; Stoffers and Muller 1972; Hume and Nelson 1985) have shown that lateral and vertical variations in clay mineralogy can be attributed largely to supply of clay minerals from differing onland source rocks. The areal distribution of halloysite and allophane, and of kaolinite and illite are considered to reflect mainly the factors of supply and provenance. In order to determine the provenance of the core sediments, samples were taken from the Waihou and Waitoa Rivers and their tributaries, the Piako and Ohinemuri Rivers. The two major river systems supplying sediment to the Firth of Thames, are the Waitoa-Piako and Waihou Rivers. Sediment discharge from the Waihou River has been estimated at 3,430,000 tonnes per year and from the Piako River about 820,000 tonnes per year (Griffiths and Glasby 1985). The streams draining the Coromandel and Hunua Ranges are considered to be responsible only for localised deposition on adjacent delta fans in close proximity to the shoreline (Dravitzki 1988), and are not thought to play a large role in influencing the overall composition of the Firth of Thames sediments, as Figure 5.9 indicates. To avoid sampling sediment that may have been resuspended and transported back upstream from the coast by tidal currents, the samples were collected well beyond any tidal influence. Figure 5.10 shows the collection sites and the whole sediment compositions for all rivers sampled. Also shown in Figure 5.10 is the average composition of surficial sediment from 12 sites in the Firth of Thames.

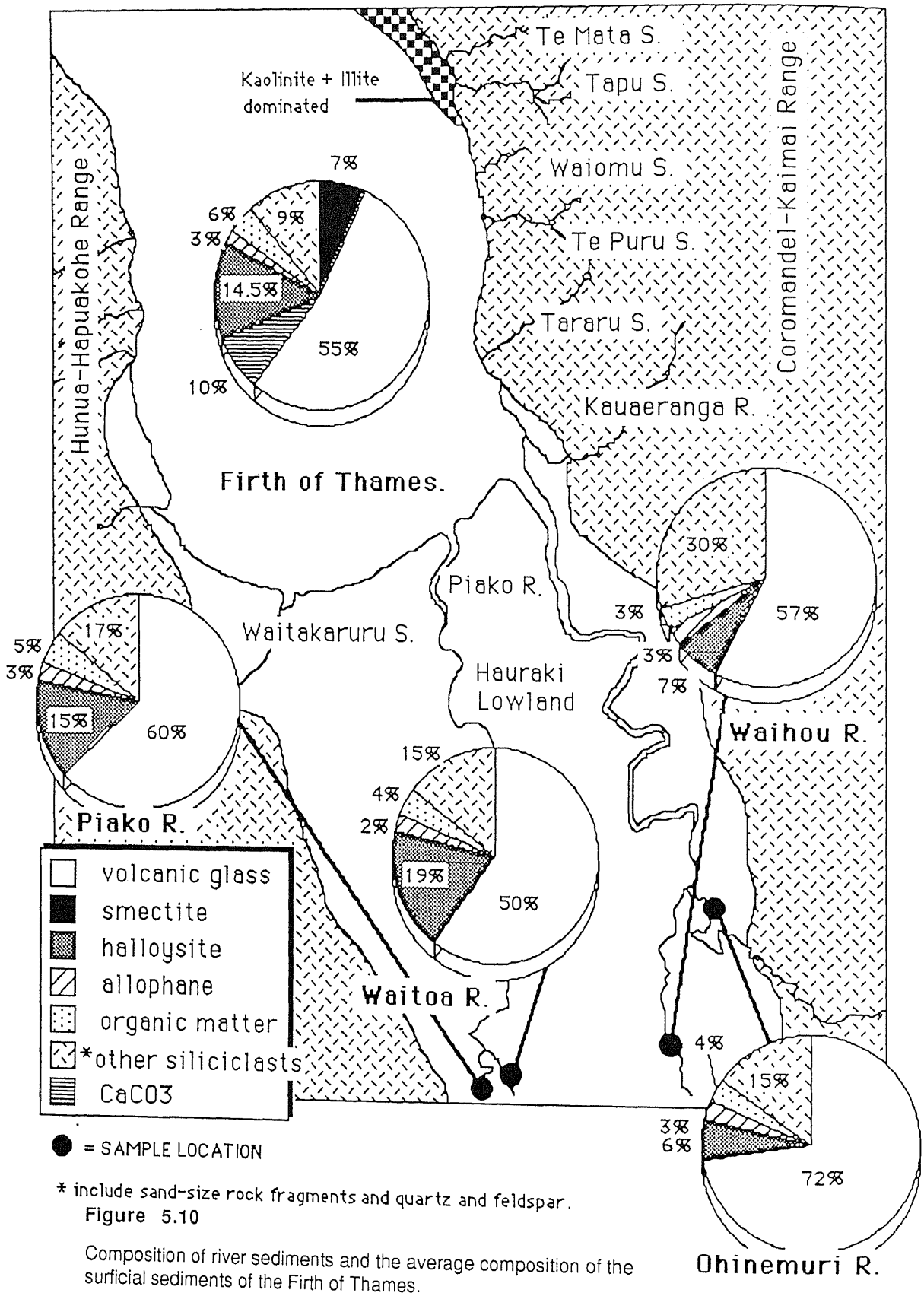

* include sand-size rock fragments and quartz and feldspar.

Figure 5.10

Composition of river sediments and the average composition of the surficial sediments of the Firth of Thames.

The provenance characteristics discussed in Chapter 2 can clearly account for the composition of the riverine sediments. The silicic nature of the volcanic source rocks is reflected by abundant rhyolitic glass shards, quartz, pumice, feldspar and rhyolitic and andestic rock fragments in the sand fraction, and the subaerial weathering of acidic volcanic detritus to yield halloysite and allophane is well known (e.g. Kirkman 1975; Parfitt et al. 1983; Stevens and Vucetich 1985) and is the likely source of these clay minerals. Analysis of the clay mineralogy of tephras by Birrell and Pullar (1973) and Kirkman (1975, 1976) has established that allophane is the dominant secondary mineral in most TVZ paleosols developed on rhyolitic tephras, with halloysite additionally present in older tephras. The composition of the Firth sediments is similar to that of the rivers supplying detritus to it, with the exception of the anomalous occurrence of smectite. In the absence of an adjacent onland catchment or shelf source, the possibility of a diagenetic origin must be considered.

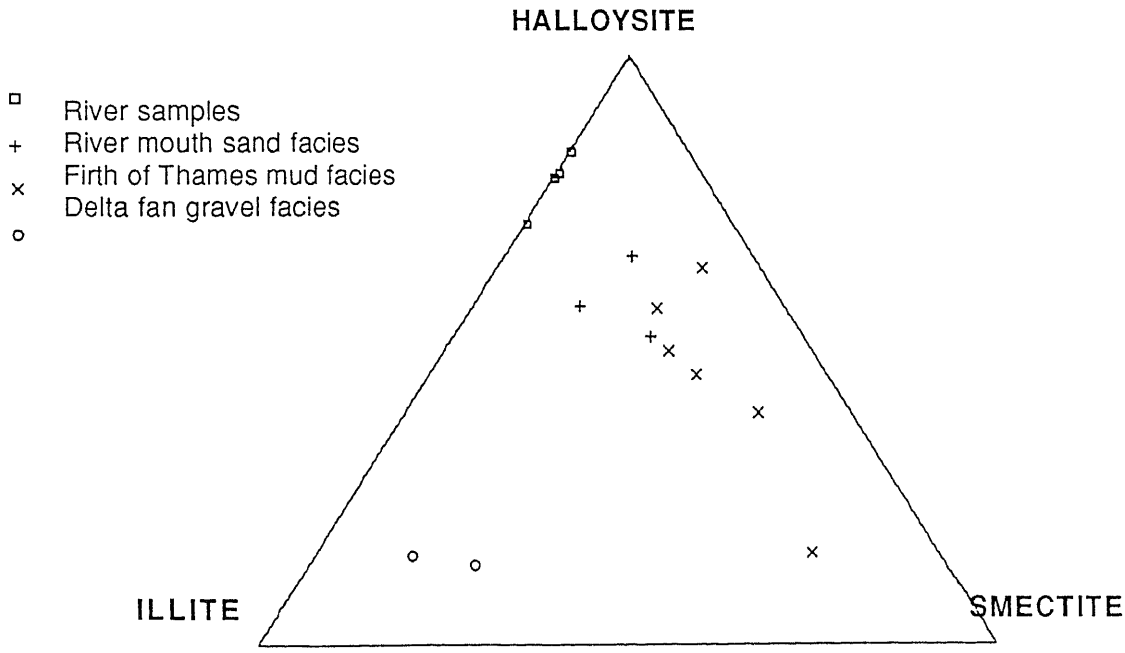

Figure 5.11

Ternary diagram of illite-halloysite-smectite. Illite-dominated sediments from the delta fan facies adjacent to Te Mata and Tapu reflect greywacke derivation. Smectite content of samples increases seaward from the river mouth sand facies to the Firth of Thames mud facies. River sample are devoid of smectite.

From the ternary composition diagram in Figure 5.11 locally significant abundances of illite and kaolinite ± chlorite reflect the greywacke source lithology north of Tapu (see Section 2.4, Regional Geology). The catchment and sediment discharge of the Tapu River is significantly higher than other streams draining the Coromandel Range (Dravitzki 1988), thus diluting the volcanic-dominated clay mineral assemblage (halloysite, smectite and allophane) of the Firth of Thames mud facies with a micaceous greywacke-dominated mineral assemblage (illite, kaolinite and ± chlorite) adjacent to Tapu and Te Mata. The dominance of single-peak plagioclase feldspar (discussed in Section 5.3) noted in sediments from this region also suggests a greywacke derivation. Likewise, it is expected that a greywacke derived clay mineral assemblage would also dominate sediments adjacent to streams draining the Hunua Ranges, although analyses were not conducted on such samples from the western Firth shoreline.

Various studies on estuarine clays have shown that diagenetic changes can occur due to a seaward increase in salinity. Reinson (1977) reviews some of the more significant studies. However, most studies are concerned with the transformation of one clay mineral to another. In Chapter 7 a diagenetic origin of smectite from the dissolution of volcanic glass is discussed and salinity is shown to be an important factor controlling the smectite formation. Recent work by van Leewue (in prep.) pertaining to the salinity stucture of the Firth of Thames suggests both vertical and lateral stratification. Salinites range seaward from an average of 10 ppt (Waihou River mouth) to 30 ppt (offshore from Te Puru). Data presented in this chapter (Fig 5.9A and 5.10) illustrate a seaward increase in smectite content ranging from 0% in river samples, thus precluding a detrital origin, to a maximum of 10% offshore.

Volcanic glass is the most abundant mineral component and exhibits virtually no variation in areal distribution with the exception of the northeastern region of the study area adjacent to Te Mata and Tapu where dilution of volcanic-derived sediment occurs due to input from locally derived greywacke-dominated sediments (Fig. 5.9C). Likewise the rock fragment, quartz and feldspar component is also uniform in all samples. Carbonate concentrations occur sporadically as lenses representing living bivalve beds and accumulations of reworked or in situ skeletal carbonate detritus.

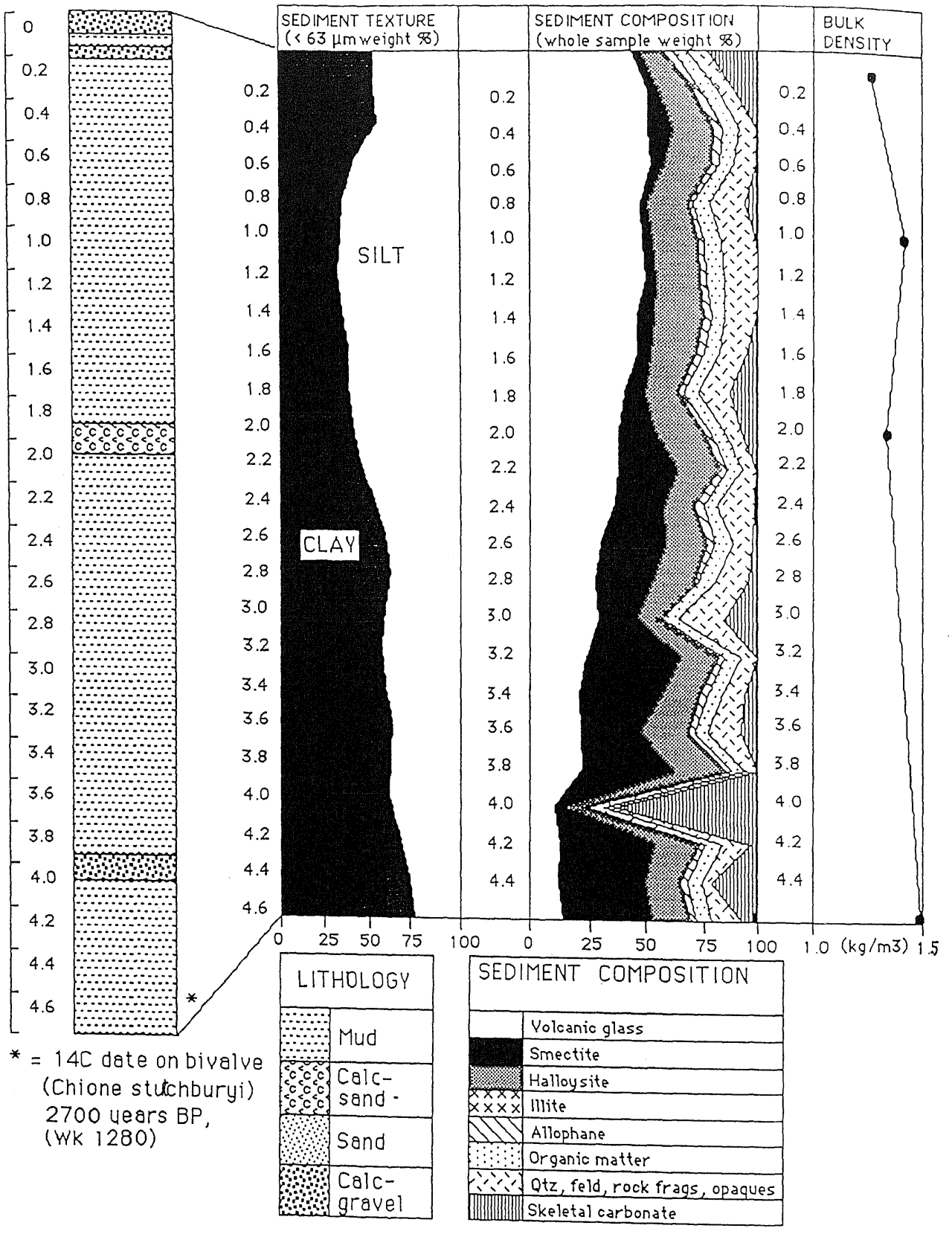

Figure 5.13A

Bulk sediment composition for Core 31

The areal distribution of carbonate in bottom sediments may be controlled by the anticlokwise movement of the residual M_2 tidal current (Bowmen and Chiswell 1982); reworked shell hash forming a lag surface where currents are strongest, along the eastern boundary of the Firth during the ebb tide and along the western boundary during the flood tide, with in situ skeletal carbonate and modern living bivalves accumulating in the central Firth.

Vertical variations in sediment mineralogy

The mineralogy of Core 31 represents a smectite-smectite/illite-halloysite-allophane-dominated clay mineral assemblage which is characteristic of the glassy acid volcanic-derived Firth of Thames mud facies accounting for the majority of the sediments in the Firth of Thames. Down-core profiles exhibit variations in composition of bulk samples and variations within the clay and silt fractions individually and are illustrated for Core 31 in Figure 5.13A and 5.12B. From the down-core composition profiles for Core 31 the following conclusions can be made:

(i) Volcanic glass dominates the surficial and upper core sediments, but decreases significantly in abundance with sub-bottom depth.

(ii) Volcanic glass is the major constituent of, and almost exclusively confined to, the silt fraction. Volcanic glass is depleted with depth in the silt fraction.

(iii) The major constituent of the clay fraction is smectite.

(iv) Smectite dominates in the lower core sediments and increases significantly in abundance with sub-bottom depth.

(v) The abundance of halloysite and allophane remains constant with sub-bottom depth on a whole

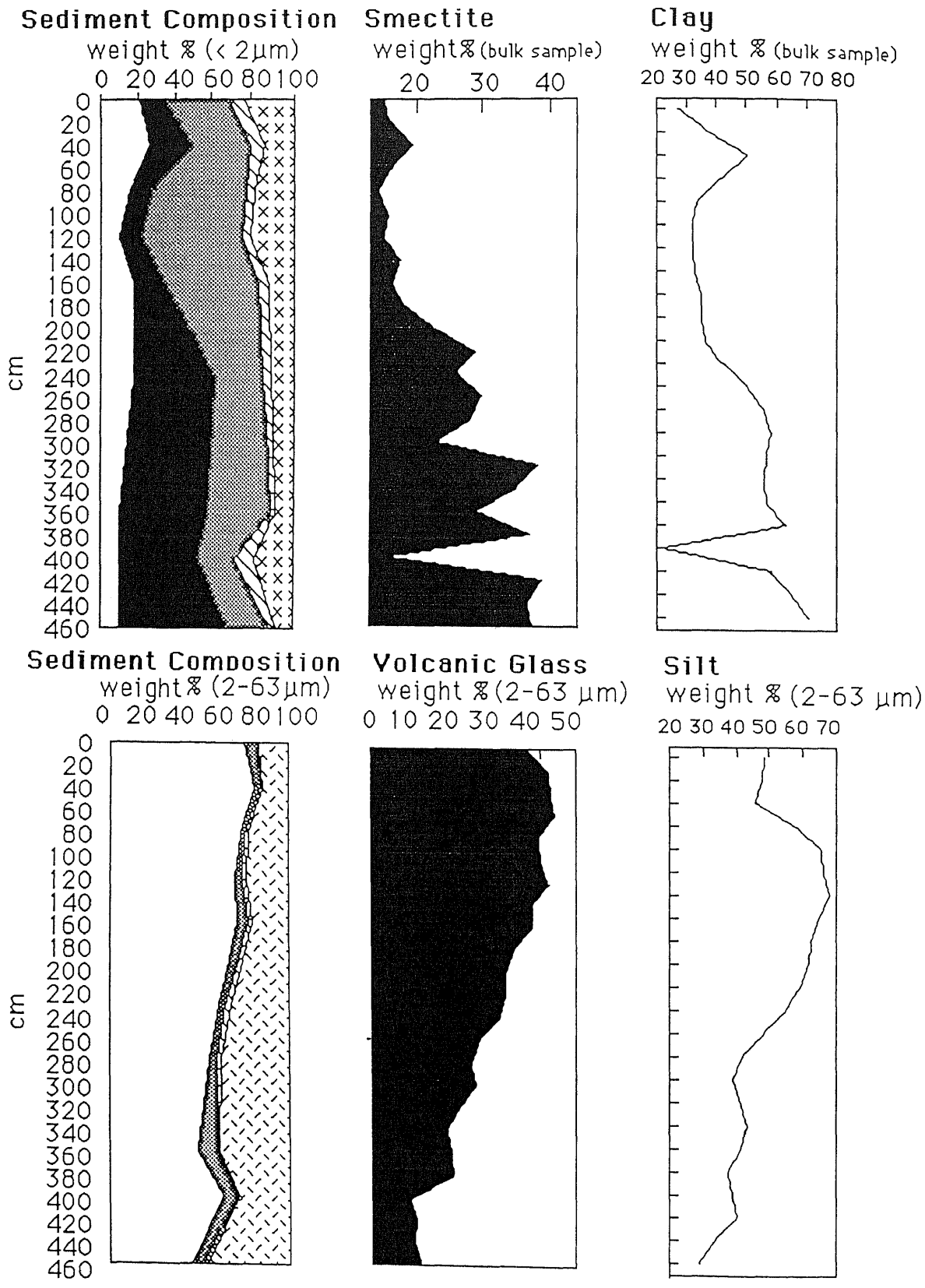

Figure 5.13B - Sediment composition of the clay and silt fraction of Core 31

sample basis, suggesting that these clay minerals are relatively stable in seawater. The abundance of halloysite and allophane decrease in the < 2 μm fraction due to the relative increase in smectite.

(vi) The distribution of calcium carbonate corresponds to the frequency of shell layers within the core.

The significance of vertical variations in mineral abundance is discussed in Chapter 7 and is related to post-depositional processes occurring within the sediments.

Sediment geochemistry

Results of a principal component analysis performed on bulk chemical data obtained by X-ray fluorescence spectroscopy for the Firth of Thames core sediments is descibed in Appendix 4. Elemental associations are represented by four factors and tend to support the mineralogy of the core sediments described in this chapter. Although geochemical data has been included in an appendix and some preliminary interpretations undertaken, a detailed discussion of sediment chemistry is not the intention of this thesis. The geochemical data presented here will probably form the basis of a future study.

-CHAPTER SIX-

SEDIMENT FAUNA

CHAPTER SIX: SEDIMENT FAUNA

6.1 INTRODUCTION

The aims of this chapter are to identify and describe the relative abundance and distribution of fauna in the late Holocene sediments of the Firth of Thames. A qualitative assessment of species abundance for Cores 21, 31 and 40 is used to make paleoenvironmental interpretations based on the ecology of the taxa present. The systematic taxonomy for all species identified is outlined in Hornibrook (1953) and Swanson (1979) for ostracods, Loeblich and Tappen (1964) for foraminifera and Powell (1979) and Beu et al. (1990) for molluscs.

6.2 MICROFOSSIL COMPONENTS

Foraminifera, ostracods and diatoms make up the majority of the microfaunal assemblage. Variations with depth in the relative abundance of various species are illustrated qualitatively for Cores 21, 31 and 40 in Figure 6.1.

Foraminifera

Foraminifera belong to the Phylum Protozoa (Class Sarcodina). They are unicellular organisms ranging in size from 50-400 μm and are characterised by a secreted or agglutinated skeletal test generally constructed of calcium carbonate (Boersma 1978). Data from micropaleontological analysis of foraminiferal assemblages have been used extensively in sedimentology, paleogeographic reconstructions, lithostratigraphy and tectonic histories of sedimentary basins. They are important because of their high diversity and occurrence in all marine environments at all latitudes in all oceans. The activity of foraminifera and their geographic location is influenced by a wide variety of factors. Therefore an understanding of foraminiferal ecology can be used in paleoenvironmental interpretation.

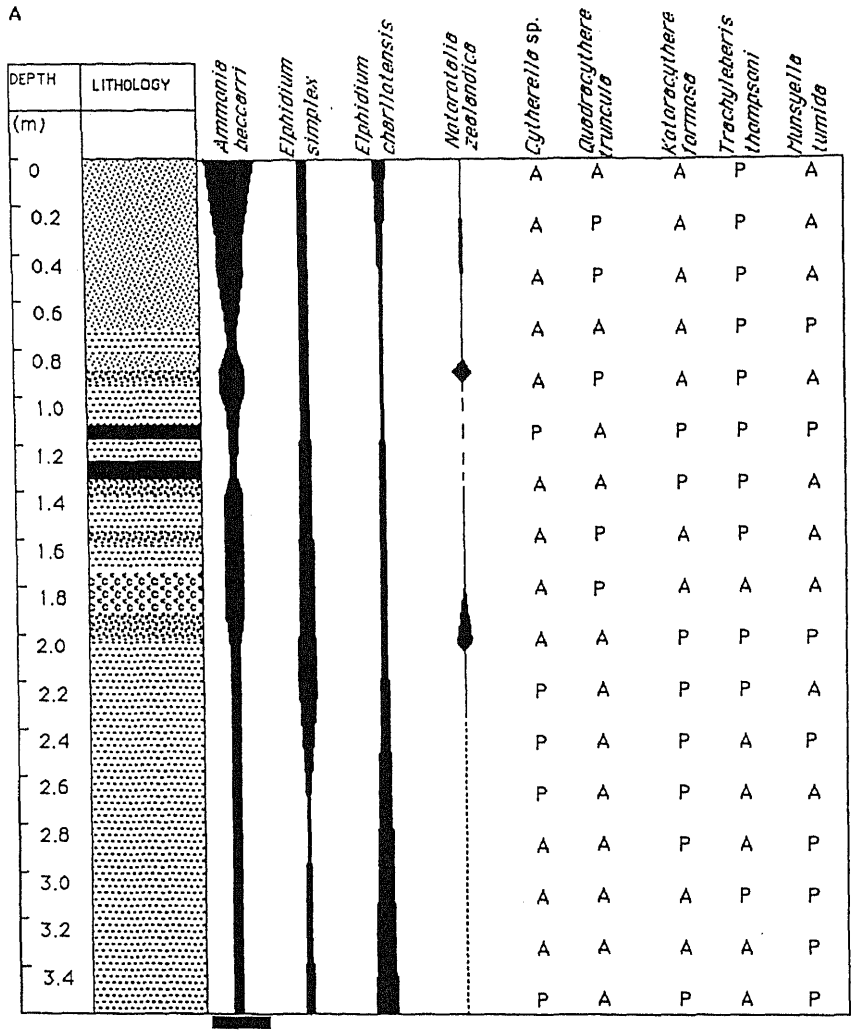
A
DEPTH
(m)
LITHOLOGY
Ammonia beccarii
Elphidium simplex
Elphidium charlottensis
Notoralilia zealandica
Cytherella sp.
Quadracythere truncula
Kotoracythere formosa
Trachyleberis thompsoni
Munseyella tumida
0
0.2
0.4
0.6
0.8
1.0
1.2
1.4
1.6
1.8
2.0
2.2
2.4
2.6
2.8
3.0
3.2
3.4

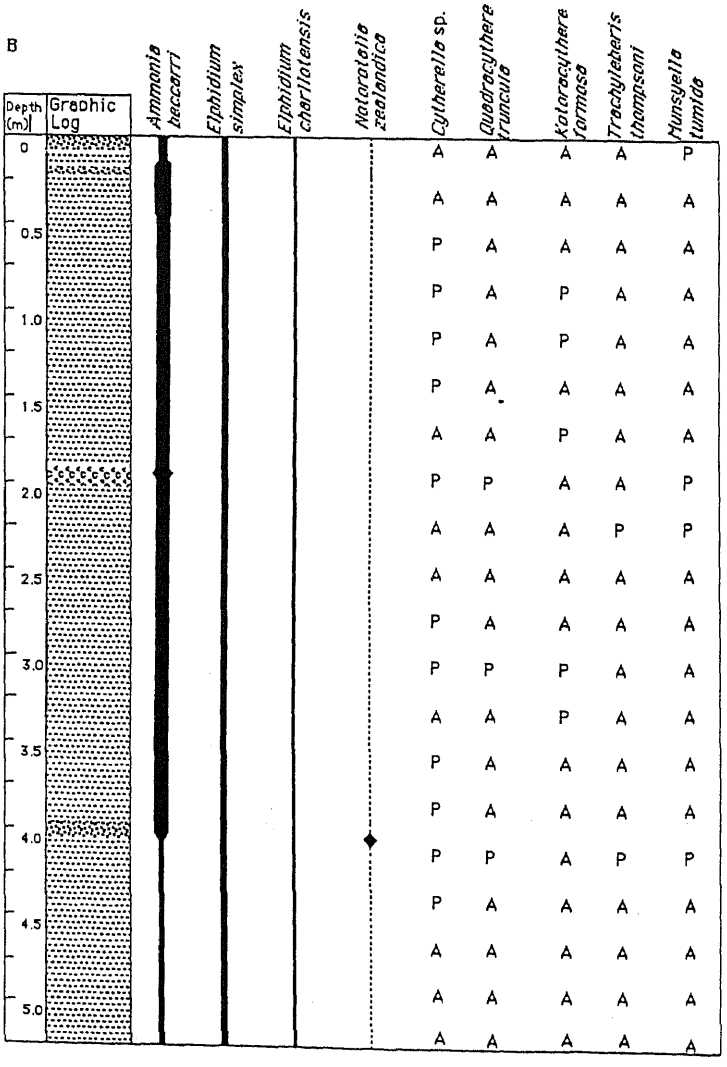
B
Depth (m)
Graphic Log
Ammonia beccarii
Elphidium simplex
Elphidium charlottensis
Notoralilia zealandica
Cytherella sp.
Quadracythere truncula
Kotoracythere formosa
Trachyleberis thompsoni
Munseyella tumida
0
0.5
1.0
1.5
2.0
2.5
3.0
3.5
4.0
4.5
5.0

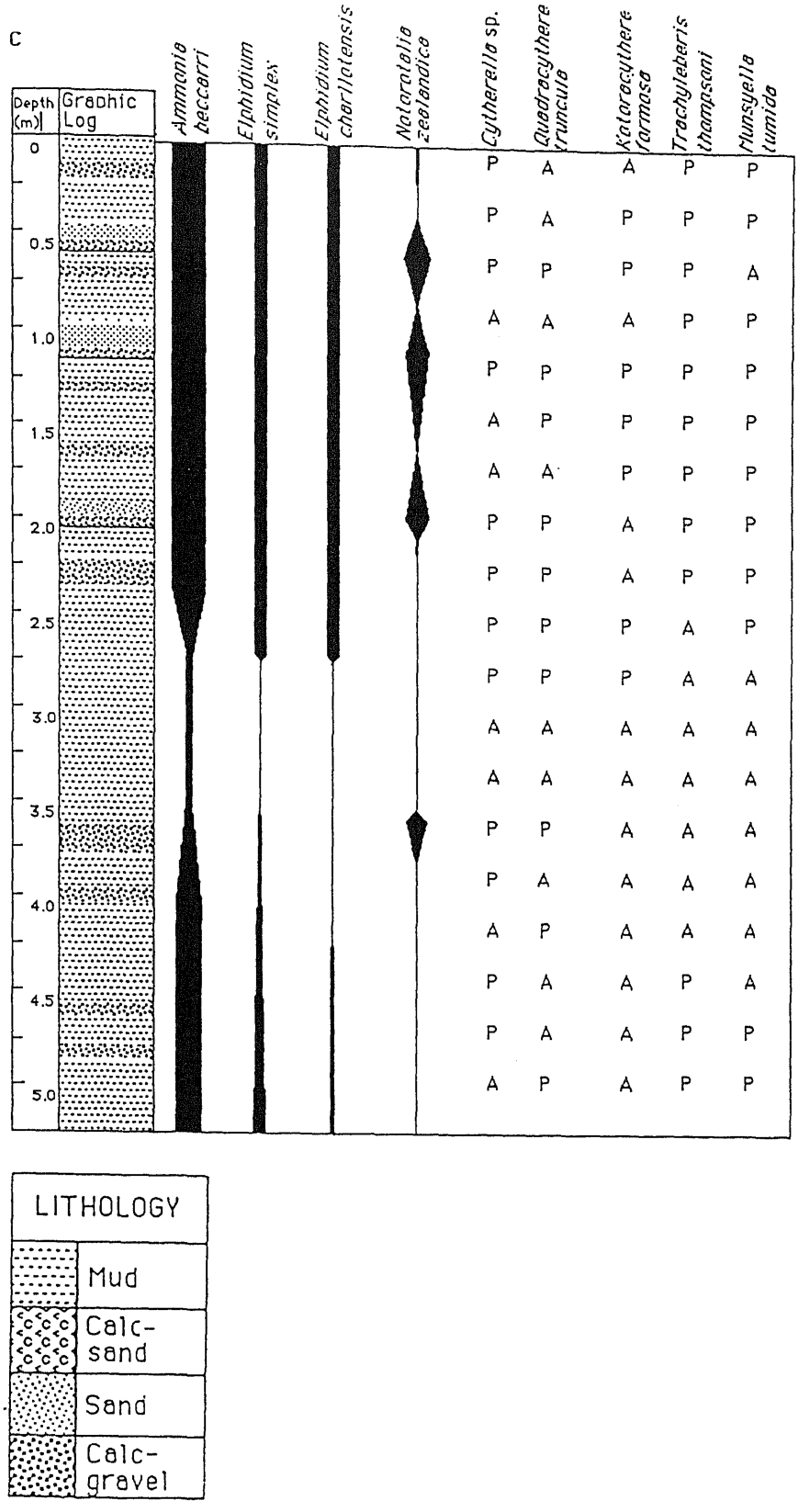

Figure 6.1

Down-core distribution of benthic taxa. Data from A) Core 21 B) Core 31 C) Core 40 (for ostracods A=absent, B=present).

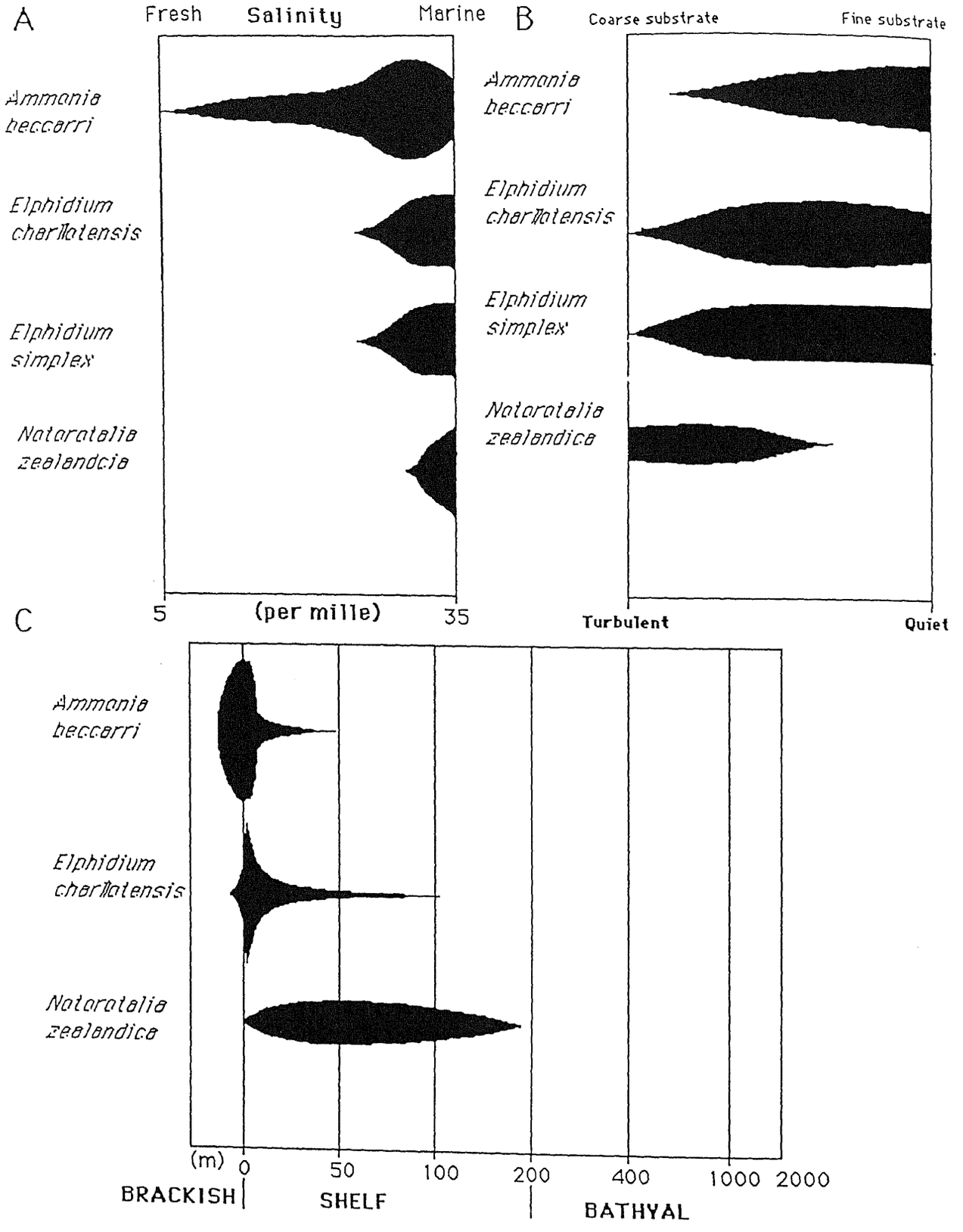

Figure 6.2

Approximate salinity ranges (A), substrate type (B) and depth range (C) of common benthic foraminifera occurring in sediments of the Firth of Thames (after Hayward 1986).

Planktonic foraminfera live in the water from the surface zone down to depths of 1000 m. The 30 modern planktonic species are grouped into two families, Globigerinidae and Globorotalidae. Temperature and salinity appear to be the major controls determining their distribution and are therefore used extensively as paleogeographic indicators of water masses. Benthic foraminifera live at the sediment water interface. They are easily distinguished from planktonic foraminifera by differences in chamber shape and wall structure and texture. Benthic forams occur at all depths and all latitudes.

A rapid paleoenvironmental assessment of faunas was undertaken for the Firth of Thames following the procedure outlined in Hayward (1986). A qualitative assessment of taxa abundance and distribution with depth is presented for Cores 21, 31 and 40 in Figure 6.1 A, B, and C. Benthic taxa dominate the foraminiferal assemblage in all samples. Rare planktonic species are recorded in samples, generally as isolated cases of one or two individuals. *Ammonia beccarri* (Plate 6.1 A) is the dominant benthic species, and in general the benthic taxa exhibit a low diversity of species characteristic of shallow marine shelf or paralic environments. Using Figure 6.2, the paleodepth range of common species can be inferred. Clearly the benthic species recorded are expected ones in marginal marine to inner shelf depths, typical of the Firth of Thames. The absence of any-deep water species indicates little or no post-mortem mixing and transportation. Hayward (1986) notes that wide variations or reductions in salinity have marked effects on the benthic foraminiferal faunas, particularly in shallow enclosed locations such as the Firth of Thames. The approximate salinity ranges and relative abundances of New Zealand shallow-water foraminifera is illustrated in Figure 6.2. It is interesting to note that *Ammonia beccarri* dominates in brackish to marginal marine salinity conditions, but is extremely versatile and is known to adapt well to a wide range of salinity conditions. The salinity conditions in the Firth of Thames vary significantly, exhibiting both lateral and vertical variations due to the large input of freshwater from the Waihou River. Average salinities, over a tidal cycle, vary from 10-30 ppt in an 8 km radius from the Waihou River mouth, while beyond this the Firth is well mixed, with maximum salinities of 32 ppt (C. van Leeuwe , pers. commun.). Consequently the taxonomic composition can be a useful guide in determining the salinity of the depositional environment in paleoenvironmental reconstructions. From

Plate 6.1

SEM photomicrographs of foraminifera identified in late Holocene core sediments of the Firth of Thames.

A *Ammonia beccarri* (130 X, 15 kV)

B *Elphidium simplex* (180 X, 15 kV)

C *Elphidium charllotensis* (200 X, 15 kV)

D *Notorotalia zealandica* (120 X, 15 kV)

E *Globorotalia inflata* (200 X, 15 kV)

F *Globigerina* sp. juvenile (250 X, 15 kV)


A

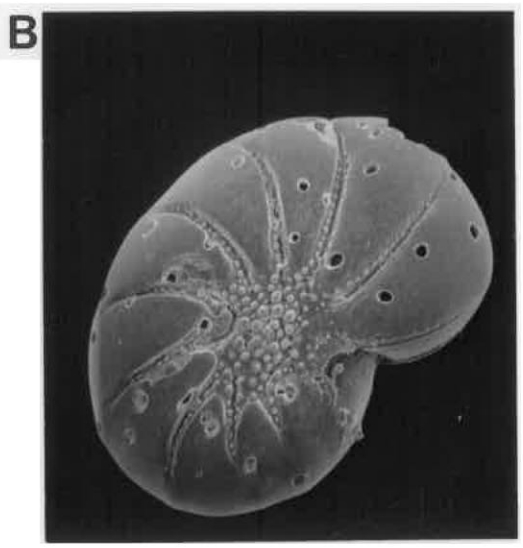
B

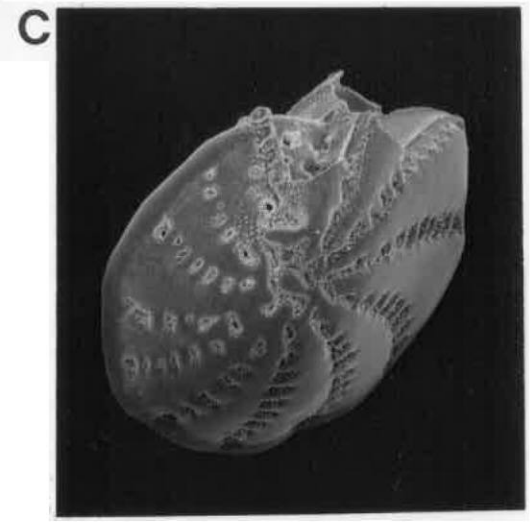
C

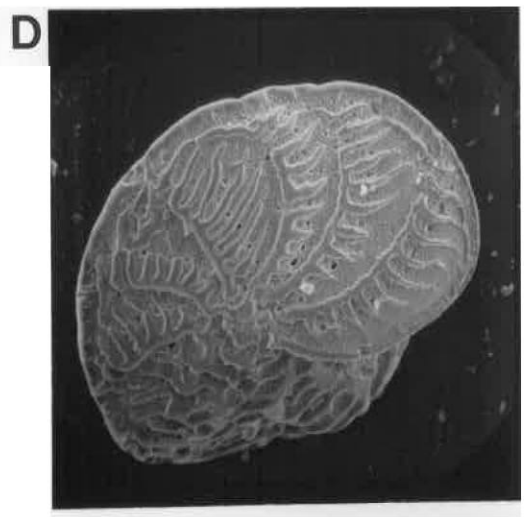
D

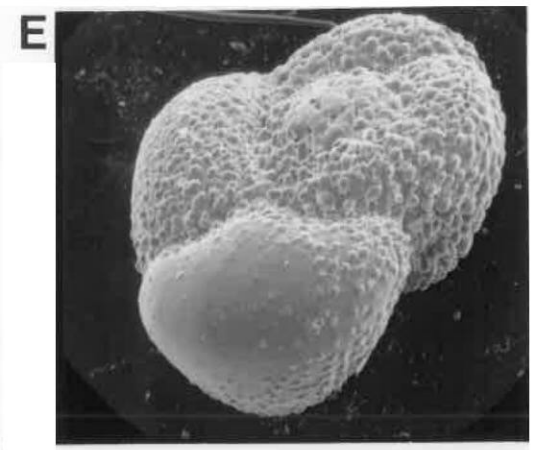
E

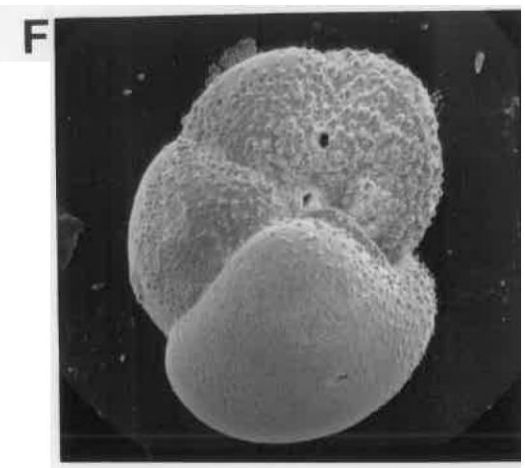
F

Figure 6.1 A *Ammonia beccarri* appears to decline in abundance with depth down Core 21 and to a lesser extent down Core 40. The sediments of Core 21 may have experienced a progressive decrease in salinity over the late Quaternary as the mouths of rivers draining the Hauraki Lowland prograded northwards. Blom (1988), in an analysis of late Quaternary core sediments from the Bass Strait, describes a shallow marginal marine/estuarine facies characterised by low diversity faunas and dominated by one species, *Ammonia beccarri.*

With the exception of *Ammonia beccarri* whose distribution appears to be salinity dependent, the down-core distribution in the relative abundance of benthic taxa does not vary substantially, indicating environmental conditions have remained fairly stable over the late Holocene. Abundances of *Ammonia beccarri* (Plate 6.1 A), *Elphidium simplex* (Plate 6.1 B) and *Elphidium charllotensis* (Plate 6.1 C) appear to be independent of substrate occurring consistently in both mud- and sand-dominated lithologies (Figure 6.1), whereas *Notorotalia zealandica* (Plate 6.1 D) is confined to sandier sediments. Figure 6.2 C illustrates the effect of wave and current action on the ranges of a selection of New Zealand inner shelf benthic faunas, including *Notorotalia zealandica* which is expected in greatest abundance in high energy environments. In Core 40 this taxa is dominant in shell-hash layers, interpreted as forming as part of storm-generated beds discussed in Chapter 3, and is unlikely to be in situ, whereas in Core 21 *N. zealandica* occurs in trace to common amounts in sandy lithologies although the decreased salinity experienced by sediments in the upper part of this core may limit numbers. Typical faunas of storm beds in Core 40 also include *Globorotalia* sp. (Plate 6.1 E), *Globigerina* sp. (Plate 6.1 F), as well as *Notorotalia zealandica,* indicating post-mortem mixing and transportation.

Ostracods

Ostracods belong to the Phylum Crustacea and are the most widely used of the crustaceans studied by stratigraphers and micropaleontologists. Like foraminifera, the study of ostracods has been

Plate 6.2

SEM photomicrographs of the ostracods and diatoms (6.2 E) identified in core sediments from the Firth of Thames.

A *Cytherella sp.* (110 X, 25 kV). 0-65m, common 37m (Swanson 1979 a,b)

B *Kotoracythere formosa* Swanson (150 X, 25 kV). 0-65m, 16-100m, common 50m, (Swanson 1979 a,b)

C *Quadracythere truncula* (Brady) (130 X, 25 kV)Common 18-30m (Hornibrook 1953), Common 13-30m, rare to 60m (Swanson 1979 a,b)

D *Trachyleberis thompsoni* Hornibrook (75 X, 25 kV)

E *Melosira* sp (780 X, 25 kV)

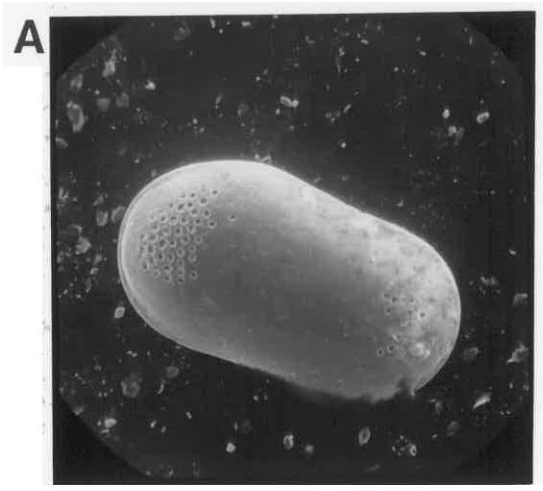
A

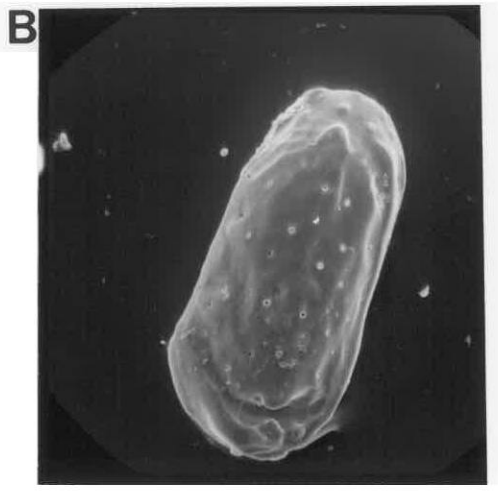
B

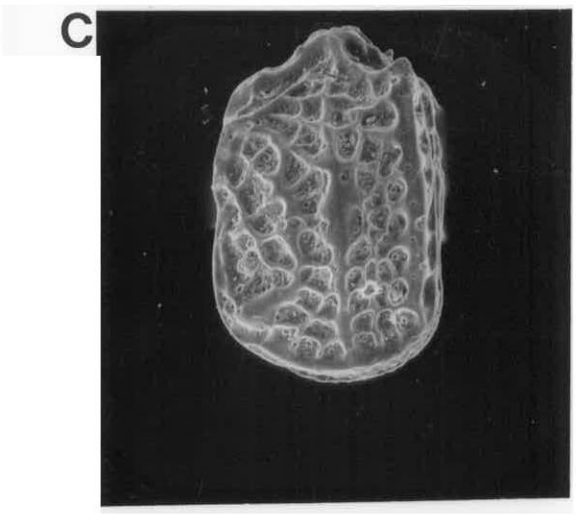
C

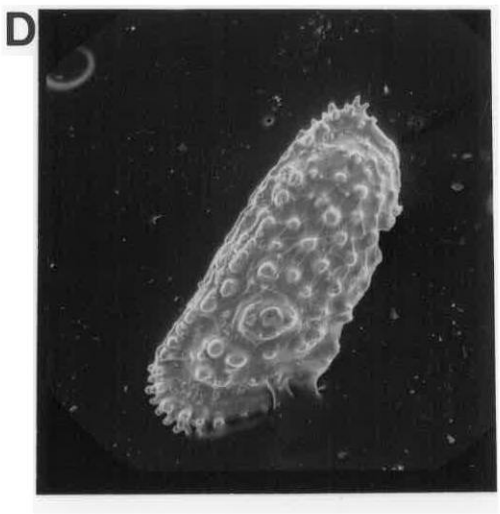
D

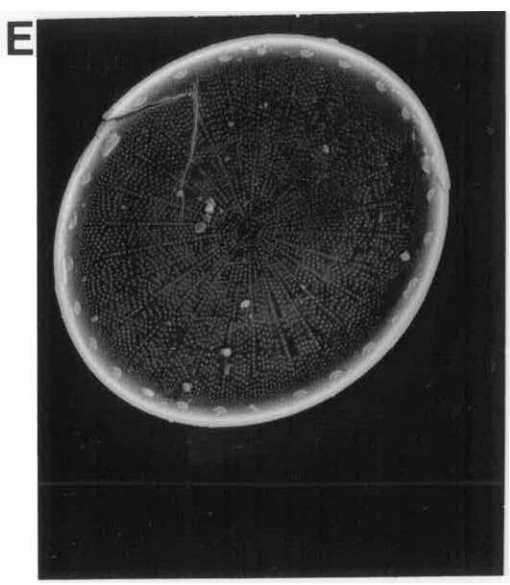
E

widely applied to stratigraphic and paleoenvironmental interpretation, and is particularly useful in shallow marine and freshwater settings where forams become less abundant. Beginning in the Cambrian, the evolutionary history of the ostracods can be followed with completion through to the present, which is unique amoung the crustaceans. The most characteristic feature of their bodies is a bivalved, well calcified and in many cases ornate carapace which fossilises easily and is well preserved in sediments. Most ostracods are 0.1-20 mm in length. The carapace possesses a considerable number of morphological features allowing taxonomic study and analysis of their ecology. Ostracods are widespread geographically. They live in fresh, brackish, saline and hypersaline waters and occur from marginal marine to abyssal depths.

The nature and distribution of New Zealand ostracods is described by Hornibrook (1953) and Swanson (1979). Ostracoda are divided into six groups (orders) based on morphologic variations of the carapace. Most post-Paleozoic to modern taxa are included in the order Podocopida and most New Zealand ostracoda are from the superfamily Cytheradae. Their most characteristic feature, at the familial taxonomic level, is the arrangement of the abductor muscle scars which are located on the internal surface of a well preserved ostracod valve and form a vertical series of four or five scars. The Cytheraceans are the most advanced family of the Podocopids in modern marine ostracod faunas. They are also the ostracod group richest in genera and species.

Ostracods are generally the most abundant microfaunal component of brackish-water sediments and become more abundant than forams as the salinity decreases. The ostracod to foram ratio is an important method in the determination of paleodepths. Substrate is thought to influence the faunal assemblage. Smooth carapace species are usually found in muds, whereas more ornate forms are found in coarser sediments. A number of ostracods are burrowers. Those which burrow into fine-grained substrates usually possess smoother elongate carapaces, whereas those which live in the interstices between grains possess a short, more robust test (Benson 1981).

Ostracods are generally not as abundant as foraminifera in the Firth of Thames sediments, typically forming less than 10% of the microfauna. The faunal assemblage identified in Core 40 is listed and illustrated in Plate 6.2. It is typical of a depth range of less than 50 m, preferring a muddy to muddy-sand substrate and influenced by relatively low energy wave conditions (Swanson 1979). *Cytherella* sp. and *Kotoracythere formosa* (Plate 6.2 A,B) generally occur in muddier sediments, whereas *Munsyella tumida*, *Trachyleberis thompsoni* (Plate 6.2 D) and *Quadracythere truncula* (Plate 6.2 C) are most abundant in gravelly muddy-sand shell layers in Core 40 (Fig. 6.1). The ostracod assemblage identified in the Firth of Thames sediments occurs at depths of less than 20 m which corresponds to the expected range of the living taxa described by Swanson (1979a) for the Otago shelf. Salinity is generally considered the most influential factor in determining the distribution of taxa. The taxa identified in core sediments are expected in salinities ranging from seawater to brackish conditions. The contemporaneous occurrence of the foram *Ammonia beccarri* indicates some form of salinity stratification controlling the distribution of benthic taxa in the Firth of Thames has existed over the late Holocene.

Diatoms

Diatoms (Plate 6.2 E) are photosynthetic single-celled algae that inhabit many aquatic and subaquatic environments. They occur as both solitary or colonial algae and secrete bivalved tests or frustules of opaline silica. They are major primary producers of silica in oceans. Diatoms may be planktonic or sessile. Most are concentric in shape and between 10-100 μm in size and comprise a significant component of the Firth of Thames sediments. The dominant taxa are characterised by circular pill box frustules. Many were observed, by optical microscopy and SEM, aligned in short sections exhibiting the thread-like form of a colony and have been identified as *Melosira* sp. (G. Gibson, pers. commun.). Diatoms are the most abundant microfauna in Cores 21 and Core 40, however a decrease in relative abundance was observed with depth and distance offshore from the Waihou River, suggesting an intimate association with fresh water input. A marked increase in abundance of

diatomaceous sediment up Core 21 probably reflects the increasing influence of freshwater from the Waihou and Piako River mouths as the shoreline prograded northwards during the late Holocene.

6.3 MACROFOSSIL COMPONENTS

A wide variety of bivalves and gastropods have been identified in the core sediments.

Bivalves

The estuarine trough shell *Mactra* (*Cyclomactra*) *ovata ovata* (Plate 6.3 C) and the nut shell *Nucula hartivigiana* are common throughout all mud-dominated sediments, but by far the most abundant bivalve is *Mactra ordinaria* (Plate 6.3 C), recognised as a small trianguarly-ovate shell, which grows up to 13 mm in length. This species appears to be confined to dense in situ shell layers and shell-hash layers, as already discussed, and is most common in sediments of the Firth of Thames mud facies (Cores 31 and 40). Like *M. ovata ovata*, *M. ordinaria* is a filter feeder and may live up to 25 cm below the sea bed. On the other hand *Austrovenus stutchburyi* (Plate 6.3 D), another abundant bivalve in mud sedments, lives at the sediment-water interface and was therefore preferred as a sample for ^{14}C dating.

The green edge mussel, *Perna canaliculus*, and the pipi, *Paphies australis,* as well as *Gari hodgei* (Plate 6.3 A) and *Tawera Spissa* (Plate 6.3B), are most abundant in nearshore sandy sediments and storm-bed shell layers. These species tolerate moderate wave action and are the major bivalve constituents of the nearshore muddy-sand (river mouth) facies (upper section of Core 21) and the sandy delta fan facies (Cores 23 and 37). *P. australe* only occurs in mud-dominated sediments as part of shell-hash layers. *Tawera spissa* (Plate 6.3 B) and *Venerupis largillierti* are members of the Veneridae family and are usually associated with sandy exposed open beach habitats. *Sigapatella novaezelandiae* is also often associated with the former species. They generally occur in coarse sediments adjacent to the delta fans of Tapu and Te Mata where exposure to wave action is higher.

Plate 6.3

Dominant molluscan species identified in core sediments from the Firth of Thames.

A *Gari hodgei*

B Shell hash containing *Tawera spissa* and *Sigapatella novaezealandiae*

C *Mactra (Cyclomactra) ovata ovata* and *Mactra ordinaria*

D *Austrovenus stutchburyi*

E *Xymene plebeius plebeius*

F *Maorioculpus roseus*

G *Penion sulcatus.*

H *Neoguraleas* sp.


A
mm 10

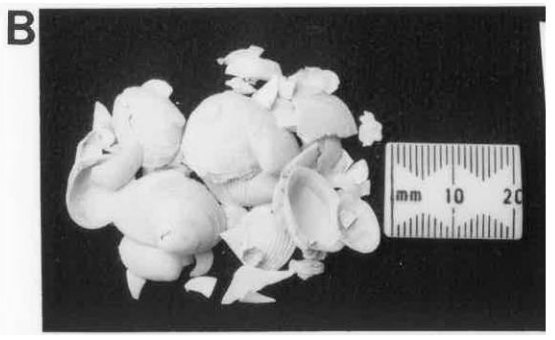
B
mm 10


C
mm 10

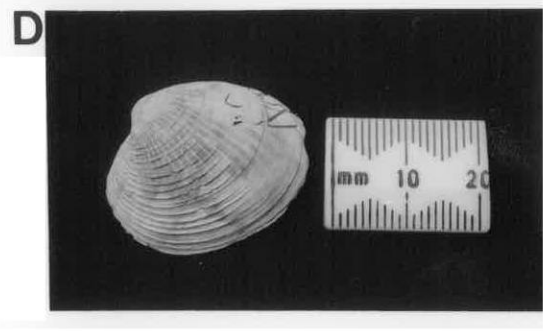
D
mm 10


E
mm 10

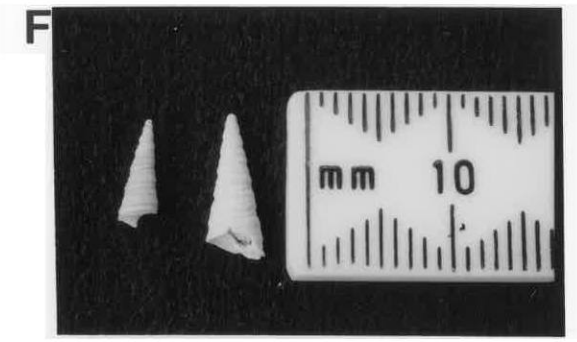
F
mm 10


G
mm 10

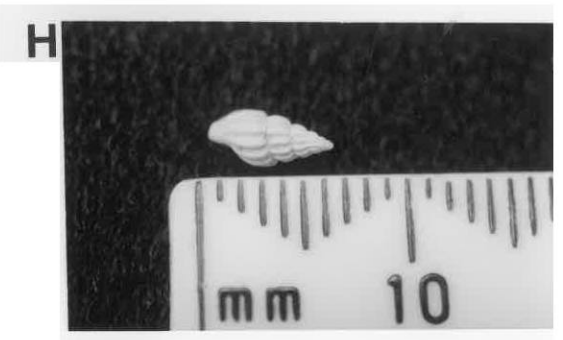
H
mm 10

A down-core transition occurs in the bivalve faunal composition of Core 21, which is related to the coarsening upwards sequence already described. *M. ordinaria*, *M.ovata*, *A. stutchburyi* and *N. hartivigiana* dominate the lower core mud facies, whereas taxa which prefer coarser substrates such as *P. canaliculus*, *P. australe*, *T. spissa* and *G.hodgei* dominate the upper core and surficial sediments.

Gastropods

Most of the gastropods identified in the core sediments are small (< 5 mm) and typical of a shallow marine sheltered mud habitat (Morton and Miller 1972). By far the most abundant species is *Xymeme plebeius* (Plate 6.3 E). *Maorioculpus roseus* (Plate 6.3 F) and the whelk *Cominella adspeisa* and *Neoguraleas* sp. (Plate 6.3 H) commonly occurs in shell-hash layers. *Penion sulcatus* was the only large species identified (Plate 6.3 G).

-CHAPTER SEVEN-

SEDIMENT DIAGENESIS

CHAPTER SEVEN: SEDIMENT DIAGENESIS

7.1 INTRODUCTION

During the analysis of core sediments of Holocene age from the Firth of Thames smectite was found to be a major component of the clay mineral assemblage, comprising up to 55% of the < 2 μm fraction. Crystalline smectite has already also been well documented in the sediments of the southern Firth of Thames and the Waihou River mouth by other workers (Stoffers et al. 1983; Henshaw 1987; Churchman et al. 1988). However, this study demonstrates that smectite is absent the bottom sediments of the major rivers draining into the Firth. Consequently the lack of any adjacent shelf or catchment source suggests the smectite may have a diagenetic origin.

"Bentonite" has been described in many deposits, both from marine sequences onland (Mosseler and Hayes 1966 ; Noh and Boles 1989) and in the marine environment (Mathews 1962; Nayudu 1964; Peterson and Griffen 1964; Biscaye 1965; Andrewsenko et al 1975; Giekes and Kastner 1971; van Rad and Rosch 1973; Melson and Thompson 1973; Hein and Scholl 1978; Hein et al. 1978; Gardner et al 1986). Bentonite is a general term for smectite clay deposits derived from altered volcanic debris (Cole and Shaw 1983). The abundance of smectite in the Firth of Thames sediments does not fall within the range used by Hein and Scholl (1978) to define "true bentonite" (> 75 wt% smectite in the < 2 μm fraction), but it does fall into the category of smectite-rich deposits (50-75 wt% smectite). Here the paragenesis of smectite is related to the alteration of detrital acidic volcanic glass in a mildly reducing, mildly anoxic marine environment.

The aims of this chapter are two-fold. Part A describes: (1) the nature and occurrence of the smectite; (2) a series of analyses of the clay mineralogy; and (3) the origin of the smectite, arguing that it is authigenic and forming as bentonitic muds. In Part B a kinetic weathering model describing the transformation of volcanic glass to smectite in sea water is presented and the rate of diagenetic alteration estimated.

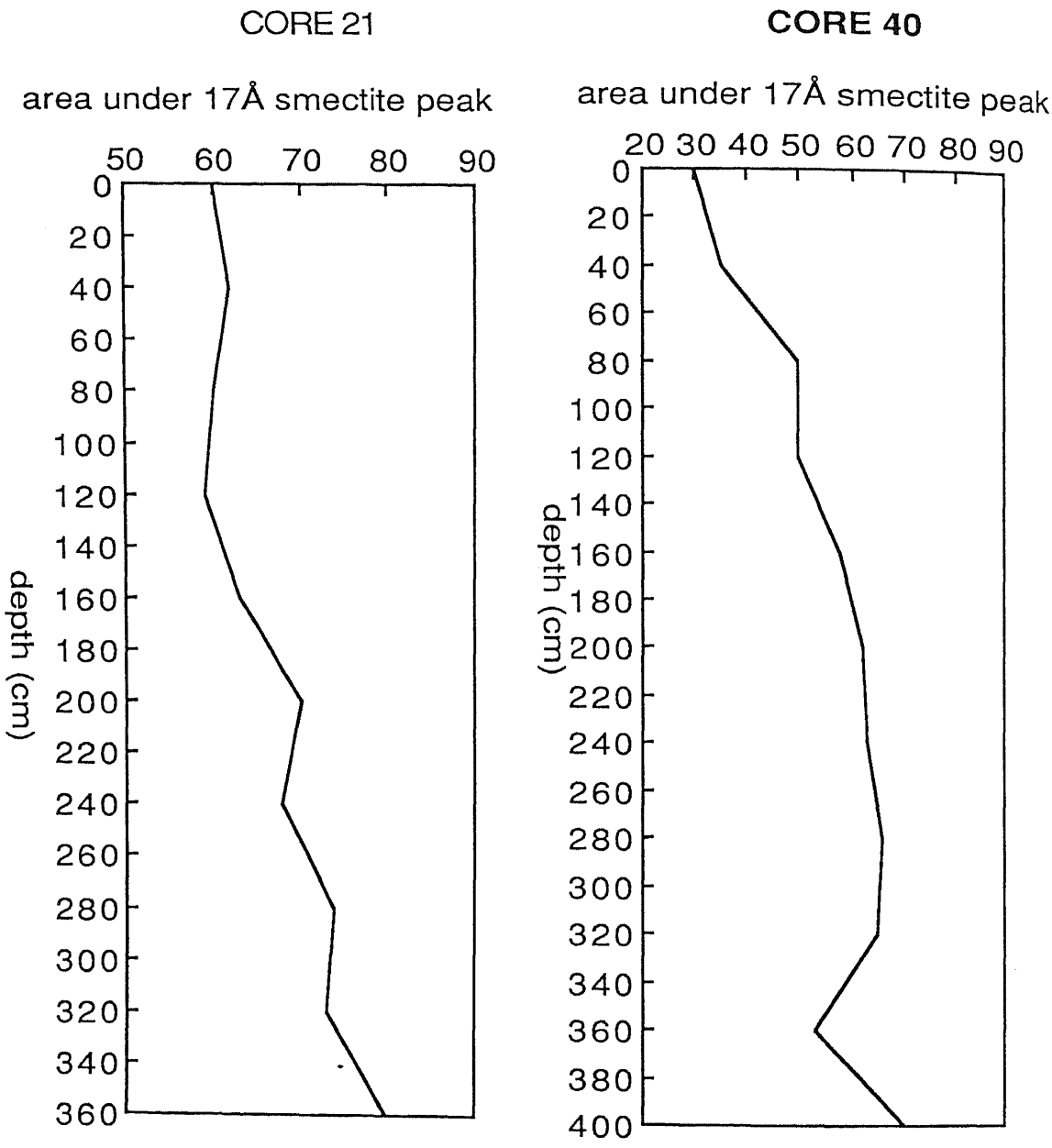

Figure 7.1

Downcore increase in the relative abundance of smectite for Core 21 and 40.

PART A: 7.2 EVIDENCE SUPPORTING A DIAGENETIC ORIGIN FOR SMECTITE

Lateral and vertical anomalies in the distribution of smectite in the Firth of Thames sediments, described in Chapter 5, seem to preclude a detrital origin. A progressive increase in smectite concentration seaward in surficial sediments, shown to correspond to an increasing salinity gradient, seems to suggest diagenetic formation. Furthermore the down-core increase in smectite content and contemporaneous decrease in volcanic glass implies an intimate association may exist between the two "minerals" (Section 5.6). It is unlikely that these vertical variations can be attributed to a gradual change in sediment supply during the late Holocene as it has already been established that the smectite has no adjacent onland source. Moreover, Pocknell et al. (1989) provide evidence from pollen characteristics in a core from the northern Firth of Thames that paleoenvironmental conditions have changed very little during the late Holocene. Consequently, it is proposed that the increase in smectite and subsequent decrease in volcanic glass down Core 31 supports diagenetic processes occurring within the sediments. The observed vertical trends in smectite abundance are not unique to Core 31 as similar trends in the relative abundance of smectite also occur down Cores 21 and 40 (Fig. 7.1).

X-ray diffraction analysis

To investigate further the role of diagenetic processes on smectite formation some additional detailed clay mineral analyses were carried out. Ten sediment samples were taken from cores 21, 31, 37 and 40. These samples were prepared for X-ray diffraction analysis by the same method described in Chapter 4. Four X-ray runs were performed on aliquots of each sample (< 2μm) : (i) an untreated sample; (ii) following ethylene glycolation for 12 hours to test for smectite; (iii) after heating to 100° C for 1hour to test for 10Å halloysite dehydration; (iv) after heating to 500° C for 1 hour to test for dehydration of smectite and for evidence of any chlorites (Hume and Nelson 1982). In addition, suspensions were saturated in 1N KOH for 15 hours and heated to 90° C for 1 hour in order to determine the degree of contraction of the smectite 001 peak owing to K^+ uptake, which can provide information on the likely nature of the source rock (Weaver 1958; Hume and Nelson 1982).

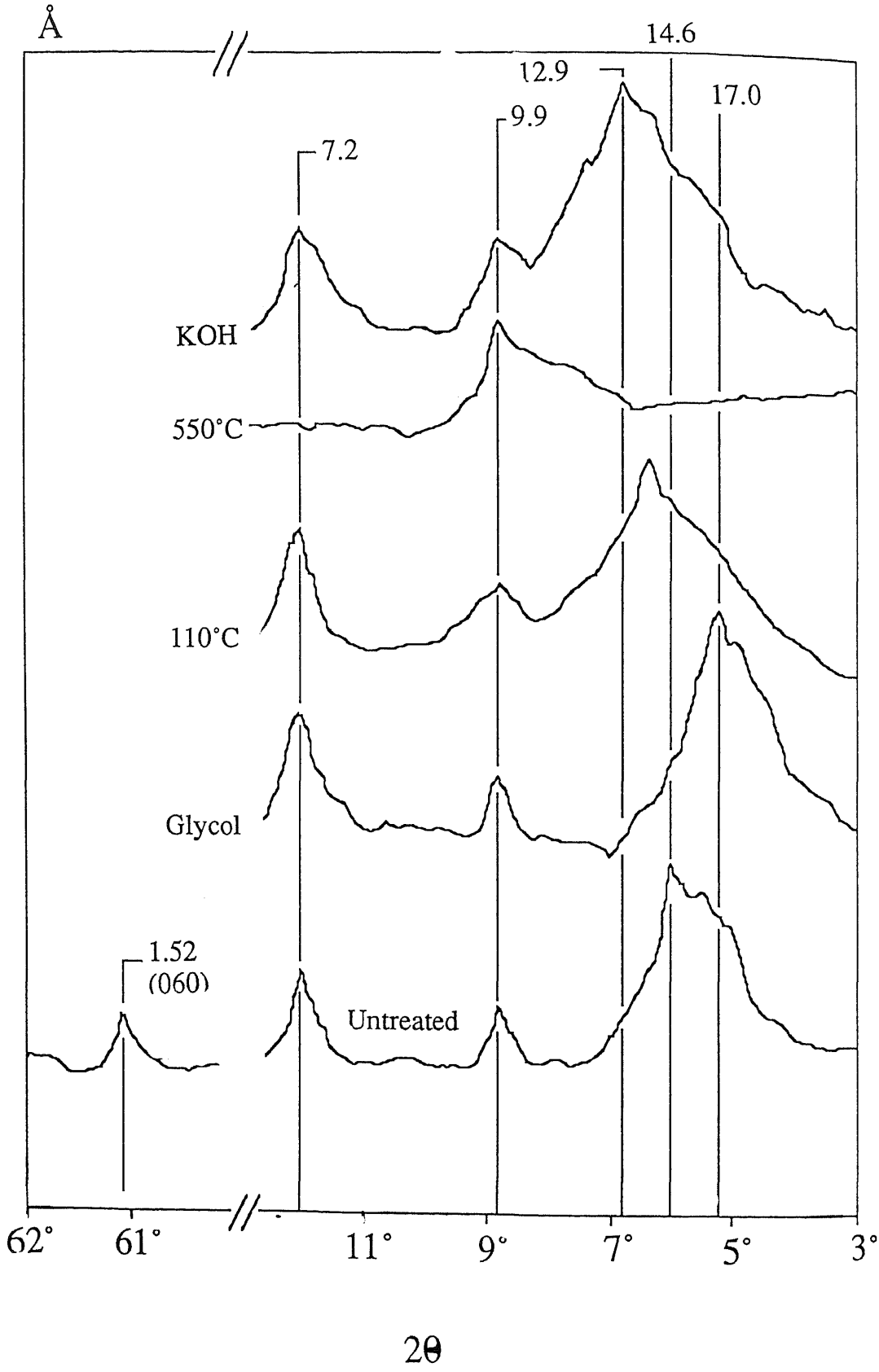

Figure 7.2

X-ray diffractograms of the < 2μm fraction for sample 31.17 following various treatments.

The results of these treatments show that the clay mineralogy of the sediments is very similar for all samples analysed (Fig. 7.2 and 7.3). A broad 001 reflection between 14 Å and 16Å, which expands to 17Å on glycolation and collapses to 9.9Å after heating to 550° C, is indicative of smectite. From the position of the 001 peak it is possible to estimate the type of exchangeable cations present (Weaver 1958; Hume 1978). In Figures 7.2 and 7.3, the untreated peak lies between 14Å and 15Å, which indicates two layers of water present and probably Ca^{2+} and/or Mg^{2+} cations present. The 001 peak exhibited only partial contraction to 12Å-13Å after KOH treatment, which suggests the smectite is derived from a low-charge non-micaceous source, such as volcanic glass. Hume (1978) also noted that smectite that was probably authigenic did not collapse to 10Å when treated with KOH.

The 060 reflection of smectite clay minerals has been used by various workers to determine whether the mineral has a trioctahedral or dioctohedral structure (Melson and Thompson 1973; Gardner et al. 1985). The 060 spacing of 1.52Å in Figure 7.2 supports a dioctahedral structure for the smectite. It should be noted that the 060 reflection was not detectable in all samples owing to the low intensities of the higher order basal reflections.

The crystallinity of smectites can be characterised by the ratio of V/P, where V is the depth measurement of the "valley" on the low-angle side of the glycolated 001 peak and P the height of the peak above background (Biscaye, 1965). The ratio is unity for perfectly crystalline smectite. On the basis of this technique many samples exhibit poor crystallinity and are characterised by very low V/P ratios, particularly in the upper portion of Core 31. Hein and Scholl (1978) describe diffuse or poorly formed 17Å smectite peaks for bentonite-bearing sediments in the upper portion of cores from the Bering Sea. They attribute this to poorly crystalline smectite and suggest that smectite becomes better crystalline with continued alteration.The morphology of smectite peaks in Figure 7.3 indicate poor crystallinity and may be due to the young age of the sediments in the Firth of Thames; however the symmetry of 17Å peak improves with sub-bottom depth.

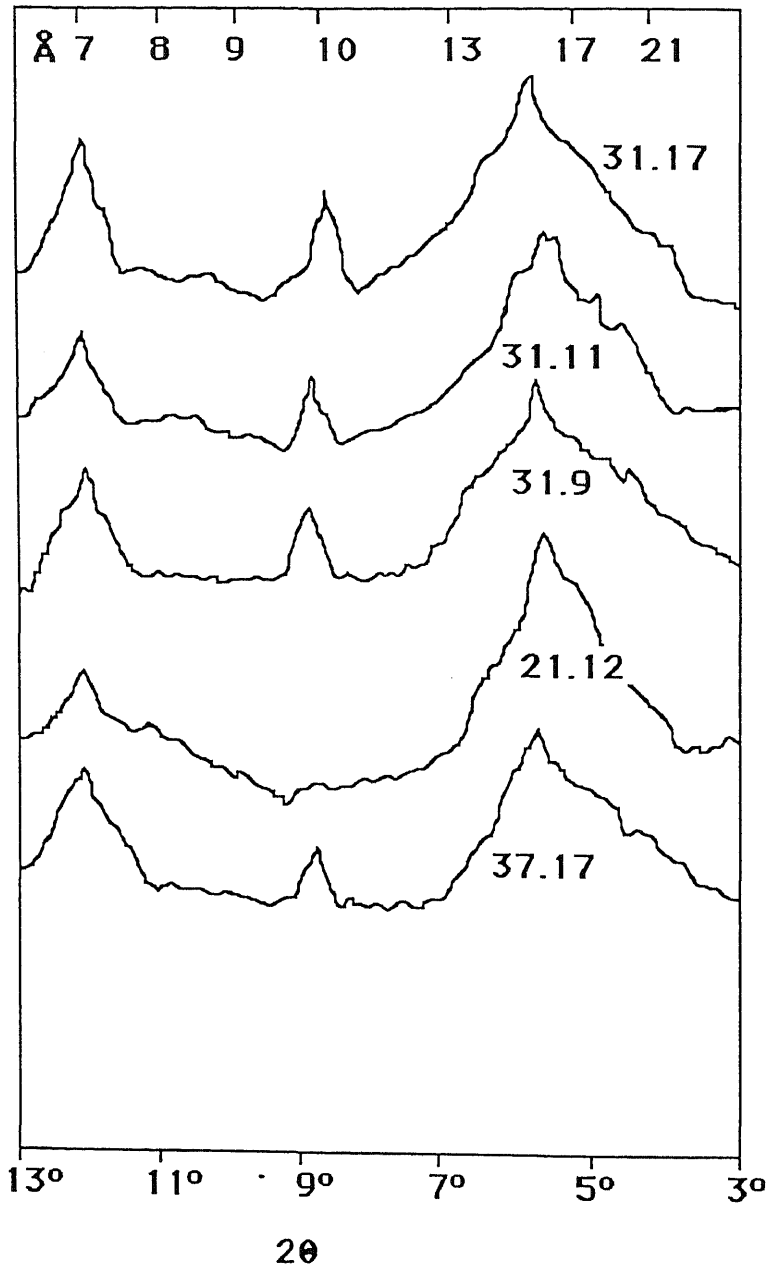

Figure 7.3

X-ray diffractograms of selected < 2μm samples demonstrate the variations in symmetry of the (001) basal smectite peak.

Some minor illite interstratification occurs in some smectites. Evidence for this is the asymmetry of the 001 peak, with smaller superimposed peaks between 14Å and 10Å on the high-angle side. Illite interstratification is a characteristic feature of smectites inherited from a detrital source, although incipient mixed layer illite-smectite is not uncommon in authigenic-volcanogenic smectite. Hein and Scholl (1978) observed up to 15% illite interstratification and suggested that this is a characteristic feature of K-bentonites. Gardner et al. (1985) suggest that mixed layer illite-smectite is formed due to argillisation of volcanic ash material on the sea floor during diagenetic alteration to smectite.

Infrared absorption analysis

Infrared (IR) spectra were recorded in the 4000-450 cm^{-1} region on a *PERKIN ELMER Model 1600 FOURIER TRANSFORM INFRARED SPECTROPHOTOMETER* (Fig. 7.4). Samples (<2 µm) were prepared in the form of KBr discs and were heated to 90° C.

Absorption bands in the 3000-4000 cm^{-1} region are due to OH stretching vibrations and indicate either structural OH groups or absorbed water (Decarreau et al.1985). The broad band at 3410 cm^{-1} is attributed to OH stretching of the remaining interlayer water after heating and has the morphology characteristic of montmorillonitic smectite (Furket and Smidt 1972). Another OH stretching absorption band was noted at 3620 cm^{-1} at a frequency range corresponding to the Al-OH-Mg stretching vibration in montmorillonitic clays (van der Marel and Beutelspacher 1976). The sharp bands at 3698 cm^{-1} and 3640 cm^{-1} are characteristic stretching vibrations of 10Å halloysite. That the 3698 cm^{-1} band is the smaller of the two generally precludes 7Å halloysite, which exhibits similar sized peaks in the OH doublet. It has been well documented by various authors that admixtures of several different aluminosilicate minerals results in overprinting of key absorption bands (Fig. 7.4), as the difference in vibrational frequencies may be very subtle. Montmorillonite spectra may be defiled by small amounts of kaolinite, halloysite or allophane (van der Marel and Beutelspacher 1976). Samples containing only 2% halloysite may exhibit strong halloysite absorption bands (Stevens and Vucetich 1986) making positive

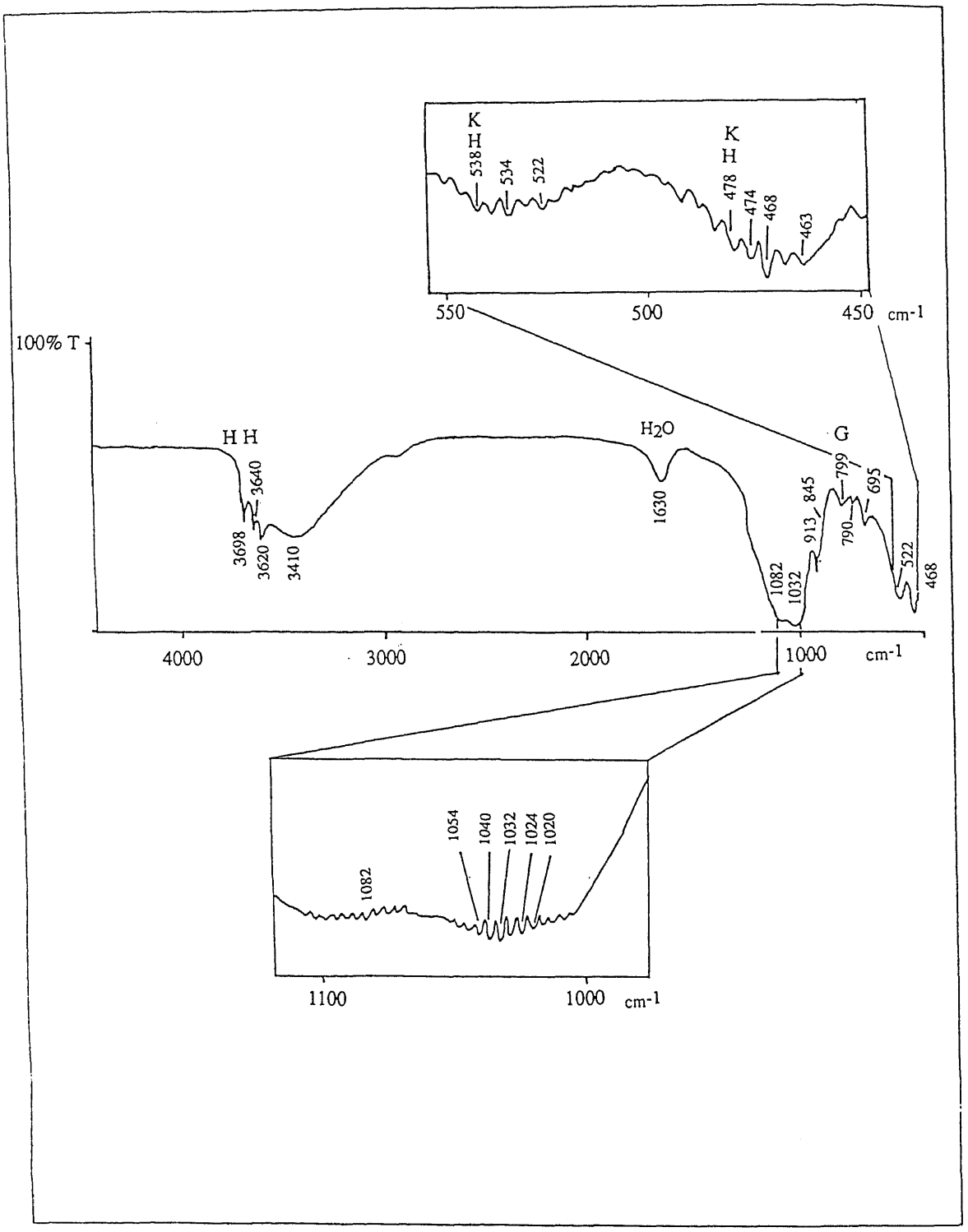

Figure 7.4

Infrared spectrum from 4000-450 cm^{-1} region for sample 31.17 (< 2 μm). The spectrum is characteristic of smectite with minor overprinting by halloysite (H), kaolinite (K) and glass (G) absorption bands.

identification of smectite difficult. An absorption band due to HOH deformation of absorbed water appears at 1630 cm^{-1}. Broad characteristic Si-O-Al stretching vibrations for montmorillonitic smectite occur at 1082 cm^{-1} and 1032 cm^{-1}. These bands may also be partly due to SiOH-AlOH deformation frequencies. Absorption bands at 790 cm^{-1}, 522 cm^{-1}, 468 cm^{-1} and 913 cm^{-1} with a shoulder at 845 cm^{-1} are characteristic bending frequencies for montmorillonitc smectite. Volcanic glass, with its diagnostic 800 cm^{-1} absorption band, probably overprints the 967 cm^{-1} smectite band. Absorption bands at 538 cm^{-1} and 478 cm^{-1} are probably due to halloysite and/or kaolinite overprinting. The IR spectra in Fig. 7.4 is characteristic of montmorillonitic smectite (dioctahedral smectite), with overprinting from halloysite , minor kaolinite and volcanic glass.

Scanning electron microscopy

Scanning electron micrographs (Plate 7.1) of smectite-rich clay exhibit authigenic smectite in various stages of formation, each characterised by distinctive growth features. Initially, as alteration begins, blebs and web-like arrays of smectite are observed on the grain surface This early formed smectite probably accounts for the asymmetry of the 17Å peak. Smectite becomes better crystallised and more highly developed with sub-bottom depth as diagenesis proceeds and occurs as crenulated honey comb-like flakes and sheets (Plate 7.1 A and B). Glass shards from the lower portion of Core 31 exhibited a rounded morphology. In most cases the conchoidal habit of the shards has been destroyed and thick clay coatings have formed on the surface, indicating increased smectite formation with depth down Core 31 (Plate 7.1).

7.3 DISCUSSION

The ability of volcanic glass dispersed in deep sea sediments to alter to smectite clay minerals is much debated in the literature and still poorly understood. The indisputable association of smectite with volcanic glass in deep sea sediments was first demonstrated by Peterson and Griffen (1964) for surficial

Plate 7.1

A Authigenic smectite coating a glass shard (sample 31.19).

B Crenulated flakes of smectite on the surface of A.

C A glass shard from surficial sediments of Core 31 exhibiting possible dissolution pits and vesicles (sample 31.1).

D Highly altered glass from the base of Core 31 completely encrusted with smectite (sample 31.21).

A

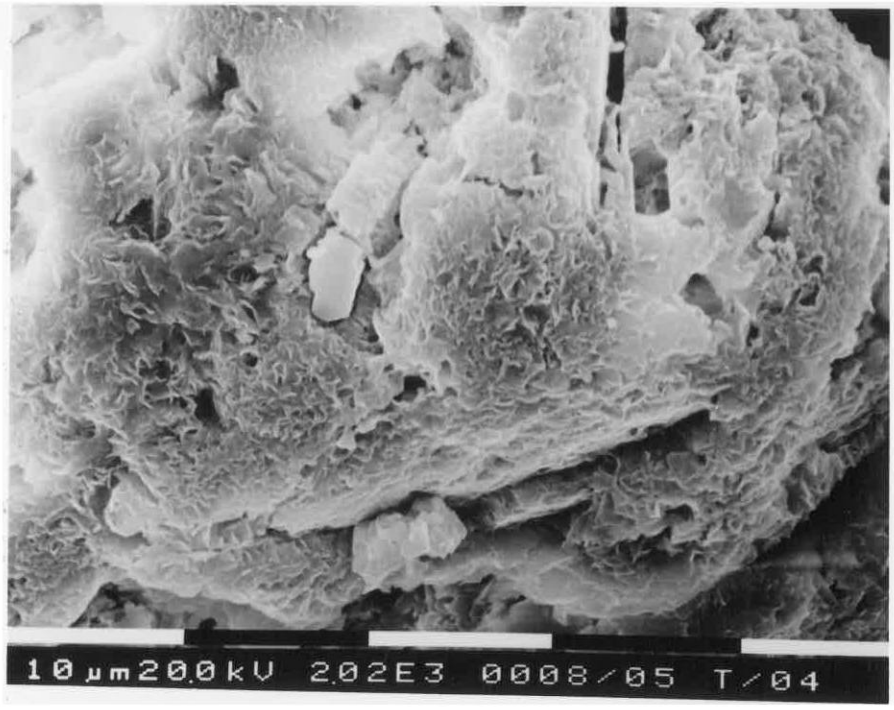

B

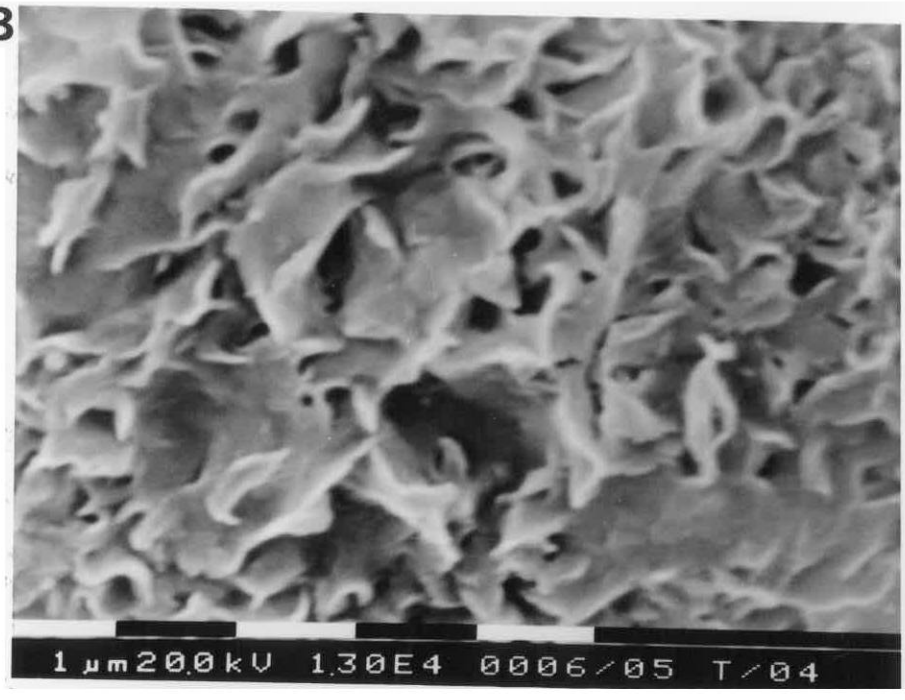

C

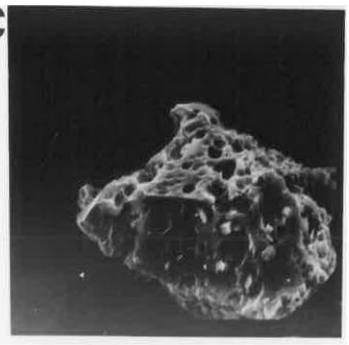

D

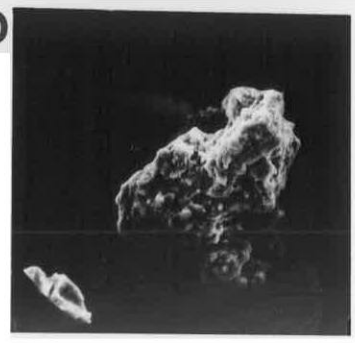

deposits of the southeastern Pacific Ocean, where basic volcanic debris was generally associated with abundant plagioclase and large proportions of smectite. Also noted was the close association of acidic volcanic detritus with smectite and potash feldspar. In both cases feldspars were assumed to have originated from a detrital source. Although the occurrence of marine bentonites forming from the alteration of volcanic detritus is widely accepted, the mechanisms of bentonite formation are poorly understood. Furthermore, bentonites actively forming in modern volcanogenic marine sediments have seldom been recognised or described.

An early diagenetic formation of smectite is described in Chamley (1971) and Keller et al. (1978) for a series of volcanic-rich oozes deposited near the Santorini archipelago, that collapsed into the eastern Mediterranean Sea about 3400 years B.P. A 7.2 m core sampled in about 280 m water depth exhibited a rapid downward increase in the abundance of smectite and contemporaneous decrease in the abundance of diatom frustules and volcanic debris. With increased depth the abundance and crystallinity of the smectite was noted to improve. Many similarities exist between this Mediterranean study and diagenetic features described for bentonites forming in the Firth of Thames. Hein and Scholl (1978a,b) describe the formation of bentonite beds from the alteration of volcanic material in late Cenozoic sediments from the southern Bering Sea and the Aleutian Ridge arc volcanics, respectively. The occurrence of " pale green laminae" in sediment from DSDP cores from the Lord Howe Rise is interpreted by Gardner et al. (1985) as evidence for the alteration of discrete ash layers. Hume and Nelson (1985) invoke a diagenetic origin to explain the occurrence of smectite in volcaniclastic sediments on the western North Island shelf.

The role of dissolved silica from diatoms in promoting diagenesis of glass is an active topic of debate. Chamley (1990) suggests that dissolved silica in interstitial waters provided from the rapid dissolution of diatomaceous material may preferentially promote the alteration of glass to smectite. Alternatively, Gardner et al. (1985) suggest low concentrations of dissolved silica in pore waters may promote the congruent dissolution of volcanic glass. However, factors such as sedimentation rates, pH and salinity may also have a profound effect on the rate of alteration. A gradual decrease of

diatomaceous material down Cores 21 and 40 described in Chapter 6 is considered to be related to water salinity and the increasing proximity of the Waihou River mouth during the late Holocene, and may also play a role in smectite formation. Volcanic glass may devitrify to palagonite (Peterson and Griffen 1964; Nayadu 1964) or incongruently dissolve to yield smectite and zeolites (Peterson and Griffen 1964; von Rad and Rosch 1972; Bonatti 1972; Noh and Boles 1989). The paragenesis from glass via smectite to alkali zeolites is considered the most likely weathering sequence of volcanic glass in most bentonitic deposits that have undergone significant burial and experienced increases in temperature and pressure.

Authigenic smectites exhibit distinctive mineralogical properties which distinguish them from detrital smectites (Hein and Scholl 1978). The recognition of these properties has been an essential part of this study. Several charcteristics of marine sediments rich in authigenic-volcanogenic smectite have been described: (i) high variability in clay mineral percentages (i.e. an incraese from 13%-55% of < 2 μm fraction downward); (ii) sections within the sediment containing more than 50% smectite; (iii) a general deviation from the typical detrital clay mineral suite of the area; (iv) the presence of only a few illite layers (< 15 %) interlayered with authigenic smectite. In contrast detrital smectite has typically up to 50% illite layers. Perry et al. (1976) have used this criteria successfully to distinguish detrital marine from authigenic-volcanogenic smectite; (v) smectite in the early stages of alteration tends to exhibit poor crystallinity. This is evident in the morphology of the 17 Å smectite peak. The symmetry of the 17Å tends to improve as diagenesis proceeds; (vi) Under SEM authigenic smectite exhibits distinctive growth features. Web-like blebs occur on the surface of glass shards which become highly wrinkled, honey comb-like flakes and sheets with continued alteration (Hein and Scholl 1978).

The abundance of smectite in sediment samples (up to 55% of the < 2μm fraction) is well within the range used by Hein and Scholl (1978) to identify smectite-rich deposits. It is unlikely that the abundance of smectite in the Firth of Thames sediments will exceed 60% assuming the degree of authigenic smectite formation is dependent on the supply of volcanic glass to the system. It has been demonstrated that the abundance of volcanic glass entering the Firth is generally 55-60 % by weight of

the total sediment. The other detrital material remains unaltered within the Firth of Thames sediments and shows little downward variation.

PART B 7.4 A PROPOSED KINETIC WEATHERING MODEL FOR THE TRANSFORMATION OF VOLCANIC GLASS TO SMECTITE

The results from the detailed mineralogical analysis previously described for Core 31 demonstrate: i) that the concentration of volcanic glass progressively declines with depth down-core and hence over time; ii) there is a contemporaneous increase in smectite abundance over time; and iii) that the concentrations of smectite and glass are intimately related and are the result of the diagenetic alteration of volcanic glass to yield smectite. The aim of this section is to consider the stability of glass and smectite in sea water. A vertical time scale for Core 31 is defined using radiocarbon ages. By allowing for variations in the rate of sediment accumulation a kinetic weathering model that describes the rate of glass transformation to smectite is presented. Rate constants and half lives of weathering are determined for the dissolution of glass and the precipitation of smectite, respectively.

Stability and thermodynamic considerations

It is possible to construct a composition-type phase diagram of the relationship between smectite, imogolite, feldspar, allophane, and zeolite following a semi-quantitative topological procedure. Topology gives geometric phase relationships (Garrels and Mc Kenzie 1982) and is a useful technique if the free energy of formation data for a mineral is lacking (i.e. volcanic glass). In this approach the molar proportions of Na_2O and SiO_2 (Table 7.1) are scaled relative Al_2O_3 (Fig. 7.5). Tie lines are drawn between phases. Other phase relationships are indicated and help to constrain the phase diagram, however other choices of tie-lines may be equally as valid. Tie lines cannot cross as this would violate the phase rule. The lines drawn normal to the tie lines have the same slope as the phase boundary. A phase diagram is then constructed by plotting $\log a_{Na^+} + pH$ vs $\log a_{H_4SiO_4}$ (Fig. 7.6). In general the topological approach does not represent the actual sizes of the individual fields or the numerical

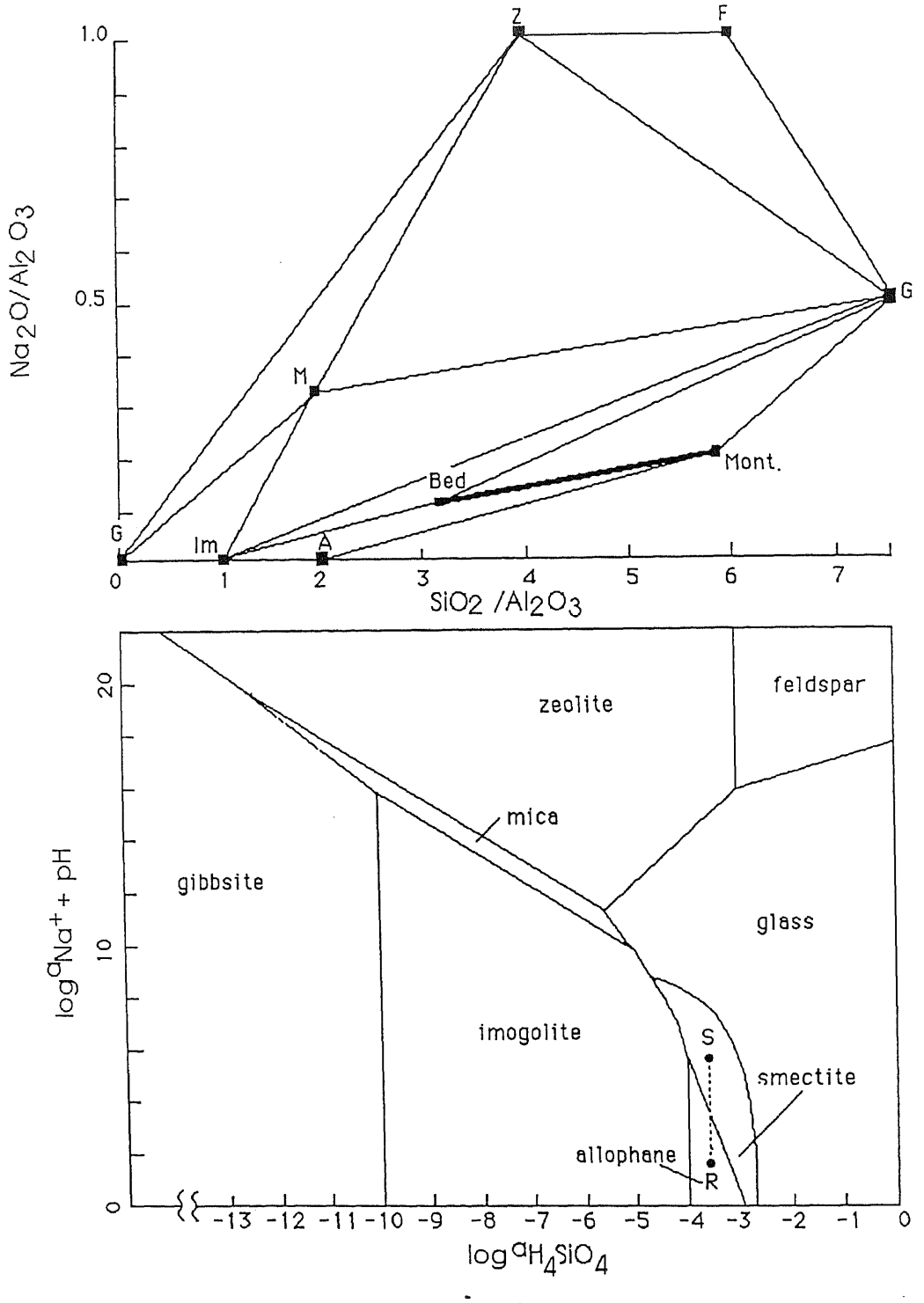

Figure 7.5

Plot of the mole proportion Na_2O and SiO_2 scaled relative to Al_2O_3 for mineral phases known to occur in the Firth of Thames.

Figure 7.6

The phase diagram representing the diagenetic weathering environment in the Firth of Thames is constructed from Figure 7.5 and boundaries quantified for the mineral compositions in Table 7.1 (discussed in text). The composition of sea water (S) and river water (R) are also plotted on the diagram and demonstrate that the formation of smectite is favoured by an increase in salinity.

position of the phase boundary axes accurately, although the geometric relationships between various phases are valid.

The phase diagram can be constrained by quantifying the phase boundaries by calculating the change in Gibb's free energy of formation (ΔG) for reactions involving mineral phases considered to be present (Table 7.1), but there remains the problem of which phases are actually present to constrain the diagram adequately.

Table 7.1
Chemical compositions and corresponding molar ratios of mineral phases used to construct Figure 7.5 and the phase diagram in Figure 7.6.

MINERAL	Na_2O/Al_2O_3	SiO_2/Al_2O_3
Analcime: $NaAlSi_2O_6.H_20$ [$1/2Na_2O.\ 1/2Al_2O_3.\ 2SiO_2.\ H_2O$]	1.0	4.0
Feldspar: $NaAlSi_3O_8$ [$1/2Na_2O.\ 1/2Al_2O_3.\ 3SiO_2$]	1.0	6.0
Imogolite: $Al_2SiO_3\ (OH)_4$ [$Al_2O_3.\ SiO_2.\ 2H2O$]	0	1.0
Montmorillonite $Si_8Al_{3.34}Mg_{0.66}\ (1/2Ca,\ Na)_{0.66}O_{20}\ (OH)_4$	0.2	4.8
Beidellite $Si_{7.34}Al_{4.66}\ (1/2Ca,Na)_2O_{0.66}(OH)_4$	0.4	3.2
Paragonite (Na-mica): $NaAl_3Si_3O_{10}\ (OH)_4$ [$1/2Na_2O.\ 3/2Al_2O_3.\ 3SiO_2.\ H_2O$]	0.3	2.0
Glass (Hodder 1985)	0.5	7.6

An assumption is made for the the composition of some of the mineral phases plotted on Figure 7. 6. An average value for the molar ratios of Na_2O/Al_2O_3 and SiO_2/Al_2O_3 typical of rhyolitic volcanic glass is used (Hodder 1985). A dioctohedral structure for smectite has already been established (Section 7.2) and therfore a composition ranging from beidillite to montmorillonite is considered valid. Evidence supporting a montmorillonitic composition is discussed in Section 7.5 and uses the nature of the basal spacing of the 001 reflection to suggest the presence of larger interlayer cations such as

Ca^{2+} and Mg^{2+}. The glass-smectite phase boundary can be somewhat constrained if glass is assumed to be in equilibrium with amorphous silica. In a soil solution amorphous silica saturation is $10^{-2.8}$ M, thus allowing a line to be plotted at $a_{H_4SiO_4} = -2.8$ which intersects the glass-smectite phase boundary. The phase diagram can be further constrained given that low-grade metamorphism of glass (Hawkins 1981) and dissolution of glass in the marine environment (Hein and Scholl 1978) can form zeolites. A tie line is assumed between glass and zeolite precluding feldspar to smectite. Compositions of the mineral phases are presented in Table 7.1. Figure 7.7 illustrates the procedure and thermodynamic calculations used to quantify the phase boundaries.

$$H_4SiO_4 + \underset{\text{Imogolite}}{Al_2SiO_3(OH)_4} \dashrightarrow \underset{\text{Allophane}}{Al_2Si_2O_5(OH)_4} + 2H_2O$$

$$\Delta G = G^\circ_{\text{allophane}} + 2G^\circ_{H_2O} + G^\circ_{H_4SiO_4} + G^\circ_{\text{imogolite}}$$
$$= (-905.61) + 2(-56.69) + 312.6 + 700.91$$
$$= -5.48 \text{ k cal mol}^{-1}$$

$$\log K = -\Delta G^\circ/RT = 5.48/1.364 = 4.02$$
$$= \underline{4.02 = -\log a_{H_4SiO_4}}$$

Therefore in Figure 7.6 $\log a_{H_4SiO_4} = 4.02$

Figure 7.7 Example of the procedure followed to calculate phases boundaries in Figure 7.6. In this example the imogolite-allophane phase boundary is quantified.

Rhyolitic glass is known to weather to allophane and imogolite in soil-forming conditions in about 3000 years.Clearly, Figure 7.6 suggests the dissolution of glass to form smectite precludes the formation of allophane. Mineral phases imogolite, allophane and halloysite are therefore considered artefacts of pre-depositional weathering of rhyolitic glass onland. This is further reinforced as no marked changes in the down-core abundance of these minerals has been found (Section 5.6). Furthermore the effective time for weathering of volcanic glass to halloysite via allophane and imogolite is 10,000-15,000 years (Birrell and Pullar 1973; Kirkman 1975). Given that the Firth of Thames sediments in Core 31 are younger than c3000 y B.P it is also unlikely that halloysite is forming post-depositionally.

From the phase diagram presented, smectite formation from the dissolution of volcanic glass is clearly favoured if the Na^+ ion activity of the interstitial water plots between that of sea water and river water (Fig. 7.9). Thus for glass dissolution smectite is the stable clay mineral in sea water, but allophane is the stable clay mineral expected with decreased salinity. This evidence supports the intimate association between the concentration of smectite in surficial sediments and salinity as discussed in Chapter 5, as it has already been suggested that the Firth of Thames may exhibit some form of salinity stratification, and it is considered that fresh water input is generally only locally significant near the mouth of the Waihou River (C. van Leeuwe , pers. commun.) where smectite concentrations are lower.

Summary of previous glass dissolution studies

Experimental laboratory dissolution studies of natural and synthetic glasses and crystalline layer silicate minerals have provided important information on the mobility and solubility of various chemical species, and have implied mechanisms for the weathering of glasses under soil-forming conditions (Berner 1978; White et al.1980; White and Claassen 1980) and in the marine environment (Lerman et al. 1975). Green (1987) provides a detailed review of many of these studies. In summary, the dissolution of glass is considered to involve an initial rapid surface exchange between aqueous hydrogen ions and cations at or near the solid/solution interface and has been demonstrated to display first order kinetics (White 1980). Subsequently, as this process approaches equilibrium with time, a slower diffusion of ions in and out of the solid becomes the rate controlling factor. This second process follows a parabolic rate law (White et al.1980).

The incongruent dissolution of glass described by parabolic kinetics implies the development of an intermediate phase, generally in the form of a hydrated surface rim through which chemical species migrate via diffusion (Lerman et al. 1975; White 1979; White and Claasson 1980). Under natural soil weathering conditions diffusion is considered to occur initially by the sorption of atmospheric water at the glass surface resulting in formation of a hydrated rim. Hodder (1985) outlines a kinetic model that

incorporates a parabolic dissolution coupled with a first order reaction to clay minerals which describes the hydration and weathering of volcanic glass. A similar model is also outlined by Murphy et al. (1986).

Most previous work has described the weathering of glass under laboratory conditions or considers the weathering of glass during soil-forming conditions. Wheather or not glass dissolution under marine conditions can be described by the same models is a question this study aims to answer. Lerman et al. (1975) show that the weathering of aluminosilicates in sea water can be described using a coupled parabolic-first order kinetic model. However, over longer durations (years) they suggest dissolution can be adequately described by first order kinetics.

Assumptions

For the following kineitic model to be valid the following assumptions are made and justified.

The diagenetic weathering of glass to yield smectite in marine sediments of the Firth of Thames has been well established from mineralogical analyses on Core 31 and is supported by theoretical thermodynamic and stability criteria previously discussed. These previous investigations indicate that the sole weathering product due to glass dissolution is smectite, despite the presence of small amounts of halloysite, allophane, illite, and kaolinite. Therefore, it is assumed that the concentration of smectite (C_S) plus the concentration of glass (C_g) at any given time must be equal to the initial concentration of glass prior to weathering (C_o) and in the following discussion concentrations will be represented by:

$C'_S = C_S / (C_g + C_S)$ for smectite and $C'_g = C_g / (C_g + C_S)$ for glass
where C'_S at $t_\infty = 1.0$ and C'_g at $t_\infty = 0$.

The ratios C'_g and C'_S are used to construct plots of concentration vs ln t for smectite and glass described in the next section. It is the same as C/C_o, a ratio used in many kinetic studies to describe the concentrations of various phases. C_g is the total glass determined by mineralogical analysis and includes hydrated glass at the grain surface and undissolved glass remaining at any given age/depth

down Core 31. In the following model C_{Σ} is used in a sequential kinetic model equation to represent total glass and is the same as C_g.

From bulk density calculations presented in Appendix 1 it is assumed that compaction of the sediment has been minimal, a reasonable assumptionand given the young age of the core sediments and their high water content. Compaction was not considered significant in a study of late Holocene mud-dominated core sediments from the Baltic Sea by Healy et al. (1987).

Sedimentation rates were calculated for a number of cores spaced evenly over the study area. These data are presented and discussed in Chapter 8. It is clear that rates of accumulation have not been constant over the late Holocene. Two major periods of sedimentation are recognised for all cores with the exception of Core 31, from which only one radiocarbon date was obtained owing to the lack of suitable shell material for dating. From 3500 y BP-1200 y B.P sedimentation rates are between 2-3 mm/y and from 1200 y B.P to present approximately 1 mm/y. It is assumed that similar conditions of sediment accumulation occurred for Core 31 and by using a radiocarbon age of 2700 y B.P obtained from shell material at 4.6 m depth and taking into account sediment accumulation rates during the late Holocene a vertical time scale for Core 31 was constructed (Table 7.2).

Kinetics of volcanic glass dissolution and smectite precipitation

Ruxton (1968) investigated the weathering of radiocarbon-dated dacitic tephras in Papua New Guinea. By assuming Al_2O_3 remained constant during weathering and that any clay mineral formation resulted from weathering of volcanic glass the loss of glass by dissolution as a function of time was shown to proceed by a first order reaction. Consequently the formation of precipitated clay minerals may also be described by a first order rate law.

$$C = C_0 e^{-kt} \qquad \text{Equation (1)}$$

Figure 7.8

A plot of concentration of smectite (Cs) vs ln t (t=years) for data from Core 31 (discussed in text).

Figure 7.9

A plot of concentration of glass (Cg) vs ln t (t=years) for data from Core 31 (discussed in text).

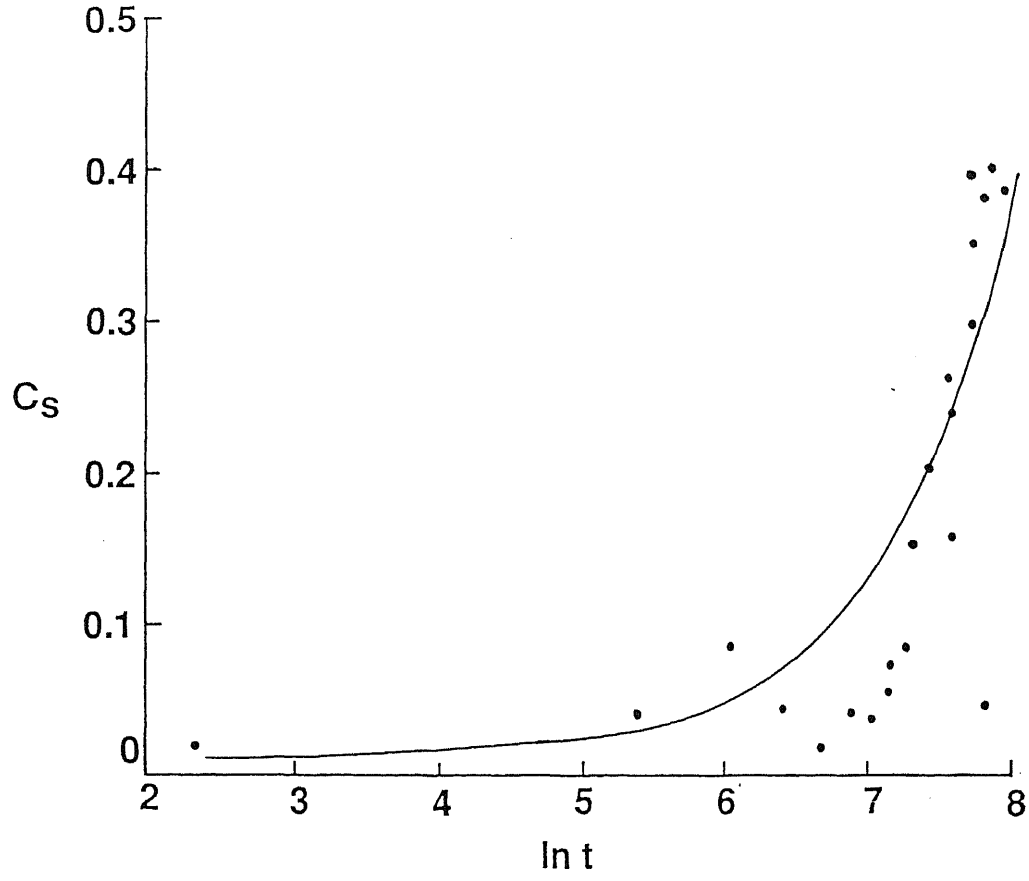
0.5
0.4
0.3
C_S
0.2
0.1
0
2
3
4
5
6
7
8
ln t

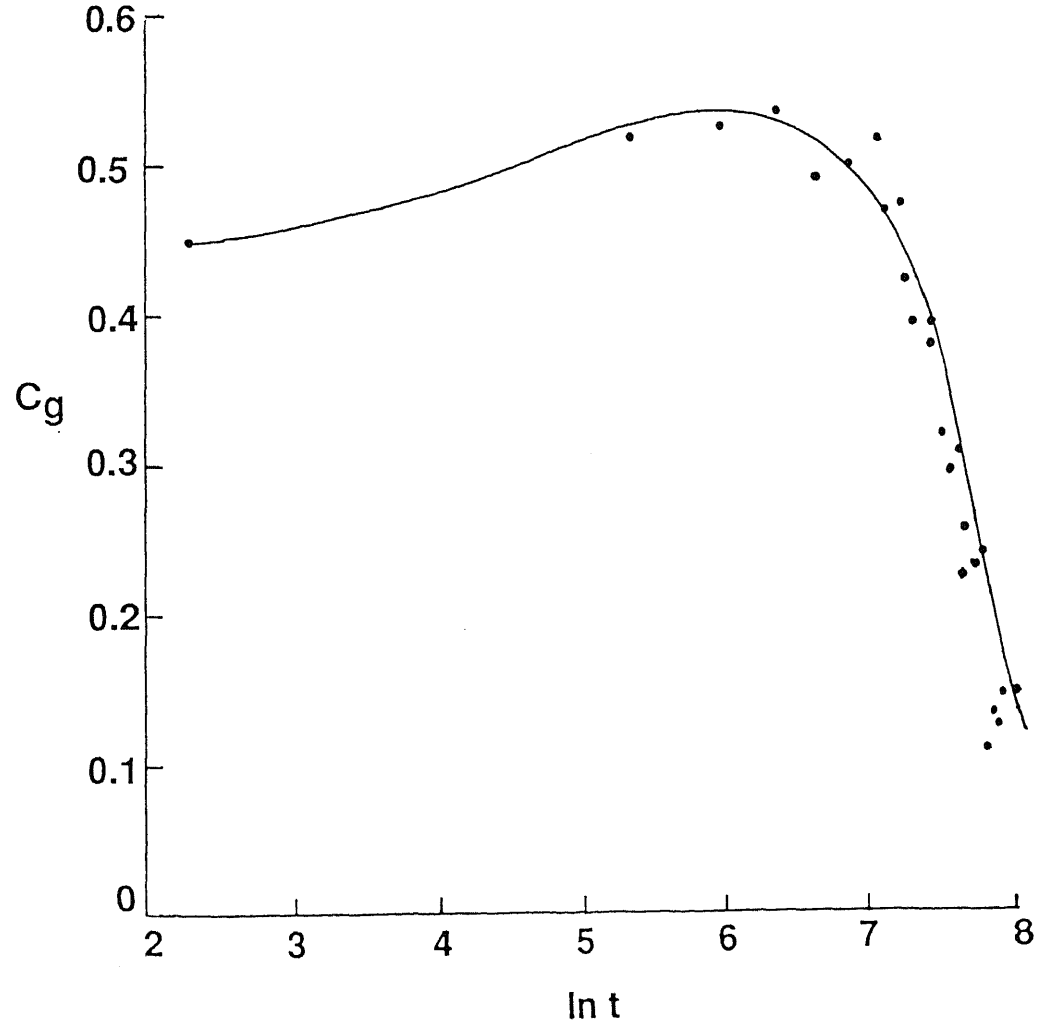
0.6
0.5
0.4
C_g
0.3
0.2
0.1
0
2
3
4
5
6
7
8
ln t

where C = concentration of glass at time (t)

C_o = original concentration of glass at time (t=0)

k = first order rate constant

e = base of the natural logarithm

t = time for weathering.

In Figure 7.8 a plot of C_s v ln t for data from Core 31 approximates an exponential curve. A good fit of data points was achieved with a regression correlation of R = 0.826. A first order rate constant of $4.63 \times 10^{-4} y^{-1}$ was calculated. Clearly the formation of smectite can be described by first order kinetics and yields a half life of formation of $t_{1/2}$ =1475 years determined by equation (1). In Figure 7.9 a plot of Cg v ln t for Core 31 data exhibits a more complex curve and suggests that the dissolution of glass cannot be described solely by first order rate law. However, the correlation improves for greater values of ln t suggesting that over prolonged periods of time (> 1000 years) dissolution may approach first order rate law. As discussed earlier, investigations into the laboratory dissolution of glass (White et al. 1980; White and Claassen 1980; White 1983) indicate that the initial stages of glass dissolution may in fact obey a parabolic rate law:

$$dC/dt = k_p t^{-1/2} \qquad \text{Equation (2)}$$

where, k_p = the parabolic rate constant.

In Figure 7.9 the the plot of Cg v ln t for Core 31 data exhibits a poor correlation with higher order parabolic curves. Poor fit of the Firth of Thames data to a parabolic function suggests that glass dissolution cannot be described solely by parabolic rate law either, although for lower ln t values there is an improved correlation.

Lerman et al. (1979) noted that neither parabolic nor linear forms of kinetics could satisfactorily describe the dissolution of glass, "as over long periods of time such reaction mechanisms may lead to physically impossible conditions of either total dissolution or an infinitely high solution concentration". A coupled kinetic model applied to the incongruent dissolution of silicate minerals in natural seawater is described by Lerman et al. (1975) and is given by the following equation:

$$dc/dt = k_p t^{-1/2} + k_1 (C_{ss} - C) \qquad \text{Equation (3)}$$

where C_{SS} = concentration at steady state.

This equation can be interpreted as a parabolic dissolution of the solid phase ($K_p t^{1/2}$) and a subsequent first order precipitation of another phase (smectite) $k_1(C_{SS}-C)$. The differential equation (3) can be integrated to give equation (4) which represents the dissolution of glass and the subsequent precipitation of a secondary mineral phase via an intermediate hydrated phase.

$$C = C_{ss} + (C_o - C_{ss})\, e^{-kt} + \beta \{Di\ (kt)^{1/2}\} \qquad \text{Equation (4)}$$

where $\beta = \{2k_p/k_1^{1/2}\}$ Equation (4a)

and $Di\ (kt)^{1/2}$ is Dawson's Integral and is evaluated using tables in Lerman (1979).

Hodder (1985) demonstrates that if the concentration of hydrated glass is initially zero ($C_{o\ (hyd)} = 0$) then equation (4) can be expressed as,

$$C = C_{ss} + (1 - e^{-kt}) + \{2k_p/k_1^{1/2}.C_{ss}\}\ \{Di\ (kt)^{1/2}\} \qquad \text{Equation (5)}$$

Furthermore, if the steady state concentration of glass $C_{ss} = 0$ at $t_\infty = 0$ (i.e. all the hydrated glass has been dissolved completely and consequently precipitated as smectite) and $C_{o\ (hyd)} = 0$, then the concentration of hydrated glass can be described by the following equation:

$$C_{(hyd)} = ß\ (Di\ (kt)^{1/2}) \qquad \text{Equation (6)}$$

Therefore the total glass concentration (C_Σ) is the sum the hydrated glass given by equation (6) and the glass remaining given by equation (1), and can be combined to give the sequential equation (7).

$$C_\Sigma = C_o e^{-kt} + ß\ (Di\ (kt)^{1/2}) \qquad \text{Equation (7)}$$

Because the concentration of glass before weathering is 100%, $C_o = 1.0$ (N.B. $C_{o\ (hyd)} = 0$ in the second expression of equation 7), equation (7) can be rewritten as:

$$C_\Sigma = e^{-kt} + ß\ (Di\ (kt)^{1/2}) \qquad \text{Equation (8)}$$

To calculate ß, the parabolic rate constant (k_p) and the first order rate constant (k_1) must be evaluated. White and Classon (1980) provide, from experimental data, a parabolic rate constant for silica released from hydrated glass of $K_p = 9 \times 10^{-7}\ s^{-1/2}$. The rate constant for the first order precipitation of smectite calculated earlier from Figure 7.12 using data in Table 7.2. yields a value of $k_1 = 4.63 \times 10^{-4}{}_y{}^{-1}$. Therefore ß can be calculated from equation (4a) thus yielding a value of 0.47. Equation (8) can be rewritten as,

$$C_\Sigma = e^{-kt} + 0.47\ D.I \qquad \text{Equation (9)}$$

where, D.I = Dawson's intergral.

Figure 7.10

The concentration of glass, expressed as the ratio C'_g, is plotted against ln t for data from Core 31 and is overlain on a series of semi-empirical curves constructed for the dissolution of glass. The curve where ß=0 is exponential and is described by first order kenetics. The other three curves represent a sequential kinetic model for the dissolution of glass given various values for ß and C_{SS}. The fit of data shows that the transformation of glass to smectite in the Firth of Thames can be described by a sequential kinetic model which involves a parabolic dissolution coupled with a first order precipitation (equation 9). For higher values of ln t dissolution becomes exponential approximating first order kinetic rate law.

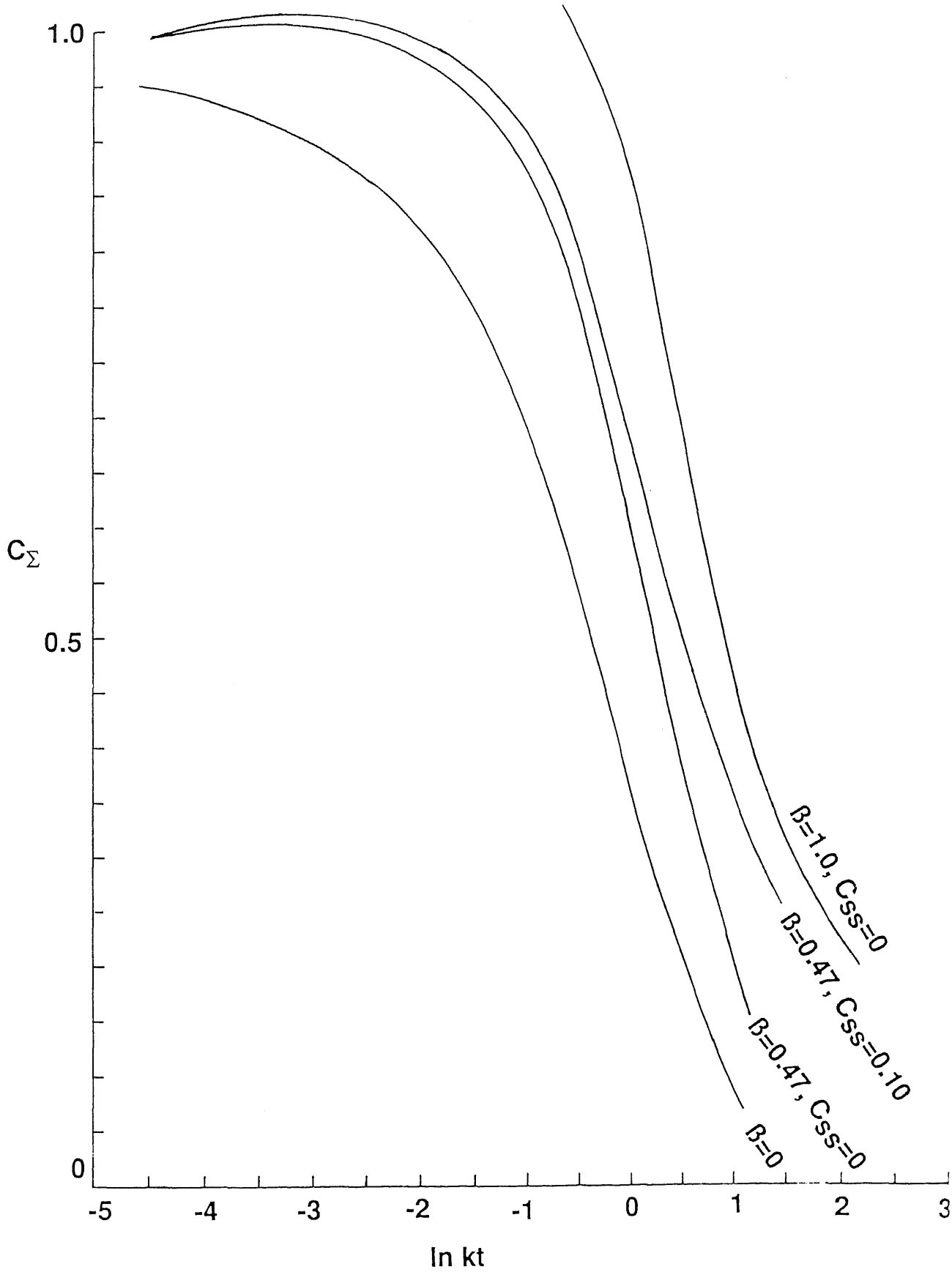
1.0
0.5
0
C_Σ
-5
-4
-3
-2
-1
0
1
2
3
ln kt
β=1.0, Css=0
β=0.47, Css=0.10
β=0.47, Css=0
β=0

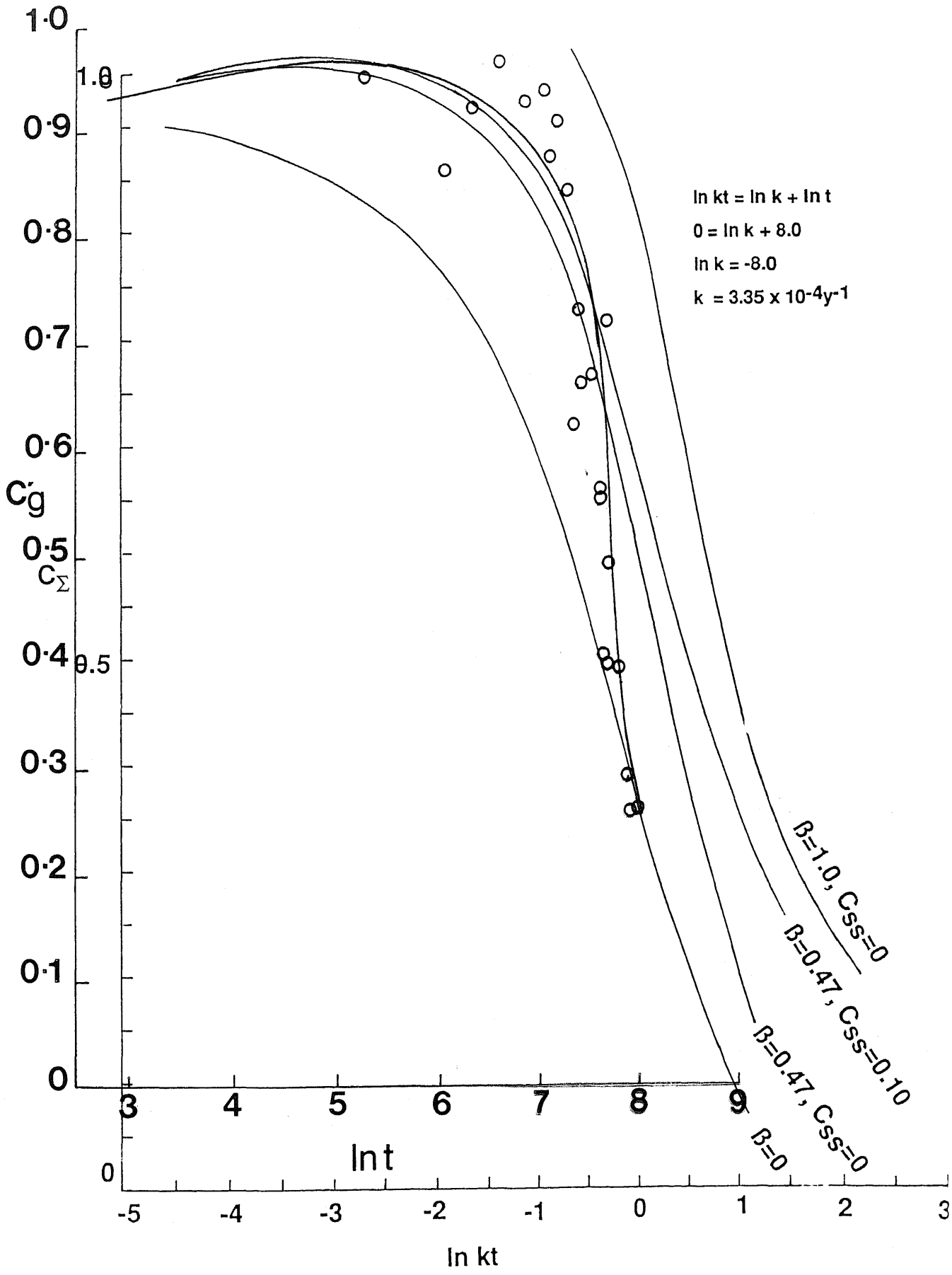
1·0
0·9
0·8
0·7
0·6
0·5
0·4
0·3
0·2
0·1
0
1.0
0.5
0
Cg
CΣ
3
4
5
6
7
8
9
Int
-5
-4
-3
-2
-1
0
1
2
3
In kt
In kt = In k + In t
0 = In k + 8.0
In k = -8.0
k = 3.35 x 10-4y-1
β=1.0, Css=0
β=0.47, Css=0.10
β=0.47, Css=0
β=0

Table 7.2

Data and calculations used to construct the semi-empirical curves in Figure 7.10 for the sequential kinetic model.

t	kt	lnkt	e^{-kt}(ß=0)	0.47 x D.I	C_Σ	C_Σ (ß=1)	$C_\Sigma(C_{SS}=0)$
0	0		1.0	0	1.0		1.0
10	0.01	-4.60	0.999	0.047	1.04	1.09	1.04
210	0.04	-3.42	0.961	0.092	1.051	1.16	1.06
410	0.09	-2.41	0.914	0.134	1.051	1.20	1.06
610	0.25	-1.39	0.779	0.199	0.978	1.202	1.00
810	0.49	-0.71	0.613	0.240	0.853	1.12	0.892
1010	0.81	-0.21	0.445	0.254	0.699	0.985	0.755
1200	1.00	0	0.368	0.252	0.620	0.904	0.683
1298	1.21	0.19	0.298	0.247	0.545	0.824	0.615
1391	1.44	0.36	0.237	0.238	0.475	0.743	0.551
1484	1.69	0.52	0.185	0.227	0.412	0.668	0.494
1577	1.96	0.67	0.141	0.215	0.356	0.600	0.442
1670	2.25	0.81	0.105	0.201	0.306	0.533	0.396
1763	2.56	0.94	0.077	0.188	0.265	0.477	0.357
1856	2.89	1.06	0.056	0.175	0.231	0.428	0.325
1949	4.00	1.38	0.018	0.142	0.160	0.320	0.258
2042	6.25	1.83	1.93×10^{-3}	0.223		0.225	
2135	9.00	2.20	1.23×10^{-4}	0.178		0.178	
2228	12.25	2.51	4.78×10^{-6}	0.150		0.150	
2321	16.00	2.77	1.13×10^{-7}	0.130		0.134	
2414	17.00	2.83	4.14×10^{-8}	0.124		0.124	
2507	18.00	2.89	1.52×10^{-8}	0.119		0.120	
2600	19.00	2.94	5.60×10^{-9}	0.114		0.110	
2786	20.00	2.99	2.06×10^{-9}	0.109		0.109	

A plot of C_Σ vs ln kt (Fig. 7.10) is constructed from data in Table 7.2 using equation (9). Also plotted are three other curves where the values of ß and C_{SS} are varied. As already discussed, where $C_{SS} = 0$, ß $= 2k_p/k_1^{1/2}$. Hodder (1985) shows that the ratio ß must therefore determine the slope of the curve C_Σ vs ln kt and represents the relative influence of first order and parabolic rate law in the sequential kinetic model. When ß = 0 the dissolution of glass is entirely first order and displays an exponential curve in Figure 7.10. When ß > 1 the curve becomes parabolic. At ß = 0.47 components of both first order and parabolic kinetics describe the dissolution of glass. When a plot of C'_g vs ln t for the Firth of Thames data is overlain on the theoretical curves good correlation is achieved with the sequential model where ß = 0.47 and $C_{SS} = 0$. The fit of data enables a rate constant of $k = 3.35 \times 10^{-4} y^{-1}$ to be calculated for the weathering of glass in the Firth of Thames (Fig. 7.10).

7.5 DISCUSSION: Implications of the sequential kinetic model

The diagenetic transformation of volacnic glass to smectite in sediments of the Firth of Thames can be described by a sequential kinetic model which involves a parabolic dissolution coupled with a first order precipitation of smectite via the formation of an intermediate hydrated glass phase. The rate constant of the first order smectite formation or precipitation reaction ($4.63 \times 10^{-4} y^{-1}$) is similar to the rate constant determined from the sequential kinetic model ($3.35 \times 10^{-4} y^{-1}$). Although the initial hydration of glass is likely to be rapid due to an excess of silica in solution the rate of continued development of the hydrated rim is determined by subsequent diffusion processes and precipitation reactions. Thus the rate of glass dissolution and the ability of smectite to precipitate is dependent on conditions in the diagenetic environment (i.e. pH, Eh, salinity and the ionic species present). Earlier stability considerations imply that the first order reaction to smectite may be thermodynamically favoured by particular conditions of pH and Na^+ and silica activity typical of interstitial fluids having sea water salinity and mildly anoxic conditions. In most environments the pH is such that much of the silica released during hydrolysis of silicic glass to smectite, is removed in solution, but in those environments where the activity of silica is sufficiently high, early silicification precludes smectite precipitation (Roberts and

Merriman 1990).

The sequential kinetic model implies that diffusion of ionic speices through a hydrated glass rim is the mechanism by which dissolution/precipitation occurs, at least initially. Berner (1978) demonstrates that particular mechanisms of glass dissolution may exhibit unique morphologies under SEM examination. Plate 7.1 C exhibits an unaltered glass shard from surficial sediments of Core 31. Surface pitting may be a result of gas vesicles or pre-depositional weathering. It was noted glass shards initially become rounded and lose much of their angular conchoidal habit and this is considered to reflect diffusion-controlled dissolution. Older glasses from lower down Core 31 tend to show minor pitting and are probably due to subsequent surface reaction dissolution of the hydrated glass as first order kinetics become rate determining (Plate 7.1 A and B).

A half life of weathering of 1475 years was determined for the first order model and compares with a half life of 1400 years calculated from the sequential model. The half life of rhyolitic glass from the Rotorua region is 18000 years (12000 years for a first order model) according to Green (1988). For andesitic glass in Taranaki, the half life is 7000 years (Neall 1977), and 1650-5000 years for dacitic glass in Papua New Guinea (Ruxton 1968). The glass entering the Firth of Thames is likely to be predominantly rhyolitic in composition with minor dacite and andesite components. The differences in estimated half lives of weathering between Firth of Thames glass and the above glasses reflect different reaction regimes in onland and marine weathering environments. The estimated rates of transformation of rhyolitic glass in the Firth of Thames cannot be compared with other similar studies as there is no published data on smectite authigenesis for marine sediments of Holocene age. The calculated rates suggest the formation of smectite in bentonite deposits is a rapid early stage diagenetic reaction and subsequent zeolitisation, which is common in older bentonites but does not occur in the Firth of Thames occurs after burial under very different conditions of temperature and pressure.

Previous studies describing authigenic smectite or "bentonite layers" in marine sediments have been associated with deep sea coring projects. Although smectite-rich deposits are recognised in

Holocene sediments (Chamley 1971) and smectite-rich layers have been identified in cores of early Pleistocene sediments from the Tasman Sea (Gardner et al. 1985), the youngest published age of bentonite deposits (completely altered ash beds, > 75% smectite) is late Pliocene (Hein and Scholl 1978). On the basis of bentonite distribution in ash layers from Aleutian Ridge arc volcanics in DSDP Leg 19 core sediments, Hein and Scholl (1978) proposed 4 or 5 x 10^6 years as the typical time required for bentonites to form from unaltered ash. However, they caution that this time may vary significantly and probably depends on the composition of volcanic detritus, pore water chemistry and the nature of the surrounding sediment. Hein and Scholl's data for bentonite formation most likely reflect the lack of recognised recent deposits in the studied sequence. Data presented here tend to favour an initial rapid alteration of glass to smectite of the order of 10^3 or 10^4 years depending upon conditions in the depositional environment. Whether or not the sediment will ever obtain "bentonite status" depends on the initial supply of volcanic detritus. After this continued alteration is likely to be slow and related more to increasing temperature and pressure associated with burial which favours the formation of zeolites (on the order of 10^5 and 10^6 years according to Hein et al. 1978).

-CHAPTER EIGHT-

THE LATE HOLOCENE SEDIMENTATION HISTORY OF THE FIRTH OF THAMES

CHAPTER EIGHT: THE LATE HOLOCENE SEDIMENTATION HISTORY OF THE SOUTHERN FIRTH OF THAMES

8.1 INTRODUCTION

In previous chapters the stratigraphy, chronology, texture, mineralogy and faunal composition of the core sediments have been described. Synthesis of this data, in conjunction with information from a peat core (Kp 8) from the Kopouatai Peat bog, described by de Lange (1989) and further analysed here, are used to reconstruct a late Holocene sedimentation history for the Firth of Thames. Other studies describing local evidence for eustatic movements in sea level and vertical tectonic movements are reviewed in the light of evidence presented in this study. The relative importance of regional subsidence and eustatic fluctuations in sea level as controls on sedimentation are determined and a developmental model for the last 6500 years is presented.

8.2 EVIDENCE SUPPORTING RAPID LATE HOLOCENE SEDIMENT INFILLING AND SHORELINE PROGRADATION

Textural, mineralogical and faunal variations with sub-bottom depth in Core 21 represent a regressive sequence and provide evidence for a late Holocene northward prograding shoreline. Essential down-core trends in Core 21 are summarised in Figure 8.1 and include the following relavent points : i) a coarsening upward of texture from mud- to sand-dominated sediments; ii) associated with this textural trend there is a progressive increase up core in the relative abundance of rock fragments; iii) an upward transition in the molluscan faunal composition from *Austrovenus stutchburyi* and *Mactra* sp. in growth position in muds to reworked shell hash layers and beds of broken *Tawera spissa, Paphies* sp. and *Perna canaliculus* near the surface - the latter species are usually associated with coarser substrates and the beach wave zone and are therefore good indicators of shoreline conditions; iv) a significant upwards increase in the abundance of the foraminifer, *Ammonia beccarri*, which is generally

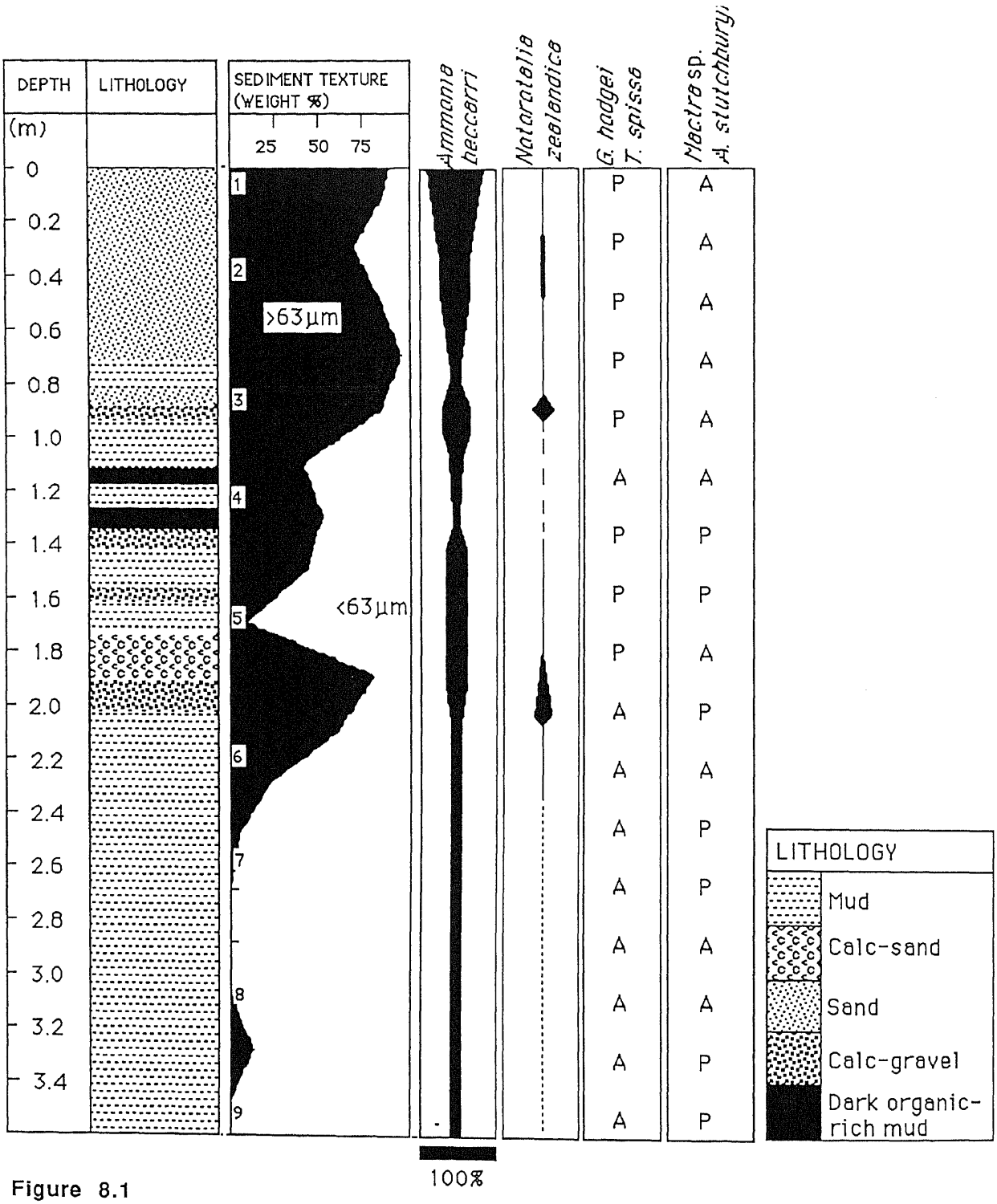

Figure 8.1

Depth variations in grainsize(CO_3-free) and faunal composition in Core 21 reflect the increased influence of fresh water and nearer proximity of the Waihou River mouth due to northwards progradation of the shoreline of the coastal Hauraki Plain during the late Holocene.

associated with reduced salinity conditions and is considered to reflect the increasing influence of freshwater input due to northward progradation of the Hauraki Lowland. Sediments from more seaward cores are largely uniform with depth. Core 31 is essentially mud-dominated, exhibiting no significant variation in faunal composition. Although more subtle variations in texture which may be suggestive of a regressive sequence occur, in particular an increase upwards in silt content, it has been demonstrated in Chapter 8 that this is most likely due to diagenetic processes transforming glass (silt size) to smectite (clay size). In Core 40 an increased frequency of storm beds in the upper portion of the core is considered to reflect a closer proximity of the shoreline in the late Holocene.

The maximum southward penetration of marine conditions in the Holocene is estimated from a core recovered from the Kopouatai Peat Bog in the Hauraki Lowland (Kp 8, see Fig. 8.3). A greenish grey basal mud, considered by de Lange (1989) to represent a marginal marine deltaic environment, was mineralogically analysed following the procedures outlined in Appendix 5. The mud has identical mineral composition to sediments of the Firth of Thames mud facies and in particular contains 45% by wt of smectite (Fig. 8.3). A radiocarbon date on peat at the peat greenish grey mud boundary gave an age of 6025 y B.P (de Lange 1989). Given that smectite has been shown to form authigenically only in marine sediments of high salinity, and to be absent in river samples, it is likely that marine conditions existed in this region of the Kopouatai Peat Bog at 6025 y B.P.

8.3 THICKNESS AND DISTRIBUTION OF THE HOLOCENE SEDIMENTS

The Firth of Thames experiences a low-energy wave climate under ambient weather conditions due to its semi-enclosed nature. Graded mixed carbonate-terrigenous layers, described in Chapter 3, are interpreted as storm beds formed under high energy conditions. Under ambient conditions the most important sediment transport mechanism is tidal currents. In particular, the anticlockwise movement around the Firth of the residual current of the M_2 tide (Bowman and Chiswell 1982) resuspends fine-grained sediments from the Waihou and Piako Rivers deposited during slack water conditions and transports them northward along the western boundary of the Firth of Thames. The velocity of the

residual tidal current is known to reach a maximum in the southern Firth of Thames and declines northwards (C. van Leeuwe , in prep). Given the limited ability of tide- and wave-generated currents to move sediment out of the Firth of Thames, except under storm conditions, the Firth can be considered a closed sedimentary system. Futhermore, Greig (1982) has mapped the northern extent of the Holocene mud (Firth of Thames) facies and notes that it laps onto the mixed-carbonate gravelly muddy sand (Central Gulf) facies of the Hauraki Gulf at a latitude roughly adjacent to Orere Point and Ponui Island suggesting that Holocene muds are prograding northwards as infilling of the Firth continues.

Rates of Sediment Accumulation

Net rates and down-core variations in the rate of sediment accumulation during the late Holocene (last 5000 years) are calculated for Cores 21, 31, 37 and 40 and illustrated graphically in Figure 8.2. Clearly there exists areal variations in the rate of sediment accumulation. These lateral variations can be used to make inferences about the thickness and extent of the Holocene sediment cover. Maximum rates of sediment accumulation have occurred in the central region, represented by Core 31 (1.9 mm/y). A significant decline in the net rate of sedimentation occurs landward, 1.2 mm/y for Core 40 and 0.6 mm/y for Core 21. Likewise, the net rate of accumulation for Core 37, adjacent to Te Puru, is 0.7 mm /y. A mean sedimentation rate of 1.5 mm/y was calculated from Cores 21, 31, 37 and 40 after weighting corrections were made. These sedimentation rates support the implications made by Bowman and Chiswell (1982) pertaining to sedimentation in the Firth of Thames. They related the modelled circulation of residual tidal currents to the modern distribution of surficial sediments described by Carter and Eade (1980) and suggested that high tidal velocities along the eastern boundary during the flood tide and along the western boundary during the ebb tide, in combination with an estuarine flow at depth from the Waihou River, may resuspend fine-grained material (Section 2.6). Consequently, a positive sediment accumulation rate is inferred for the central Firth where the velocities of the residual tidal currents are nil.

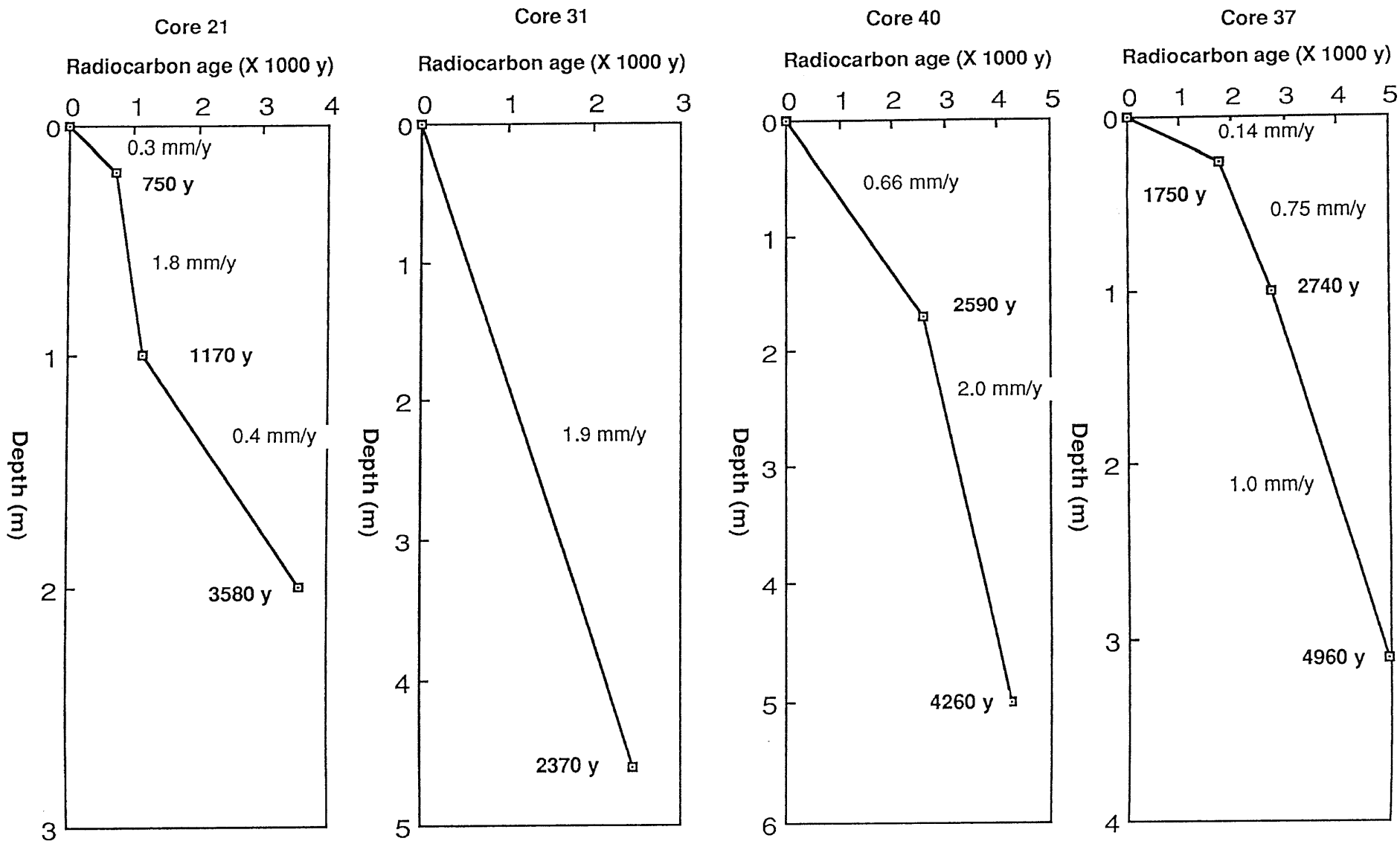

Figure 8.2
Plots illustrate variations in sedimentation rates over the late Holocene.

Progressive winnowing of mud sediments offshore by tidal currents during the late Holocene has produced an actively prograding submarine sediment wedge which reaches a maximum thickness (maximum rates of sediment accumulation) in the central region in the vicinity of Core 31 and thins significantly northward.

Seismic Stratigraphy

Because none of the cores penetrated the late Pleistocene transgressive surface the actual thickness of the Holocene sediments can only be inferred by extrapolation of sedimentation rates back to 6500 y B.P, a time considered to represent the onset of rapid mud sedimentation on the late Pleistocene transgressive surface in the southern Firth of Thames. A limited number of seismic echograms (Plate 8.1), recorded on a 3.5 kHz GIFFT recorder during a cruise of the R.V. Tangaroa in 1976 into the southern Firth of Thames, were made available by Dr L. Carter of the New Zealand Oceanographic Institute, Wellington. The tracks covered by the echograms are marked on Figure 8.4. A prominent reflector at a sub-bottom depth ranging from 5-10 m is considered to represent the post-glacial Holocene transgressive surface. Overlying this surface a seismic unit, characterised by a uniform reflection pattern from bottom to the present seabed, represents the prograding Holocene mud blanket. Greig (1982) identified a similar, but considerably thinner unit from echograms in the northern Firth of Thames. Seismic data support the above accumulation rates, where in the vicinity of Core 31 maximum rates of sediment accumulation correspond to a maximum thickness of ~ 8 m. Seaward of this position the mud blanket thins. The echograms show local variations in thickness due to irregularities protruding from the Pleistocene surface and faulting within the Pleistocene sediments. These protruberances are most pronounced in the seismic track adjacent to the Coromandel Range and may represent paleo-relief features inherited from an exposed land surface during the last glaciation - possibly the remnants of a ridge and swale topography generated by streams on local fans from the nearby Coromandel Range.

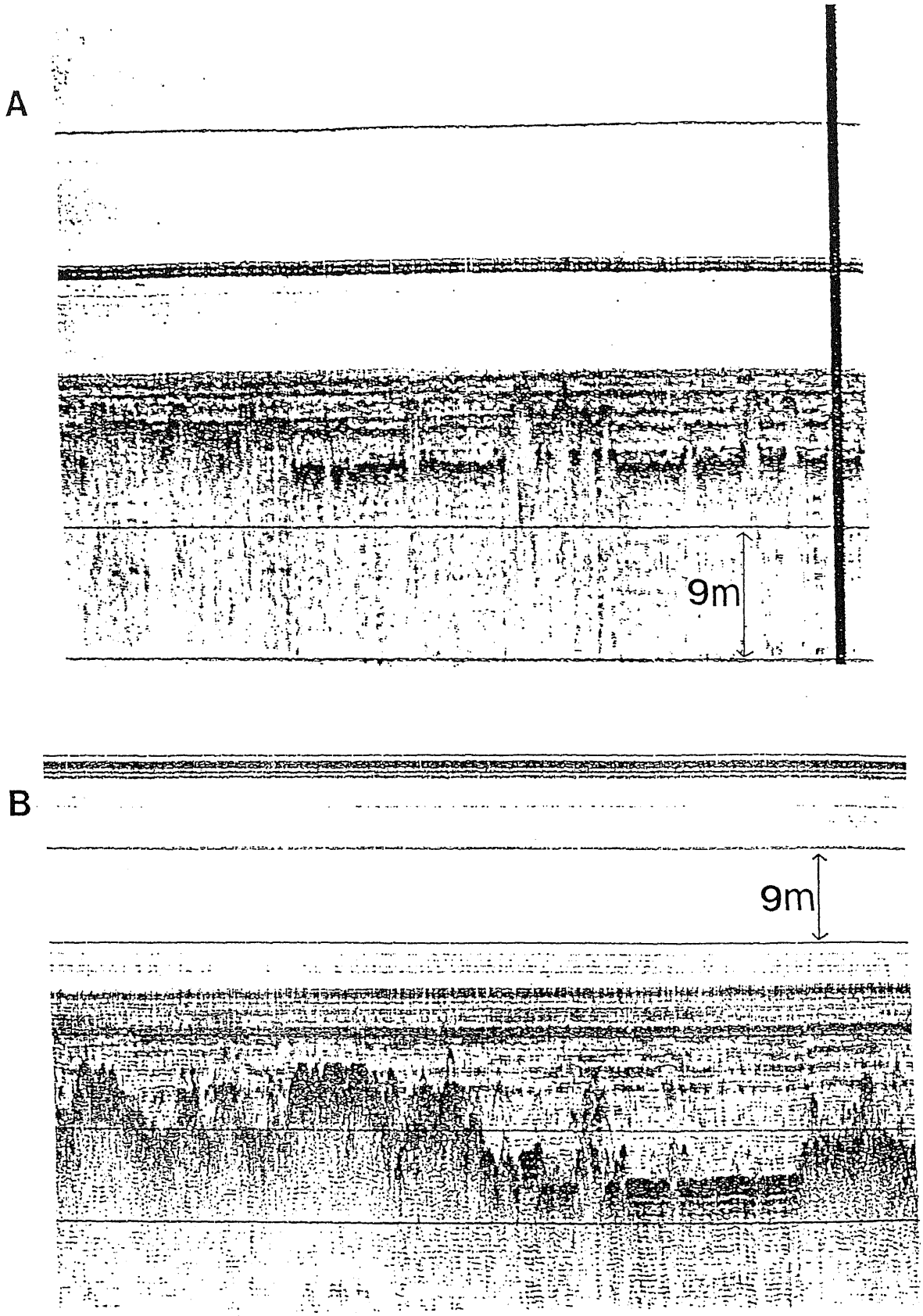

Plate 8.1

Seismic echograms were recorded on a 3.5 kHz Gift recorder. In A), a prominent reflector at a sub-bottom depth ranging from 5-10 m represents the post-glacial Holocene transgressive surface. Holocene mud sediments overly this surface. Variations in thickness of the Holocene sediments are due to irregularities protruding from the Pleistocene surface along with displacement from east-west trending faults that cross-cut the rift. The latter result in the accumulation of relatively deep pockets of Holocene sediments in B). The distance between chart lines is 9 m. The position of seismic profiles A and B are illustrated in Figure 8.4.

8.4 LATE HOLOCENE EUSTATIC MOVEMENT IN SEA LEVEL

Gibb (1986a) has summarised sea level data for a variety of sites around New Zealand and suggested that sea level reached its maximum about 6500 y B.P and has not fluctuated by more than ± 1 m since that time. However, local relative sea level movements have long been recognised for the Firth of Thames region (Schofield 1960; Woodroffe et al. 1983) and for the Northland and Auckland region (Schofield 1973). Marks and Nelson (1979) cite dune progradation at Omoro barrier spit during the late Holocene as evidence for a 2 m lowering of sea level in the last 5000 years. Schofield (1960) described the extensive beach ridge system near Miranda as evidence for a 2 m lowering of sea level in the last 4000 years. More recently Woodroffe et al. (1983) have interpreted new data from the same area and suggested that sea level showed a eustatic lowering of 0.7-0.9 in the last 3900 years and reached it's present level about 1200 y B.P. Both Schofield (1960) and Woodroffe et al. (1983) found no evidence to suggest vertical uplift has occurred during the late Holocene along the Firth of Thames Fault (Fig. 8.4). From the data of Woodroffe et al. (1983) the rate of late Holocene lowering of sea level is estimated at 0.2 mm/y.

8.5 VERTICAL FAULT MOVEMENTS: An estimated rate of regional subsidence for the late Holocene

A rate of regional subsidence for the last 6025 years is calculated using lithological and age data from Core Kp 8 (Fig. 8.3). Hauraki Catchment Board surveys of the bog surface provide a datum of 6 m above mean sea level (de Lange 1989, from Harris 1978). A radiocarbon age of 6025 y B.P for basal peat at 7 m depth, at the marine mud-peat boundary, is assumed to represent the position of the shoreline at about 6050 y B.P, which further assumes there was no substantial lag between the recession of sea level and the colonisition of peat on the mud surface. Regional subsidence is therefore the summation of the depth of the 6050 y B.P surface below present mean sea level (1.0 m) and the eustatic lowering of sea level over the same period, estimated by Woodroffe et al. (1983) to be 0.9 m (Fig. 8.3). This yields a regional subsidence rate (RSR) of 0.3 mm/y, which compares to a rate of

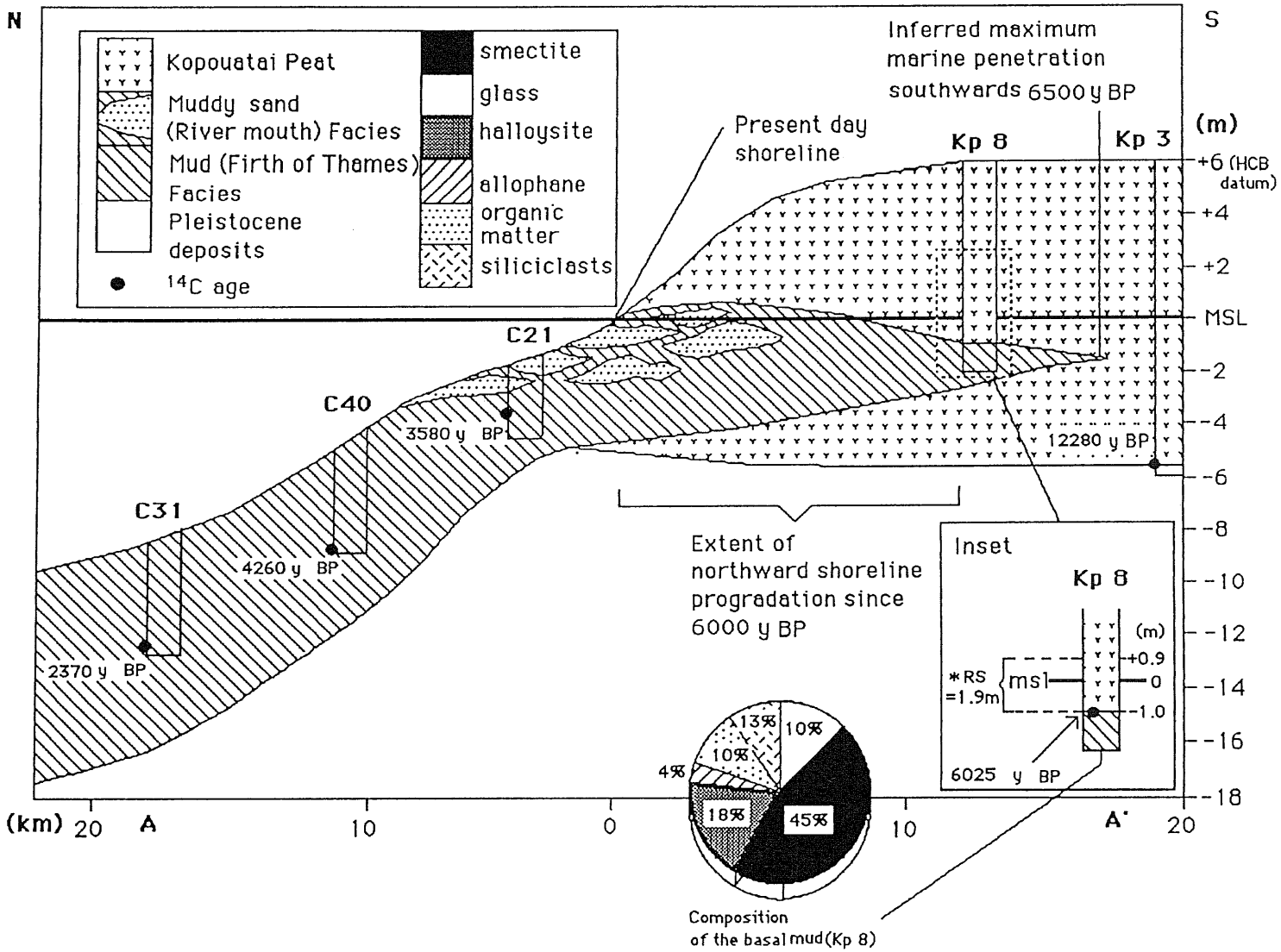

Figure 8.3
A schematic x-section from north to south through the Firth of Thames and northern Hauraki Plain. The position of the transect is marked on Figure 8.4 (see text for details).

1.5 mm/y for the late Quaternary suggested by Pillans (1986) and would suggest that the tempo of vertical tectonic movements has declined during the late Holocene. One third of this vertical movement can be accounted for by displacement across the Kerepehi Fault, estimated to be 0.13 mm/y for the last 10,000 years in the vicinity of Kopouatai Peat Bog (de Lange 1989). The other two thirds is probably due to vertical movement along the Hauraki Fault because the Firth of Thames Fault was inferred by Hochstein and Nixon (1979) to be only a minor hinge fault. With respect to the estimated late Holocene RSR, movement on the Kerepehi Fault may be a rather more significant control on sedimentation than originally suggested by de Lange (1989) who considered the effects of subsidence in the Kerepehi Depression to be largely overidden by regional subsidence.

8.6 ESTIMATED RATES OF SEDIMENT INFILLING AND SHORELINE PROGRADATION

The average rate of sediment accumulation (1.5 mm/y) outweighs the RSR (0.3 mm/y, Section 8.5) and supports the sedimentological evidence that substantial infilling and shoreline progradation has occurred during the late Holocene. A net rate of relative vertical sediment accretion of 1.2 mm/y can then be estimated by subtracting the RSR from the average rate of sediment accumulation. Given that 15 km of shoreline progradation has occurred since 6050 y B.P (from position of Kp 8 in Figs. 8.3 and 8.4), a rate of lateral progradation of 2.5 m/y is determined.

From Figure 8.2 it can be seen that rates of sediment accumulation have varied over the late Holocene. In general there has been a gradual decline in the rate of sedimentation. The most rapid sedimentation occurred between 3500 and 1200 y B.P when accumulation rates were in excess of 2 mm/y. This corresponds to, and was probably accelerated by, a period of sea level lowering as suggested by evidence from the Miranda Chenier Plain (Woodroffe et al. 1983) and adds weight to the likelihood of a real lowering of sea level during the late Holocene.

The rates of shoreline progradation estimated here are high compared to other studies around the

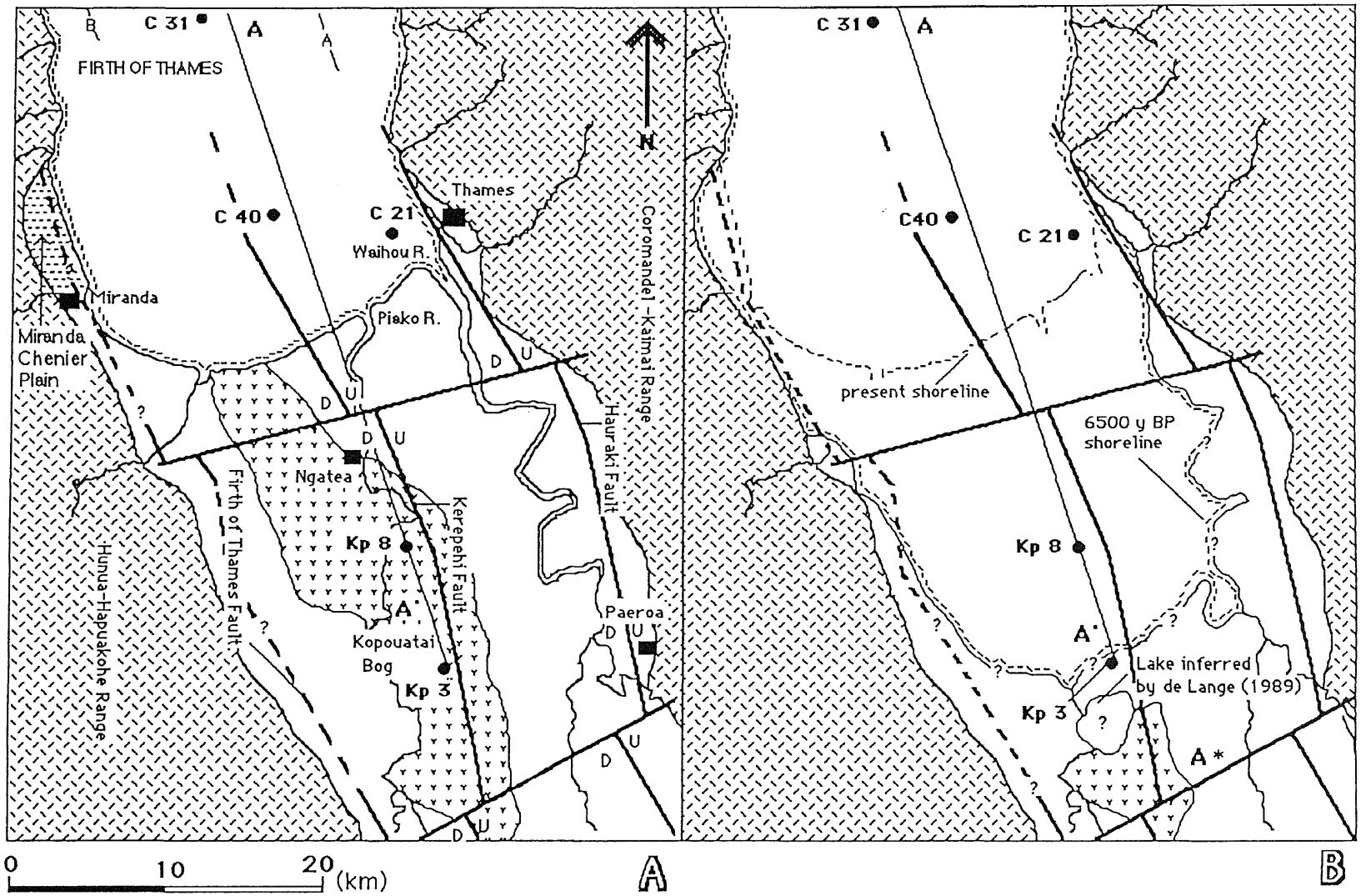

Figure 8.4

A) Present day shoreline morphology of the Firth of Thames. **B)** A paleo-reconstruction of shoreline at the height of the Holocene transgression, approximately 6500 y BP. The exact nature of the shoreline is inferred from the present geomorpholgy of the Hauraki Lowlands and maximum southward penetration of marine conditions is inferred from lithological data from Kp 8 and Kp 3 (Fig. 8.3). **A*** = Awaiti dune field.

New Zealand coastline, for example a rate of 1.2 m/y over the last 8000 years for the Rangitaiki Plain (Pullar and Selby 1971) and a rate of 0.15 m/y over the last 5000 years for Pauanui Beach (Gibb and Aburn 1986). However, it is significant that each of these locations is unique and they are characterised by very different conditions of uplift, subsidence, sediment supply and shelf and coastal plain geometry. For the Firth of Thames a high rate of sediment supply into a low energy, protected embayment has been the major factor controlling active progradation. Moreover the narrow width of the coastal Hauraki Plain, a consequence of the confining effect of the Hauraki Graben, has restricted the area available for lateral distribution of sediment alongshore and consequently favoured rapid seaward accretion. Due to very low gradients of 1: 2000 of the sea floor in the southern Firth of Thames rather small fluctuations in sea level would have had a profound effect on shoreline progradation and it is probable that maximum progradation occurred during 3500-1200 y B.P when sea level was receding.

From 1200 y B.P to Recent accumulation rates have been substantially lower, generally less than 1.0 mm/y. During historic times progradation has been minimal. Sea level, however, has been rising at the rate of 1.2 mm/y since 1900 according to a rigorous statistical anaysis of tidal gauge data, from several locations around New Zealand, by Hannah (1988). This rise approximates the modern rate of sediment accumulation and therefore would not promote shoreline progradation.

8.7 A LATE HOLOCENE DEVELOPMENTAL HISTORY FOR THE FIRTH OF THAMES

Time zones in the following reconstructions are based largely on significant variations in sedimentation rates and sea level movements. Therefore the boundaries between individual periods should not be considered precise.

6500-3500 y B.P

Rising sea level associated with the Holocene marine transgression culminated between 6500-6000 y B.P, forcing the rivers draining the Hauraki Lowland to aggrade. Greenish grey volcanic

glass-dominated muds, which soon altered to smectite-bearing muds, were deposited in shallow marine conditions at least as far south as Core Kp 8, 15 km south of the present coastline. Sea level at this time was approximately 1 m above present sea level. Marine conditions did not penetrate much beyond Kp 8 because weathered pumiceous alluvial gravels, inferred to be of late Pleistocene age, and not marine muds were encountered by de Lange (1989) in a transect of cores further south near the Awaiti dune field (Kp 3, Figs. 8.3 and 8.4). A lake may have developed in the Kopouatai Depression around this time, as a consequence of river and stream aggradation. In the northern Kopouatai Depression, in the vicinity of Kp 8, a pre-exsisting peat bog inferred by de Lange (1989) to have formed during a lower sea level was probably overlain by marine mud during the Holocene transgression but remained untouched in the south. de Lange (1989) cites as evidence for this a progressive increase in age of basal peats southwards. Sea level probably remained stable during this period and sedimentation rates were initially high (> 1.5 mm/y) due to a period of base level readjustment in response to a stabilising sea level.

3500-1500 y B.P

As sea level receded, peat soon recolonised in the northern Kopouatai Depression and the Waihou River migrated across the western Hauraki Plain reworking Holocene marine mud and Pleistocene alluvial sediments. Coarser sediments are deposited in close proximity to the river mouth on top of the finer muds giving rise to the characteristic coarsening upwards sequence recorded in Core 21. Eustatic lowering of sea level forms a series of stranded beach ridges and intertidal flats in a prograded coastal plain near Miranda and causes rivers to incise into the Hauraki Plain producing an increased supply of fine-grained volcanic glass-dominated sediments to the Firth of Thames. Sedimentation rates are highest during this period, >2 mm/y. Rapid shoreline progradation ensued , and given the low gradients of the coastal plain, seafloor progradation rates may have been in excess of 2.5 m/y. Sea level was lowering at a rate of 0.2 mm/y and a regional rate of subsidence of 0.3 mm/y determined in Section 8.5 is inferred.

1500 y B.P - Recent

Sea level stabilises and probably remained constant until historic times (last 150 years), since when it has probably been rising. Continued progradation of the shoreline northwards is due solely to infilling, but sediment accumulation rates are now lower (~1 mm/y) and the rate of progradation has declined. Progradation is accompanied by continued peat growth in the Kopouatai Depression. Historically rising sea levels have largely offset progradation.

-CHAPTER NINE-

SUMMARY AND CONCLUSIONS

CHAPTER NINE: SUMMARY AND CONCLUSIONS

This chapter summarises the principal conclusions of this study as they relate to the objectives outlined in the introduction.

Stratigraphy of the late Holocene sequence

A total of 45 shallow-marine sediment cores, 5 cm in diameter and up to 5.5 m long, were collected from the southern Firth of Thames. Analytical data from 13 of these cores form the basis of this study. Offshore cores (e.g., Cores 31 and 40) are dominated by a greenish grey (10GY 5/1) plastic mud, typically bioturbated and massive, with sporadic uncorrelatable interbedded shell layers comprising intact or disarticulated bivalves, particularly the fragile *Mactra ordinaria* and sometimes *Mactra ovata* and *Austrovenus stutchburyi*. Shell hash layers, some of which are associated with normally graded mixed terrigenous-carbonate sequences, also occur (e.g. Core 40) and show many similarities to graded storm-beds described by other workers (Hayes 1967; Gagen et al. 1989).

The muds range from silty clays to clayey silts and consist mainly of volcanic glass, smectite and halloysite, with smaller amounts of other siliciclasts such as quartz, feldspar, volcanic rock fragments (ignimbrite, rhyolite and andesite) and allophane and illite, as well as skeletal carbonate (mainly aragonite) and organic matter. Radiocarbon dating of the basal sediments from the cores reveals a range of late Holocene basal ages from 2700 y B.P to 5000 y B.P. This mud dominated-lithology has been termed the Firth of Thames mud facies and although the cores did not penetrate the entire Holocene sequence, seismic evidence indicates it is laterally extensive, approximately 10 m thick and appears to be prograding northwards.

Nearer shore, the upper parts of sediment cores (e.g., Cores 21 and 37) are usually coarser, and include siliciclastic (muddy) sand (river mouth sand facies) and/or more prevalent interbeds of sand and shell-hash material within mud (delta fan gravel facies). Such coarsening-upwards sequences have

resulted from the late Holocene infilling of the Firth of Thames once sea level reached its present height about 6500 y B.P (Gibb 1986). The lower portion of the nearshore Core 21 is a volcanic glass-dominated mud unit, the same as constitutes all of offshore Core 31, and typical of the modern siliciclastic Firth of Thames mud facies that infills the bulk of the Firth.

Late Holocene sediment infilling and shoreline progradation

Up to 15 km of northward shoreline progradation of the Hauraki coastal plain has been estimated to have occurred since 6050 y B.P, at an average rate of 2.5 mm/y. Essential evidence supporting this contention is summarised below:

1) A coarsening upwards of texture in cores from mud- to sand-dominated sediments accompanied by a progressive increase up-core in the relative abundance of rock fragments.

2) An upwards transition in the molluscan faunal composition from *Austrovenus stutchburyi* and *Mactra* sp. in growth position in muds to reworked shell hash layers and beds of broken *Tawera spissa, Paphies* sp. and *Perna canaliculus* near the surface - the latter species are usually associated with coarser substrates and/or the beach wave zone and are therefore good indicators of shoreline conditions.

3) A progressive up-core increase in the abundance of the foraminifer *Ammonia beccarri*, a prevalent species in nearer shore cores, which is a good indicator of brackish water conditions suggests the influence of freshwater input from the Waihou River has increased during the late Holocene.

4) The ostracods *Munsyella tumida, Trachyleberis thompsoni* and *Quadracythere truncula* increase in abundance up Core 21 and are generally associated with coarser substrates.

5) Smectite-bearing basal marine muds overlain by peat dated at 6025 y B.P in a core (Kp 3) from the onland Kopouatai Peat Bog suggest that marine conditions existed in this inland region of the Hauraki Depression prior to 6025 y B.P.

A regional subsidence rate of 0.3 mm/y during the late Holocene is estimated for the Hauraki Depression in the vicinity of the Firth of Thames (Section 8.5). This compares to a proposed rate of 1.5 mm/y and suggests that the tempo of vertical tectonic movement has declined during the Holocene. A mean rate of offshore vertical sediment accumulation of 1.5 mm/y is estimated for the Firth of Thames which clearly overrides the rate of regional subsidence.

The estimated rates of shoreline progradation are high in comparison to those from other studies around the New Zealand coastline (Section 8.6). For the Firth of Thames a high rate of sediment supply into a low energy, protected embayment has been the major factor controlling active progradation. Moreover the narrow width of the coastal plain has restricted the area available for lateral distribution of sediment alongshore and consequently favoured more rapid seaward accretion.

Given the low gradient of 1:2000 of the sea floor in the southern Firth of Thames, small reductions in sea level can also have a profound effect on shoreline progradation. Maximum progradation probably coincided with, and was accelerated by, a period of eustatic sea level lowering of up to 0.9 mm/y over the period from 3500-1200 y B.P. This is supported by evidence from the Miranda Chenier Plain and that there appears to be no evidence of uplift in the western Firth of Thames along the inferred Firth of Thames Fault during the Holocene.

From 1200 y B.P to the present day the accumulation rates have been considerably lower (<1.0 mm/y). Indeed, since 1900 sea level has been rising at an average rate of 1.2 mm/y (Hannah 1988). Consequently shoreline progradation during historic times has been minimal.

Sediment Mineralogy

Down-core variations in sediment composition have been traced in detail for Core 31, and profiles have been presented in Chapter 5 for the whole sediment and for the clay and silt fractions. The following conclusions can be drawn:

i) Volcanic glass dominates the surficial and upper core sediments (45-55%), but decreases in abundance with increasing sub-bottom depth (15%).

ii) Volcanic glass resides principally in the silt fraction and dominates it's composition.

iii) Smectite dominates in the lower core sediments (up to 45%), increasing significantly in abundance with increasing sub-bottom depth (.

iv) Smectite is a/the major constituent of the clay fraction and its abundance within this fraction increases with increasing sub-bottom depth. This relationship also holds in Cores 21 and 40.

v) Halloysite (10-15%), allophane (2-4%) and illite ± kaolinite (3-8%) abundances remain more or less constant throughout the core.

vi) Calcium carbonate abundance relates mainly to the distribution of shell layers within the core.

Nature of smectite

Clearly an intimate association between smectite and volcanic glass is well established from the down-core composition profiles. To better characterise the nature of the smectite a range of more specific clay mineral analyses were carried out on 10 samples from 4 cores. Important features include:

i) The position of the untreated 001 smectite peak between 14 and 15Å indicates Ca^{2+} and Mg^{2+} are the dominant interlayer cations present, and partial contraction of this peak to 12Å to 13Å after KOH treatment suggests smectite is derived from a low-charge non-micaceous source, such as volcanic glass.

ii) An 060 smectite reflection at 1.52Å supports a dioctahedral structure for the smectite.

iii) The above XRD analysis and diagnostic infrared absorption spectra (Chapter 7) suggest smectite is dominantly montmorillonitic in composition.

iv) A general lack of interstratified illite does not support a detrital origin for smectite.

v) Asymmetry of the 001 peak, particularly in samples from the upper core sediments, is diagnostic of the early formation of poorly crystalline authigenic smectite. The symmetry of the peak generally improves down-core as the smectite becomes more crystalline.

vi) Under SEM authigenic smectite exhibits distinctive growth features. Web-like blebs occur on the surface of glass shards which become highly wrinkled, honey comb-like flakes and sheets with increasing sub-bottom depth in cores.

Origin of smectite

The short streams draining the bounding Coromandel and Hunua Ranges are considered to be responsible for only localised deposition on small delta fans along the shoreline of the Firth of Thames and play a subordinate role in the overall budget of offshore mud sedimentation. Their greywacke-derived clay components are dominated by illite, kaolinite and chlorite, not smectite.

Sediment supply to the Firth comes principally from the Waihou and Piako/Waitoa Rivers via the Hauraki Lowland and southern catchments. The composition of the Hauraki Lowland riverine bottom sediments has been compared to the average of 13 surficial sediment samples from the Firth of Thames. The modern river sediments are dominated by silicic volcanic glass, pumice, quartz, feldspar, rock fragments of ignimbrite, rhyolite and andesite, and halloysite and allophane. They are compositionally similar to the widespread Quaternary terrigenous sedimentary deposits covering the Hauraki Depression and, like them, intimately reflect detrital derivation from the surrounding provenance of predominantly silicic (to intermediate) volcanic rocks, particularly the pumice-rich ignimbrites or, as for the halloysite and allophane, their subaerial weathering products.

The composition of the siliciclastic fraction in the Firth of Thames sediment cores is similar to that being supplied by the rivers draining Hauraki Lowland, except for the anomalous presence of smectite, which can therefore not have a detrital origin.

Late Holocene diagenetic transformation of volcanic glass to smectite

The diagenetic transformation of volcanic glass to smectite in sediments of the Firth of Thames has been described by a sequential kinetic model which involves a parabolic dissolution coupled with a first order precipitation of smectite via the formation of an intermediate hydrated glass phase. The rate constant of the first order smectite formation or precipitation reaction ($4.63 \times 10^{-4} y^{-1}$) is similar to the rate constant determined from the sequential kinetic model ($3.35 \times 10^{-4} y^{-1}$).

The rate at which glass will dissolve to yield smectite in sediments of the Firth of Thames is dependent upon conditions in the diagenetic environment (ie., pH, Eh, salinity and the ionic species present). Thermodynamic stability considerations imply that the first order precipitation of smectite may be catalysed by particular conditions of pH and Na^+ activity typical of interstitial fluids having sea water salinity under mildly anoxic conditions.

The mechanism of dissolution implied by the sequential kinetic model is supported by SEM evidence. Initially the glass shards become rounded and lose much of their angular conchoidal habit, a reflection of diffusion-controlled dissolution (Berner 1978). Older glasses from lower down-core tend to exhibit minor pitting due to subsequent surface reaction dissolution of the hydrated glass as first order kinetics become rate determining .

A half-life of weathering of 1475 y has been determined for the first order model and compares with a half-life of 1400 y calculated from the sequential model. Both are considerably lower than known half-lives for the subaerial weathering of rhyolitic glass (Section 7.5). The calculated weathering rates for glass in the Firth of Thames are unique and suggest that the formation of smectite in bentonite deposits can be a rapid early stage diagenetic reaction. Subsequent zeolitisation, which is common in older bentonites, but not found in the Firth of Thames deposits, occurs only after burial and greatly increased temperatures and pressures.

The ability of volcanic glass dispersed in deep-sea sediments to alter to smectite clay minerals is much debated in the literature and still poorly understood. Previous studies describing authigenic smectite or "bentonite layers" in marine sediments have been discussed in Chapter 7 and are generally associated with deep-sea coring projects and sediments of Pleistocene or older. However smectite-rich deposits have been recoreded in Holocene sediments. The youngest published dates of bentonite deposits (completely altered ash beds, > 75% smectite) are late Pliocene. The transformation of glass to smectite, although widely accepted as an early diagenetic process, has largely been considered to occur slowly (10^5 to 10^6 y to attain "full bentonite status"). The half-lives of weathering and reaction rates presented in this study demonstrate that under mildly anoxic, saline conditions the transformation of glass to smectite is a rapid early stage diagenetic reaction.

-APPENDICES-

APPENDIX 1: CORE DESCRIPTIONS

Appendix 1 contains descriptive logs of 11 cores that are analysed and referred to in this thesis. Cores are logged largely on the basis of a qualitative assessment of sediment texture and faunal and mineral composition. Radiocarbon ages and corresponding sample locations are noted. For Master Cores, graphic profiles of sediment texture are plotted along with bulk density calculations. Graphics used to represent lithotypes are illustrated in Figure A1.1 along with any additional graphics used.

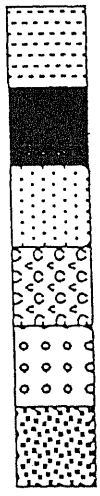

Mud

Organic-rich mud

Sand

Calcareous sand (> 50% by wt CaCO3)

Gravel

Calcareous gravel (> 50% by wt CaCO3)

S Individual intact shells

Mud with sand intercalations

Rootlets and other organic debris

Plant fragment lineations

Figure A1.1

Graphic symbols used for classification of sediment-type in core logs.

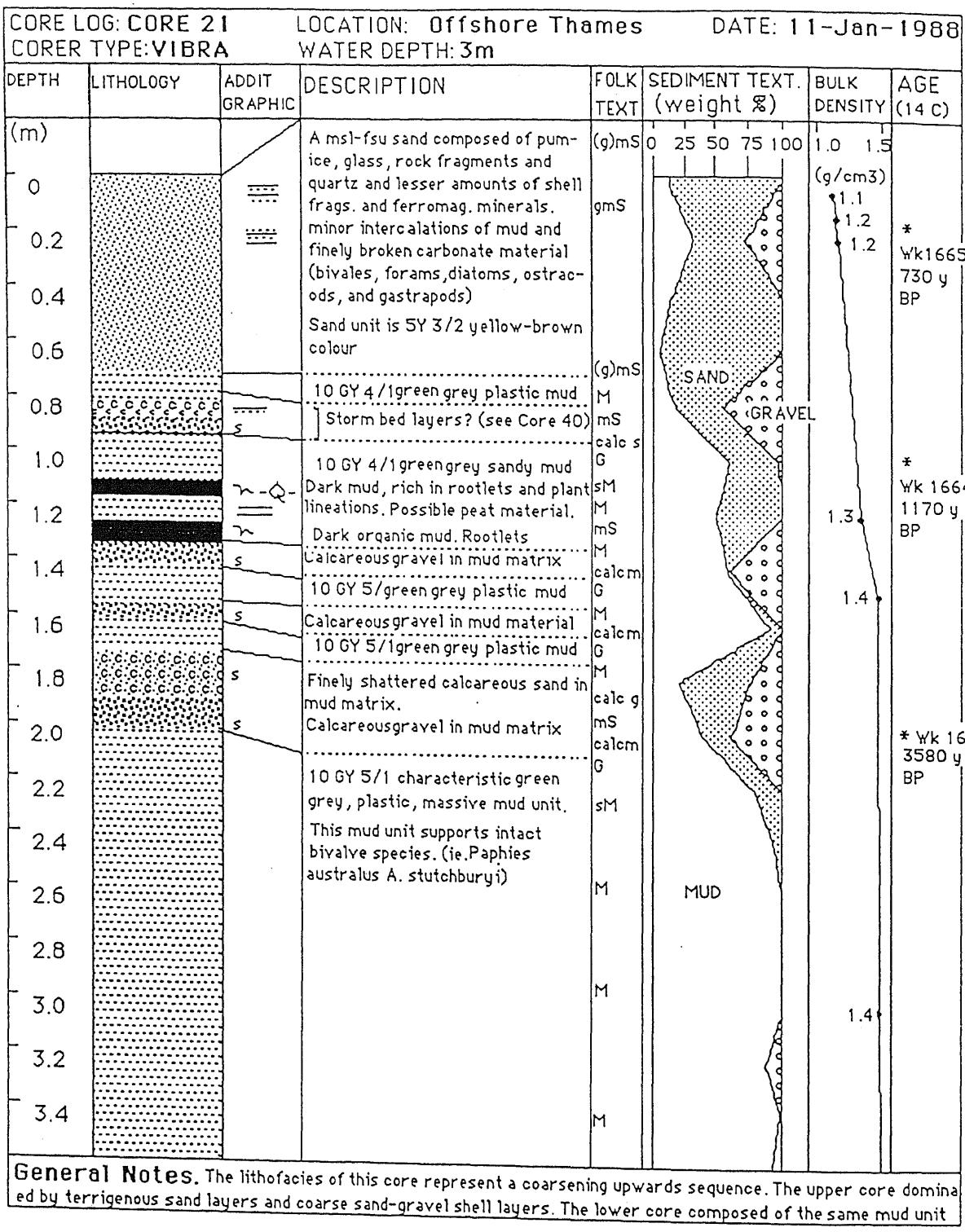

General Notes. The lithofacies of this core represent a coarsening upwards sequence. The upper core domina ed by terrigenous sand layers and coarse sand-gravel shell layers. The lower core composed of the same mud unit

CORE LOG: CORE 23 LOCATION: Offshore Tapu South DATE: 12-Jan-198[illegible]

CORER TYPE: Livingstone WATER DEPTH: 2.2m GRID REF:

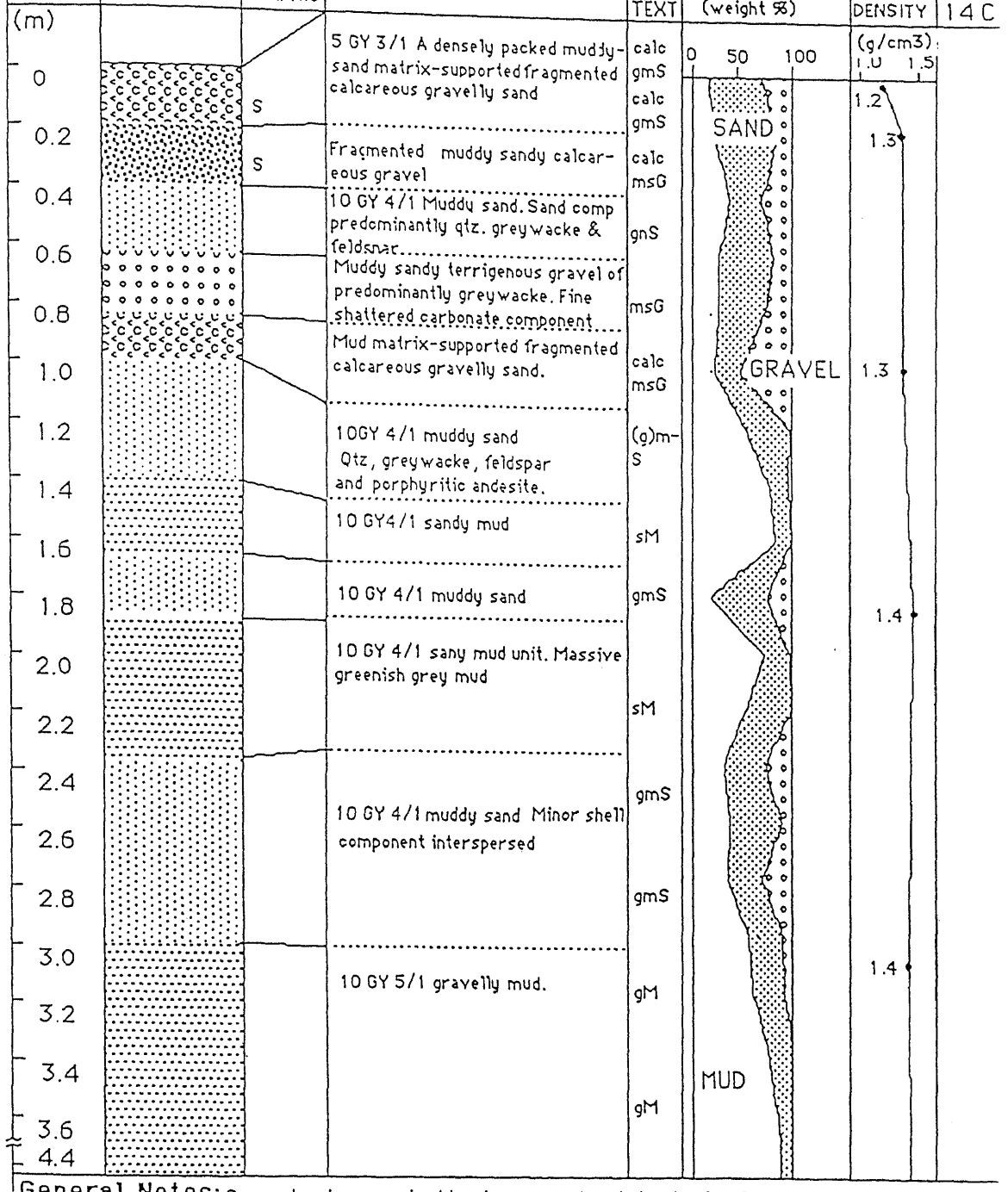

General Notes: Coarse terrigenous, mixed terrigenous-carbonate bands of poorly sorted greywacke qtz and feldspar are interbeded in the lower core by characteristic sticky massive green grey mud unit

CORE LOG: CORE 31 LOCATION: Central Firth of Thames DATE: 13-Jan-1988
CORER TYPE: Livingstone WATER DEPTH: 10.4 m GRID REF:

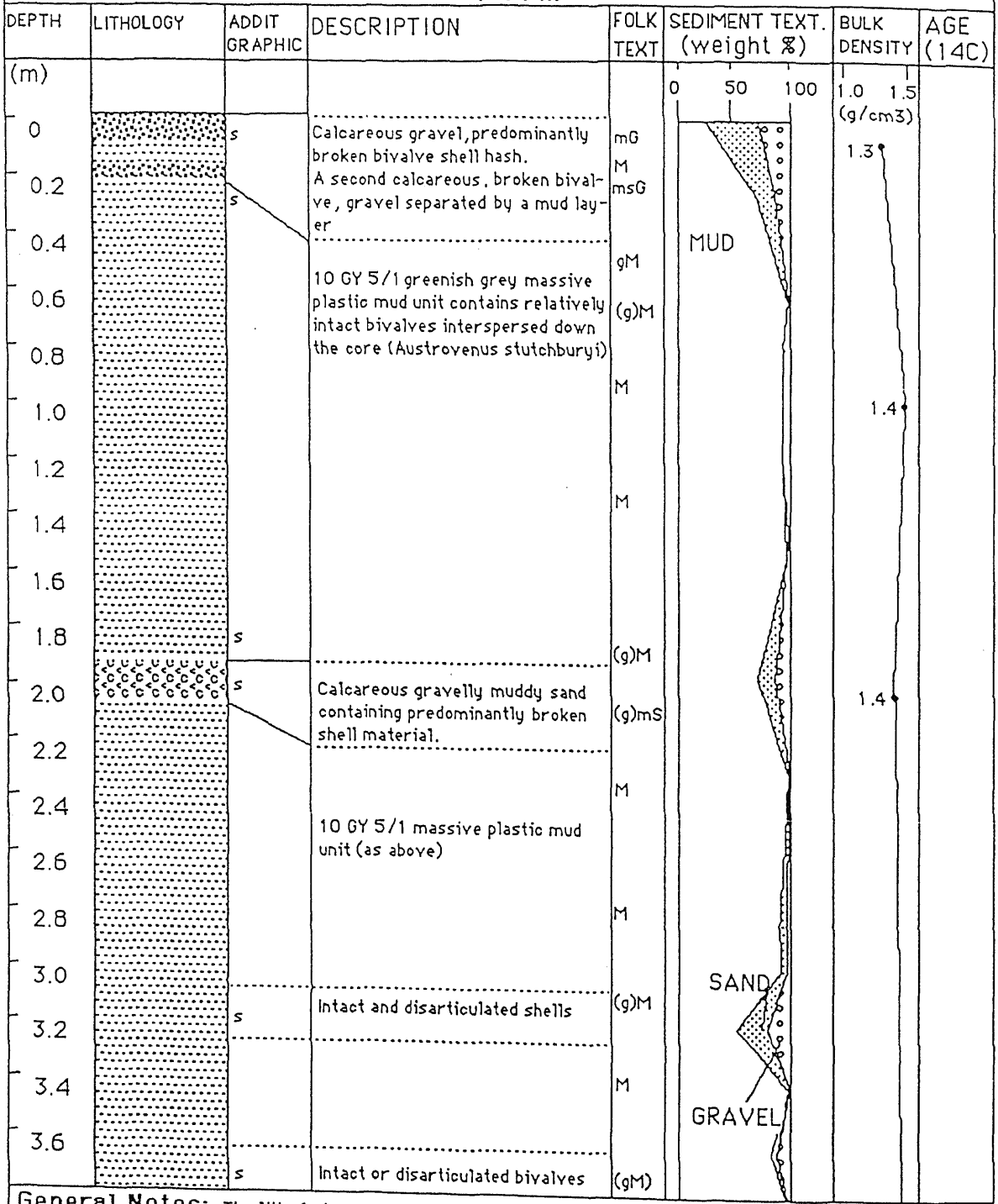

General Notes: The lithofacies represented in Core 31 are characterised by an extensive 10 GY 5/1 green grey massive plastic mud unit with interspersed layers of shattered bivalve gravels. Typical of central Firth mud facies

CORE LOG: CORE 31 LOCATION: Central Firth of Thames DATE: 13-Jan-1988
CORER TYPE: Livingstone WATER DEPTH: 10.4 m

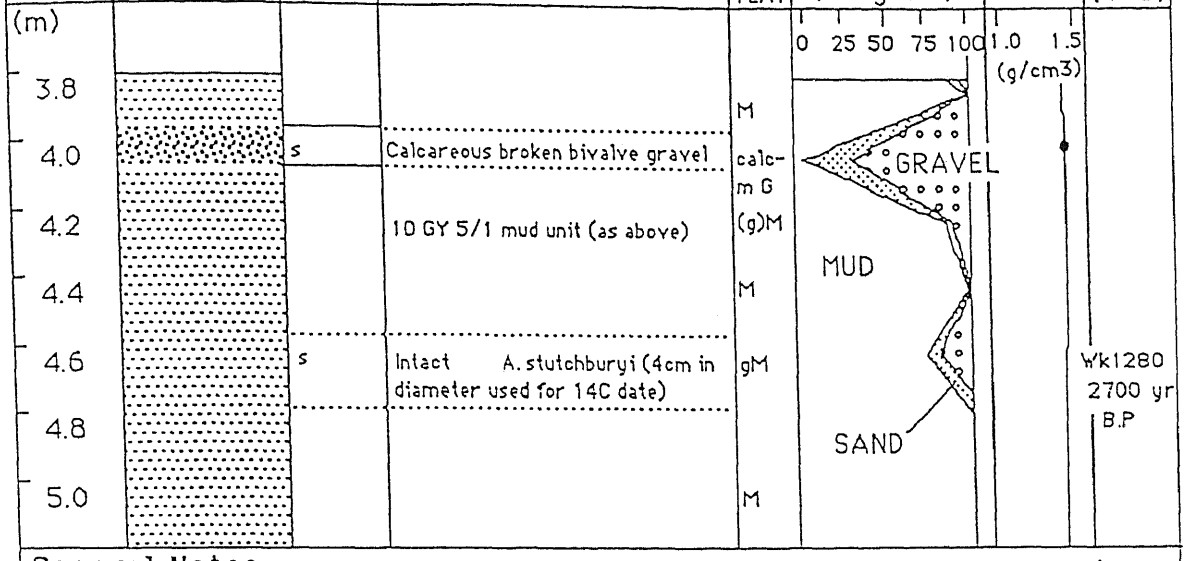

General Notes: The lithofacies represented in Core 31 are characterised by an extensive 10 GY 5/1 green grey massive plastic mud unit with interspersed layers ofshatteredbivalve gravels. Typical of central Firth mudfacies

CORE LOG: CORE 37 LOCATION: Offshore Te Puru DATE: 13-Jan-1988
CORER TYPE: Livingstone WATER DEPTH: 3m

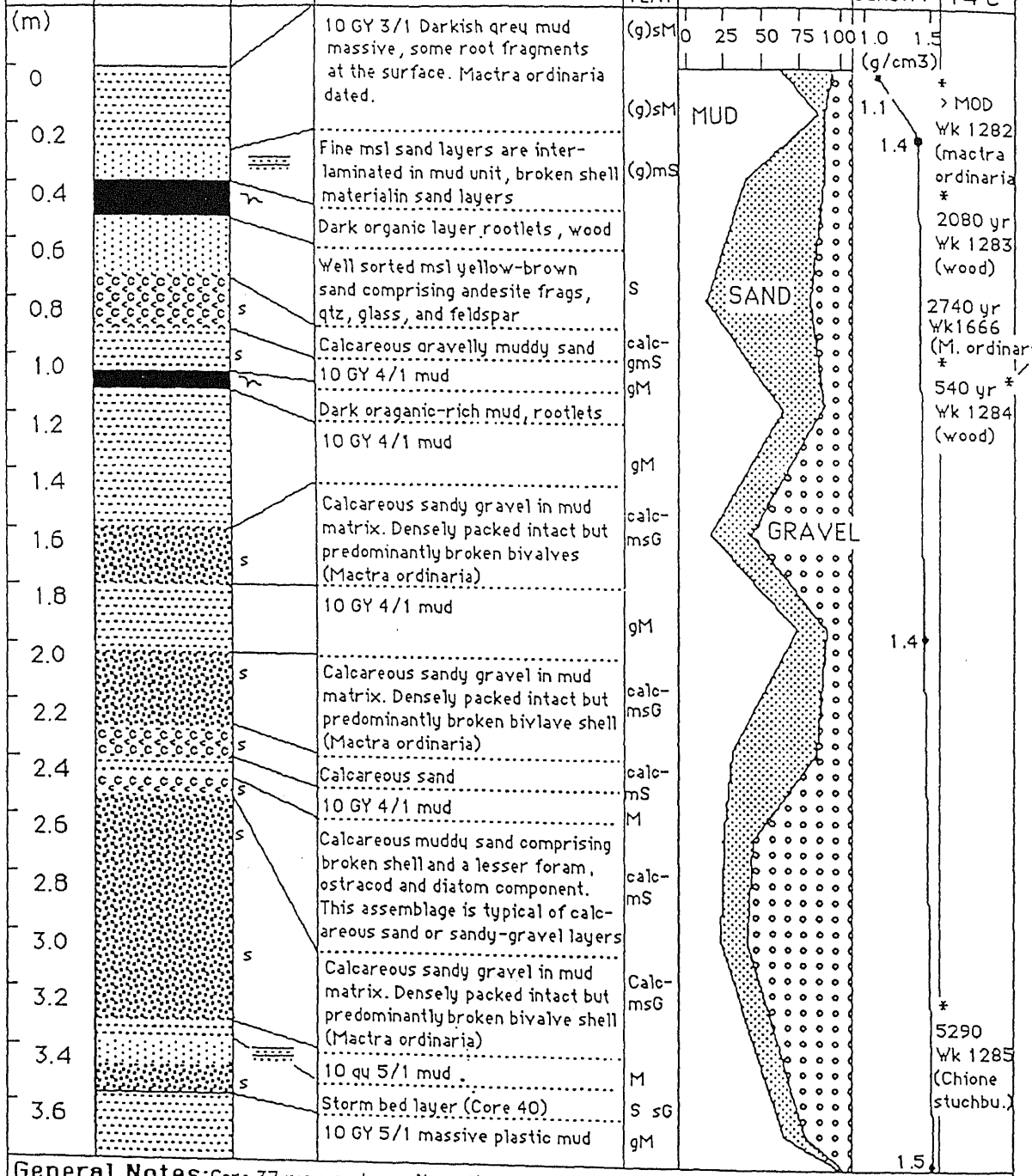

General Notes: Core 37 represents an alternating sequence of calcareous sands and gravels supported and and interlayered in a mud unit. The coarser lithofacies of the upper core reflect the proximity to the Te Puru · delta fan

CORE LOG: CORE 37 LOCATION: Offshore Te Puru DATE: 13-Jan-1988

CORER TYPE: Livingstone WATER DEPTH: 3m

DEPTH (m)	LITHOLOGY	ADDIT GRAPHIC	DESCRIPTION	FOLK TEXT	SEDIMENT TEXT. 0 25 50 75 100	BULK DENSITY 1.0 1.5 (g/cm3)	AGE 14 C
4.0			10 GY 5/1 greenish grey plastic massive gravelly-mud . Gravel is intact and disarticulated bivalve shells (A. stutchburyi) Mud unit is characteristic of the mud facies described for all cores	(g)M			
4.2		s					
4.4							

General Notes: Core 37 represents an alternating sequence of calcareous sands and gravels supported and and interlayered in a mud unit. The coarser lithofacies of the upper core reflect the proximity to the Te Puru delta fan

CORE LOG: CORE 40 LOCATION: Southern Firth of Thames DATE: 14-JAN-1988
CORER TYPE Livingstone WATER DEPTH: 4m

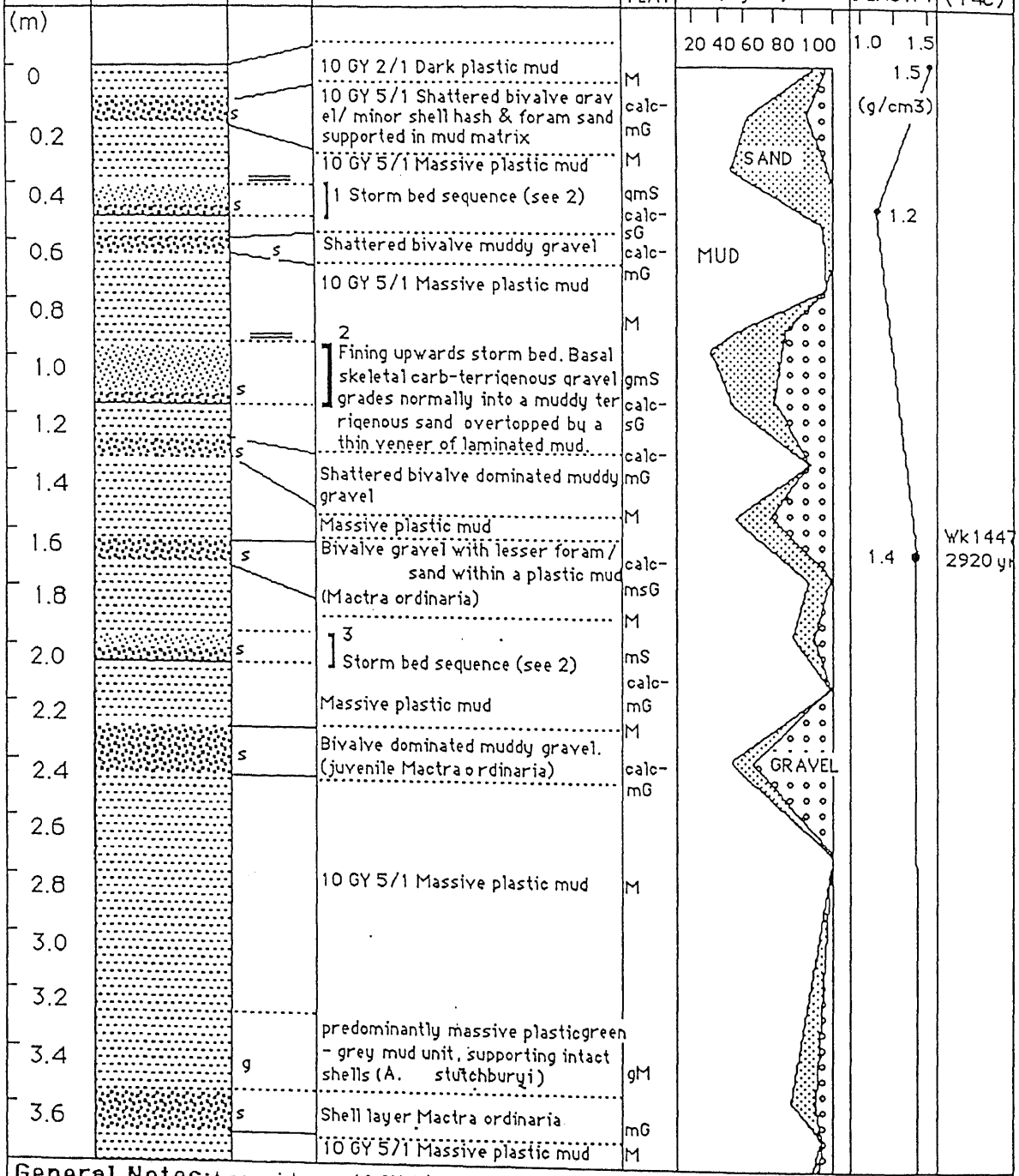

General Notes: A greenish grey 10 GY 5/1 sticky plastic massive mud is the dominant unit. This unit is interlayered with relatively intact shell gravel layers and graded terrigenous-shell beds.

CORE LOG: CORE 40 LOCATION: Southern Firth of Thames DATE: 14-Jan-1988

CORER TYPE: Livingstone WATER DEPTH: 4m

DEPTH	LITHOLOGY	ADDIT GRAPHIC	DESCRIPTION	FOLK TEXT	SEDIMENT TEXT.	BULK DENSITY	14C AGE
(m)		s	Intact and disarticulated bivalve gravelsupported in a (10 GY 5/1) mud matrix	mG	MUD	1.4	
4.2		s					
4.4			10 GY 5/1 mud	gM			
4.6		s	Mud supported bivalve gravel	mG	GRAVEL		
4.8		s	As above, but more broken shells	M mG			
5.0		s	10 GY 5/1 Typical massive mud unit. Disarticulatedbivalve sampled for14C date (Chione stuch buryi)	(g)M			* 4590 yrs Wk 1448 (A. stutch.)
5.2							

General Notes: A greenish grey10GY 5/1 sticky plastic massive mud is the dominant unit. This unit is interlayered with relatively intact shell gravel layers and finning upwards shell hash storm beds.

DATE: 12-Jan-1988

CORE LOG: **CORE 4** LOCATION: **450 m off Tararu**
CORER TYPE: **Livingstone** WATER DEPTH: **1.3m**

DEPTH (m)	LITHOLOGY	ADDIT GRAPHIC	DESCRIPTION	FOLK TEXT
0		S	2.5Y 4/2 Dark greyish yellow gravelly sand. Gravel component is due to carbonte shell material. Predominantly Austrovenus stutchburyi, Paphies australus, Tawera spissa. Terrigenous sand composed of rock fragments, qtz glass and feldspar. Mud content of this unit increases with depth.	gS
0.2				
0.4				
0.6				gS
0.8			5 Y 4/2 Greenish olive	
1.0				
1.2				
1.4				gS
1.6				
1.8				
2.0			7.5 Y 4/2 Greyish olive	gmS
2.2				
2.4			10 Y 4/2 Olive grey	gS
2.6				
2.8				
3.0				
3.2				
3.4				
3.6				

General Notes:

DATE: 1-Jan-1988

CORE LOG: **CORE 6** LOCATION: **2 km off Tararu**

CORER TYPE: **Livingstone** WATER DEPTH: **4.0 km**

DEPTH (m)	LITHOLOGY	ADDIT GRAPHIC	DESCRIPTION	FOLK TEXT
0				
0.2			Greenish-grey (10GY 5/1) massive mud with individual intact or disarticulated valves of Austro venus stutchburyi. Thin sand lenses are intercalated with muds at the base of this mud unit	gM
0.4				
0.6		S		
0.8			Calc-muddy gravel-shell hash	calc-msG
1.0			calc-gravelly sand composed of mixed terrigenous-carbonate sed. -shell hash.	calc-gS
1.2				
1.4			Greenish grey (10 GY 5/) mud with intact valves of Austrovenus stutchburyi	gM
1.6		S		
1.8				
2.0				M
2.2		S		gM
2.4				
2.6				
2.8				
3.0				
3.2				
3.4				
3.6				

General Notes:

DATE: **12-Jan-1988**

CORE LOG: **CORE 26** LOCATION: **500 m off Te Mata Bridge**

CORER TYPE: **Livingstone** WATER DEPTH: **2.0 m**

DEPTH (m)	LITHOLOGY	ADDIT GRAPHIC	DESCRIPTION	FOLK TEXT
0			gravelly sand	gS
0.2		s	sandy shell hash in terrig. sand	
0.4			Gravelly muddy sand	gmS
0.6		s	mixed calc-terrig sand	
0.8			gravelly muddy sand	(g)mS
1.0			Interbedded mud and terrig. sand layers	
1.2			10 GY 5/1 greenish grey sandy mud.	
1.4				
1.6				
1.8			Log of wood encountered	gM
2.0				
2.2				
2.4				
2.6				
2.8				
3.0				
3.2				
3.4				
3.6				

General Notes: Mixed terrig-carbonate muddy sand-gravelly sand. Muddier near base.

DATE: 13-Jan-1988

CORE LOG **CORE 32** LOCATION: **6 Nm E of Wharekawa**

CORER TYPE: **Livingstone** WATER DEPTH **8.0 m**

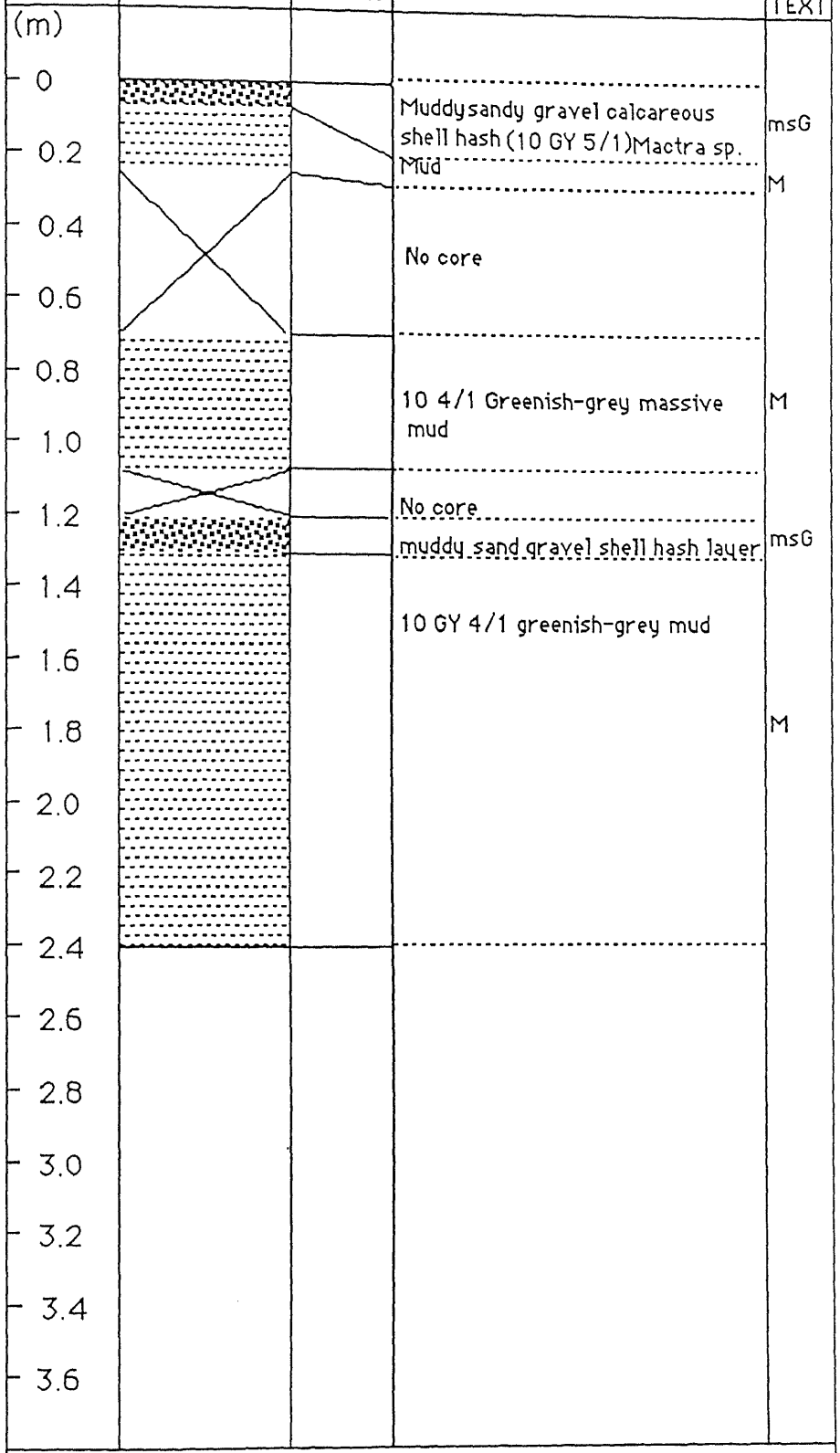

General Notes: Greenish grey muds typical of the Firth of Thames mud facies

DATE: 13-Jan-1988

CORE LOG: Core 33 LOCATION: 2.7 km WofTePuru
CORER TYPE: Livingstone WATER DEPTH: 7.5 m

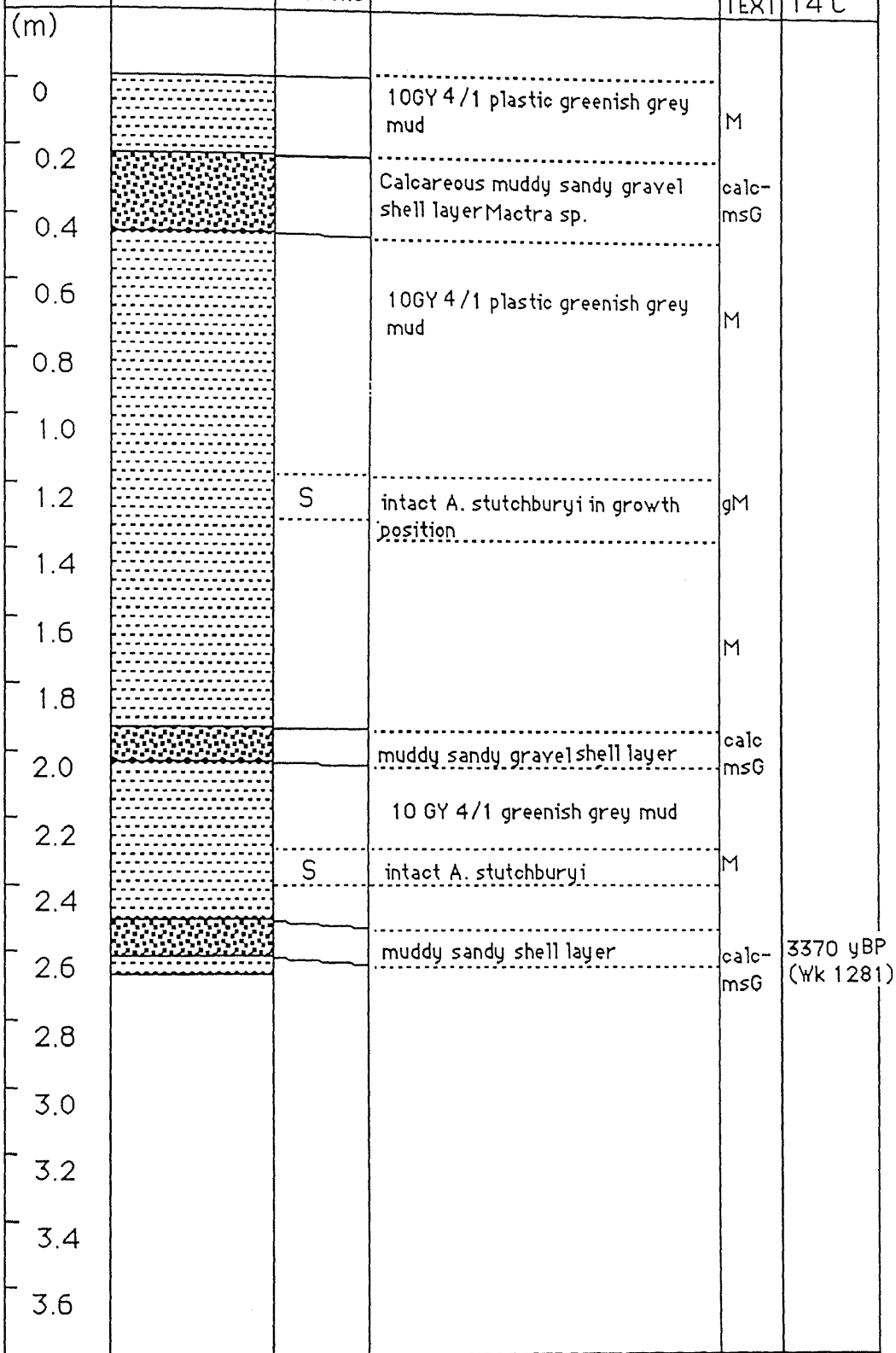

General Notes: Predominantly a greenish-grey mud unit typical of the Firth of Thames facies. Interbedded shell layers of Mactra sp.

DATE: 12-Jan-1988

CORE LOG: **CORE 41** LOCATION: **Waiomu Sth - 400 m offshore**

CORER TYPE: **Livingstone** WATER DEPTH: **3.5 m**

DEPTH (m)	LITHOLOGY	ADDIT GRAPHIC	DESCRIPTION	FOLK TEXT
0 – 0.8			10 GY 5/1 greenish grey mud with fine sand intercalations. Unit increases in sand content with depth	(g)sM / M / (g)sM / gsM
0.8 – 1.0			Dark organic-rich mud layer contains wood fragments, roots, and leaves.	M / S
1.0 – 1.2			msl-fsu sand	
1.2 – 1.8			10 GY 4/1 greenish-grey gravelly sandy mud Gravel component due to shell fragments	(g)s M
2.0		S	In situ Mactra sp.	gM
2.2 – 4.8			10 GY 4/1 greenish grey mud. Intact shells occur throughout. Predominantly A. stutchburyi.	gsM

General Notes: Core 41 is dominated a typical greenish grey mud. However a significant terrigenous sand componenet also occurs

APPENDIX 2: SEDIMENT TEXTURE DATA

Presented in this appendix are the results of analysis of core sediment texture. A graphic core log and locations of samples for which carbonate-free textural data were determined is presented for the Master Cores (Cores 21,23,31,37 and 40). Ternary textural plots corresponding to the respective cores are also included, which illustrate down-core variations in texture of the acid-insoluable residue discussed in Chapter 4.

Table A2.2

Core 23 - texture data.

SAMPLE#	DEPTH (M)	CLAY%	SILT%	SAND%	GRAVEL%
23.01	0.0	5.3	4.2	61.1	29.4
23.02	0.2	10.8	0.2	64.0	18.1
23.03	0.4	24.9	7.1	36.0	32.0
23.04	0.6	10.5	9.1	59.8	20.7
23.05	0.8	17.6	2.5	48.9	31.1
23.06	1.0	10.6	3.8	29.4	56.2
23.07	1.2	30.4	20.6	46.9	2.0
23.08	1.4	34.0	40.9	20.4	4.8
23.09	1.6	54.0	29.6	16.4	0.0
23.10	1.8	6.5	1.6	64.0	27.9
23.11	2.0	24.0	45.4	28.8	1.8
23.12	2.2	1.6	48.7	49.7	0.0
23.13	2.4	14.2	10.9	45.4	29.4
23.14	2.6	20.1	13.5	56.0	10.4
23.15	2.8	8.8	20.1	38.5	23.6
23.16	3.0	29.9	22.8	36.9	10.4
23.17	3.2	34.0	24.3	35.3	6.4
23.18	3.4	59.0	12.8	27.8	0.4
23.19	3.6	21.4	60.4	17.7	0.6

Carbonate-free analysis

SAMPLE#	CLAY%	SILT%	SAND%
23.01	7.5	5.9	86.6
23.03	36.7	10.4	52.9
23.05	25.5	3.6	70.9
23.07	31.1	21.0	47.9
23.12	1.6	48.7	49.7
23.15	13.1	29.9	57.1
23.19	21.5	60.7	17.8
23.21	18.8	61.8	19.4

Table A2.1

Core 21 - texture data.

SAMPLE#	DEPTH (cm)	CLAY%	SILT%	SAND%	GRAVEL%
21.01	0.0	4.6	8.6	84.1	2.6
21.02	20-22	16.0	15.0	41.3	27.7
21.03	40-42	0.8	14.7	83.7	0.8
21.04	60-62	0.6	4.0	94.3	1.2
21.05	80-82	8.6	7.0	37.0	47.5
21.06	100-102	34.6	24.5	37.7	3.2
21.07	120-122	24.0	24.7	51.0	0.3
21.08	140-142	29.9	27.5	3.4	39.2
21.09	160-162	50.1	40.5	8.7	0.0
21.10	180-182	1.5	18.1	56.3	24.1
21.11	200-202	19.2	20.0	21.1	39.7
21.12	220-222	10.5	67.7	21.9	0.0
21.14	260-262	55.8	38.2	6.0	0.0
21.15	280-282	51.9	48.0	0.1	0.0
21.16	300-302	44.9	55.0	0.1	0.0
21.17	320-322	69.3	30.0	0.7	0.0
21.18	340-342	5.1	81.6	13.3	0.0
21.19	360-362	70.2	29.6	0.2	0.0

Carbonate-free analysis

SAMPLE#	CLAY%	SILT%	SAND%
21.01	4.7	8.9	86.4
21.03	0.8	14.9	84.3
21.06	35.7	25.3	39.0
21.08	49.2	45.3	5.6
21.10	2.0	23.8	74.2
21.12	10.5	67.7	21.9
21.14	55.8	38.4	6.0
21.16	44.9	55.0	0.1
21.18	5.1	81.6	13.3

Table A2.3

Core 31 - texture data.

SAMPLE #	DEPTH (cm)	CLAY%	SILT%	SAND%	GRAVEL%
31.01	0	26.8	25.0	24.2	24.0
31.02	20-22	37.2	46.9	9.0	7.1
31.03	40-42	50.3	43.2	2.1	4.4
31.04	60-62	41.3	57.6	0.0	1.4
31.05	80-82	33.6	63.7	2.8	0.0
31.06	100-102	32.1	65.2	2.8	0.0
31.07	120-122	31.8	67.1	1.1	0.0
31.08	140-142	34.0	65.6	0.9	0.6
31.09	160-162	34.7	57.9	3.5	4.0
31.10	180-182	35.7	49.2	7.1	8.7
31.11	200-202	36.2	52.0	11.2	0.6
31.12	220-222	42.5	55.7	1.5	0.8
31.13	240-242	50.3	47.1	2.2	0.5
31.14	260-262	56.9	41.6	2.4	0.0
31.15	280-282	58.4	37.8	3.0	0.9
31.16	300-302	57.2	20.0	12.3	10.7
31.17	320-322	56.1	43.3	0.6	0.0
31.19	340-342	56.5	35.0	5.5	3.0
31.20	380-382	63.2	36.3	0.5	0.0
31.21	400-402	21.3	14.2	19.0	45.5
31.22	420-422	58.0	33.5	2.4	6.1
31.23	440-442	65.0	33.8	1.2	0.0
31.24	460-462	70.6	11.8	5.0	12.7

Carbonate-free analysis

SAMPLE #	CLAY%	SILT%	SAND%
31.01	35.3	32.9	31.8
31.03	52.6	45.2	2.2
31.05	33.6	63.7	2.8
31.07	31.8	67.1	1.1
31.09	86.2	60.3	3.6
31.11	36.5	52.3	11.3
31.13	50.5	47.3	2.2
31.15	58.9	38.1	3.0
31.17	56.1	43.3	0.6
31.19	58.6	35.7	5.7
31.21	39.1	26.1	34.8
31.23	70.6	28.2	1.2

Table A2.4

Core 37 - texture data.

SAMPLE #	CLAY%	SILT%	SAND%	GRAVEL%
37.01	21.6	36.0	40.7	1.7
37.02	21.8	60.3	11.0	6.9
37.05	0.0	11.7	67.9	20.4
37.09	2.2	11.1	44.4	42.4
37.11	18.3	38.7	34.5	8.5
37.13	3.6	23.2	31.2	42.1
37.15	9.6	14.4	38.4	37.6
37.17	0.0	55.0	7.7	37.3
37.21	24.6	69.8	5.7	0.0
37.24	32.4	66.4	1.3	0.0

Carbonate-free analysis

SAMPLE#	CLAY%	SILT%	SAND%
37.01	22.0	36.6	41.4
37.02	23.5	64.7	11.8
37.05	0.0	14.6	85.4
37.09	3.8	19.2	77.0
37.11	42.8	42.8	14.5
37.13	6.2	40.4	53.4
37.15	15.4	23.1	61.6
37.17	0.0	87.7	12.3
37.21	24.6	69.8	5.7
37.24	32.4	66.4	1.3

Table A2.5

Core 40 - texture data.

SAMPLE #	DEPTH(cm)	CLAY%	SILT%	MUD %	SAND %	GRAVEL%
40.01	0.0	32.6	63.2	95.8	3.9	0.3
40.02	20-22	20.2	17.6	37.8	44.9	16.3
40.03	40-42	14.1	15.1	29.2	47.9	22.8
40.04	60-62	23.8	73.1	96.9	1.7	1.4
40.05	80-82	63.7	34.0	97.6	1.8	0.5
40.06	100-102	17.8	7.8	13.7	53.0	33.3
40.07	120-122	19.0	10.9	29.9	30.5	39.9
40.08	140-142	16.9	64.9	81.8	6.0	12.0
40.09	160-162	12.9	15.9	28.8	29.0	42.7
40.10	180-182	12.0	73.5	85.5	11.6	2.9
40.11	200-202	17.9	47.8	65.7	16.7	17.6
40.12	220-222	22.3	74.4	96.7	2.6	0.7
40.13	240-242	12.3	17.9	30.2	16.7	52.6
40.14	260-262	30.2	67.8	98.0	1.9	0.0
40.15	280-282	43.8	54.0	97.7	2.2	0.1
40.16	300-302	48.7	49.9	98.6	1.3	0.0
40.17	320-322	56.2	39.1	95.3	3.1	1.6
40.18	340-342	52.3	33.0	85.3	9.3	5.3
40.19	360-362	49.7	19.5	69.2	12.8	18.0
40.20	380-382	35.9	55.4	91.3	4.5	4.2
40.21	400-402	23.9	15.0	38.9	24.9	36.2
40.22	420-422	37.3	43.2	80.5	11.5	7.7
40.23	440-442	51.9	44.9	96.7	3.4	0.0
40.24	460-462	24.0	1.2	25.2	11.4	63.4
40.25	480-482	25.6	28.3	53.9	13.4	32.7
40.26	500-502	34.3	55.8	90.1	7.2	2.8
40.27	520-522	48.1	30.0	78.1	9.3	12.1

Carbonate-free analysis

SAMPLE #	CLAY%	SILT%	SAND%
40.01	32.7	63.4	3.9
40.03	18.3	19.6	62.1
40.05	64.0	34.2	1.8
40.07	27.9	21.6	50.5
40.09	20.8	29.0	50.2
40.11	38.5	41.2	20.3
40.13	26.3	38.1	35.6
40.15	43.8	54.0	2.2
40.17	57.1	39.7	3.2
40.19	60.7	23.7	15.6
40.21	37.5	23.5	39.0
40.23	51.8	44.8	3.4
40.25	38.0	42.1	19.9
40.27	54.7	34.7	10.6

Table A2.6

Texture data from other cores.

SAMPLE#	DEPTH (m)	MUD%	SAND%	GRAVEL%
CORE 41				
41.1	0.1	91.0	8.8	0.2
41.2	0.3	16.0	79.2	4.8
41.5	1.0	49.8	50.2	0.0
CORE 4				
4.1	0.1	2.4	92.5	5.1
4.2	0.4	1.3	88.0	10.7
4.3	1.2	0.0	95.5	4.5
4.4	2.0	4.7	91.3	4.0
CORE 32				
32.1	0.0	13.2	37.5	49.3
32.2	0.9	99.0	1.0	0.0
32.4	1.9	94.2	5.7	0.1
CORE 33				
33.1	0.2	96.3	3.7	0.0
33.4	0.7	93.1	3.7	3.3
CORE 26				
26.1	0.0	1.2	85.0	13.8
26.3	1.2	87.1	9.3	3.6
CORE 34				
34.1	0.1	12.6	64.4	64.7
CORE 6				
6.1	0.0	84.2	12.2	3.6
6.2	0.2	27.1	62.5	10.4
6.3	0.4	12.5	76.8	10.7
6.4	1.3	7.6	68.3	24.1
6.6	2.3	99.2	0.8	0.0

Table A2.7

Surficial, river and peat core (Kp3) sediment texture data.

SAMPLE#	CLAY%	SILT%	SAND%
8.1	48.3	42.8	8.9
10.1	1.8	0.3	98.0
11.1	32.7	28.7	38.6
28.1	9.0	16.9	74.1
29.1	32.0	64.1	3.9
39.1	3.0	4.5	92.6
RIVER SAMPLES			
SAMPLE#	CLAY%	SILT%	SAND%
PIAKO	12.1	17.7	58.2
WAIHOU	6.0	29.7	76.4
WAITOA	43.9	17.9	38.2
OHINEMURI	10.3	19.3	71.2
PEAT CORE			
Kp 8	0.0	60.5	39.5

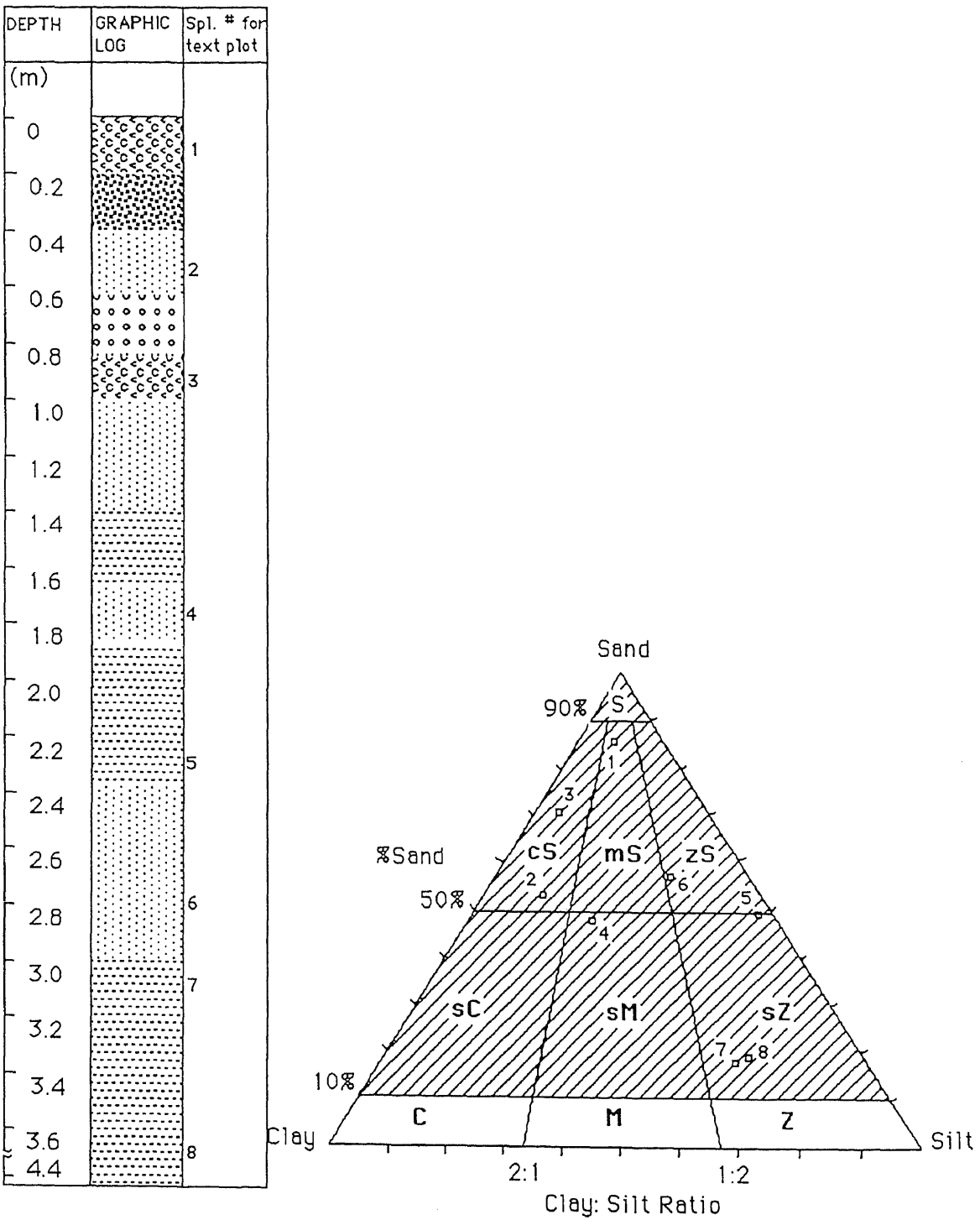

Figure A2.1

Carbonate-free textural classification of Core 23 sediments.

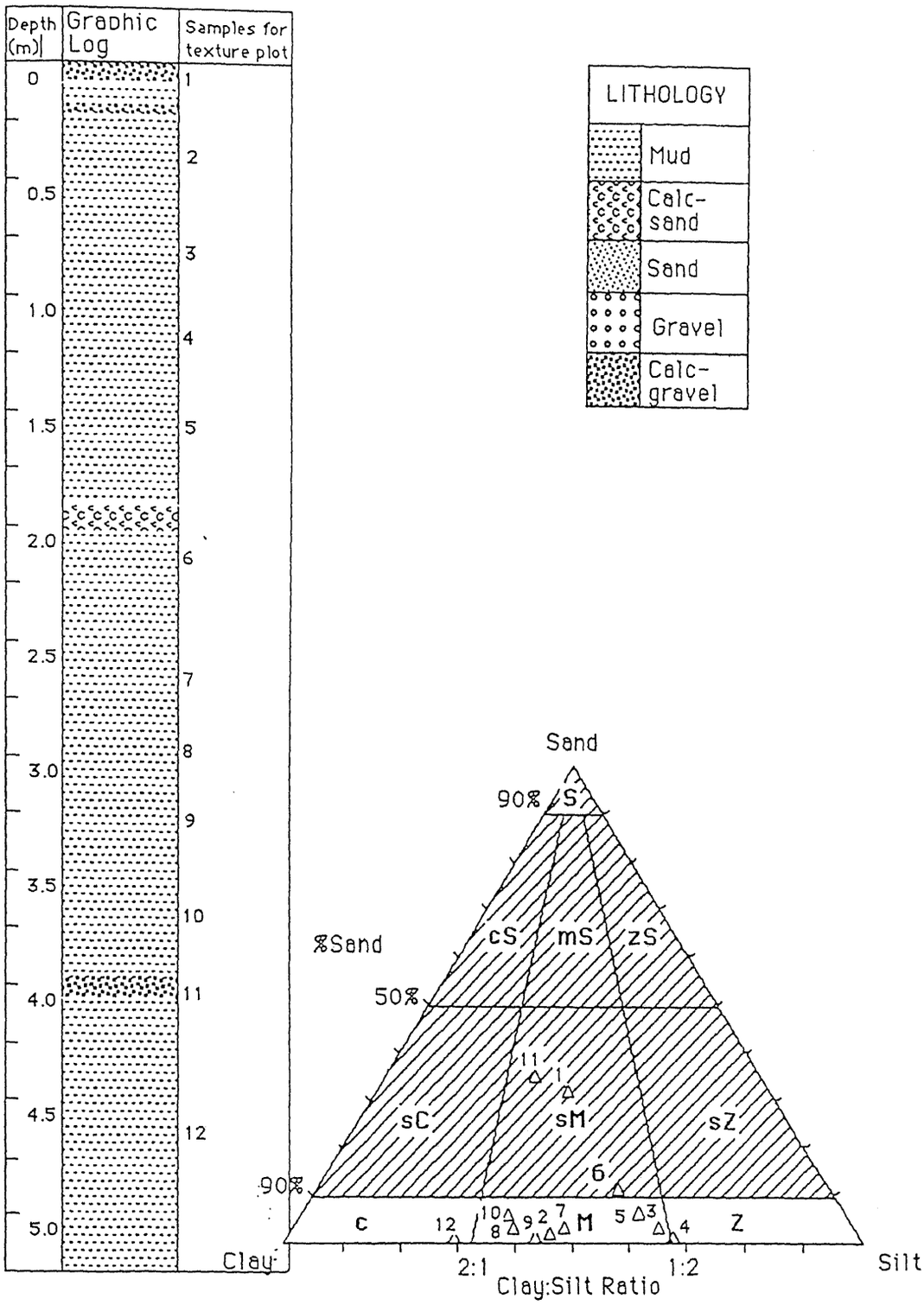

Figure A2.2

Carbonate-free textural classification of Core 31 sediments.

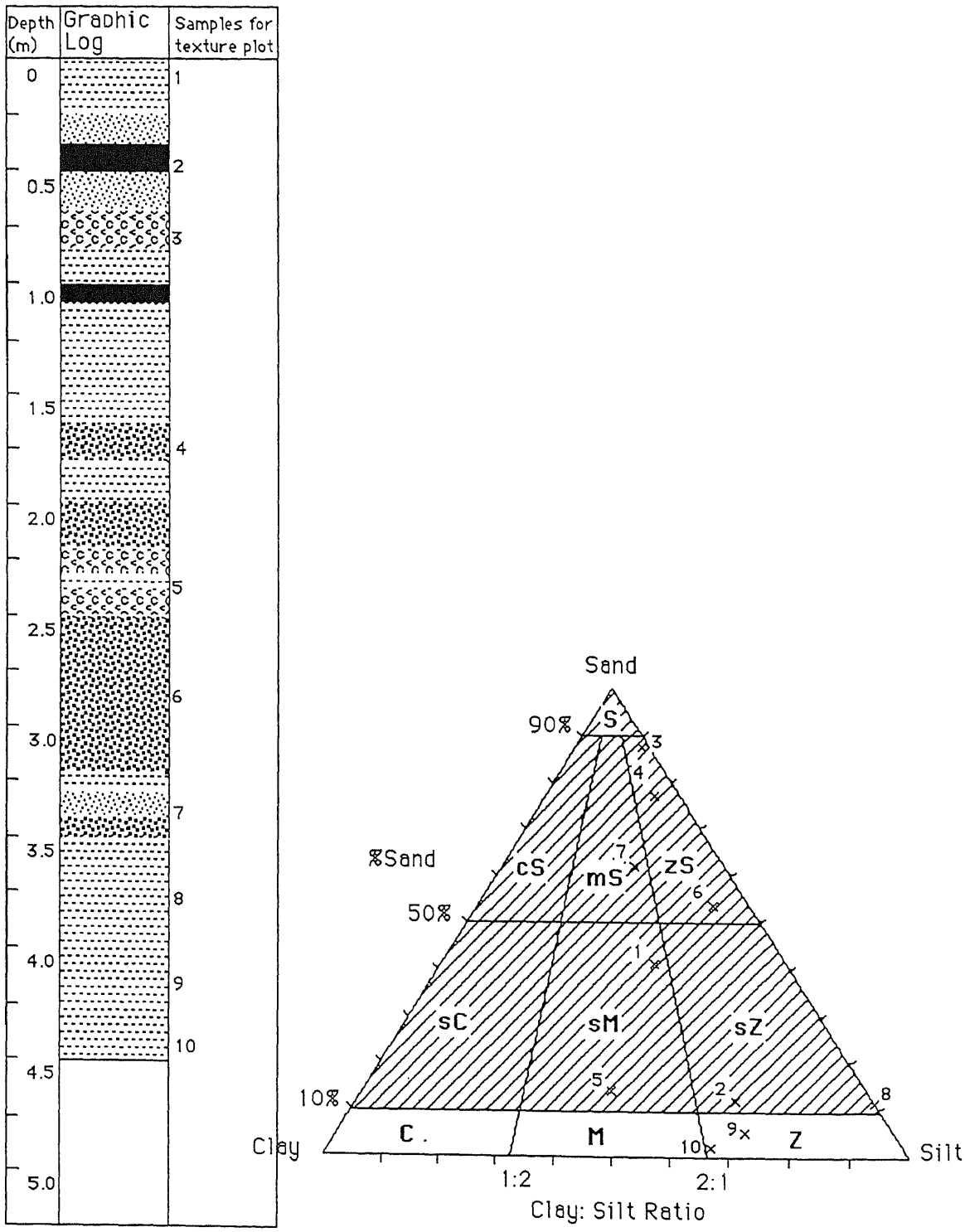

Figure A2.3

Carbonate-free textural classification of Core 37 sediments.

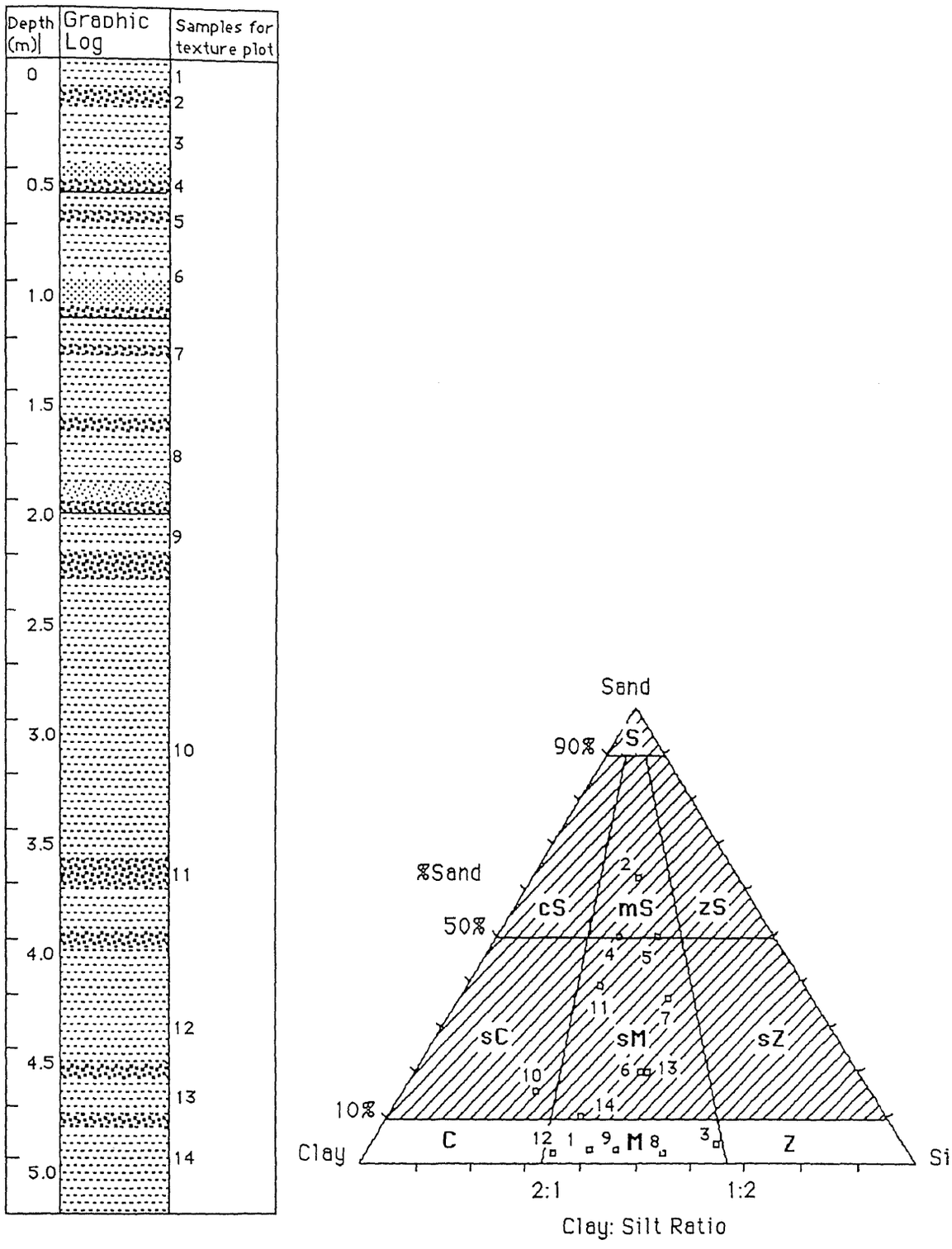

Figure A2.4

Carbonate-free textural classification of Core 40 sediments

APPENDIX 3: SEDIMENT MINERALOGY DATA

Presented in this appendix are the results of a quantitative analysis of mineralogy for Core 31 sediments (bulk, 2 μm-63 μm and < 2 μm), surficial core sediments and riverine bottom sediments.

Table A3.1

Bulk sediment mineral composition, Core 31.

Depth (cm)	Sample#	Volcanic Glass	Smectite	Halloysite + Illite	Allophane	Terrig. Detritus	CaC03	Organic Matter
0-2	31.1	45.2	3.4	11.0	3.5	8.4	24.9	6.7
20-22	31.2	52.1	4.3	16.2	3.0	7.5	10.0	6.9
40-42	31.3	52.6	10.3	17.8	4.0	7.0	4.4	7.3
60-62	31.4	53.8	5.2	21.0	3.2	9.0	1.0	6.8
80-82	31.5	49.3	2.1	18.9	2.2	15.3	5.1	6.5
100-102	31.6	50.1	4.2	20.0	2.6	15.2	1.0	7.0
120-122	31.7	51.9	3.4	19.7	3.1	16.3	2.5	7.4
140-142	31.8	47.3	7.2	22.3	3.0	13.4	0.5	6.3
160-162	31.9	47.6	5.3	20.7	3.4	11.9	6.6	6.4
180-182	31.10	42.0	8.5	15.0	2.8	13.5	12.0	6.2
200-202	31.11	39.5	15.6	21.6	2.7	7.0	7.1	6.5
220-222	31.12	39.6	25.3	19.5	3.0	5.0	1.0	6.6
240-242	31.13	38.1	20.6	14.5	3.5	15.9	1.2	5.7
260-262	31.14	32.1	27.2	18.9	3.7	8.5	2.1	7.5
280-282	31.15	29.6	24.5	18.7	2.1	14.6	3.5	6.9
300-302	31.16	30.9	15.8	10.2	2.0	20.0	13.9	7.2
320-322	31.17	25.7	40.5	16.8	3.0	7.0	0.1	6.9
340-342	31.18	22.4	35.9	17.4	2.8	10.0	5.2	6.3
360-362	31.19	23.3	25.3	22.4	2.1	14.3	7.1	5.6
380-382	31.20	24.0	38.5	24.2	2.2	5.2	0.0	5.9
400-402	31.21	11.2	4.6	7.2	2.4	4.6	63.4	7.9
420-422	31.22	13.2	41.5	20.3	2.8	12.0	3.5	6.9
440-442	31.23	12.4	38.2	16.1	3.2	4.0	20.1	6.0
460-462	31.24	14.8	39.1	17.8	2.5	12.9	5.1	6.2

N.B.Halloysite and illite also includes kaolinite.

Table A3.2

Mineral composition of the silt (2 μm-63 μm) fraction, Core 31.

Depth (cm)	Volc. Glass	Halloysite	Allophane	Terrig. Det
0-2	75.2	7.6	1.0	12.0
40-42	80.6	4.3	1.2	13.9
80-82	72.9	3.0	1.6	23.6
120-122	70.1	4.4	2.4	23.1
160-162	71.1	6.4	2.5	20.0
240-242	60.0	3.4	3.0	33.6
280-282	55.1	5.1	1.5	38.3
320-322	50.2	6.1	1.2	40.0
360-360	49.2	10.5	1.8	38.3
400-402	63.1	7.5	2.1	26.9
460-462	45.3	7.0	2.0	45.7

Table A3.3

Mineral composition of the clay (<2 μm) fraction, Core 31.

Depth (cm)	Volc. Glass	Smectite	Halloysite	Allophane	Illite
0-2	20.1	12.9	48.3	8.2	10.5
40-42	25.5	20.5	37.7	7.0	9.3
80-82	15.0	10.1	59.0	3.5	10.6
120-122	10.0	10.5	62.4	4.7	12.4
160-162	17.4	15.2	51.6	5.4	10.4
240-242	16.9	40.9	29.9	4.2	8.5
280-282	15.2	42.1	33.0	2.5	7.2
320-320	13.1	44.4	32.2	2.2	8.1
360-362	10.0	44.4	36.1	2.6	6.3
400-402	10.2	38.7	28.3	9.8	13.0
460-462	10.1	55.4	22.8	2.7	8.0

Table A3.4

Mineral composition of surficial core sediments and riverine bottom sediments.

Sample#	Allophane	Smectite	Illite	Halloysite (+kaolinite)	Volcanic glass	Calcium carbonate	Organic matter	Terrig. detritus
4.1	2.0	3.0	3.0	11.5	64.3	10.0	3.1	5.0
6.1	2.2	5.0	4.0	9.7	60.2	0.0	5.1	6.7
21.1	2.5	2.5	5.0	10.0	50.5	20.0	4.3	10.3
23.1	3.0	5.0	10.0	0.0	27.8	29.0	3.9	17.0
26.1	7.6	2.5	15.0	0.0	15.9	7.0	4.8	30.0
32.1	2.3	15.5	4.0	3.5	60.3	7.0	5.1	0.0
33.1	2.2	7.5	5.0	12.3	71.3	0.0	4.1	0.0
34.1	2.3	5.5	4.0	12.5	62.7	5.0	6.0	2.7
37.1	2.0	2.0	3.0	10.7	47.3	5.0	5.3	25.0
39.1	2.9	15.0	4.0	12.2	50.4	20.0	2.0	0.0
40.1	3.3	10.0	5.0	12.5	58.2	0.0	8.9	0.0
41.1	1.7	7.0	2.0	16.0	59.3	5.0	8.3	5.0
Average	3.0	7.0	5.3	9.2	55.0	10.0	6.0	9.0
RIVER SAMPLES								
Ohinemuri	3.0	0.0	3.0	3.0	72.0	0.0	4.0	15.0
Waitoa	2.0	0.0	5.0	14.0	50.0	0.0	4.0	15.0
Piako	3.0	0.0	4.0	11.0	60.0	0.0	5.0	17.0
Waihou	3.0	0.0	2.0	5.0	57.0	0.0	3.0	30.0

APPENDIX 4: BULK SEDIMENT GEOCHEMISTRY

X-ray fluorescence spectroscopy was used to analyse 52 samples from all Master Cores and a number of other cores (Table A4.1) for 20 elements. Analyses were carried out at the Victoria University Analytical Facility. Results are listed in Tables A4.2 and A4.3. Although bulk elemental analyses were determined for the Firth of Thames core samples the results are not described in detail in this thesis because of insufficient available time to do full justice to them. Some initial interpretations are made here, which should provide a baseline for further geochemical surveys of the sediments of the Firth of Thames.

Core sediment geochemistry can be an important tool in environmental impact investigations. Anthropogenic heavy metal-bearing pollutants accumulating in sediments of lakes, estuaries, harbours and coastal waters are becoming an increasing environmental problem which is receiving much greater awareness and this is attested to by the increasing number of pollution-orientated publications in recent years (Shrimp et al. 1971; Syers et al. 1973; Forstner and Muller 1973; Stoffers et al. 1986; Giovanni et al. 1990). The determination of concentrations of heavy metals in sediments of the Firth of Thames, which could be related to mining activities in the Coromanadel Range during historical times, is an interesting and pertinent application of this line of research in future studies.

A4.1 PRINCIPAL COMPONENT ANANLYSIS

A matrix of correlation coefficients is listed in Table A4.4. A principal component analysis performed on total elemental data for all samples confirms most of the element associations deduced from the correlation matrix and agrees with the trends observed by Stoffers et al. (1983) in a similar study. Four factors account for 99% of the total variance of the data. The factor loadings are shown in Table A4.5.

Factor 1: High loadings of SiO_2 and Na_2O and negative loadings of CaO and Sr are considered to represent the mutually exclusive nature of carbonate vs. terrigenous sedimentation (volcanic glass-dominated). Also in this factor are high loadings of K_2O, Rb, Ba, and Al_2O_3 which represent the influence of micaceous source rock (i.e., greywacke). This factor explains 38% of the variance in the data.

Factor 2: High loadings of TiO_2, Fe_2O_3, MgO, and V may represent a chlorite or heavy mineral factor. This factor explains 24% of the variance in the data.

Factor 3: High loadings of Pb, Cu, Zn, As and MnO are considered to represent an anthropogenic factor due to mining in the Coromandel Peninsula. Factor 3 accounts for 23% of the variance in the data.

Factor 4: This is an unusual factor being characterised by high loadings of P_2O_5, MgO and Na_2O and a negative Rb loading and may be an authigenic factor representing the formation of Mg-rich smectite. In Figure A4.1 a strong correlation between P_2O_5 and clay content is illustrated. P_2O_5 concentrations may be closely associated with authigenic smectite formation. The strongly negative Rb loading could be suggestive of the lack of a detrital origin for elements represented in this factor.

A seperate principal component analysis was also performed on elemental data from the surficial core sediments only and factor loadings are shown in Table A4.6. Three factors accounted for 96% of the total variance. In general the same geochemical associations are observed as for the bulk core elemental data. However, the anthropogenic factor (factor 2) accounts for 35% of the variance in the data suggesting Pb, Cu, Zn and As are concentrated in the surficial sediments. Also noted is the lack of an authigenic factor in the surficial sediments supporting a post-depositional diagenetic mineral genesis and consequently an increase in smectite abundance with sub-bottom depth in cores.

Vertical variations in Pb, Cu, Zn and As

The study of marine sediments represents a useful tool for determining the actual state of environmental pollution. Under ideal conditions where almost no physical and biological disturbances have occurred, sediments can be an invaluable historical record of environmental pollution. Accurate chronologies of sedimentation are requried in order to calculate rates of sedimentation and elemental influxes. A commonly used dating technique on a time scale of 100-200 y is by means of the natural isotope ^{210}Pb, followed by confirmation using the artificial isotope ^{137}Cs (Giovanni et al. 1990). Another useful technique, providing biological reworking of the sediment has not occurred, is by palynological analysis. In New Zealand, pollen horizons corresponding to Polynesian and European occupation may be identified. This technique is often backed up with radiocarbon dates on shell material.

Down-core profiles of the concentration of Pb, Cu, Zn and As are plotted for a number of cores from the Firth of Thames (Fig. 3.1) in Figure A4.2. Radicarbon ages are also shown where available. Cores 6 (adjacent to Tararu Stream), 21 (adjacent to Thames foreshore) and 37 (adjacent to Te Puru Stream) show a significant decrease in concentration of all four elements in the top 20 cm of each core. A radiocarbon age of 730±70 y B.P (Wk 1665, Table 5.1) on A. *stutchburyi* at 20 cm depth down Core 21 corresponds

to the position at which heavy metal concentrations appear to reach "normal background levels". Metal concentrations were generally an order of magnitude higher prior to this date and within the upper 20cm of the core. A high resolution chronolgy from 750 y B.P to present was not available and would probably have required the application of the dating methods mentioned above. However, it would appear reasonable to suggest that the increased metal concentrations in the sediments of the Firth of Thames are due to mining and mining-related activities over the last 150 years. A similar down-core trend in metal concentrations is observed for Core 40 (Fig. A4.2). However Core 31, in the central southern Firth of Thames showed no significant down-core variation (Fig. A4.2). The highest concentrations of Pb, Cu, Zn and As are in sediments adjacent to the mouths of streams draining the Coromandel Range, further relating the distributions to anthropogenic activities. These concentrations decrease progressively with distance offshore but are still significantly high in the vicinity of Core 40, 7km west of Tararu (Fig.3.1).

Geoaccumulation indices have been applied in various studies (Muller 1979; Stoffers et al. 1986) to compare the present day metal contamination with pre-civilisation background levels. Further research in the Firth of Thames could include such an investigation and may also include the evaluation of the mobility of metals in sediments of the Firth of Thames and consequently a discussion of the environmental implications.

Table A4.1
Sample positions and corresponding sample numbers for XRF analyses. Organic carbon contents and bulk densities are also shown

XRF Sample No.	Sample type	Sample position	Internal Sample No.	%C(org)	Bulk(kgm-3) density
TN-001	Sediment	C4 10-12 cm	C4 4.1	1.8	1275
TN-002	Sediment	C4 40-42 cm	C4 4.2	1.9	1260
TN-003	Sediment	C4 120-122 cm	C4 4.3	2.3	1319
TN-004	"	C4 200-202 cm	C4 4.4	---	1356
TN-005	"	C6 1-2 cm	C6 6.1	3.0	1390
TN-006	"	C6 5-6 cm	C6 6.1	3.7	1400
TN-007	"	C6 25-27 cm	C6 6.1	3.8	1410
TN-008	"	C6 75-77 cm	C6 6.2	---	1250
TN-009	"	C6 215-217 cm	C6 6.6	4.0	1430
TN-010	"	C21 2-4 cm	C21 21.1	2.6	1213
TN-011	"	C21 15-17 cm	C21 21.2	2.8	1183
TN-012	"	C21 20-22 cm	C21 21.2	2.9	1183
TN-013	"	C21 100-103 cm	C21 21.6	3.2	1303
TN-014	"	C21 140-142 cm	C21 21.8	3.3	1450
TN-015	"	C21 200-202 cm	C21 21.11	---	1195
TN-016	"	C21 300-303 cm	C21 21.17	4.3	1475
TN-017	"	C23 5-7 cm	C23 23.1	2.3	1225
TN-018	"	C23 20-22 cm	C23 23.2	2.7	1307
TN-019	"	C23 50-52 cm	C23 23.4	---	1325
TN-020	"	C23 120-122 cm	C23 23.7	3.7	1424
TN-021	"	C23 225-227 cm	C23 23.12	3.2	1417
TN-022	"	C23 370-372 cm	C23 23.19	3.0	1423
TN-023	"	C26 3-4 cm	C26 26.1	2.4	1190
TN-024	"	C26 115-117 cm	C26 26.3	4.7	1391
TN-025	"	C31 3-5 cm	C31 31.1	3.0	1250
TN-026	"	C31 100-102 cm	C31 31.6	2.8	1385
TN-027	"	C31 200-202 cm	C31 31.11	4.0	1315
TN-028	"	C32 7-9 cm	C32 32.1	4.1	1075
TN-029	"	C32 100-102 cm	C32 32.2	3.2	1412
TN-030	"	C32 200-202 cm	C32 32.4	4.2	1450
TN-031	"	C33 1-3 cm	C33 33.1	3.6	1420
TN-032	"	C33 110-112 cm	C33 33.4	3.9	1417
TN-033	"	C33 200-202 cm	C33 33.8	3.7	1439
TN-034	"	C34 2-4 cm	C34 34.1	4.0	1331
TN-035	"	C34 80-82 cm	C34 34.4	3.7	1390
TN-036	"	C37 3-5 cm	C37 37.1	3.5	1090
TN-037	"	C37 10-12 cm	C37 37.2	3.9	1111
TN-038	"	C37 15-17 cm	C37 37.2	3.5	1373
TN-039	"	C37 20-22 cm	C37 37.2	3.5	1373
TN-040	"	C37 110-112 cm	C37 37.7	---	1385
TN-041	"	C37 200-202 cm	C37 37.11	3.1	1270
TN-042	"	C37 300-302 cm	C37 37.16	---	1450
TN-043	"	C37 480-482 cm	C37 37.24	2.7	1515
TN-044	"	C40 3-5 cm	C40 40.1	9.8	1436
TN-045	"	C40 28-30 cm	C40 40.3	3.7	1180
TN-046	"	C40 150-152 cm	C40 40.8	3.3	1099
TN-047	"	C41 2-4 cm	C41 41.1	3.5	1395
TN-048	"	C41 5-6 cm	C41 41.1	3.5	1395
TN-049	"	C41 16-18 cm	C41 41.2	2.5	1285
TN-050	"	C41 111-113 cm	C41 41.5	15.4	1413
TN-051	"	C41 150-152 cm	C41 41.7	2.4	1403
TN-052	"	C41 210-212 cm	C41 41.7	2.5	1320

Table A4.2

Major element analyses for sediment samples from the Firth of Thames

Sample No.	SiO2 %	TiO2 %	Al2O3 %	Fe2O3 %	MnO %	MgO %	CaO %	Na2O %	K2O %	P2O5 %	LOI %	Total %
TN-001	64.20	0.64	9.62	5.21	0.24	1.42	7.23	1.28	1.16	0.10	9.67	99.76
TN-002	48.07	0.59	8.39	3.69	0.04	1.50	19.85	1.55	0.86	0.09	18.03	99.44
TN-003	54.17	0.55	9.20	4.51	0.04	1.71	14.21	1.45	0.91	0.08	15.05	99.23
TN-004	58.50	0.61	11.45	5.09	0.04	1.90	7.09	2.17	1.34	0.08	14.06	99.80
TN-005	54.85	0.46	11.41	4.36	0.15	1.80	7.22	3.27	1.57	0.15	17.26	99.69
TN-006	61.86	0.53	12.42	4.38	0.10	1.62	1.90	3.59	1.83	0.13	13.15	99.66
TN-007	52.62	0.50	12.04	4.66	0.09	1.73	6.66	3.23	1.61	0.15	19.99	99.63
TN-008	59.12	0.58	10.91	4.24	0.07	1.63	7.67	2.54	1.43	0.09	13.25	99.90
TN-009	55.99	0.55	13.47	5.20	0.08	1.83	2.03	3.85	1.61	0.11	18.19	99.26
TN-010	59.47	0.46	12.79	5.00	0.17	1.45	4.37	2.83	1.86	0.11	12.86	99.06
TN-011	55.78	0.33	11.26	3.40	0.07	1.16	10.17	2.99	2.00	0.08	14.53	99.24
TN-012	60.10	0.35	11.64	3.21	0.06	1.09	7.45	3.04	2.20	0.06	11.98	99.50
TN-013	58.22	0.62	12.81	4.90	0.06	1.82	3.81	3.23	1.58	0.10	14.68	99.85
TN-014	57.25	0.57	12.95	5.17	0.09	1.93	3.81	3.35	1.56	0.13	15.18	99.92
TN-015	57.67	0.54	13.17	5.10	0.09	1.69	2.86	3.14	1.59	0.11	16.34	100.08
TN-016	58.95	0.57	14.00	5.49	0.09	1.73	0.64	3.07	1.59	0.10	15.98	100.13
TN-017	31.58	0.59	7.83	3.54	0.05	1.95	31.46	1.76	0.47	0.11	24.97	99.20
TN-018	32.10	0.43	8.07	2.79	0.04	1.78	31.46	1.80	0.52	0.15	26.22	99.37
TN-019	28.66	0.41	7.20	2.98	0.04	1.82	34.78	1.55	0.41	0.11	28.03	99.10
TN-020	49.10	0.49	10.72	3.98	0.04	1.82	12.56	3.02	1.40	0.15	19.94	99.28
TN-021	58.69	0.68	13.46	4.90	0.04	1.80	3.68	3.19	1.57	0.11	13.501	00.10
TN-022	54.48	0.82	15.19	6.21	0.06	2.11	5.17	2.75	1.37	0.11	13.24	99.82
TN-023	54.25	0.83	15.26	6.12	0.06	2.08	5.16	2.69	1.35	0.11	13.74	99.89
TN-024	51.29	0.56	12.97	4.73	0.05	1.95	7.63	3.23	1.41	0.13	19.00	99.47
TN-025	50.62	0.43	10.83	3.67	0.04	1.63	11.22	3.31	1.47	0.20	19.77	99.67
TN-026	59.27	0.47	11.76	3.89	0.04	1.51	4.54	3.52	1.63	0.17	15.16	99.84
TN-027	57.71	0.54	13.03	5.11	0.05	1.90	1.30	3.82	1.60	0.16	17.15	99.19
TN-028	49.52	0.44	10.74	3.98	0.05	1.69	11.29	3.30	1.35	0.16	21.08	99.34
TN-029	60.12	0.49	11.80	4.23	0.04	1.66	2.92	3.99	1.62	0.25	15.85	99.54
TN-030	59.55	0.51	12.83	4.73	0.05	1.70	1.49	3.77	1.58	0.15	15.64	99.16
TN-031	53.75	0.47	11.61	4.30	0.06	1.87	6.29	3.91	1.60	0.14	18.85	99.19
TN-032	58.65	0.51	12.80	4.89	0.05	1.83	1.03	3.83	1.57	0.14	17.05	99.07
TN-033	54.97	0.52	12.40	4.85	0.07	1.84	4.55	3.75	1.61	0.15	18.31	99.09
TN-034	54.30	0.56	13.73	5.17	0.07	2.05	2.20	4.48	1.68	0.14	18.36	99.19
TN-035	55.83	0.50	12.37	4.93	0.05	1.79	3.44	3.53	1.51	0.17	18.69	99.06
TN-036	58.68	0.59	13.03	5.01	0.10	1.85	2.39	3.25	1.71	0.14	15.15	99.16
TN-037	57.36	0.63	13.90	5.32	0.10	1.99	1.63	3.58	1.71	0.14	15.67	99.13
TN-038	53.88	0.68	11.46	4.63	0.04	1.69	9.35	1.81	1.26	0.10	17.67	99.21
TN-039	56.73	0.64	22.23	5.27	0.06	1.91	3.64	2.89	1.63	0.13	15.60	99.10
TN-040	57.53	0.54	12.67	4.75	0.04	1.70	3.73	2.92	1.58	0.15	16.65	99.09
TN-041	59.93	0.55	12.74	4.59	0.06	1.48	3.20	2.63	1.60	0.10	14.96	99.29
TN-042	58.25	0.58	13.34	4.85	0.05	1.61	3.64	2.36	1.63	0.13	15.55	99.14
TN-043	60.20	0.64	15.21	4.78	0.05	1.37	2.50	2.06	1.80	0.09	12.63	99.08
TN-044	61.73	0.52	12.39	4.63	0.11	1.60	1.89	3.17	1.78	0.12	13.60	99.19
TN-045	56.14	0.51	12.40	4.71	0.07	1.97	2.47	4.49	1.70	0.13	18.05	99.10
TN-046	59.42	0.53	12.48	4.56	0.06	1.61	2.76	3.45	1.67	0.15	15.19	99.19
TN-047	54.05	0.65	13.40	5.04	0.09	1.75	6.53	2.48	1.48	0.13	16.73	99.40
TN-048	57.14	0.62	13.87	5.64	0.11	2.03	1.52	3.06	1.72	0.14	16.33	99.08
TN-049	56.98	0.76	11.33	5.26	0.07	1.72	9.10	1.74	1.23	0.13	13.15	99.18
TN-050	57.02	0.74	17.48	6.29	0.08	1.63	0.96	1.35	1.70	0.05	14.47	99.28
TN-051	59.63	0.62	12.15	4.41	0.05	1.58	6.74	1.79	1.43	0.08	12.91	99.21
TN-052	60.33	0.68	14.15	5.07	0.07	1.60	2.82	1.81	1.66	0.08	13.23	99.29

Table A4.3
XRF trace element analyses of core sediment samples from the Firth of Thames.
Results are reported in ppm.

SAMPLE	Ga	Pb	Rb	Sr	Th	U	Y	As	V	Cr	Ba	Ni	Cu	Zn
TN-001	9.1	70.2	45.3	293.2	4.8	1.1	15.0	33.8	114.0	124.2	233.2	10.9	34.5	206.1
TN-002	7.7	11.0	36.4	721.3	3.2	0.5	13.6	12.1	90.0	76.5	199.4	8.5	11.1	45.8
TN-003	9.4	11.3	40.0	674.9	3.6	2.0	14.9	16.1	102.2	78.2	174.5	10.6	14.0	62.6
TN-004	12.2	13.5	49.6	328.3	5.4	1.1	16.2	17.2	102.9	100.4	196.4	13.6	15.9	74.5
TN-005	13.0	91.4	55.2	266.3	6.4	1.2	16.2	23.4	87.1	79.4	223.8	13.8	29.7	246.0
TN-006	12.8	32.4	60.7	124.2	6.2	2.0	16.4	22.4	82.8	88.6	283.8	14.3	25.0	117.8
TN-007	12.5	20.3	53.4	244.0	5.6	1.2	15.6	35.4	84.7	70.0	247.3	13.8	15.7	70.8
TN-008	12.0	11.6	48.5	301.0	5.3	1.9	15.9	13.0	83.7	102.8	242.4	11.7	9.6	57.3
TN-009	14.7	15.2	53.9	113.7	6.2	1.5	16.9	13.4	101.2	77.8	191.8	15.4	15.5	71.7
TN-010	13.5	95.2	62.7	176.1	6.7	2.1	19.1	32.6	81.6	79.9	293.0	13.7	25.2	214.4
TN-011	13.7	11.8	65.2	359.4	7.1	2.3	21.7	9.7	56.1	63.6	378.5	9.3	7.4	55.9
TN-012	11.8	13.5	70.4	269.0	8.2	1.8	21.4	9.4	53.0	96.7	429.7	10.3	8.0	49.9
TN-013	13.8	11.2	51.3	172.0	6.5	1.3	18.9	8.5	93.8	78.1	240.4	14.4	11.6	65.6
TN-014	13.6	12.8	51.5	206.2	5.7	1.1	17.7	12.8	94.4	72.9	211.5	15.0	11.1	68.5
TN-015	14.1	14.6	53.8	140.5	7.7	2.1	18.3	12.2	96.1	61.1	208.8	15.7	13.2	71.0
TN-016	15.5	15.1	57.7	64.6	7.8	1.8	16.0	10.3	100.0	65.9	202.4	14.3	12.4	73.8
TN-017	8.0	7.7	22.4	1390.4	1.9	1.6	11.1	13.5	82.4	57.3	141.1	9.3	8.3	36.8
TN-018	6.7	8.6	22.6	1492.0	2.0	0.0	8.8	8.7	65.5	48.0	137.8	8.0	7.9	33.0
TN-019	6.7	8.5	19.6	1685.6	2.7	0.7	10.6	10.2	71.0	60.3	121.4	8.8	11.5	34.0
TN-020	12.8	8.7	42.1	574.0	4.4	3.0	13.4	12.9	86.0	63.9	185.0	13.0	10.6	53.5
TN-021	13.3	10.4	51.0	187.3	5.5	2.1	15.7	13.7	104.6	73.5	233.6	15.2	17.7	65.6
TN-022	13.4	13.7	53.2	283.1	6.5	2.4	16.9	12.4	92.8	60.5	245.4	13.9	13.8	61.9
TN-023	16.2	34.0	42.9	234.6	5.0	1.8	15.2	16.4	147.8	71.2	215.8	15.0	21.5	99.2
TN-024	13.9	12.6	43.8	357.0	6.3	3.0	15.3	9.9	105.7	55.9	210.0	14.0	14.0	61.5
TN-025	11.6	21.6	50.4	277.9	7.9	2.6	15.9	8.4	73.8	57.9	224.8	13.0	13.9	68.0
TN-026	11.9	12.3	55.3	237.0	6.3	1.7	15.8	8.7	74.4	61.2	253.3	12.5	10.6	58.7
TN-027	12.8	15.0	53.9	95.1	6.6	1.2	17.4	8.9	94.6	68.6	192.6	15.4	11.2	72.3
TN-028	11.0	13.4	46.3	376.7	5.2	1.4	15.3	7.9	78.0	60.7	190.5	13.6	7.4	58.7
TN-029	11.7	15.6	54.0	139.5	6.3	1.7	16.3	7.1	83.9	66.0	219.4	13.9	9.9	63.8
TN-030	12.9	14.0	54.9	111.4	6.5	1.2	16.8	9.0	88.5	78.9	214.5	14.5	10.7	70.1
TN-031	12.8	16.6	51.4	225.9	7.3	1.9	17.2	6.9	77.9	62.5	224.2	13.4	11.3	65.8
TN-032	13.5	14.7	54.3	85.2	6.4	1.8	16.6	9.4	94.1	70.3	194.0	17.0	16.0	72.1
TN-033	14.8	13.8	53.7	198.5	7.1	1.4	16.4	9.6	87.8	70.0	199.9	15.7	9.4	68.2
TN-034	13.8	20.5	55.5	131.3	6.6	2.0	17.4	7.3	91.2	72.3	216.5	16.8	15.6	75.1
TN-035	13.1	14.0	51.8	163.5	7.7	1.6	16.2	10.5	96.2	69.5	194.6	16.1	9.7	67.9
TN-036	13.9	49.0	58.3	129.8	5.7	1.1	15.8	19.5	102.5	78.5	225.2	15.9	33.2	178.3
TN-037	14.7	71.1	59.1	113.7	6.4	1.2	16.8	21.4	118.3	88.4	217.1	15.6	38.0	195.5
TN-038	11.9	12.0	48.6	353.7	4.0	1.3	12.5	12.2	115.8	98.9	199.8	14.1	17.7	58.8
TN-039	13.3	17.7	56.4	179.2	5.2	2.1	15.7	10.2	105.1	108.0	226.8	15.6	15.5	75.8
TN-040	14.8	13.4	53.7	185.6	6.0	2.3	16.6	12.1	102.4	106.5	195.7	15.9	12.7	70.7
TN-041	12.6	11.4	55.6	160.0	6.5	2.4	16.1	12.0	90.6	83.1	218.5	14.8	17.1	68.9
TN-042	13.0	14.6	57.8	172.8	6.0	2.3	17.2	8.8	95.1	99.2	227.0	15.9	15.8	69.5
TN-043	15.1	17.2	64.7	149.9	7.7	1.8	18.8	10.9	95.6	76.5	276.1	14.6	15.7	69.8
TN-044	13.7	61.1	63.1	120.7	6.5	1.9	17.6	14.2	81.4	92.3	244.7	14.4	21.2	192.1
TN-045	12.3	15.6	55.7	135.1	6.3	1.5	17.5	6.6	86.7	68.4	226.0	15.4	11.4	70.3
TN-046	13.0	12.3	54.9	147.7	6.3	1.6	17.5	9.6	82.3	73.8	239.9	14.3	9.2	65.6
TN-047	14.0	64.0	55.2	228.1	5.3	1.0	14.9	18.9	118.6	88.5	215.5	14.9	30.4	169.9
TN-048	14.4	96.8	61.9	104.8	7.2	1.7	16.5	23.3	114.6	87.6	210.6	16.4	36.0	226.1
TN-049	12.2	72.8	48.3	368.4	4.0	1.4	13.5	26.0	121.7	101.7	219.2	13.6	73.3	427.6
TN-050	15.8	20.9	57.0	94.5	5.1	1.2	15.3	15.1	158.4	98.5	240.3	19.4	33.4	74.7
TN-051	13.0	14.0	52.5	323.3	4.6	2.6	17.0	17.3	97.8	89.3	234.7	13.4	13.4	68.1
TN-052	15.7	16.2	62.2	157.9	7.4	2.3	16.9	12.0	109.6	80.5	262.3	15.5	16.8	76.6

Table A4.4
Correlation coefficient matrix for major and minor element data; n=52.

	SiO2	TiO2	AL2O3	Fe2O3	MnO	MgO	CaO	Na2O	K2O	P2O5	Pb	Rb	Sr	As	V	Cr	Ba	Ni	Cu	Zn
SiO2	1.000	0.203	0.565	0.533	0.287	-0.250	-0.929	0.363	0.846	-0.060	0.201	0.880	-0.930	0.119	0.233	0.429	0.558	0.609	0.202	0.249
TiO2		1.000	0.489	0.749	-0.024	0.437	-0.254	-0.345	-0.086	-0.302	0.126	0.008	-0.217	0.209	0.829	0.352	-0.175	0.426	0.465	0.252
Al2O3			1.000	0.741	0.227	0.173	-0.703	0.208	0.582	-0.093	0.136	0.593	-0.663	0.030	0.526	0.384	0.268	0.730	0.206	0.109
Fe2O3				1.000	0.320	0.469	-0.693	0.124	0.365	-0.133	0.290	0.418	-0.641	0.260	0.789	0.326	-0.032	0.807	0.429	0.318
MnO					1.000	0.005	-0.331	0.193	0.416	-0.074	0.791	0.448	-0.329	0.353	0.089	0.175	0.277	0.269	0.446	0.611
MgO						1.000	-0.003	0.244	-0.317	0.282	0.099	-0.354	0.057	0.030	0.417	-0.189	-0.650	0.337	0.138	0.086
CaO							1.000	-0.539	-0.862	-0.076	-0.213	-0.862	0.983	-0.080	-0.346	-0.362	-0.410	-0.816	-0.197	-0.217
Na2O								1.000	0.555	0.582	0.042	0.416	-0.538	-0.205	-0.269	-0.266	0.149	0.400	-0.195	-0.028
K2O									1.000	0.014	0.240	0.963	-0.876	0.080	0.011	0.314	0.747	0.572	0.099	0.177
P2O5										1.000	0.103	-0.063	-0.093	-0.119	-0.226	-0.360	-0.301	0.138	-0.051	0.087
Pb											1.000	0.318	-0.224	0.693	0.251	0.289	0.124	0.216	0.739	0.877
Rb												1.000	-0.874	0.142	0.066	0.413	0.736	0.565	0.193	0.267
Sr													1.000	-0.084	-0.309	-0.361	-0.458	-0.770	-0.193	-0.228
As														1.000	0.273	0.305	0.111	0.076	0.624	0.641
V															1.000	0.403	-0.250	0.611	0.552	0.312
Cr																1.000	0.259	0.318	0.438	0.368
Ba																	1.000	-0.005	0.022	0.086
Ni																		1.000	0.309	0.218
Cu																			1.000	0.911
Zn																				1.000

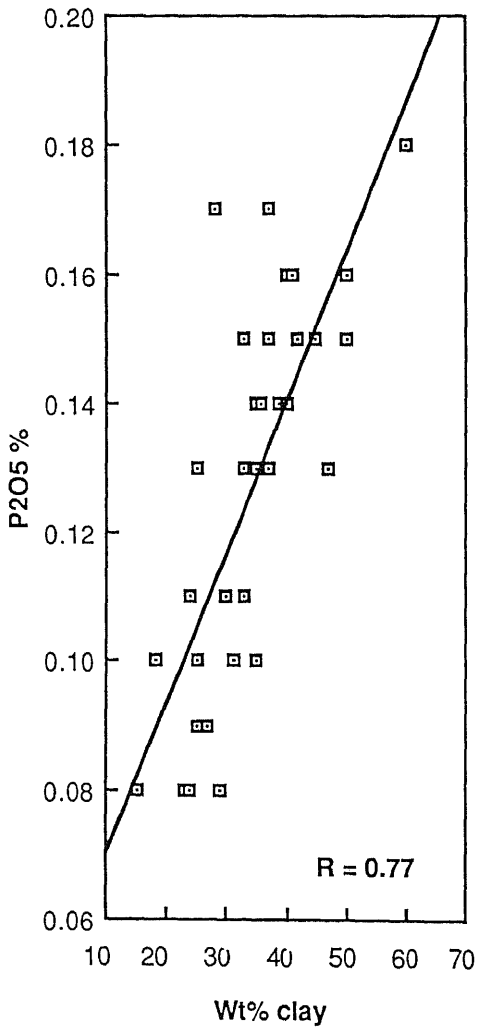

Figure A4.1
Relationship between phosphate and clay content.

Table A4.5
R-mode factor matrix for major and minor elements
from all core samples. Statistically significant factor loadings (> 0.5)are bolded.

	Factor 1	Factor 2	Factor 3	Factor 4
SiO2	**0.913**	0.142	0.113	-0.111
TiO2	0.007	**0.862**	0.111	-0.326
Al2O3	**0.644**	**0.558**	-0.004	-0.070
Fe2O3	0.442	**0.826**	0.204	-0.003
MnO	0.315	-0.652	**0.773**	0.086
MgO	-0.295	**0.688**	0.047	**0.529**
CaO	**-0.920**	-0.322	-0.086	-0.124
Na20	**0.531**	-0.111	-0.070	**0.782**
K20	**0.972**	-0.104	0.125	0.035
P2O5	-0.011	-0.073	0.048	0.843
Pb	0.127	0.056	**0.942**	0.084
Rb	**0.957**	-0.061	0.202	**-0.820**
Sr	**-0.928**	-0.260	-0.100	-0.117
As	-0.013	0.070	**0.823**	-0.172
V	0.072	**0.888**	0.211	-0.233
Cr	0.356	0.250	0.292	-0.564
Ba	**0.687**	-0.460	0.097	-0.378
Ni	**0.624**	**0.649**	0.097	0.227
Cu	0.033	0.363	**0.816**	-0.163
Zn	0.091	0.145	**0.921**	0.000
Cumulative variance explained	38%	62%	85%	99%

Variance explained by each factor
Factor 1 - 38%, Factor 2 - 24%, Factor 3 - 23%, Factor 4 - 14%

Table A4.6
R-mode factor matrix for major and minor element data from surficial core samples.
Statistically significant factor loadings (>0.5) are bolded.

	Factor 1	Factor 2	Factor 3
SiO2	**0.718**	**0.608**	0.105
TiO2	-0.123	0.005	**0.979**
Al2O3	**0.816**	-0.126	**0.508**
Fe2O3	0.477	**0.271**	**0.811**
MnO	0.026	**0.959**	0.062
MgO	0.000	-0.767	0.476
CaO	**-0.935**	-0.261	-0.149
Na2O	**0.713**	-0.559	-0.309
K2O	**0.960**	0.173	-0.176
P2O5	0.267	-0.462	-0.600
Pb	0.303	**0.865**	0.029
Rb	**0.902**	0.332	-0.210
Sr	**-0.938**	-0.230	-0.036
As	-0.071	**0.928**	0.210
V	0.067	0.134	**0.951**
Cr	0.089	**0.849**	0.296
Ba	**0.700**	0.579	-0.127
Ni	**0.905**	0.236	0.233
Cu	0.298	**0.767**	0.372
Zn	0.332	**0.864**	0.056
Cumulative variance explained.	39%	74%	96%

Variance explained by each factor
Factor 1 - 39%, Factor 2 - 35%, Factor 3 - 22%

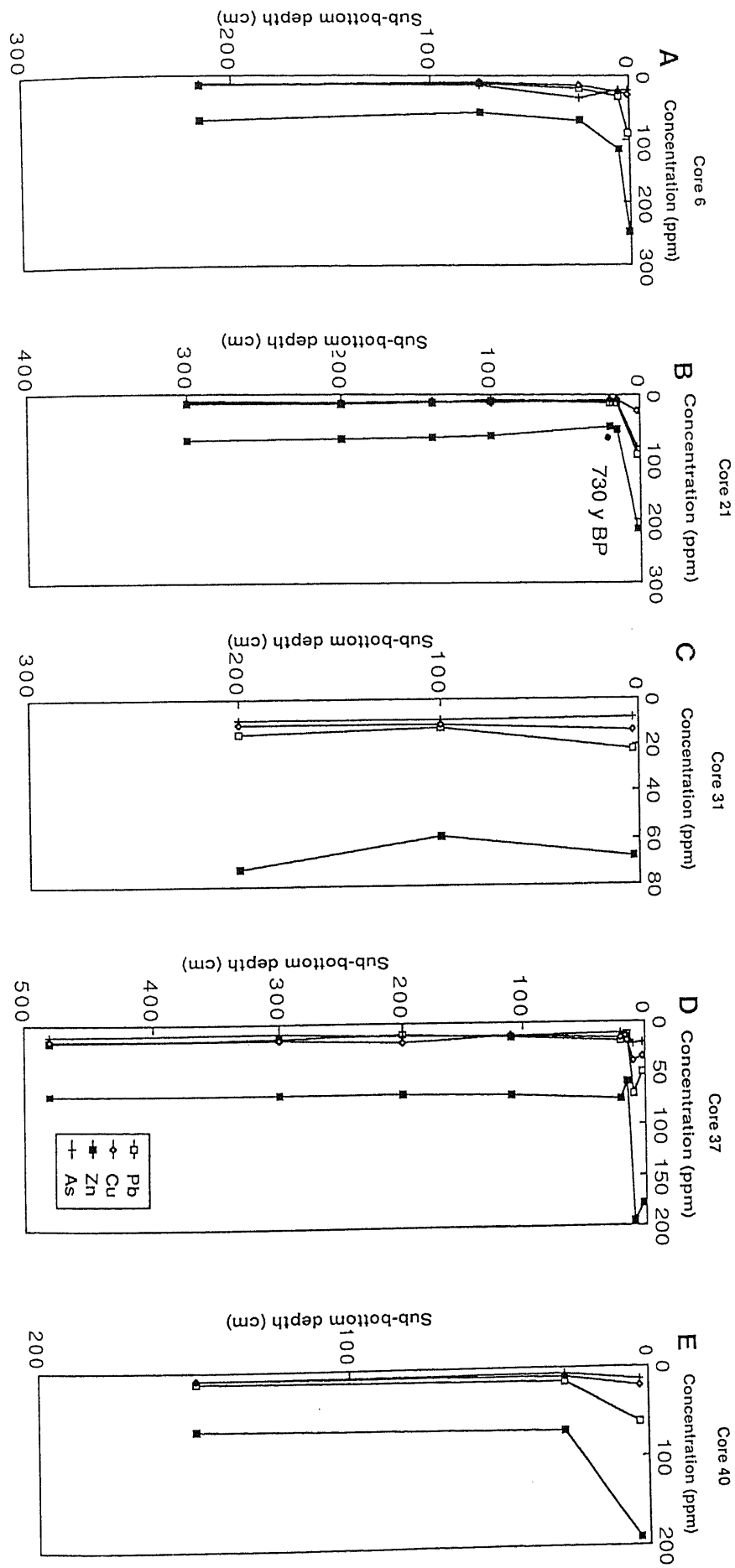

Figure A4.2
Down-core variations in the concentration of Pb, Cu, Zn and As for A) Core 6, B) Core 21, C) Core 31, D) Core 37 and E) Core 40.

APPENDIX 5. METHODOLOGY

Figure A5.1 is a flow diagram which shows the procedures followed and the various analyses undertaken in this study. There were three basic lines of analytical procedure: preparation and determination of major grain-size fractions; separation and preparation of sand, silt and clay fractions for mineralogical analysis; and preparation of bulk samples for chemical analysis.

A5.1 SEDIMENT TEXTURE

Approximately 30-40 g of available sediment was used for laboratory analysis. A sub-sample (15-20 g) was used for chemical analysis of organic carbon and elemental analysis by X-ray fluorescence spectroscopy (Chaps. 4 & 6, respectively). The remaining sediment was treated with 10% H_2O_2 and heated to remove organic matter. Samples were then gently washed with a washing solution (4g $NaHCO_3$ + 1g $NaCO_3$) upon a 63 µm sieve with as little physical abrasion as possible. The washing solution has a pH of approximately 9.4 and ensures no fine-grained calcareous elements are dissolved.

The coarse fraction was rinsed with distilled water and placed in an ultra-sound bath for 30 minutes in order to remove fine particulates adhering to the sand grains and then re-washed through a 63 µm sieve with distilled water onto filter paper and dried at 30°C for 24 hours. The <63 µm fraction was allowed to settle for a few days and the excess solution decanted off. The fine sediment was stored in 100 ml glass jars in washing solution away from sunlight to prevent any algal growth.

The >63 µm fraction was then passed through a 2 mm sieve to separate the gravel (> 2 mm) and sand (63 µm-2mm) fractions. The two fractions were then weighed to three decimal places using a *METTLER Pan Balance*. The <63 µm fraction was subjected to a pipette analysis according to the procedure outlined by Lewis (1983) after Folk (1968) to determine the percentage by weight of clay and silt.

The <63 µm fraction was transferred to a 1L measuring cylinder. 0.5-1.0 g of sodium metahexaphosphate ("Calgon") was added as a dispersent to prevent flocculation of the clays. The column was then topped up to 1000 ml with distilled water and thoroughly stirred using a stirring rod. A beaker is also filled with tap water and the temperature taken with a thermometer. Corrected pipette insertion depths were then calculated using the tables in Lewis (1983, page 99) from Folk's (1974) formula based on Stokes Law. Immediately after stirring a 20 ml pipette is inserted to 20 cm depth and a sample extracted at exactly 20 seconds. The first withdrawal represents everything finer than 63 µm (that is total mud). Another withdrawl is taken at 2hr at a depth 10 cm corresponding to 4 µm (for total

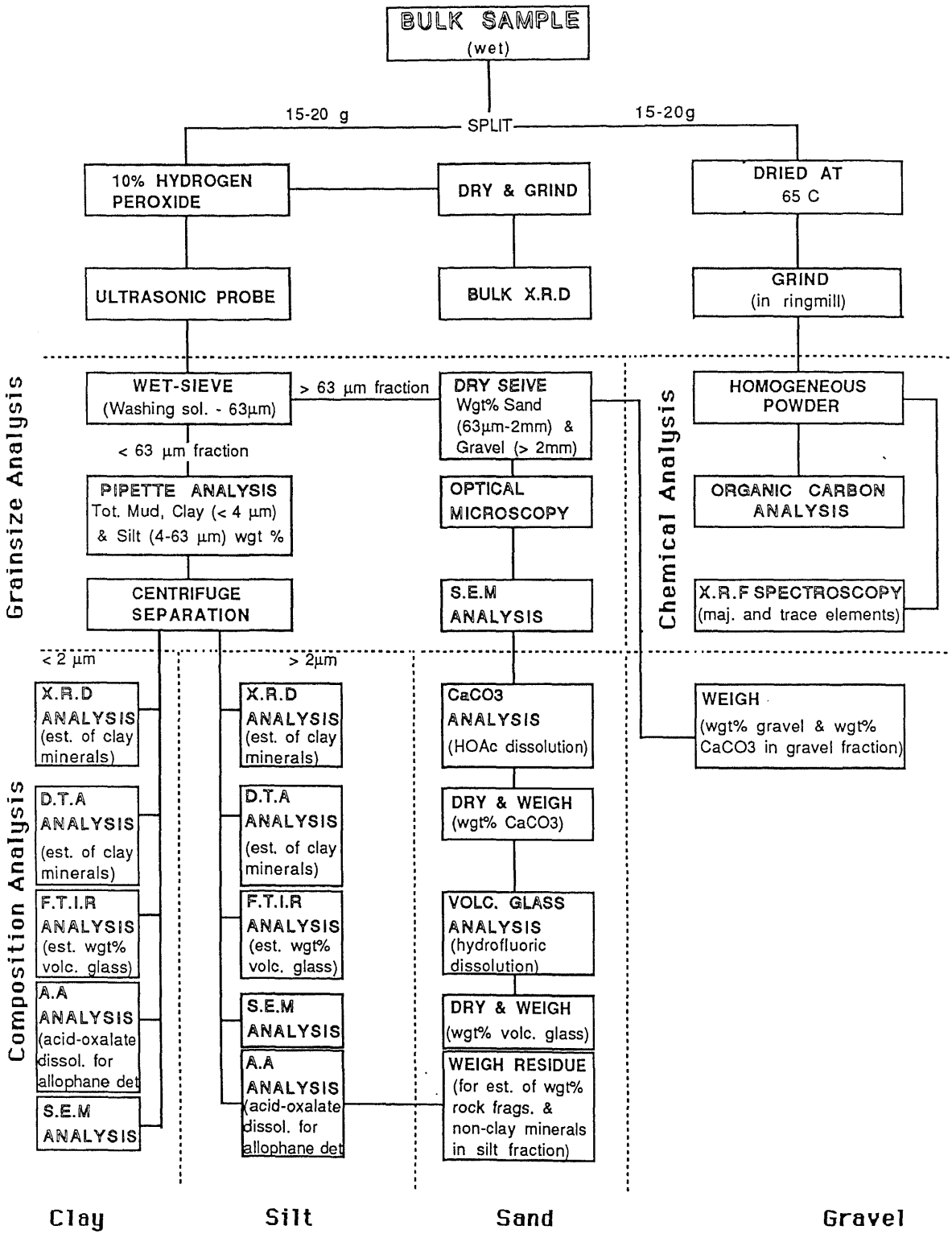

Figure A5.1
Laboratory procedure followed during analysis of the core sediments.

clay). The withdrawn samples are passed through pre-weighed filter paper, oven-dried at 65°C and reweighed. To calculate the weight percent of silt and clay:

a) The weight of filter paper is subtracted from the weight of the filter paper and plus dried sediment.

b) The weight of sediment from the <63 μm sample is multiplied by 50 and the weight of dispersent is then subtracted. This gives the value for the weight of mud. Adding this value to the weight of the >63 μm fraction provides the total sample weight.

c) The weight of sediment from the < 4μm sample is multiplied by 50 following the same procedure in b). This gives the value for the weight of clay. This value subtracted from the weight of mud calculated in b) provides the weight of silt in the sample.

d) Weight percent abundances for the size fractions (i.e., gravel, sand, silt and clay) are then obtained by dividing the individual size fractions by the total weight of sediment and multiplying by 100.

Master Cores 21, 23, 31, 37 and 40 were sampled at 20 cm intervals for textural anlyses, while Cores 4, 6, 26, 32, 33 and 34 were only sampled at obvious changes in lithology down core. Surficial sediments from Cores 8,9,19,11, 26, 28 and 39 were sampled for textural analysis.

A5.2 ORGANIC CARBON

Organic carbon content was determined by the Schollenberger method outlined by Allison (1965). This method uses potassium dichromate to oxidise the organic matter. The excess dichromate is then back-titrated with ammonium ferrous sulphate solution using barium diphenylamine sulphanate indicator. 0.785 g of potassium dichromate is added to 1 g of sample and about 10 ml of distilled water and gently heated for half an hour. A blank containing no sample is also prepared. After allowing time to cool 100 ml of distilled water is added and 5 ml of phosphoric acid. This is then titrated with 0.5 M ferrous ammonium sulphate solution to a greenish colour. At this stage 2 ml of barium diphenylamine sulphonate indicator is added. The titration is continued untill a green color is achieved once again.

A5.3 BULK DENSITY

Bulk density is the ratio of mass to unit volume of sediment. As the volume of sediment includes air space, bulk density is related to porosity and thus packing and grainsize. Undisturbed sediment samples of known volume in field-moist condition were used to determine bulk density. Only predominantly mud sediments were sampled at broad intervals downcore (see Appendix 1). All bulk

density determinations in Appendix 1 are presented on a field-moist basis and are therefore lower than would be expected for equivalent material on a dry density basis (i.e. taking into account soil moisture).

Sediments of similar grainsize (i.e. mud) were sampled in order that the bulk density could be related to the degree of compaction. There is a gradual increase in bulk density down all cores, from approximately 1100 kg/m^3 in surficial samples, to 1500 kg/m^3 at the base of the core. The results indicate no significant compaction or shortening of the sediment due to coring or core extrusion processes. The gradual increase in bulk density can be related to the increasing overburden weight of the sediment and, most importantly decreasing water content with depth.

A5.4 X-RAY DIFFRACTION ANALYSIS

All samples from master cores 21, 23, 31, 37 and 40, and surficial samples from cores 4,6,8,10,32,33,34,41 and 26 and river samples were prepared for x-ray diffraction analysis (XRD) of the < 63 μm fraction. The sand fraction (>63 μm) was removed by wet sieving during textural analysis procedures previously described in Appendix 5. Quantitative determination of sediment composition is carried out for the sand fraction independently and is discussed in Chapter 5. Although procedures are outlined by Nelson and Cochrane (1970), Hume and Nelson (1982) and Gibbs (1967) concerning the semi-quantitative determination of primary minerals by XRD (i.e. quartz and feldspar), it was concluded that due to the nature of the sediment such a technique would be unsuitable. The following are factors precluding the quantitative XRD analysis of sand fraction minerals.

i) Short-range order components such as volcanic glass and allophane are X-ray amorphous and tend to decrease the intensity of reflections from more crystalline minerals because of their significant absorption affect.

ii) The generally low concentrations of primary mineral components occurring in the silt fraction made accurate measurement of peak height above background problematic.

iii) The determination of feldspar percentage is further complicated when more than one species is present. Hume and Nelson (1982) acknowledge these difficulties. In particular confusion between minor X-ray peaks and the position of generally discrete plagioclase peaks can create inaccuracies.

iv) Significant variations in background noise level due to iron in samples affected peak

intensities and the recognition of peak positions.

v) Grinding samples during preparation causes the breakdown of rock fragments of andesite, greywacke and rhyolite to their mineral components producing higher concentrations of quartz and feldspar than traditional point counting techniques would reveal.

Therefore the purpose of using XRD analysis was: 1) to determine qualitatively minerals present in the silt (2-63 μm) and clay (< 2 μm) fractions; 2) To semi-quantitatively estimated the abundance of clay species present in the clay fraction.

Sample preparation and pretreatments

For analysis of the individual silt and clay fraction seperation of the < 2 μm and the 2-63 μm size range was achieved by a centrifugation technique following the method outlined by Lowe (1981). Silt samples were gently ground with a mortar and pestle until a homogeneous paste was produced. Grinding procedures were minimised as much as possible as overgrinding may destroy the structure of the clay minerals present. Orientated paste mounts were prepared using the smear on glass slide method (SOGS) after Hume (1978). The silt slides were then dried under an infrared lamp.

The clay separate was also prepared as an orientated mount by the SOGS method. However the clay samples were not dried rapidly under heat as this caused cracking of the sample due to the presence of short-range order constituents and also smectite. Instead the mounted specimens were dried slowly over distilled water in a dessicator for 72 hours. This procedure was adopted as it was suspected from preliminary X-ray runs of the clay fraction that 10Å halloysite may be present and drying by rapid heating can dehydrate it to its 7Å state at about 100° C. Unequivocal distinction between halloysite and kaolinite is difficult if halloysite is expected to be in the dehydrated 7Å form. Conversely, rehydration of 7Å halloysite is unlikely using this method.

For positive identification of clay mineral species it is necessary to identify changes in intensity and position of the basal reflections in response to various pre-treatments. The treatments used and their effects on clay minerals and corresponding variations in diffraction pattern are outlined by Brown and Brindly (1980), Hume and Nelson (1982) and Eslinger and Peaver (1986). Five X-ray runs were performed on aliquots of each sample after the following pre-treatments (Fig. 5.3):

i) An untreated sample (UT)

ii) Vapour solvation with ethylene glycol for 12 hours in order to distinguish between smectite, vermiculite and chlorite (G)

iii) Heating sample to 110° C causes dehydration of 10Å halloysite and a subsequent increase in the intensity of the 7Å peak. Thus used to distinguish 7Å and 10Å halloysite (110)

iv) Formamide is applied to an untreated specimen slide in order to distinguish between 7 Å halloysite and kaolinite. This method is outlined by Churchman et al. (1984) and is based on the relative abilities of 7 Å halloysite to intercalate polar organic compounds. Samples were sprayed with a fine film of formamide and analysed 1 hr later. It is important to analyse samples soon after treatment as kaolinte will also intercalate formamide, although more slowly.

v) Heating at 500° C for 1 hour to test for illite and chlorite.

Specimens were scanned from 3 to 15 °2O (clay) and 3 to 30 °2O (silt) on the Universty of Waikato *Philips PW 1840 X-Ray Diffractometer* using the following instrument settings.

kV = 20
mA = 20
T.C = 1 sec
Chart speed = 10 mm min^{-1}
Scanning speed = varied from 0.01-0.05 mm min^{-1}
Slit width = 0.1 mm
Range = $1*10^{-3}$

Semi-quanititative procedure for estimating clay mineral contents

Details of the weighting method for determining semi-quantitatively the abundance of clay minerals in the < 2 μm fraction are as follows:

1) All components are compared to the illite phase 10Å(110) which is obtained by measuring the area under the 10Å peak after heating to 110° C to remove 10Å halloysite.

2) To obtain the percentage smectite, area under the 14.0 Å(110) peak is measured and divided by 3 to correct for low-angle polarisation. The corrected peak intensities are then divided by the 10Å(110) value.

3) As the purpose of this analysis is primarily to determine the relative abundance of smectite in the clay fraction the remaining clay mineral phases, which are represented by the 7Å peak, are calculated as a group. On the diffractogram of the heated sample (110° C) (Fig. 5.3), total halloysite, kaolinite and chlorite is represented by the 7Å(110) peak and can be compared to 2 times that of the 10Å(110) peak.

The following is an example of a semi-quantitative calculation of clay mineral abundance for sample 31.17 in Figure 5.3. Peak areas were measured to give:

$10Å_{(110)}$ = 5 units^2
$14Å_{(110)}$ = 50 units^2
$7Å_{(110)}$ = 20 units^2

I	= 10Å(110)/10Å(110)	= 5/5	= 1.0	= 16%
S	= 14Å(110)/10Å(110) * 2 =	50/10	= 3.3	= 52%
K+H+C	= 7Å(110)/10Å(110) * 2	= 20/10	= 2.0	= 32%
			Total = 6.3	

Hence the clay mineral composition of the < 2 μm fraction is illite 16%, smectite 52%, halloysite and kaolinite and chlorite 32%. For the calculations to be valid the following assumptions are made:

i) The reported clay minerals comprise 100% of the sample. This however is not the case as X-ray amorphous allophane and volcanic glass are also present and are identified and determined quantitatively by other methods described later. The abundance of clay minerals in the < 2 μm fraction is then recalculated taking into account the amount of allophane and volcanic glass determined by other techniques, and the results are presented in Appendix 3 accordingly.

ii) For the weighting corrections selected for individual clay mineral species to be valid it is necessary to assume that the peaks on the heated diffraction trace represent the total conversion of 10Å to 7Å halloysite. Thus the 10Å(110) peak is solely due to illite and consequently there is minimal degradation of smectite to 10Å illite after heating to 110° C. Comparison of the untreated and heated 001 smectite peak would tend to reinforce this assumption.

A5.5 DIFFERENTIAL THERMOGRAVIMETRIC ANALYSIS

Aliquots of < 2 um and bulk samples seperated for XRD analysis were air dried and lightly ground in a mortar. Due to the length of time required for each analysis (3 hr), samples were carefully selected and only samples from Core 31 and river samples were analysed. Duplicates of random samples were run in order to test the reproducibility of results. 25-30 mg of sample were carefully weighed and inserted into a sample holder. Al_2O_3 is also added in a 1:1 ratio as a reference. Samples were heated from ambient temperature to 700° C at a rate of 10° min^{-1}. Analysis were made at the University of Waikato using a *Shimadzu DT-40 Thermal Analyser* coupled to a *Shimadzu Chromatopac C.R6A V1.0 microcomputer.*

Differences in temperature between a sample and a reference material (Al_2O_3) are recorded as the sample is heated at a controlled rate. A simultaneous gravimetric anaysis is also carried out. The loss in weight corresponding to changes in temperature, characteristic of halloysite (500°C), between the sample and the reference is calculated and compared to a 100% standard.

A5.6 INFRARED ABSORPTION ANALYSIS

Samples were prepared for analysis as KBr discs following the procedure outlined by Lowe and Nelson 1983 in which 1 mg of sample was mixed with 200 mg of oven-dry, spectrographically pure KBr. Gentle mixing in a mortar was sufficient to ensure a homogeneous mixture. The entire sample was then transferred to a vacuum die and evacuated for 2 minutes at a pressure of 1700 psi and heated to 70° C

Volcanic glass standards were prepared by mixing measured quantities of pure ground glass extracted from the sand fraction of the sample in question with measured quantities of pure halloysite. 1 mg of homogenised standard sample was mixed with 200 mg of KBr and prepared as disks by the above procedure. Ten standards were constructed ranging from 0 -10% volcanic glass. The length of the 800 cm^{-1} band in Figure 5.8, characteristic of volcanic glass, is measured and plotted against the known weight % abundance of the glass to form a standard calibration curve. By extrapolating values from the curve the weight% abundance of volcanic glass can be estimated for the silt and clay fractions. Infrared spectra were recorded in the 4000-450 cm^{-1} on a *PERKIN ELMER Model 1600 FOURIER TRANSFORM INFRARED SPECTROPHOTOMETER*.

A5.7 HYDROFLUORIC ACID DISSOLUTION ANALYSIS

1 g of sample is immersed in 10 ml of concentrated HF for 30 seconds, which was considered the optimum time for successful dissolution of volcanic glass. A boric acid solution was used to quench the reaction and the residue was washed through filter paper several times with distilled water. The

remaining mineral fraction was dried, weighed and the abundance of volcanic glass estimated. It should be noted that glass subjected to HF dissolution was not used in the subsequent SEM analysis described later. The fraction remaining after HF dissolution represents predominantly quartz, feldspar and rock fragments.

A5.8 DETERMINATION OF ALLOPHANE CONTENT

The methods of Parfitt and Wilson (1986) are used for the estimation of allophane. 1.5 g of field-moist soil is shaken with 100 ml of 0.2 M ammonium oxalate solution at pH 3 in a plastic centrifuge tube for 3 hours in the dark at 20° C on a horizontal reciprocating shaker. The contents were then centrifuged for 10 min at 2000 rpm and the clear supernatant stored in plastic bottles. Al and Si were determined using a *PHILLPS SP9 UNICAM ATOMIC ABSORPTION SPECTROPHOTOMETER* at the University of Waikato.

A5.9 SCANNING ELECTRON MICROSCOPY

Various methods of sample preparation were employed for SEM analysis. Sand-sized samples were subjected to ultrasonic vibration in freon for 10 seconds using a *DAWE 7530A SONIPROBE* in order to remove adhering fine particulates. Grains were then blown onto double sided-cellotaped brass stubs and a fine coating of gold applied. Silt-and sand-sized samples were prepared following the methods outlined in Lowe (1981). Microfossil specimens were hand picked under an optical binocular microscope.

APPENDIX 6: Waikato University, Department of Earth Sciences, archive numbers

Samples listed in the Appendices and referred to in this thesis are held in the Department of Earth Sciences rock and sediment store and are listed here with their corresponding Waikato (WT) archive numbers. All samples have been split into three fractions and stored individually as muds(>63μm), sands(2-63μm) or gravels(>2μm) and are labeled "WT sample No" M, S or G. Cores 1-45 are also stored.

Waikato No.	Thesis sample No.
WT 27368	21.01
WT 27369	21.02
WT 27370	21.03
WT 27371	21.04
WT 27372	21.05
WT 27373	21.06
WT 27374	21.07
WT 27375	21.08
WT 27376	21.09
WT 27377	21.11
WT 27378	21.12
WT 27379	21.14
WT 27380	21.15
WT 27381	21.16
WT 27382	21.17
WT 27383	21.18
WT 27384	21.19
WT 27385	23.01
WT 27386	23.02
WT 27387	23.03
WT 27388	23.04
WT 27389	23.05
WT 27390	23.06
WT 27391	23.07
WT 27392	23.09
WT 27393	23.11
WT 27394	23.12
WT 27395	23.13
WT 27396	23.14
WT 27397	23.15
WT 27398	23.16
WT 27399	23.17
WT 27400	23.18
WT 27401	23.19
WT 27402	31.01
WT 27403	31.02
WT 27404	31.03

WT 27405	31.04
WT 27406	31.05
WT 27407	31.06
WT 27408	31.07
WT 27409	31.08
WT 27410	31.09
WT 27411	31.10
WT 27412	31.11
WT 27413	31.12
WT 27414	31.13
WT 27415	31.14
WT 27416	31.15
WT 27417	31.16
WT 27418	31.17
WT 27419	31.19
WT 27420	31.20
WT 27421	31.21
WT 27421	31.22
WT 27422	31.23
WT 27423	31.24
WT 27424	37.01
WT 27425	37.02
WT 27426	37.05
WT 27427	37.07
WT 27428	37.09
WT 27429	37.11
WT 27430	37.13
WT 27431	37.15
WT 27432	37.17
WT 27433	37.19
WT 27434	37.21
WT 27435	37.23
WT 27436	40.01
WT 27437	40.02
WT 27438	40.03
WT 27439	40.04
WT 27440	40.05
WT 27441	40.06
WT 27442	40.07
WT 27443	40.08
WT 27444	40.09
WT 27445	40.10
WT 27446	40.11
WT 27447	40.12
WT 27448	40.13
WT 27449	40.14
WT 27450	40.15
WT 27451	40.16
WT 27452	40.17
WT 27453	40.18
WT 27454	40.19
WT 27455	40.20
WT 27456	40.21
WT 27457	40.22
WT 27458	40.23
WT 27459	40.24

WT 27460	40.25
WT 27461	40.26
WT 27462	40.27
WT 27463	41.01
WT 27464	41.02
WT 27465	41.05
WT 27466	4.01
WT 27467	4.02
WT 27468	4.03
WT 27469	4.04
WT 27470	32.01
WT 27471	32.02
WT 27472	32.04
WT 27473	33.01
WT 27474	33.04
WT 27475	26.01
WT 27476	26.03
WT 27477	34.01
WT 27478	6.01
WT 27479	6.02
WT 27479	6.04
WT 27480	6.06
WT 27481	8.01
WT 27482	10.1
WT 27483	11.1
WT 27484	28.1
WT 27485	29.1
WT 27486	39.1
WT 27487	PIAKO R.
WT 27488	WAIHOU R.
WT 27489	WAITOA R.
WT 27490	OHINEMURI R.
WT 27491	PEAT CORE (Kp 8)

Core archive numbers (Sample location of all cores shown in Figure 3.1)

WT 27492	CORE 1
WT 27493	CORE 2
WT 27494	CORE 3
WT 27495	CORE 4
WT 27496	CORE 5
WT 27497	CORE 6
WT 27498	CORE 7
WT 27499	CORE 8
WT 27500	CORE 9
WT 27501	CORE 10
WT 27502	CORE 11
WT 27503	CORE 12
WT 27504	CORE 13
WT 27505	CORE 14
WT 27506	CORE 15
WT 27507	CORE 16
WT 27508	CORE 17

WT 27509	CORE 18
WT 27510	CORE 19
WT 27511	CORE 20
WT 27512	CORE 21
WT 27513	CORE 22
WT 27514	CORE 23
WT 27515	CORE 24
WT 27516	CORE 25
WT 27517	CORE 26
WT 27518	CORE 27
WT 27519	CORE 28
WT 27520	CORE 29
WT 27521	CORE 30
WT 27522	CORE 31
WT 27523	CORE 32
WT 27524	CORE 33
WT 27525	CORE 34
WT 27526	CORE 35
WT 27527	CORE 36
WT 27528	CORE 37
WT 27529	CORE 38
WT 27530	CORE 39
WT 27531	CORE 40
WT 27532	CORE 41
WT 27533	CORE 42
WT 27534	CORE 42
WT 27535	CORE 44
WT 27536	CORE 45

-REFERENCES-

REFERENCES

Alison L.E. 1965: *In* Black C.A. (ed), *Methods of soil analysis. Part 2.* American Society of Agronomy, Madison, Wisconsin. 1367-1378.

Andrushchenko N.F., Gradusov B.P., Yeroshchev-Shak V.A., Yanshina R.S., Borisovskiy S.Ye. 1975: Composition and stucture of metamorphosed ferromanganese nodules, new vein formations of manganese hydroxides, and the surrounding pelagic sediments in the Southern Basin of the Pacific Ocean floor. *Internatational Geology Reviews*, 17: 865-1392.

Benson R.H. 1961: Ecology of ostracode assemblages. In Moore R.C. (ed.), *Crustacea, Ostracoda: Treatise on inveterbrate paleontology, Part Q, Arthropoda 3.* Geological Society of America and University of Kansas Press, 441pp.

Berner R.A. 1978: Rate control of mineral dissolution under earth surface conditions. *American Journal of Science*, 278: 1235-1252.

Beu A.G., Maxwell P.A. 1990: Cenozoic mollusca of New Zealand. *New Zealand Geological Survey Paleontological Bulletin*, no. 38.

Beutelspacher H., van der Marel H.W. 1968: *Atlas of electron microscopy of clay minerals and their admixtures.* Elsevier, New York, 333pp.

Birrell K.S., Pullar W.A. 1973: Weathering of paleosols in Holocene and late Pleistocene tephras in central North Island, New Zealand. *New Zealand Journal of Geology and Geophysics*, 16: 687-702.

Birrell K.S., Pullar W.A., Searle P.L. 1977: Weathering of Rotoehu ash in the Bay of Plenty district. *New Zealand Journal of Science*, 20: 303-310.

Biscaye P.E. 1965: Mineralogy and sedimentation of recent deep-sea clay in the Atlantic Oean and adjacent seas and oceans. *Bulletin of the Geological Society of America*, 76: 803-832.

Blom W.M. 1988: *Late Quaternary facies of Bass Basin, southeastern Australia: their environmental significance and response to sea-level changes,* Unpublished D.Phil. Thesis , Department of Geology and Geophysics, University of Sydney, Australia,250pp.

Bohor B.F., Hughes R.E. 1971: Scanning electron microscopy of clays and clay minerals. *Clays and Clay Minerals*, 19: 49-54.

Boldrin A., Bortollrri G., Frascari F., Guerzoni S., Rabitti S. 1988: Recent deposits and suspended sediments off the Po Della Pila (Po River Main Mouth), Italy. *Marine Geololgy*, 79: 159-169.

Boles J.R., Franks S.G. 1979: Clay diagenesis in Wilcox sandstones of Southwest Texas: Implications of smectite diagenesis on sandstone cementation. *Journal of Sedimentary Petrology*, 49,1: 55-70.

Bonatti E., 1972: Authigenesis of minerals - marine. In Fairbridge R.W. (Ed), *Encyclopedia of Geochemistry and Environmental Sciences*. New York (Van Nosrand Reinhold Co.), 48-46pp.

Bowman M.J., Chiswell S.M. 1982: Numerical tidal simulations within the Hauraki Gulf, New Zealand. In; Nihoul J.C.J. (ed), *Hydrodynamics of semi-enclosed seas*. Elsevier Scientific Publishing Company, Amsterdam; 349-384.

Brindley G.W., Brown G. (eds). 1980: Crystal structures of clay minerals and their X-ray identification. *Mineralogical Society Monograph No. 5, Mineralogical Society, London*, 495pp.

Butler V.L., and Stein J.K. 1988: Comments on "Changing late Holocene flooding frequencies of the Columbia River, Washington" by James C. Chatters and Kairn A Hoover. *Quaternary Research* 29: 186-187.

Carroll D., Starkey H.C. 1971: Reactivity of clay minerals with acids and alkalies. *Clays and Clay Minerals*, 19: 321-333.

Carter L. 1975: Sedimentation on the continental terrace around New Zealand: A review, *Marine Geology*, 19: 209-387.

Carter L., Eade J.V. 1980: *Hauraki sediments*. New Zealand Oceanographic Institute Coastal Chart Series 1:200 000.

Chamley H. 1971: Recherches sur la sedimentation argileuse en Mediterranee. *Sci. Geol.*, Strasbourg, mem, 35: 225 pp.

Chamley H. 1990: *Clay Sedimentology.* Springer-Verlag Berlin, 623pp.

Churchman G.J., Whitton J.S., Clariage G.G.C., Theng B.K.G. 1984: Intercalation method using formamide for differentiating halloysite from kaolinite. *Clays and Clay Minerals*, 32 (4): 241-248.

Churchman G.J., Hunt J.L., Glasby G.P., Renner R.M., Griffiths G.A . 1988: Input of river-derived sediment to New Zealand continental shelf: II mineralogy and composition. *Estuarine, Coastal and Shelf Science*, 27: 397-411.

Cole T.G., Shaw H.F. 1983: The nature and origin of authigenic smectites in some recent marine sediments. *Clay Minerals*, 18: 239-252.

Cuthbertson A.S. 1981: *The Hinuera Formation in the southern Hauraki Lowland*, Central North Island. Unpublished MSc Thesis, University of Waikato, New Zealand.

de Lange P.J. 1989: *Late Quaternary development of the Kopouatai Peat Bog, Hauraki Lowland, and some paleoenvironmental inferences.* Unpublished MSc Thesis, University of Waikato, New Zealand.

de Lange P.J., Lowe D.J. 1990: History of vertical displacement of Kerepehi Fault at Kopouatai Bog, Hauraki Lowlands, New Zealand, since c10 700 years ago, *New Zealand Journal of Geology and Geophysics*, 33 (2): 277-285.

Decarreau A., Bonnin D., Badaut-Trauth D., Couty R., Kaiser P. 1987: Synthesis and crystallogenesis of ferric smectite by evolution of Si-Fe coprecipitates in oxidising conditions. *Clay Minerals*, 22: 207-223.

Dravitzki M.L. 1988: *Littoral drift of mixed sand and gravel sediments on four gravel delta fans, western Coromandel, New Zealand.* Unpublished MSc. Thesis, University of Waikato, New Zealand, 188pp.

Eberl D.D. 1984: Clay mineral formation and transformation in rocks and soils. *Philosophical Transanctions of the Royal Society of London*, 311: 241-257.

Eslinger E., Pevear D. 1988: Clay minerals for petroleum geologists and engineers, *Society of Ecomonic Paleontologists and Mineralogists Short Course* no. 22.

Farmer V.C. 1974: The infrared spectra of minerals. *Mineralogical Society*, London, 539pp.

Farmer V.C., Fraser A.R., Russell J.D., Yoshinaga N. 1977: Recognition of imogolite structures in allophanic clays by infrared spectroscopy. *Clays and Clay Minerals*, 12: 55-57.

Farmer V.C., Fraser A.R., Tait J.M., Palmieri F., Violante P., Nakai M., Yoshinaga N. 1978: Imogolite and proto-imogolite in an italian soil developed on volcanic ash. *Clays and Clay Minerals*, 13: 271-275.

Folk R.L. 1968: *Petrology of sedimentary rocks.* University of Texas, Hemphill's, Austin, Texas, 170pp.

Folk R.L., Andrews P.B., Lewis D.W. 1970: *Detrital sedimentary rock classification and nomenclature for use in New Zealand.* University of Canterbury, New Zealand.

Forstner U., Muller. 1973: Heavy metal accumulation in river sediments: a response to environmental pollution. *Geoforum*, 14:53-63.

Furket R.J., Smidt R.E. 1972: Soil Bureau Laboratory Methods. *New Zealand Soil Bureau Scientific Report* 10, NZ DSIR.

Gagan M.K., Johnson D.P., Carter R.M. 1988: The Cyclone Winifred storm bed, central Great Barrier Reef Shelf, Australia. *Journal of Sedimentary Petrology*, 58 (5) 845-856.

Gardner J.V., Nelson C.S., Baker P.A. 1985: Distribution and character of pale green laminae in sediment from Lord Howe Rise: a probable late Neogene and Quaternary tephrostratigraphic Record. *In: Initial Reports of the Deep Sea Drilling Project*, 90: 1145-1159.

Gibb J.G. 1986: A New Zealand regional Holocene eustatic sea level curve and its application to determination of vertical tectonic movements. *Royal Society of New Zealand Bulletin,* 24: 377-395.

Gibb J.G., Aburn J.H. 1986: Shoreline fluctuations and an assessment of a coastal hazard zone along Pauanui Beach, eastern Coromandel Peninsula, New Zealand. *Ministry of Works, Water and Soil Technical Publication,* No 27.

Gibbs R.L. 1967: Quantitative X-ray diffraction analysis using clay mineral standards extracted from the samples to be analysed. *Clay Minerals*, 7: 79-90.

Gieskes J.M., Kastner M. 1975: Evidence for extensive diagenesis, Madagascar Basin, D.S.D.P site 245. *Geochimica et Cosmochimica Acta*, 39: 1385-1393.

Green B.E. 1987: *Weathering of buried paleosols on late Quaternary rhyolitic tephras, Rotorua region, New Zealand.* Unpublished M.Sc. Thesis, University of Waikato, New Zealand.

Greig A. 1982: *Sediments and recent geological history of the Hauraki Gulf.* Unpublished M.Sc. Thesis, University of Auckland, New Zealand, 205pp.

Greig M.J., Proctor R.1988: A numerical model of the Hauraki Gulf, New Zealand. *New Zealand Journal of Marine and Freshwater Research*, 22: 379-390.

Griffiths G.A., Glasby G.P. 1985: Input of river-derived sediment to the New Zealand Continental Shelf. I. Mass. *Estuarine, Coastal and Shelf Science*, 21: 773-787.

Hannah J. 1988: Analysis of mean sea level trends in New Zealand form historical tidal data. *Dept. of Survey and Land Information*, report No. 2.

Haq B.U., Boersma A. 1978: *Introduction to marine micropaleontology*. Elsevier, New York, 376p.

Hayes M.O. 1967: Hurricanes as geological agents: case studies of Hurrican Carla, 1961, and Cindy, 1963. University of Texas, *Bureau of Economic Geolology, Rept Inv*, 61-54.

Hayward B.W. 1986: A guide to paleoenvironmental assessment using New Zealand Cenozoic foraminiferal faunas. *New Zealand Geological Survey Paleontological Report* 109.

Heath R.A 1977: Phase distribution of tidal constituents around New Zealand. *New Zealand Journal of Marine and Freshwater Research*, 11: 383-392.

Healy T.R., Kirk R.M. 1982: Coasts, *In* Soons J.M., Selby M.J. (eds.), *Landforms of New Zealand.* 392pp. Longman Paul Ltd. Auckland New Zealand.

Healy T.R., Erlenkeuser H., Werner F., Winn K. 1987: Theoretical post-glacial sedimentation rates for a semi-enclosed sea; example of the Kieler Bucht, Western Baltic. *Boreas*, 16: 207-213.

Healy T.R., Werner F. 1987: Sediment budget for a semi-enclosed sea in a near homogeneous

lithology; example of the Kieler Bucht, Western Baltic. *Senkenbergiana marit*, 19: 195-222.

Healy J., Schofield J.C., Thompson B.N. 1964: Sheet 5 - *Rotorua*. Geological map of New Zealand 1:250000. Wellington, New Zealand. Department of Scientific and Industrial Research.

Healy J. 1969: Geological report on proposed tunnel line, Kaimai Railway Deviation. Unpublished New Zealand Geological Survey Report. 65p.

Hein J.R., Scholl D.W. 1978: Diagenesis and distribution of late Cenozoic volcanic sediment in the South Bering Sea. *Geological Society of America Bulletin*, 89: 197-210.

Hein J.R., Scholl D.W., Miller J. 1978: Episodes of Aleutian Ridge explosive volcanism. *Science*, 199: 137-141.

Henshaw G.S. 1988: Sorption of trace metals on suspended sediment of the Waihou River. Unpublished MSc Thesis, University of Auckland, New Zealand.

Hochstein M.P., Nixon I.M. 1979: Geophysical study of the Hauraki Depression, North Island, New Zealand. *New Zealand Journal of Geology and Geophysics*, 22, 1: 1-19.

Hochstein M.P., Tearney K., Rawson S., Davey F.J., Davidge S., Henrys S., Backshall D. 1986: Structure of the Hauraki Rift (New Zealand). *Royal Society of New Zealand Bulletin,* 24: 333-348

Hodder A.P.W. 1985: Effect of composition on hydration kinetics in colcanic glasses: Implications for dating. *Journal of Colloid and Interface Science*, 103, 1: 45-49.

Hornibrook N.de B. 1952: Tertiary and recent marine ostracoda of New Zealand. *Palaeontological Bulletin,* 8: 82pp.

Houghton B.F., Cuthbertson A.S. 1989: Sheet T14 BD - *Kaimai*. Geological map of New Zealand 1:50000 : Department of Scientific and Industrial Research.

Hume T.M., Sherwood A.M., Nelson C.S. 1975: Alluvial sedimentology of the Upper Pleistocene Hinuera Formation, Hamilton Basin, New Zealand. *Journal of the Royal Society of New Zealand* 5: 421-462.

Hume T.M. 1978: *Clay petrology of Mesozoic to recent sediments of central Western North Island, New Zealand.* Unpublished D.Phil. Thesis , University of Waikato, New Zealand.

Hume T.M., Nelson C.S. 1982: X-ray diffraction analytical procedures and some mineralogical characteristics for South Auckland region sediments and sedimentary rocks, with special reference ot their clay fraction. Occasional Reprot No.10, University of Waikato, Department of Earth Science, 33pp.

Hume T.M., Nelson C.S. 1986: Distribution and origin of clay minerals in surfical shelf sediments Western North Island, New Zealand. *Marine Geology*, 69: 289-308.

Isla F.I. 1989: Holocene sea level fluctuation in the Southern Hemisphere. *Quaternary Science Rviews*, 8: 359-368.

Kear D., Tolley W.P. 1957: Notes on Pleistocene and Jurassic beds near Morrinsville. *New Zealand Journal of Science and Technology*, sB,General 38: 500-506.

Kellar J., Ryan W.B.F., Ninkovitch D., Altherr R. 1978: Explosive activity in the Mediterranean over the last 200,000 y as recorded in deep-sea sediments. *Geological Society of America Bulletin*, 89: 591-604.

Kirkman J.H. 1975: Clay mineralogy of some Tephra Beds of Rotorua area, North Island, New Zealand. *Clays and Clay Minerals*, 10: 437-449.

Kirkman J.H. 1976: Clay mineralogy of thirteen paleosols developed in Holocene and late Pleistocene tephras of central North Island, New Zealand. *New Zealand Journal of Geology and Geophysics*, 19: 179-187.

Kirkman J.H. 1977: Possible structure of halloysite disks and cylinders oberved in some New Zealand rhyolitic tephras. *Clay Minerals*, 12: 12-18.

Kirkman J.H., McHardy W.J. 1980: A comparative study of the morphology, chemical composition and weathering of rhyolitic and andesitic glass. *Clay Minerals*, 15: 165-173.

Kirkman J.H. 1980: Clay mineralogy of a sequence of Andesitic Tephra Beds of Western Taranaki, New Zealand. *Clays and Clay Minerals*, 15: 157-163.

Kiwi Gold Exploration Co Ltd. 1987: Preliminary geological assessment, E.L. 33 290 Firth of Thames, New Zealand. Prep. by Applied Geology Associates Ltd.

Kreisa R.D. 1981: Storm-generated sedimentary structures in subtidal marine facies with examples from the middle and upper Ordovician of south western Viginia. *Journal of Sedimentary Petrology*, 51: 823-848.

Lerman A., MacKenzie F.T., Bricker O.P. 1975: Rates of dissolution of aluminosilicates in sea water. *Earth and Planetary Science Letters*, 25: 82-88.

Lewis D.W.1984: *Practical sedimentology.* Hutchinson Ross Publishing Company, 229pp.

Loeblich A.R., Tappen H. 1964: *Sarcondina, cheifly "Thecamoebians" and Foraminiferida: Treatise on invertebrate paleontology, part c, Protista* 2, v. 1-2. Geological Society of America and University of Kansas.

Lowe D.J. 1981: *Origin and composite nature of late Quaternary airfall deposits*, Hamilton Basin, New Zealand. Unpublished M.Sc. Thesis, University of Waikato, New Zealand.

Lowe D.J., Nelson C.S. 1983: Guide to the nature and method of analysis of the clay fraction in tephras from the South Auckland region, New Zealand, Occasional Report No.11. Department of Earth Sciences, University of Waikato, New Zealand, 69pp.

MacKenzie R.C (ed) 1970: *Differential thermal analysis.* Vol 1, fundamental aspects. Academic Press, London and New York, 775pp.

McKyes E., Sethi A., Yong R.N. 1974: Amorphous costings on particles of sensitive clay soils. *Clays and Clay Minerals*, 22: 427-233.

Male A.G.B., Cochrane G.R. 1978: Analysis of suspended sediment patterns in the Firth of Thames, In: Landsat 2 over New Zealand. New Zealand D.S.I.R Bulletin , Ellis P.J., Thomas L.L. (eds). 221: 411-413.

Marks G.P., Nelson C.S. 1979: Sedimentology and evolution of Omaro spit, Coromandel Peninsula, *New Zealand Journal of Marine and Freshwater Research*, 13(3): 347-372.

Mathews D.H. 1962: Altered lavas from the floor of the eastern North Atlantic. *Nature*, 194: 368-369.

Melson W.G., Thompson G. 1973: Glassy abyssal basalts, Atlantic Sea floor near St Paul's Rocks: Petrography and composition of secondary clay minerals. *Geological Society of America Bulletin*, 84: 703-716.

Middleton A. 1987: *The distribution and weathering of the Martha Mine Tailings.* Unpublished MSc. Thesis, University of Waikato, New Zealand, 306pp.

Mossler J.H., Hayes J.B. 1966: Ordovician potassium bentonites of Iowa. *Journal of Sedimentary Petrology*, 36, 2: 414-427.

Murphy W.M., Oelkers E.H., Lichtner P.C. 1989: Surface reaction versus diffusion control of mineral dissolution and growth rates in geochemical processes. *Chemical Geology*, 78, 3/4: 357-358.

Nadeau P.H., Wilson M.J., McHardy W.J., Tait J.M., 1985: The conversion of smectite to illite during diagenesis: evidence from some illitic clays from bentonites and sandstones. *Mineralogical Magazine*, 49: 393-400.

Naidu A.S., Burrell D.C., Hood D.W. 1971: Clay mineral composition and geological significance of some Beaufort Sea sediments. *Journal of Sedimentary Petrology*, 47: 691-694.

Nayudu Y.R. 1964: Palogonite tuffs (hyaloclastites) and the products of posteruptive processes. *Bulletin Volcanology*, 27: 332-341.

Nelson C.S., Cochrane R.H.A. 1970: A rapid X-ray method for the quantitative determination of selected minerals in fine grained and altered rocks. *Tane*, 16: 152-162.

Nelson C.S. 1977: Grainsize parameters of insoluble residues in mixed terrigenous-skeletal carbonate sediments and sedimentary rocks: some New Zealand examples. *Sedimentology* 24: 31-52.

Nelson C.S., Hume T.M. 1977: Relative intensity of tectonic events revealed by the Tertiary sediment record in the North Wanganui Basin and adjacent areas, New Zealand. *New Zealand Journal of Geology and Geophysics*, 20 (2): 369-392.

Nelson C. H. 1982: Modern shallow water graded and layers from storm surges, Bering Shelf: a mimic of Bouma sequences and turbidite systems. *Journal Sedimentary Petrology*, 52: 537-545.

Noh J.H., Boles J.R. 1989: Diagenetic alteration of perlite in the Guryongpo area, Republic of Korea. *Clays and Clay Minerals*, 37, 1: 47-58.

Odom I.E. 1984: Smectite clay minerals; properties and uses, *Philosophical Transactions of the Royal Society of London*, 311: 391-409.

Parfitt R.L., Furkert R.J., Henmi T. 1980: Identification and structure of two types of allophane from volcanic ash soils and tephra, *Clays and Clay Minerals*, 28 (5): 328-334.

Parfitt R.L., Hemni T. 1980: Structure of some allophanes from New Zealand. *Clays and Clay Minerals* 28 (4): 285-294.

Parfitt R.L., Henmi T. 1982: Comparison of an oxalate extraction method and an infrared spectroscopic method for determining allophane in soil clays. *Soil Science and Plant Nutrition*, 28 (2): 183-190.

Parfitt R.L., Russell M., Orbell G.E. 1983: Weathering sequence of soils from volcanic ash involving allophane and halloysite, New Zealand. *Geoderma*, 29: 41-57.

Parfitt R.L., Wilson A.D., 1986: Estimation of allophane and halloysite in three sequences of volcanic soils, New Zealand. In "Volcanic Soils" (E. Fernandez Caldas and H. Yaalon, eds.) *Catena Supplement 7*, Braunschweig: 1-8.

Parfitt R.L. 1990: Allophane in New Zealand - A Review *Austrailian Journal Soil Research*, 28: 343-360.

Pecsok R.L., Shields L.D., Cairns T., McWilliams I.G. 1976: (2nd ed) *Modern method of chemical analysis.* Wiley and Sons, 573pp.

Pejrup J. 1988: *In,* de Boer P.L., van Gelder A., Nio S.D. (eds.), *Tide-influenced sedimentary environments and facies.* Kluner Academic Press.

Perry E., Beckles E.C., Newton R.M. Chemical and mineralogical studies, sites 322 and 325, *In* Hollister C.D., Craddock C., and others, *Initial reports of the Deep Sea Drilling Project,* 35, Washington, D.C., U.S. Government Printing Office, p. 465-469.

Peterson M.N.A., Griffin J.J. 1964: Volcanism and clay minerals in the southeastern Pacific. *Journal of Marine Research*, 22: 287-312.

Pierce J.W., Siegel F.R. 1969: Quantification in clay mineral studies of sediments and sedimentary rocks. *Journal of Sedimentary Petrology*, 39: 187-193.

Pillans B. 1986: A late Quaternary uplift map for North Island, New Zealand. *Royal Society of New Zealand Bulletin*, 24: 409-417.

Pocknall D.T., Gregory M.R., Greig D.A. 1989: Palynology of Core 80/20 and its implications for understanding Holocene sea level changes in the Firth of Thames, New Zealand. *Journal of the Royal Society of New Zealand*, 19 (2): 171-179.]

Powell A.W.B. 1979: *New Zealand Mollusca - marine, land and freshwater shells*. Collins, London.

Pullar W.A., Selby M.J. 1971: Coastal progradation of Rangataiki Plains. *New Zealand Journal of Scienece*, 14 (2): 419-434.

Reineck H.E., Singh .B. 1971: Genesis of laminated sand and graded rythmites in storm-sand layers of shelf mud. *Sedimentology*, 123-128.

Reinson G.E. 1977: Hydrology and sediments of a temperate estuary - Mallacoota Inlet, Victoria. Department of National Resources Bureau of Mineral Resources, *Geology and Geophysics, Bulletin 178*,91pp.

Rhodes E.G. 1984: Depositional model for chenier plain, Gulf of Carpentaria Australia. *Sedimentology*, 29 (2): 201-223.

Roberts B., Merriman R.J. 1990: Cambrian and Ordivician metabentonites and their relevance to the origins of associated mudrocks in the northern sector of the Lower Paleozoic Welsh marginal basin. *Geological Magazine*, 127 (1): 31-43.

Ross C.S., Hendricks S.B. 1945: Minerals of the montmorillonite group. *U.S. Geological Survey Professional Paper* 205: 23-79.

Ruxton B.P. 1968: Rates of weathering of Quaternary volcanic ash in north-east Papua. *Transactions 9th International Congress of Soil Science*, 367-376.

Sayers J.K., Iskander J.K., Keeney D.R. 1973: Distribution and background levels of Mercury in sediment cores from selected Wisconsin Lakes. *Water-air-soil pollution*, 2: 105-118.

Scafe D.W., Kunze G.W. 1971: A clay mineral investigation of six cores from the Gulf of Mexico. *Marine Geology*, 10: 69-85.

Schofield J.C. 1959: Tauranga Group. In: Fleming C.A. (ed.) *Lexique Stratigraphique International* 6 (4): 387pp.

Schofield J.C. 1960: Sea level fluctuations during the last 4000 years as recorded by a Chenier Plain, Firth of Thames, New Zealand. *New Zealand Journal of Geology and Geophysics*, 3 (3): 467-485.

Schofield J.C. 1973: Postglacial sea-levels of Northland and Auckland. *New Zealand Journal of Geology and Geophysics*. 16 (3): 359-366.

Schofield J.C. 1975: Sea level fluctuations cause perodic post-glacial progradation south Kaipara barrier, North Island, New Zealand. *New Zealand Journal of Geology and Geophysics*. 18 (2): 295-316.

Siever R., Kastner M. 1967: Mineralogy and petrology of some Mid-Atlantic Ridge sediments, *Marine Research*, 25: 263-278.

Shrimp N.F., Scheilacher J.A., Ruck R.R., Heck D.B., Leland H.V., 1971: Trace element and organic carbon accumulation in the most recent sediments of southern Lake Michigan. *Illinois Geological Survey Environmental Geology Note* 41:25p.

Skinner D.M.B. 1986: Neogene volcanism of the Hauraki volcanic region, In: Late Cenozoic volcanism in New Zealand. *Royal Society of New Zealand Bulletin*, 23:.

Stevens K.F., Vucetich C.G. 1985: Weathering of upper Quaternary tephras in New Zealand. *Chemical Geology*, 53: 237-247.

Stoffers P., Glasby G.P., Pluger W.L., Walter P. 1983: Reconnaissance survey of the mineralogy and geochemistry of some New Zealand lake and nearshore sediments. *New Zealand Journal of Marine and Freshwater Research*, 17: 461-480.

Stoffers P., Glasby G.P., Wilson G., Davis R., Walter P. 1986: Heavy metal pollution in Wellington Harbour. *New Zealand Journal of Marine and Freshwater Research*, 20: 495-512.

Stoffers P., Muller G. 1972: Clay mineralogy of Black Sea sediments. *Sedimentology*, 18: 113-121.

Swanson K.M. 1979: The marine Fauna of New Zealand: Ostracods of the Otago shelf. *New Zealand Oceanographic Institute Memoir*, 78: 55pp.

Symes R.E., Wells N. 1973: Mineral content of topsoils on coastal terraces from Mount Egmont to Palmerston North, New Zealand. *New Zealand Journal of Geology and Geophysics*, 16: 651-656.

Van der Marel H.W., Beutelspacher H. 1976: *Atlas of infrared spectroscopy of clay minerals and their admixtures.* Elsevier, Amsterdam, 396pp.

Van Leeuwe C. in prep. Mud transportation in the Firth of Thames?. Unpublished MPhil. Thesis. University of Waikato, New Zealand.

Von Rad U., Rosch H. 1972: Mineralogy and origin of clay minerals, silica and authigenic silicaties in leg 14 sediments, *In*: Hayes D.E., Pimm A.C. et al., *Initial Reports of DSDP leg14*: Washington (US Govt. Printing Office), 727-751.

Wada K. 1977: Allophane and imogolite, *In*: Dixon J.B., Weed S.B. (eds). Minerals in soil environments. *Soil Science Society of America*, Madison, 603-658.

Wada K. 1978: Allophane and imogolite, *In*: Sudo T., Shioda S. (eds). *Clays and clay minerals of Japan.*. Developments in sedimentology. Kodansha and Elsevier, Tokyo, 26: 147-185.

Walker R.G. (ed) 1984: *Facies models* (2nd ed.). Geoscience, Canada, 318pp.

Weaver C.E. 1958: The effects and geological significance of potassium "fixation" by expandable clay minerals derived from muscovite, biotite, chlorite and volcanic material. *American Mineralogist*, 43: 839-861.

Wigley G.N.A 1990: *Holocene evolution of the Te Puke Lowland, western Bay of Plenty, New Zealand.* Unpublished MSc. Thesis, University of Waikato, New Zealand.

White A.F., 1979: Geochemistry of groundwater associated with a tuffaceous aquifer, Oasis Valley, Nevada. *United States Geological Survey Professional Paper*, 712-E, 26 pp.

White A.F., Claasson H.C. 1980: Kinetic model for the short-term dissolution of rhyolite glass. *Chemical Geology*, 28: 91-109.

White A.F., Claasson H.C., Benson L.V., 1980: The effect of dissolution of volcanic glass on the water chemistry in a tuffaceous aquifer, Rainer Mesa, Nevada. *United States Geological Survey Water Supply Paper* 1535-Q, 32pp.

White A.F. 1983: Surface chemistry and dissolution kinetics of glassy rocks at 25°C. *Geochimical et Cosmochimica Acta*, 47: 805-815.

Wilson M.D., Pittman E.D. 1977: Authigenic clays in sandstones: Recognition and influcence on reservoir properties and paleoenvironmental analysis. *Journal of Sedimentary Petrology*, 47 (1): 3-31.

Woodroffe C.D., Curtis R.J., McLean R.F. 1983: Development of a Chenier Plain, Firth of Thames, New Zealand. *Marine Geology*, 53: 1-22.

Yoshinaga N., Tait J.M., Soong 1973: Occurrence of imogolite in some volcanic ash soils of New Zealand. *Clay Minerals*, 10: 127-130.